This electronic thesis or dissertation has been downloaded from the King's Research Portal at https://kclpure.kcl.ac.uk/portal/

The Molecular Basis of the Frank-Starling Relationship

Zhang, Xuemeng

Awarding institution:
King's College London

The copyright of this thesis rests with the author and no quotation from it or information derived from it may be published without proper acknowledgement.

END USER LICENCE AGREEMENT

Unless another licence is stated on the immediately following page this work is licensed under a Creative Commons Attribution-NonCommercial-NoDerivatives 4.0 International licence. https://creativecommons.org/licenses/by-nc-nd/4.0/

You are free to copy, distribute and transmit the work

Under the following conditions:

- Attribution: You must attribute the work in the manner specified by the author (but not in any way that suggests that they endorse you or your use of the work).
- Non Commercial: You may not use this work for commercial purposes.
- No Derivative Works - You may not alter, transform, or build upon this work.

Any of these conditions can be waived if you receive permission from the author. Your fair dealings and other rights are in no way affected by the above.

Take down policy

If you believe that this document breaches copyright please contact librarypure@kcl.ac.uk providing details, and we will remove access to the work immediately and investigate your claim.

Download date: 14. Jan. 2025

The Molecular Basis of the Frank-Starling Relationship

Doctor of Philosophy

Xuemeng Zhang

2015

A thesis submitted in accordance with the requirements of

The Randall Division of Cell and Molecular Biophysics, King's College London

献给齐文和张志刚，

我亲爱的父母

To Qi Wen and Zhang Zhigang

Abstract

Frank-Starling law of the heart describes a proportional relationship between the end-diastolic ventricular volume and the systolic output in the heart on a beat-to-beat basis. It is largely due to a phenomenon called length dependent activation (LDA) on the level of cardiomyocytes. With the increasing SL, there are two outcomes of LDA: the increasing maximum force production, and the increasing Ca^{2+} sensitivity.

Ca^{2+} binding to cardiac troponin C (cTnC) triggers a series of changes in thin filament structure that enable heart muscle cells to contract. A polarized fluorescence technique, F*IS*S, was used to investigate the role of cTnC in the LDA. Using a purposely-built experimental set-up, force development and cTnC structural change were measured simultaneously as functions of $[Ca^{2+}]$ at SLs 1.9 and 2.3 μm. With the increasing SL, the Ca^{2+} sensitivity for force and cTnC structural change increased in a similar fashion, whereas the increase in maximum force production was not accompanied by an increase in the amplitude of cTnC structural change.

Although the inhibition of active force by 25 μM blebbistatin reduced the amplitude of cTnC structural change upon Ca^{2+} activation, the SL-dependent increase in the Ca^{2+} sensitivity was still presented. These results suggested that the force-generating cross-bridges were not essential for the SL-dependent changes of Ca^{2+} sensitivity in LDA. Taken together, our results suggested that the LDA was likely controlled via two signalling pathways. The SL-dependent Ca^{2+} sensitivity was mainly regulated by the thin filament, while the SL-dependent maximum force generation was controlled by the thick filament.

In addition, mimicking the SL stretching-induced reduction in interfilament spacing with 1% dextran did not reproduce the SL-dependent increase in the Ca^{2+} sensitivity, whereas further compression with 4% dextran significantly increased the Ca^{2+} sensitivity. This suggested that there might be another mechanism in the regulation of Ca^{2+} sensitivity by osmotic compression, which depends on the degree of the compression rather than the alteration in the interfilament spacing.

Acknowledgements

First of all, I would like to express my deepest gratitude to my supervisors Dr. Yin-Biao Sun and Professor Malcolm Irving for the opportunity of this fantastic project, for their countless hours of guidance throughout the entire project, and for constantly encouraging me and having faith in me, especially when I was not sure if I was capable of building the extremely complex experimental set-up. Now that I look back, the joy and gain this project has brought to me is more than words can describe. I would also like to thank Professor David Trentham for the scientific advice and discussions throughout my PhD.

I appreciate all the amazing lab members who have been more than friendly and generous to make my 3 years in the lab an incredible experience. I am particularly indebted to Dr. Ian Robertson, not only for sharing invaluable scientific ideas with me, helping me with my thesis, but also for all the fun conversations and experiences we had. I am very grateful to Dr. Thomas Kampourakis and Dr. Ivanka Sevrieva for introducing me to almost all the lab work, sharing wisdoms with me, helping me, and kindly teaching me in so many ways. I would never have accomplished building the set-up without the patient help and suggestions from Dr. Luca Fusi. I would also like to extend my special thanks to Dr. Andrea Knowles for showing me the biochemical experiments. Many thanks go to former lab member Rebecca (Becci) Scott for the unforgettable lunchtime. Also thanks to Ziqian Yan for the friendship. I would also like to thank some former members of the Randall Division: Dr. Daopeng Yuan and Dr. Zhisheng Lu, who helped me get used to the brand new environment when I first started.

Thanks to all my friends in Britain and China who took really good care of my crazy thoughts from time to time. I am eternally grateful to my best friends Yuan Zhao and Sean Song for the pleasant time we spent together, the experience they selflessly shared with me, and constantly soothing my panic attack, they are forever families to me.

I cannot begin to think of how grateful I am to have such wonderful and

understanding parents and families who have been nothing but caring and supporting and enduring in every possible way. They helped me grow into an optimistic and independent woman which I believe I will benefit from for my entire life.

Last not least, I would like to thank King's College London and China Scholarship Council for the generosity in sponsoring me and this project.

Table of Contents

Chapters Page

List of Abbreviations

ADP	Adenosine-5’-O-diphosphate
AP	Action Potential
ATP	Adenosine-5’-O -triphosphate
BDM	2,3-butanedione-monoxime
BR	Bifunctional Rhodamine (Bis-iodoacetamidorhodamine)
BR-cTnC	BR-labelled recombinant cardiac troponin C
BR-cTnC-C	BR-labelled recombinant cardiac troponin C mutant carrying the following substitutions Cys35Ser, Cys84Ser, Glu55Cys and Asp62Cys, whereby the BR molecule is cross-linked with Cys55 and Cys62
BR-cTnC-E	BR-labelled recombinant cardiac troponin C mutant carrying the following substitutions Cys35Ser, Cys84Ser, Glu95Cys and Arg102Cys, whereby the BR molecule is cross-linked with Cys95 and Cys102
BR-hcTnC	BR-labelled human cardiac troponin C
cCTnC	C-terminal domain (C-lobe) of cardiac troponin C
cCTnI	C-terminus of cardiac troponin I
cCTnT	C-terminus of cardiac troponin T
cMyBP-C	Cardiac Myosin binding protein C
cNTnC	N-terminal domain (N-lobe) of cardiac troponin C
cNTnT	N-terminus of cardiac troponin T
CrP	Creatine phosphate
cTn	Cardiac troponin complex
cTnC	Cardiac troponin C

cTnI	Cardiac troponin I
cTnT	Cardiac troponin T
Da	Dalton
DAQ	Data acquisition
DMSO	Dimethyl Sulphoxide
DTT	Dithiothreitol
E.coli	Escherichia coli
EGTA	Ethyleneglycoltetraacetic acid
ELC	Essential light chains
ESPVR	End-systolic pressure-volume relationship
ESV	End-systolic volume
F-actin	Filamentous actin (polymer)
F*IS*S	Fluorescence for *In Situ* Structure
fsTnC	Fast skeletal troponin C
G-actin	Globular actin (monomer)
HMM	Heavy meromyosin
IATR	Iodoacetamidotetramethylrhodamine
IT arm	Elongated domain of troponin containing cTnC residues 93–161 rigidly integrated between cTnI residues 42–136 and cTnT residues 203–271
KPr	Potassium propionate
LCD	Light chain domain
LDA	Length dependent activation
LMM	Light meromyosin
MgADP	Magnesium adenosine-5'-O-diphosphate
MgATP	Magnesium adenosine-5'-O-triphosphate
MHC	Myosin heavy chains
MLC	Myosin light chains
MW	Molecular weight

NEM-S1	Subfragment 1 of myosin that was reacted with N-ethylmaleimide
NMR	Nuclear magnetic resonance
PM	Photomultiplier
PMT	Photomultiplier tube
Pi	Inorganic phosphate
PV loop	Pressure-volume loop
RLC	Regulatory light chains
RP-HPLC	Reverse phase high performance liquid chromatography
RyRs	Ryanodine receptors
S1	Subfragment 1 of myosin
S2	Subfragment 2 of myosin
SA node	Sinoatrial node
SEM	Standard error of the mean
SL	Sarcomere length
SR	Sarcoplasmic reticulum
ssTnI	Slow skeletal muscle troponin I
sTnC	Skeletal muscle troponin C
TFA	Trifluoroacetic acid
Tm	Tropomyosin
Tn	Troponin
TnC	Troponin C
TnI	Troponin I
TnT	Troponin T
TnT1	The extension region, N-terminus of troponin T
Tris	Tris-hydroxymethyl-methylamine
v/v	Volume per volume
w/v	Weight per volume

List of Figures

List of Tables

Chapter 1

Introduction

1.1 General Introduction – from Heart to Cardiac Muscle

The heart is a hollow, muscular organ found in all organisms with circulatory systems. It works as a pump that drives blood throughout the pulmonary and systemic blood vessels of the entire body by repeated contracting (beating). The pulmonary circulation exchanges the deoxygenized blood and carbon dioxide with freshly oxygenized blood from the lungs, which enters into the systemic circulation to transport oxygen to the body. The blood-flow continuously provides the body tissues with oxygen and nutrition, and removes the waste products to maintain homeostasis.

The heart beats nonstop about 3 million times throughout an average human life span. These repeated, rhythmic contractions are triggered by a series of electrical impulses (action potentials, AP), that originated from the sinoatrial node (SA node, often known as the cardiac pacemaker) and propagated through the elaborate electrical conduction system of the heart to stimulate the rest of the cardiac muscle. It is the ordered stimulation of the myocardium that allows efficient contraction of the entire heart, thereby allowing blood to be pumped throughout the body.

The vertebrate heart is principally made of connective tissue and cardiac muscle cells (cardiomyocytes). Cardiac muscle is an involuntary striated muscle that is found exclusively in the walls of the heart, especially in the myocardium which is the thick middle layer of the heart's wall (Figure 1.1.1 A). It accounts for about 0.5% of the lean body mass in human.

Like skeletal muscle, cardiac muscle is composed of individual cells that separated from each other by enclosing in endomysium. Generally, cardiac muscle cells are about 100 μm long and 20 μm wide, which are shorter and wider than skeletal muscle cells. They are predominantly mononucleated and typically branched instead of linear as the skeletal muscle cells. Cardiomyocytes contain a further thread-like collection of elongated structures — myofibrils, which can be of variable length and are composed by chains of the repeating subunits — the sarcomeres (Figure 1.1.1 B & Figure 1.1.2).

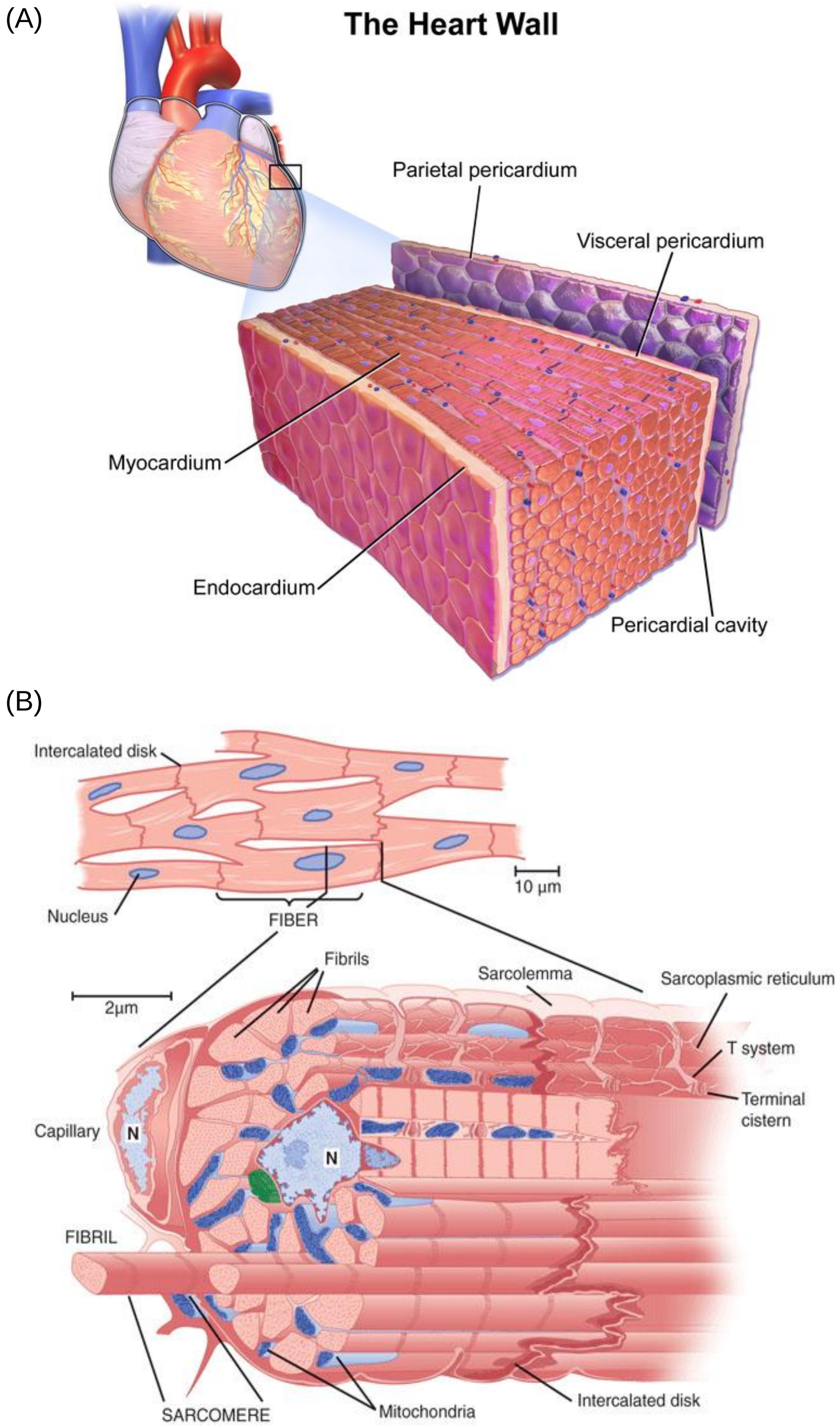

Figure 1.1.1: Cartoon representation of (A): the composition of the heart wall, the middle layer myocardium contains the biggest part of the cardiomyocytes (Blausen.com staff. "Blausen gallery 2014". *Wikiversity Journal of Medicine*. DOI:10.15347/wjm/2014.010. ISSN 20018762); and (B): the major constitution within a cardiomyocyte. (Figure from http://s3.amazonaws.com/rapgenius/morphology%20cardiac%20muscle.jpg).

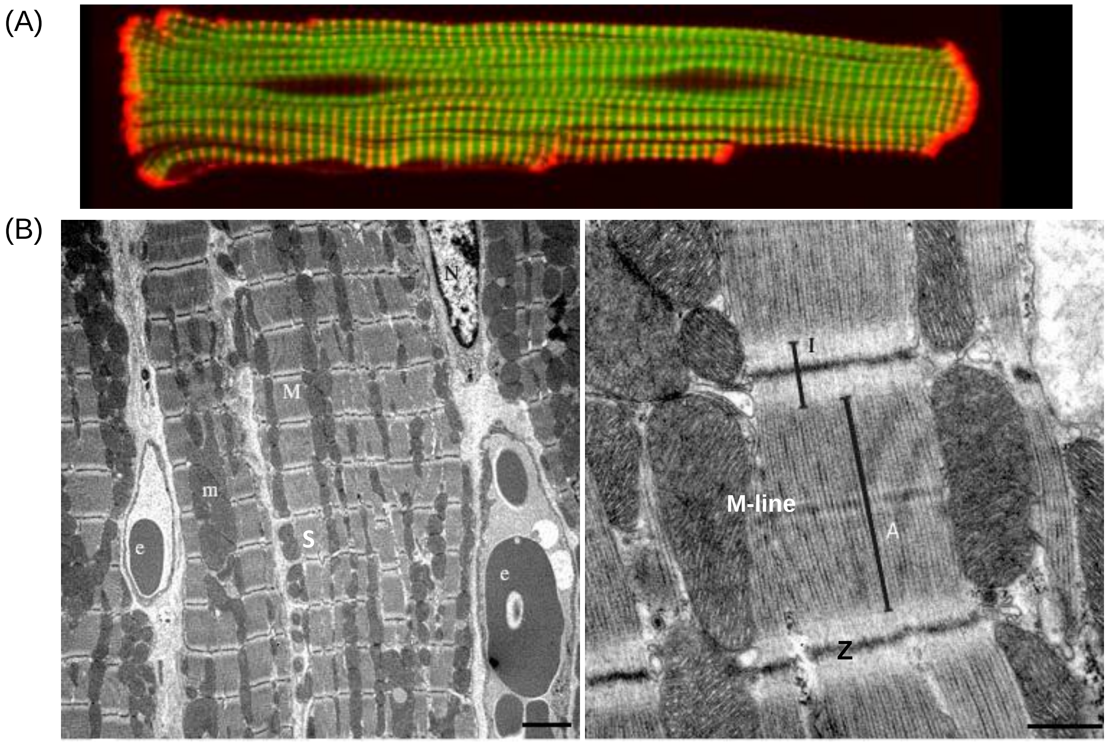

Figure 1.1.2: Cardiomyocyte geometry. (A): Confocal image of an adult rat cardiomyocyte stained sarcomeric actin (Green) and α-actinin (Z-lines, red), nucleus not shown. Image taken from http://diseasebiophysics.seas.harvard.edu/research/mechanotransduction/ (B): Electron microscopy image of the longitudinally sectioned rat's cardiomyocytes which contains sarcomere units that repeat along the length of it. **(a):** Red blood cells (e), mitochondria (m), myofibrils (M) and a cellular nucleus (N) are visible. Chains of sarcomeres (S) show the presence of striated pattern. Scale bar is 2 μm; **(b):** Highly ordered sarcomere unit clearly shows the A-bands (A) and I-bands (I). The Z-disks (Z) define the length of one sarcomere unit. M-line in the centre of the sarcomere is also visible (detailed description in Section 1.2.1). Scale bar is 500 nm. Micrographs were from http://www.trincoll.edu/~alehman/PhotoBIOL152.htm.

1.2 Ultrastructure of Cardiac Muscle

1.2.1 The Sarcomere

The sarcomere is the basic structural and functional unit in all striated muscle. It is primarily responsible for the striated appearance and the basic machinery for muscle contraction. The repeating cross-banding pattern in myofibrils are characterised by the relatively high- and low-density regions in sarcomere units under electron microscopy (Figure 1.1.2). The striation pattern in cardiomyocyte results from the various optical properties of the proteins that make up the sarcomere. The establishment of myosin and actin as the major sarcomeric proteins causing the striation pattern within the sarcomere was through the work of Hanson and Huxley (1953) using electron microscopy and X-ray diffraction. They discovered that myosin and actin are localised differently on the filaments of the myofibrils (the myofilaments). The myofilaments are further divided into two types according to the diameter and protein constitution: the myosin-containing thick filament and the actin-containing thin filament.

Each sarcomere is defined by two highly dense bands called the Z-disks or Z-lines. The length of the sarcomere — the distance between two adjacent Z-lines, typically ranges from 1.7 μm to 2.3 μm in human cardiomyocytes under physiological condition. Within each sarcomere, surrounding the Z-lines are the lighter, less dense I-bands which are composed of actin filaments without being superimposed by myosin filaments. The thin filaments extend to the Z-line on one side and run into the darker, denser A-band on the other. The A-band contains the entire length of a single thick filament, yet it has both the myosin and actin filaments as the components. In the central of the A-band there is a paler actin filament-free region called the H-zone where there is no myofilaments overlap. In the middle of the H-zone lies a thin darker M-line formed of cross-connection elements of the cytoskeleton. Electron microscopy images showing the main features of the striation pattern in sarcomeres are in Figure 1.1.2, and the schematic drawing is shown in Figure 1.2.1. In the sarcomere, the overlapping myofilaments are organised in a hexagonal arrangement, in which each thick filament is surrounded by six thin filaments while each thin filament is surrounded by three thick filaments (Huxley, 1953a; Huxley, 1953b) (Figure 1.2.1).

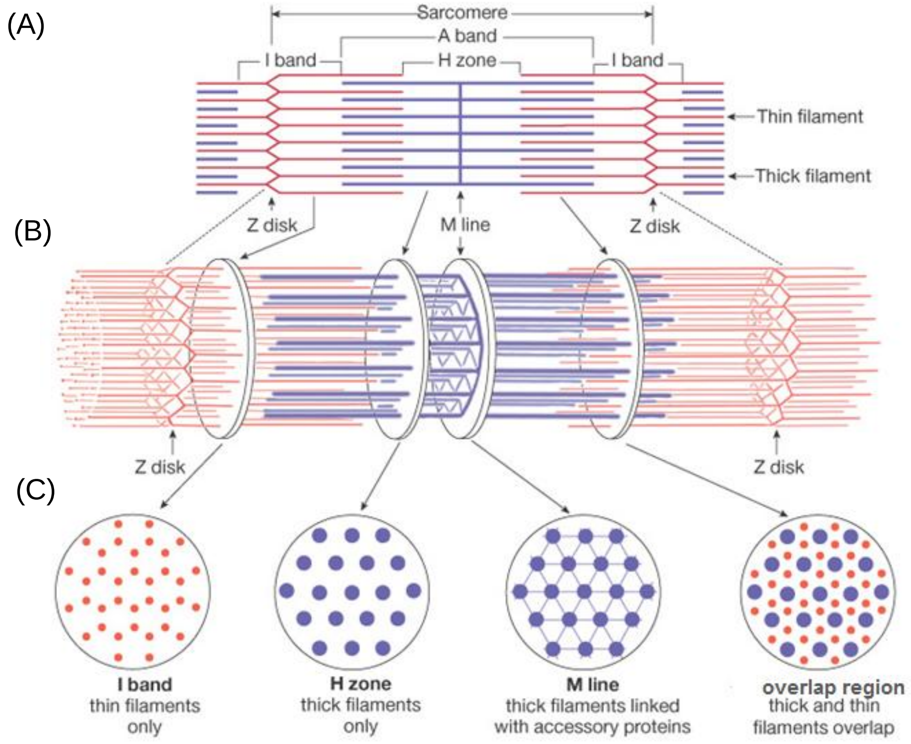

Figure 1.2.1: Cartoon representation of the striation pattern in the sarcomere. (A) and (B): The two- and three-dimensional organisation of a sarcomere. The thick filaments are shown in blue and the thin filaments in red; (C): The cross-sectional patterns generated by the myofilaments are shown below their respective zones. Figure taken from http://faculty.pasadena.edu/dkwon/chapt_11/textmostly/slide30.html.

Striated muscle contraction is achieved by the interactions between actin and myosin filaments (the actomyosin interaction) in the A-band of the sarcomere. In cardiac muscle, sarcomeric function plays a central role in the performance of the myocardium contraction, thus of the cardiac pump function. It is determined by the properties of the multiple protein constitutions in the sarcomere. Alterations in sarcomeric protein composition under pathological conditions will influence the contractile performance of the heart (Hamdani *et al*., 2008). The major proteins contained in the sarcomere are illustrated in Figure 1.2.2, including actin, tropomyosin (Tm), troponin (Tn) in the thin filament; myosin molecules and myosin binding protein C (MyBP-C) in the thick filament; the giant protein titin extends from the Z-line to the M-line of the sarcomere; the Z-line protein α-actinin; the M-line proteins myomesin, etc. The sarcomere is a complex system where every protein is essential to assure the structural and functional integrity of it. The unltrastructure of the major proteins involved in muscle contraction is discussed below.

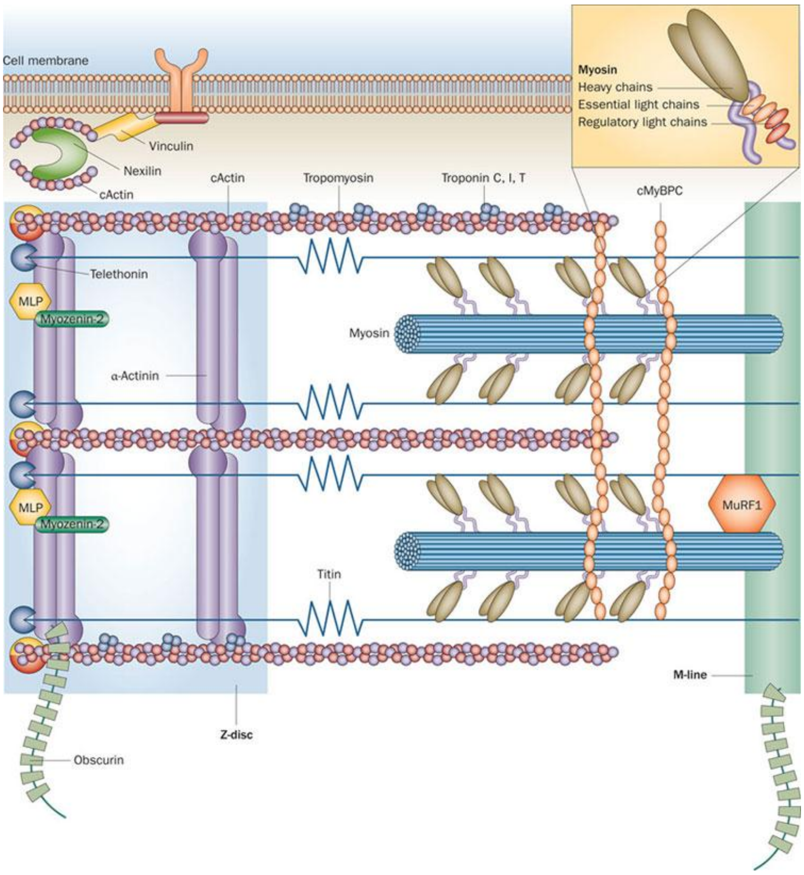

Figure 1.2.2: Major protein components in the sarcomere. Detailed description is in the text. cActin denotes α-actin, the actin isoform presents in cardiac muscle sarcomere. Figure taken from Frey *et al*. (2012).

1.2.2 The Thin Filament

1.2.2.1 Actin

The multi-protein complex of the thin filament is essentially comprised of three major proteins: actin, tropomyosin and troponin (Figure 1.2.3).

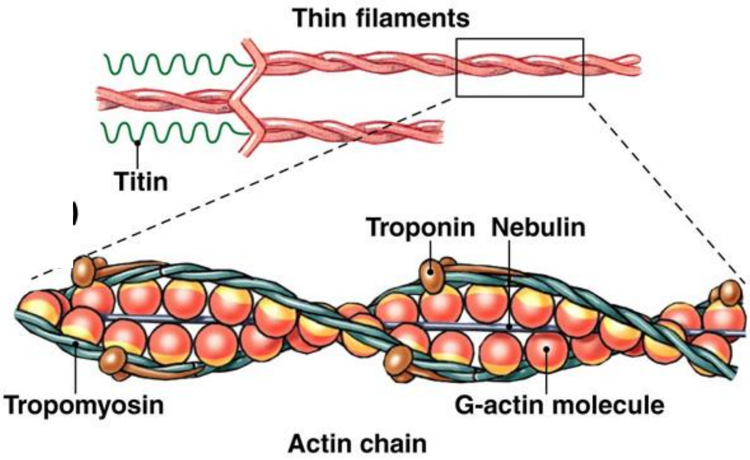

Figure 1.2.3: Schematic representation of the thin filament organisation, containing the double-stranded actin helix as the core of the filament, another double helical polymer tropomyosin and the ternary troponin complex. Each Tm spans seven actin monomers per strand in each 38 nm axial repeat, connects with adjacent molecules in a head-to-tail fashion. Picture illustrated by Benjamin Cummings.

Actin monomer is a globular multi-functional protein with a molecular mass of ~42kDa (G-actin). It is structurally divided into four sub-domains (I-IV) (Kabsch *et al*., 1990) with an ATP and Ca^{2+} binding site in the cleft at the centre of the molecule (Figure 1.2.4 A). Due to the smaller mass of the sub-domain II, G-actin monomers are polarized — the exposed areas of sub-domains I and III are referred to as the “barbed” ends, whilst the exposed areas of domains II and IV are termed the “pointed" ends.

G-actin monomers polymerize into filamentous actin (F-actin) in a double-stranded helical conformation which forms the core of the thin filament. An atomic structure of F-actin has been determined by a combination of X-ray crystallography and X-ray diffraction, as illustrated in Figure 1.2.4 B (Fujii *et al*., 2010; Holmes et al., 1990). The double-stranded filament has seven actin monomers per strand in each ca.38nm axial repeat. The assembly of one Tm and one Tn molecule binding with these seven actins in a ratio of 1:1:7 is often referred to as a regulatory unit (Ebashi et al., 1969). Under physiological conditions, actin polymerisation occurs preferentially at the barbed (+) end of the G-actin monomers powered by ATP hydrolysis, whereas depolymerisation takes place at the pointed (-) end (Figure 1.2.4 C). Within the sarcomere, actin is orientated with the (+) end in the Z-line and the (-) end pointing towards the M-line, preventing it from spontaneous depolymerisation by actin capping proteins.

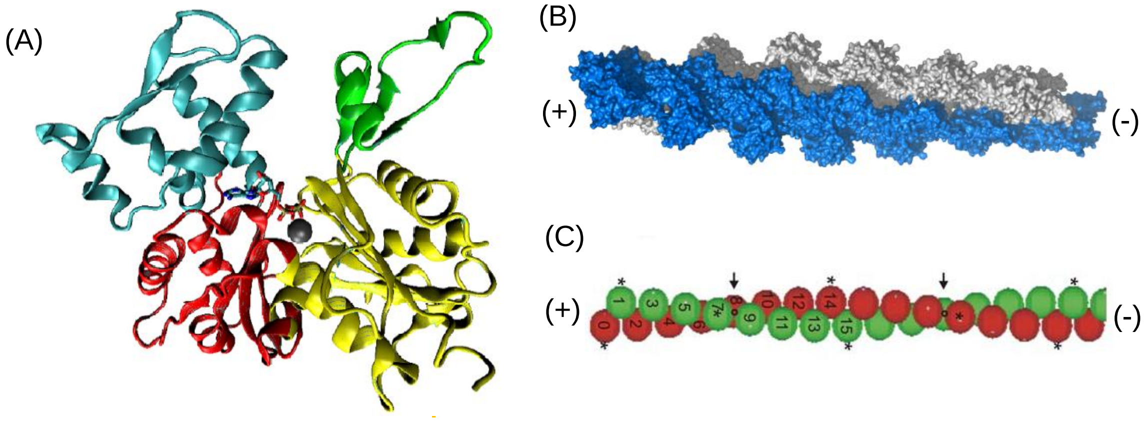

Figure 1.2.4: (A): Atomic structure of G-actin (PDB 1ATN) (Kabsch *et al*., 1990). G-actin consists of four sub-domains: I~IV. The central cleft with Ca^{2+} is shown in grey and the bound nucleotide is ATP ; (B): Atomic structure of F-actin based on the actin filament model of Holmes *et al*. (1990). The barbed- and pointed-end of the polarised filament are represented by (+) and (-), respectively. (Figure taken from http://en.wikipedia.org/wiki/Actin#mediaviewer/File:Actin_filament_atomic_model.png.); (C): The polymerization process occurs at the barbed (+) end of the filament and is associated with the hydrolysis of ATP by each actin monomer. Figure adapted from Luther (2009).

1.2.2.2 Tropomyosin

Tropomyosin is also a double-stranded α-helical coiled-coil protein that resides in the thin filament. The two polypeptide chains of Tm bind symmetrically alongside each of the helical strands of filamentous actin (Brown *et al*., 2005) (Figure 1.2.3). Each of this 400 Å long and 20 Å wide molecule spans seven actin monomers on each strand of F-actin over the 385 Å length of the thin filament. Neighbouring Tm molecules are linked up in a head-to-tail fashion, forming a continuous, flexible structure with high persistence length (Li *et al*., 2011).

Tm is involved in regulating the interactions between actin and myosin by guarding the myosin heads binding sites on actin filament, thus plays a pivotal role in regulating muscle contraction.

1.2.2.3 Troponin

The troponin complex (Tn, relatively molecular mass ~80 kDa) was first identified as the regulatory unit of the thin filament by Ebashi *et al*. (1967). One Tn is associated with one Tm which binds to seven actin monomers at an interval of 38 nm along each strand of F-actin. This ternary complex consists of three subunits: troponin C (TnC, ~18 kDa), the Ca^{2+} binding subunit; troponin I (TnI, ~24 kDa), the inhibitory subunit; and troponin T (TnT, ~35 kDa), the Tm binding subunit (Figure 1.2.5).

The Ca^{2+} binding induced structural rearrangement in Tn is known to be the first step that initiates muscle contraction. Studies using electron microscopy and low-resolution X-ray crystallography divided Tn into two domains: the TnT1 extension domain, and the rest of Tn — the core domain, which contains most of the regulatory function of Tn complex (Flicker *et al*., 1982; Ohtsuki, 1979; Ohtsuki *et al*., 1988; Takeda *et al*., 1997; White *et al*., 1987). The crystal structure of the core domain of human cardiac troponin (cTn) in the Ca^{2+}-saturated form was published by Takeda *et al*. (2003). The core domain of cTn is dominated by α-helices and is further organised into two structurally distinct sub-domains: the regulatory head and the IT arm (Figure 1.2.5). The regulatory head contains the N-terminal lobe of cTnC (cNTnC) which provides the Ca^{2+} binding site, and binds with the switch peptide of cTnI upon Ca^{2+} binding. The IT arm is a rigid and asymmetrical structure (~80 Å long) which has an arrowhead shape containing a long α-helical coiled-coil formed between cTnT and cTnI, with the C-terminal lobe of cTnC (cCTnC) sandwiched between them. The two sub-domains are connected via flexible linkers, characterising the highly flexible feature of the entire Tn molecule. The structures of the three subunits are discussed below.

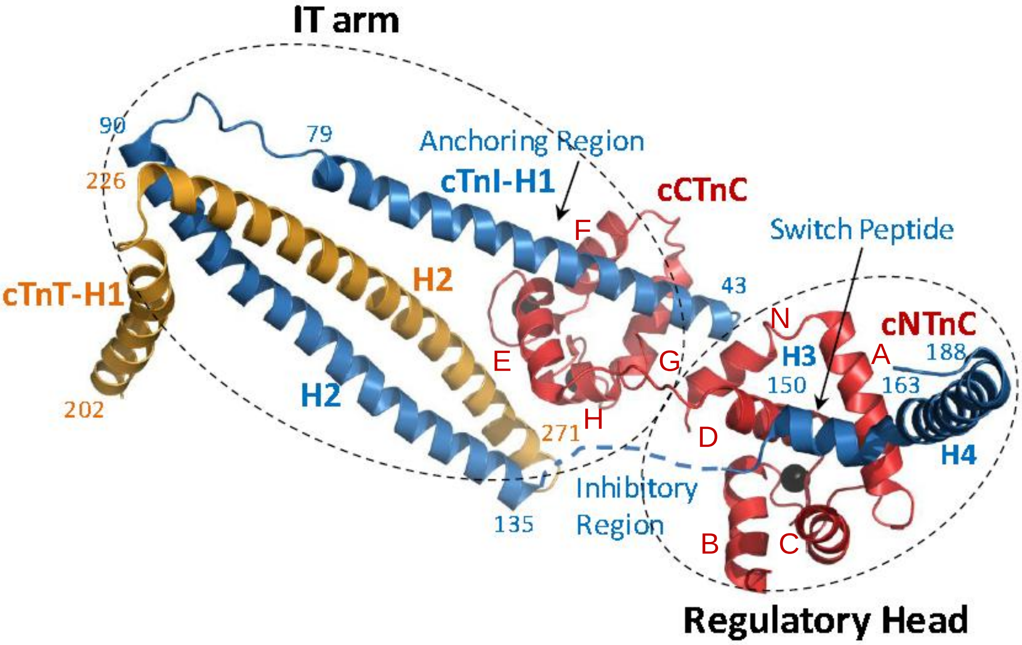

Figure 1.2.5: X-ray crystal structure of the Ca^{2+}-bound troponin core domain containing cTnC (red), cTnI (blue) and cTnT (gold) (PDB 1J1E, modified from Takeda *et al*. (2003)). The core domain can be divided into two sub-domains: the regulatory head and the IT arm. The two globular lobes in cTnC, i.e. the N-lobe and C-lobe are presented as cNTnC and cCTnC, respectively. The three Ca^{2+} ions bound to the Ca^{2+} binding sites II-IV are represented by black spheres (vision of the two high-affinity sites III and IV in cCTnC are obscured by the α-helices of the C-lobe). The inhibitory region of cTnI was not seen in the crystal structure and is represented as dashed line. Each helix within cTnI and cTnT is indicated by helix number, whereas those in cTnC are denoted by capital letter (A-H and N).

cTnC has a dumbbell-shaped structure which consists of two globular lobes — the regulatory N-lobe and the structural C-lobe, connected by a flexible linker formed by helices D and E (the D/E-linker, Figure 1.2.5) (Herzberg and James, 1985). cTnC is the Ca^{2+} binding protein. It contains two high affinity divalent cation binding sites (Ca^{2+}/Mg^{2+} sites, III and IV) in the C-lobe, and only one low-affinity Ca^{2+} binding site (II) in the N-lobe. There is an additional low-affinity binding site (I) in the N-lobe of skeletal

TnC. Due to amino acid substitutions at three coordinating positions in the loop, the functional site I is inactive in cTnC (Sia et al., 1997; van Eerd and Takahshi, 1976). Under physiological conditions, the high-affinity sites in the C-lobe are mostly always occupied with divalent metal ions. The open conformation of the C-lobe exposes a hydrophobic patch which binds the first N-terminal amphiphilic α-helix of cTnI (the cTnI-H1 helix in Figure 1.2.5), thus plays a structural role in anchoring cTnC in the cTn complex (Gasmi-Seabrook *et al*., 1999). The low-affinity binding site in the N-lobe of cTnC, on the other hand, is bound with Ca^{2+} ions upon an increase in the intracellular [Ca^{2+}]. As the regulatory Ca^{2+}-sensor, the N-lobe opens up a hydrophobic patch upon Ca^{2+} binding which interacts with the second amphiphilic α-helix of cTnI (the H3 helix, residues 147-163, known as the “switch peptide”). The binding of $cTnI_{147\text{-}163}$ only occurs in the Ca^{2+}-saturated state of the N-lobe to form a 1:1 cTnI/cTnC complex. This interaction between cNTnC and $cTnI_{147\text{-}163}$ triggers the relocation of Tm along the actin filament which represents an essential step in the signally pathway of muscle contraction (further discussed later).

Structure of the regulatory domain cNTnC in apo (Ca^{2+}-free), Ca^{2+}-saturated, and cNTnC $\cdot Ca^{2+}\cdot$ $cTnI_{147\text{-}163}$ states was confirmed by NMR studies (Li *et al*., 1999; Sia *et al*., 1997; Spyracopoulos *et al*., 1997). As illustrated in Figure 1.2.6, the conformation transition in cNTnC upon Ca^{2+} binding does not involve an opening of the N-lobe and the exposure of a substantial hydrophobic area, rather, it presents a similarly closed conformation as the apo state, in contrast with the skeletal TnC. Yet subsequent binding of the switch peptide of $cTnI_{147\text{-}163}$ to the small hydrophobic surface of cNTnC largely open the regulatory domain by moving helices B and C away from N, A and D. The interaction between cTnI and cTnC stabilizes the open conformation of cNTnC via interfering with the AB helical interface. It leads to a series of conformation steps in muscle contraction.

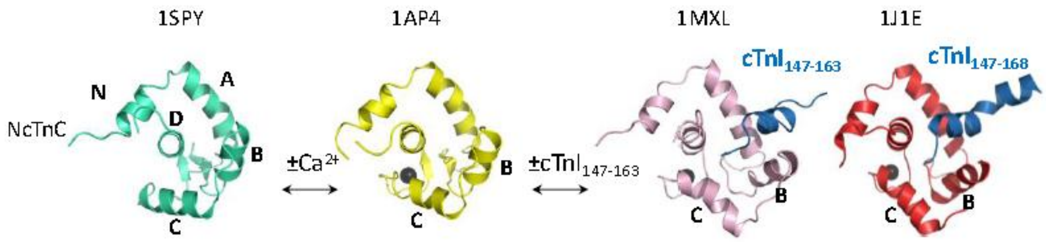

Figure 1.2.6: Closed to open transition in the conformation of cNTnC (NMR structures as indicated). Left to right — cNTnC apo (Ca^{2+} free), cNTnC·Ca^{2+}, cNTnC·Ca^{2+}·cTnI$_{147\text{-}163}$ and cNTnC·Ca^{2+}·cTnI$_{147\text{-}168}$. Binding of Ca^{2+} alone only induces minor changes in the conformation. The subsequent binding of the switch peptide fully opens the N-lobe and stabilizes the open conformation. See text for detailed description.

As the inhibitory subunit of cTn, cTnI inhibits the interactions between actin and myosin heads via the inhibitory binding to the actin filament at low [Ca^{2+}] (Farah et al., 1994; Syska et al., 1976; Talbot and Hodges, 1981). There are two regions in cTnI which are essentially responsible for the inhibitory binding of cTnI to actin in the absence of Ca^{2+} — the inhibitory region (residues 137-148) and the C-terminus of cTnI (cCTnI, residues 169-210). In the sequence between these two regions lies the switch peptide of cTnI (residues 147-163), which specifically binds with the hydrophobic cleft of cNTnC in the presence of Ca^{2+} (Figure 1.2.6). Thus, the interactions between cNTnC and the switch peptide of cTnI must remove both the inhibitory region and the C-terminal portion of cTnI from actin, resulting in the release of inhibition and the subsequent shifting of the equilibrium position for Tm (Campbell and Sykes, 1991; Kobayashi et al., 1999). As the link that connects helices H2 and H3 of cTnI, the inhibitory region is not well defined due to the flexible feature.

cTnT is the largest subunit in the cTn complex, which has an essential role in anchoring the cTn complex on the thin filament via interacting with Tm. There are two distinct Tm binding portions in cTnT: the N-terminus of cTnT (also known as the cTnT1 extension region) and the C-terminus of cTnT (denoted as cCTnT) (Ohtsuki, 1979; Tanokura *et al*., 1983), neither of them is included in the crystal structure elucidated by Takeda *et al*. (2003), thus not presented in Figure 1.2.5. Even though cTnT1 is not part of the Tn core complex, it exclusively interacts with Tm to anchor the Tn complex independent of the intracellular [Ca^{2+}] level, whereas cCTnT binds Tm in a more Ca^{2+} sensitive manner, i.e. stronger interaction occurs at low [Ca^{2+}] (Pearlstone and Smillie, 1983). As shown in Figure 1.2.5, the H2 helix of cTnT forms a parallel α-helical coiled-coil with the H2 helix of cTnI. Together with the upstream α-helical H1 helix of cTnT and the H1 helix of cTnI, these long helices are integrated in a rigid and asymmetrical domain — the IT arm. The amino acid residues in the rigid domain are well conserved between species, suggesting the important physiological roles it must hold in characterising the function of cTn. The IT arm does not have direct interaction either with Tm or with actin.

1.2.2.4 Structural Role of Troponin on Thin Filament

The conformational rearrangements of the cTn complex upon Ca^{2+} binding are the first steps in the elusive signalling pathway of cardiac muscle contraction.

Under physiological conditions, the interactions between cTnI and actin, cTnT and Tm stabilize the cTn complex onto the thin filament. All these interactions are Ca^{2+} sensitive except for the binding of the N-terminus of cTnT (cTnT1) to Tm. cTnT1 remains binding to Tm regardless of the relaxation or activation of the muscle. At low [Ca^{2+}], Tm is trapped in a position which covers the myosin heads binding sites on the actin filament by cTnT1, together with the two regions of cTnI which perform the inhibitory binding on actin in the absence of Ca^{2+} — the inhibitory region and the C-terminus of cTnI (cCTnI). The regulatory domain of cTn — the N lobe of cTnC (cNTnC), which is connected with the rest of cTn complex via the D/E-linker, rotates around its central D-helix searching for binding the switch peptide of cTnI (Sevrieva *et al*., 2014). As mentioned before (Figure 1.2.6), with an increasing [Ca^{2+}] over the physiological range, cNTnC undergoes a transition from an apo Ca^{2+} free state to a slightly opened Ca^{2+}-saturated state, and ends up in a substantially opening state with the subsequent binding of cTnI switch peptide, which in turn stabilizes cNTnC in the open conformation. As a consequence, the interaction between cTnI and cNTnC triggers the release of the two adjacent regions of cTnI switch peptide — the inhibitory region and the cCTnI from their actin binding inhibitory sites, which enables the movement of Tm from its kept position along the actin filament and facilitates the actomyosin interactions to generate force. Thus, the conformational dynamics of the cNTnC upon Ca^{2+}-activation surely play an important role in the regulation of cardiac muscle contraction. The IT arm of the cTn complex, on the other hand, does not move during activation, suggesting the C-lobe of cTnC (cCTnC), together with the coiled-coil helices of cTnT and cTnI, acts as a scaffold holding cNTnC and the actin binding regions of cTnI (Sevrieva *et al*., 2014). A cartoon representation of the interactions between components of cardiac thin filament upon Ca^{2+}-activation is in Figure 1.2.7.

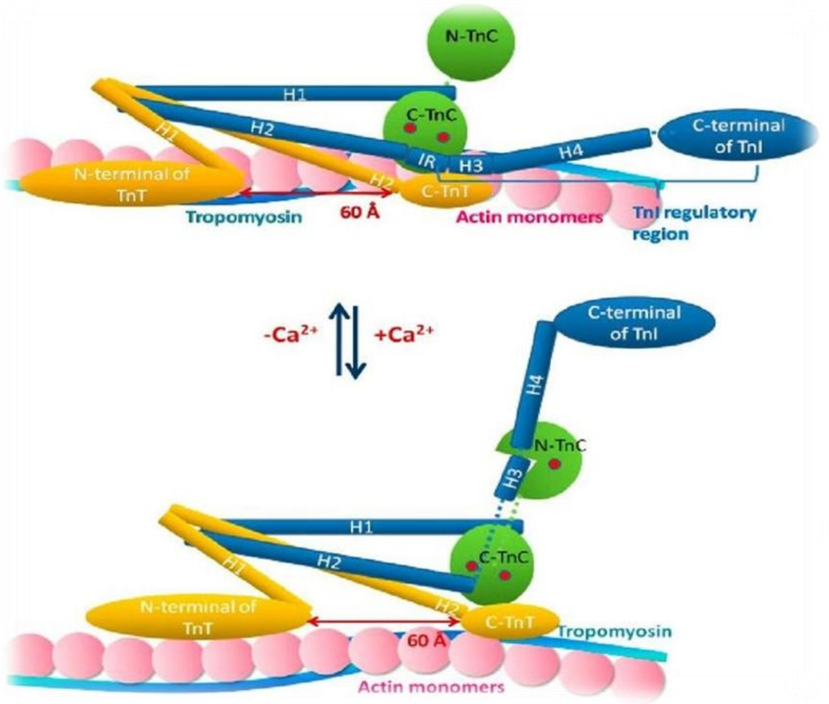

Figure 1.2.7: Schematic representation of the Ca^{2+}-dependent interactions between components of cardiac thin filament (figure adapted from Takeda *et al*. (2003)). The three subunits of cTn complex — cTnC is in green with three Ca^{2+} binding sites (site II on NTnC, site III and IV on CTnC, Ca^{2+} ions are denoted by red dots), cTnI is in blue (IR denotes the inhibitory region) and cTnT in yellow. Actin and Tm strands are in pink and cyan, respectively. See text for details of the Ca^{2+}-regulated thin filament activation.

1.2.3 The Thick Filament

The thick filament is mainly composed of myosin molecules and associated proteins, such as titin and myosin binding protein C (cMyBP-C) (Figure 1.2.2). Myosin is the most abundant component which forms the core of the thick filament. Titin is a giant elastic protein which spans 1 μm across half of the sarcomere with its N-terminus anchoring the Z-disk and C-terminus embedding in the M-line (Fukuda et al., 2009; Labeit and Kolmerer, 1995). It has an important role in generating passive force when the sarcomere is stretched beyond its slack length in the physiological SL range (Granzier and Irving, 1995; Linke et al., 1996).Titin interacts with both the thin and thick filament in the sarcomere. cMyBP-C is a myosin-associated protein which locates in the C-zone of the thick filament (C-zone — two 350nm long regions that flank the cross-bridge bare zone) (Previs et al., 2013). It was thought to bind to both myofilaments (Craig *et al*., 2014; Luther *et al*., 2011).

Myosin is a highly asymmetric, hexameric molecule which contains six separate protein chains: two myosin heavy chains (MHC), two regulatory light chains (RLC) and two essential light chains (ELC) (Figure 1.2.8 A). The two heavy chains wrap together as a parallel coiled-coil at the C-terminus of myosin, extend over most of the length of the molecule to form the myosin rod/tail portion, and end in two globular domains (known as the myosin heads) at the N-terminus. Proteolytic digestion of myosin with trypsin divided the molecule into two fragments: a light meromyosin (LMM) and a heavy meromyosin (HMM) (Szent-Gyorgyi, 1953). Further proteolysis of the latter fragment HMM with trypsin yields two subfragments: the globular S1 and the coiled-coil S2 (Mueller and Perry, 1962). As shown in Figure 1.2.8 A, subfragment S2 and LMM form the rod portion/tail of the myosin molecule. Subfragment S1, on the other hand, is the myosin head which forms the force-generating cross-bridge via interacting with actin. Structurally, S1 is divided into a motor domain which contains the ATP and actin binding sites, and a light chain domain (LCD, also known as the lever-arm) contains the regulatory and essential light chain. Figure 1.2.8 B is the X-ray structure of the chicken skeletal myosin S1 (Rayment *et al*., 1993b).

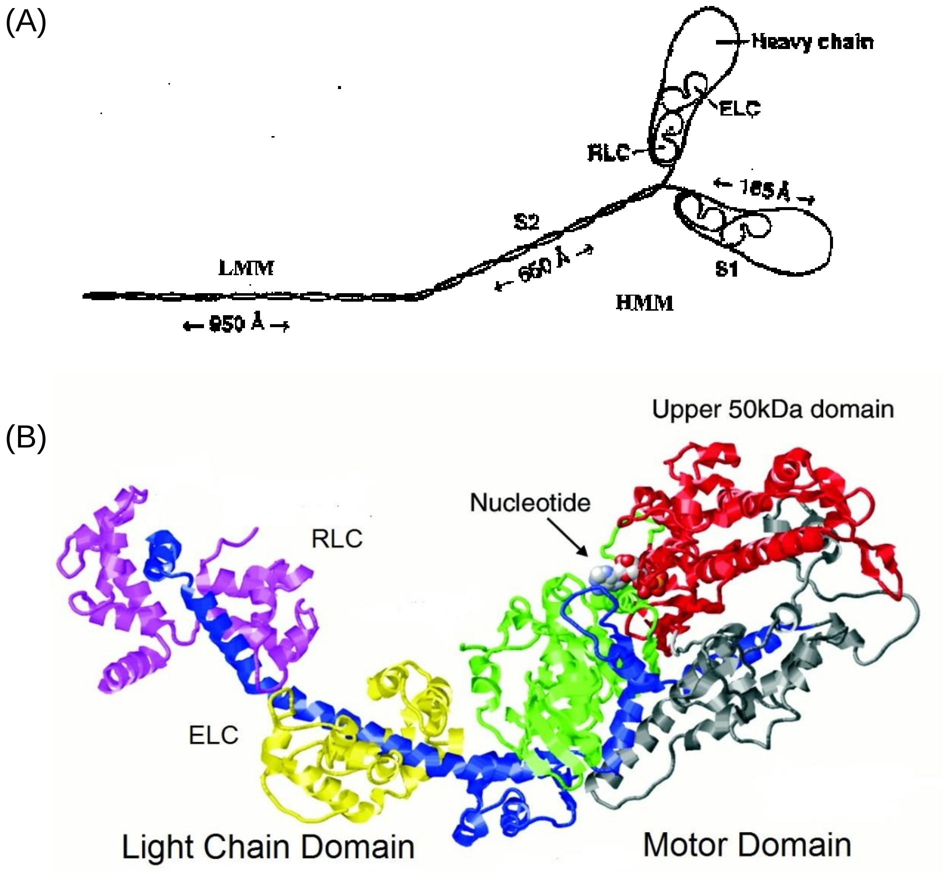

Figure 1.2.8: Myosin organisation. (A): Schematic representation of the hexameric molecule consisting two heavy chains, two RLCs and two ELCs. The myosin molecule can be divided into two major fragments, LMM is an extended coiled-coil, whereas HMM contains two subfragments — the globular S1 (myosin heads) and S2. S2 and LMM form the backbone of the thick filament. Figure taken from https://www.uic.edu/classes/phyb/phyb516/BaranyUpdate4/Myosin/Myosin.html; (B): X-ray crystallographic structure of chicken skeletal myosin subfragment S1. S1 can be divided into the globular motor domain which has the actin- and nucleotide-binding site, and the extended light chain domain which contains the essential and regulatory light chains. The green, red/grey, and blue segments represent the 25 kDa, 50 kDa, and 20 kDa segments of the heavy chain. The yellow and magenta parts correspond to the ELC and RLC respectively. (PDB 2MYS (Rayment *et al*., 1993b), figure modified from (Ruegg *et al*., 2002)).

1.2.3.1 The Cross-Bridge Cycle

In striated muscle contraction, the subfragment S1 of the myosin molecule, also known as the myosin head region, is the molecular motor which interacts with the actin filament in a cyclic manner to form cross-bridges and generate force (Cooke, 1997). The cyclic formation of cross-bridges is fuelled by ATP hydrolysis. In each cross-bridges cycle, the ATP-driven myosin motor undergoes a series of conformational changes in order to connect with actin and generate force (power stroke).

Current investigations agree with a “swinging lever-arm” model, in which the S1 myosin heads do not tilt as a whole, rather, the major conformational change determining the power stroke is confined to the LCD of the myosin molecule (Rayment et al., 1993a; Uyeda et al., 1996; Uyeda and Spudich, 1993). This model proposed that during the power stroke, the motor domain of myosin is relatively immobile, whereas the LCD acts as a rigid lever-arm which amplifies small conformational changes in the motor domain to produce an axial movement at the head-rod junction (Figure 1.2.9 A), producing pulling force at the cross-bridges which slides the actin filament towards the centre of the sarcomere (see Section 1.3.1 for the “sliding filament” theory). The “swinging lever-arm” model has received ample experimental supports by *in vitro* motility measurements with engineered lever-arms and *in situ* fluorescence polarization measurements in muscle fibres (Anson *et al*., 1996; Irving *et al*., 1995).

In an entire ATP-driven cross-bridge cycle, starting from the pre-power stroke state (from ④-① in Figure 1.2.9 B) for clear description, one molecule of ATP is hydrolyzed by myosin into ADP and Pi, swinging the lever-arm up and switching the myosin heads into high-energy configuration in preparation for the power stroke. At this state, myosin heads are attaching to actin forming weak binding cross-bridges with the lever-arm up. With the products of ATP hydrolysis dissociate from myosin heads, the conformational changes in the motor domain are amplified by the converter domain, which swings the LCD (the lever-arm) by ~70°, allowing switching to strong binding cross-bridges to generate force and slide actin filaments in the power stroke (working stroke) state (Geeves and Holmes, 1999; Llinas et al., 2012). When a new ATP is attached, the interaction between actin and myosin heads ends with the cross-bridge detached and lever swinging down. Hydrolysis of the new ATP molecule induces the entering of the pre-power stroke state where the cocking of the myosin heads by upward swinging lever-arm occurs, ready to undergo another cycle.

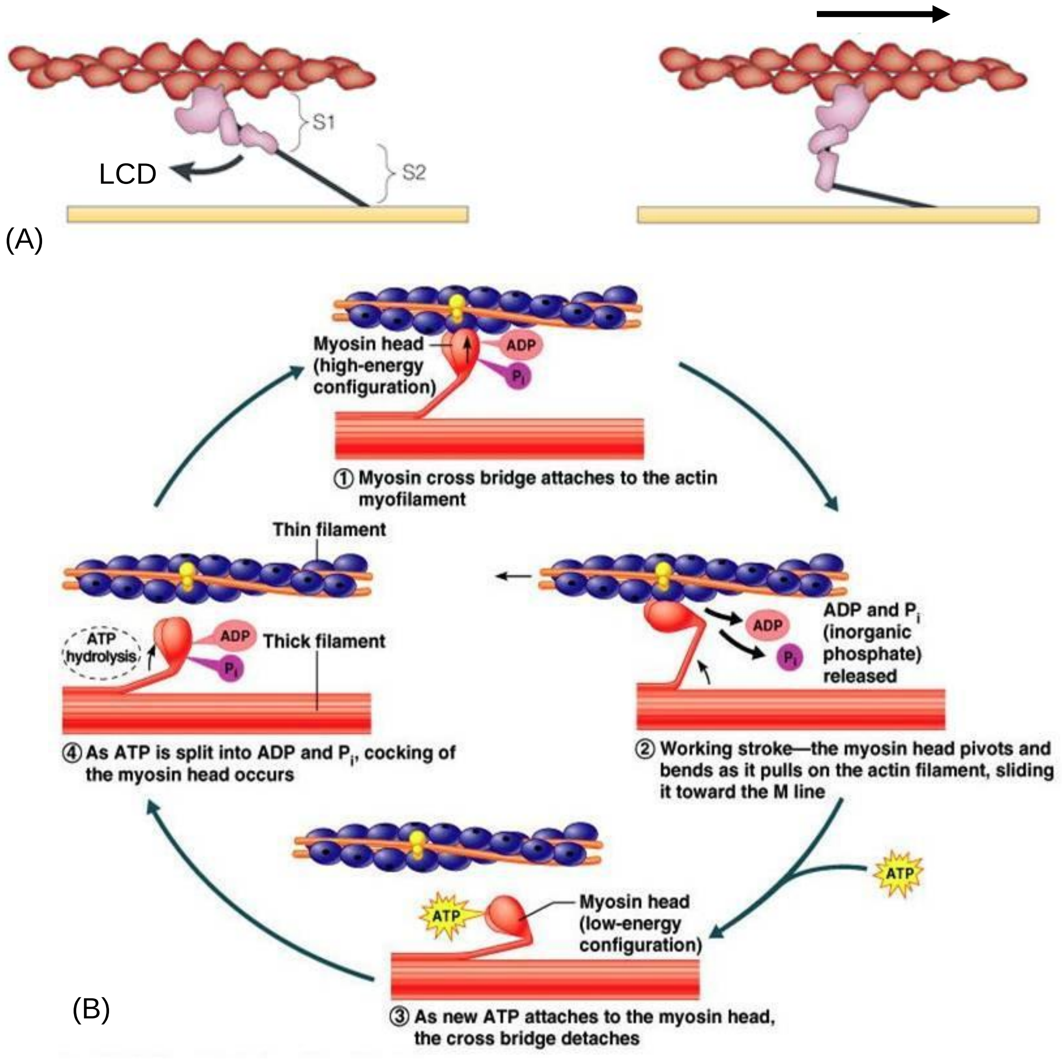

Figure 1.2.9: (A): Cartoon representation of the power stoke of the “swinging lever-arm” model. The conformation change of a cross-bridge from pre-power stroke state (left) to post-power stroke state (right) is determined by the tilting of the light chain domain (LCD) Figure modified from Spudich (2001); (B): A typical cross-bridge cycle powered by ATP hydrolysis based on the “swinging lever-arm” model (see text for description). Figure illustrated by Benjamin Cummings.

1.3 Regulation of Cardiac Muscle Contraction

1.3.1 The Sliding Filament Theory

In the heart, the contraction-induced shortening of the cardiomyocytes, as a result of the shortening of the aligned sarcomere units on the molecular level, reduces the size of the ventricular chambers, thus ejects blood into two circulation systems. The molecular mechanism underlying the sarcomere shortening during muscle contraction was described as the sliding of the thin filaments with respect to the thick filaments — the "sliding filament" theory (Huxley and Niedergerke, 1954; Huxley and Hanson, 1954). Using high resolution microscopy, researchers observed that during contraction, the A-bands of the sarcomere remained relatively central and constant in length, whereas the I-bands and H-zones shortened along with the sarcomere, indicating the sliding of the thin filaments towards the centre of the sarcomere is the cause of the sarcomere and muscle shortening. Neither of the two myofilament systems changes length when sliding occurs. The formation of cross-bridges by actomyosin interactions was first discovered and characterized as the motor that causes the sliding between myofilaments by Huxley (1957) using electron microscopy studies of rabbit psoas and frog sartorius muscle. When strongly bound, these cyclic interactions generate a pulling force on the actin filament, propelling them towards the centre of the sarcomere. The pulling force transmits from the actin filaments towards the ends of each sarcomere — the Z-disks, where through the mechanical coupling with the extracellular collagen network, ultimately reaches the heart's cavity to cause myocardium shortening and produce ventricular pressure. The trigger for initiating all these events in muscle contraction was identified as the binding of Ca^{2+} to the thin filament protein-cTnC. The significance of Ca^{2+} in the regulation of muscle contraction is discussed below.

1.3.2 The Ca^{2+} Regulation of Muscle Contraction

Contraction of striated muscle is triggered by Ca^{2+} binding to the regulatory protein Tn in the actin-containing thin filaments, leading to an azimuthal movement of the Tm around the filament that reveals the myosin heads binding sites, allowing cyclic actomyosin interactions and force generation (Ebashi et al., 1969; Gordon et al., 2000; Greaser and Gergely, 1971). In cardiac muscle cell, the rapid rising of intracellular $[Ca^{2+}]$ ($[Ca^{2+}]_i$) from resting (~160 nM) to active (~2.7 μM) occurs with the arrival of action potentials (AP) from the pacemaker cells in the heart (Kirschenlohr *et al.*, 2000). AP stimulation depolarises the cell membrane, leading to a small influx of Ca^{2+} entering the cell via the voltage-gated calcium channels in the membrane. However, the Ca^{2+} entry at this point is insufficient to induce a normal contraction. It binds to the ryanodine receptors (RyRs) on the sarcoplasmic reticulum (SR) and triggers the release of more Ca^{2+} from these intracellular Ca^{2+} stores — the Ca^{2+}-induced Ca^{2+} release. The combination of Ca^{2+} entry and SR Ca^{2+} release transiently increases the $[Ca^{2+}]_i$, which binds to the regulatory N-lobe of cTnC and initiates the contraction at the sarcomere level by the sliding of actin over myosin filaments. At the end of the AP, voltage-dependent Ca^{2+} channels in the membrane become inactive, most of the Ca^{2+} is recaptured by the SR and extruded by the Na/Ca exchanger. Relaxation occurs when $[Ca^{2+}]_i$ falls towards the resting level and Ca^{2+} dissociate from cTnC. The events in the sarcomere regulated by Ca^{2+} binding or dissociation during activation and relaxation are described next.

1.3.2.1 The steric blocking model

The molecular basis for the Ca^{2+}-regulated activation was first established after the identification of Tn and Tm as the principal proteins of Ca^{2+} regulation (Ebashi et al., 1967; Ebashi and Endo, 1968). In these investigations, researchers characterised that Tn is the actual Ca^{2+} binding constituent of thin filaments. The position of Tm on the thin filament is key to myosin binding, depending on the presence or absence of Ca^{2+} on Tn. A steric blocking model describing the Ca^{2+}-regulated thin filament activation was proposed based on the X-ray diffraction experiments (Haselgrove and Huxley, 1973; Parry and Squire, 1973). This model postulated a Ca^{2+}-free (OFF) state when Tm sterically blocks the myosin heads binding sites on actin, along with a Ca^{2+}-bound (ON) state when Tm moves azimuthally away from the binding sites upon Ca^{2+} binding to Tn, allowing actomyosin interactions. This simple two-state model was supported by electron microscopy and image reconstitution results which indicated Tm shifts along the actin filament from a periphery, closer to myosin binding sites position towards a closer to actin filament groove position upon Ca^{2+} activation (Lehman et al., 1994; Lehman et al., 1995; Milligan and Flicker, 1987; Spudich et al., 1972; Vibert et al., 1997; Xu et al., 1999) (Figure 1.3.1 A).

The two-state model was later updated to a three-state model where Tm was found to move further along the inner groove of the actin filament upon myosin heads binding (Figure 1.3.1 B), resulting in an equilibrium three states of Ca^{2+}-dependent thin filament activation: blocked, closed, and open state (Lehrer, 1994; McKillop and Geeves, 1993). In association with the three thin filament states, there are two cross-bridge states: a weak binding cross-bridge (A-state) and a strong binding cross-bridge (R-state). In the absence of Ca^{2+}, Tm occupies a position in which it imposes a steric hindrance to myosin binding, whereby no cross-bridges can be formed (blocked state). With the binding of Ca^{2+} to cTnC, conformational rearrangements in the Tn complex allow Tm to relocate towards the groove of the actin double helix, which partially exposes the myosin binding sites (closed state). At this state, myosin heads are able to interact weakly with actin to form weak binding cross-bridges with no force generation (A-state). The weak binding cross-bridges then undergoes an isomerisation to the strong binding, force-generating state (R-state) with high rates of ATP hydrolysis. Transition from weak to strong binding state is related with a further movement of Tm into the groove of the actin filament, shifting thin filament to a fully-activated open state. The further displacement of Tm fully exposes the myosin binding sites on actin filament at which more force-generating cross-bridges can be formed.

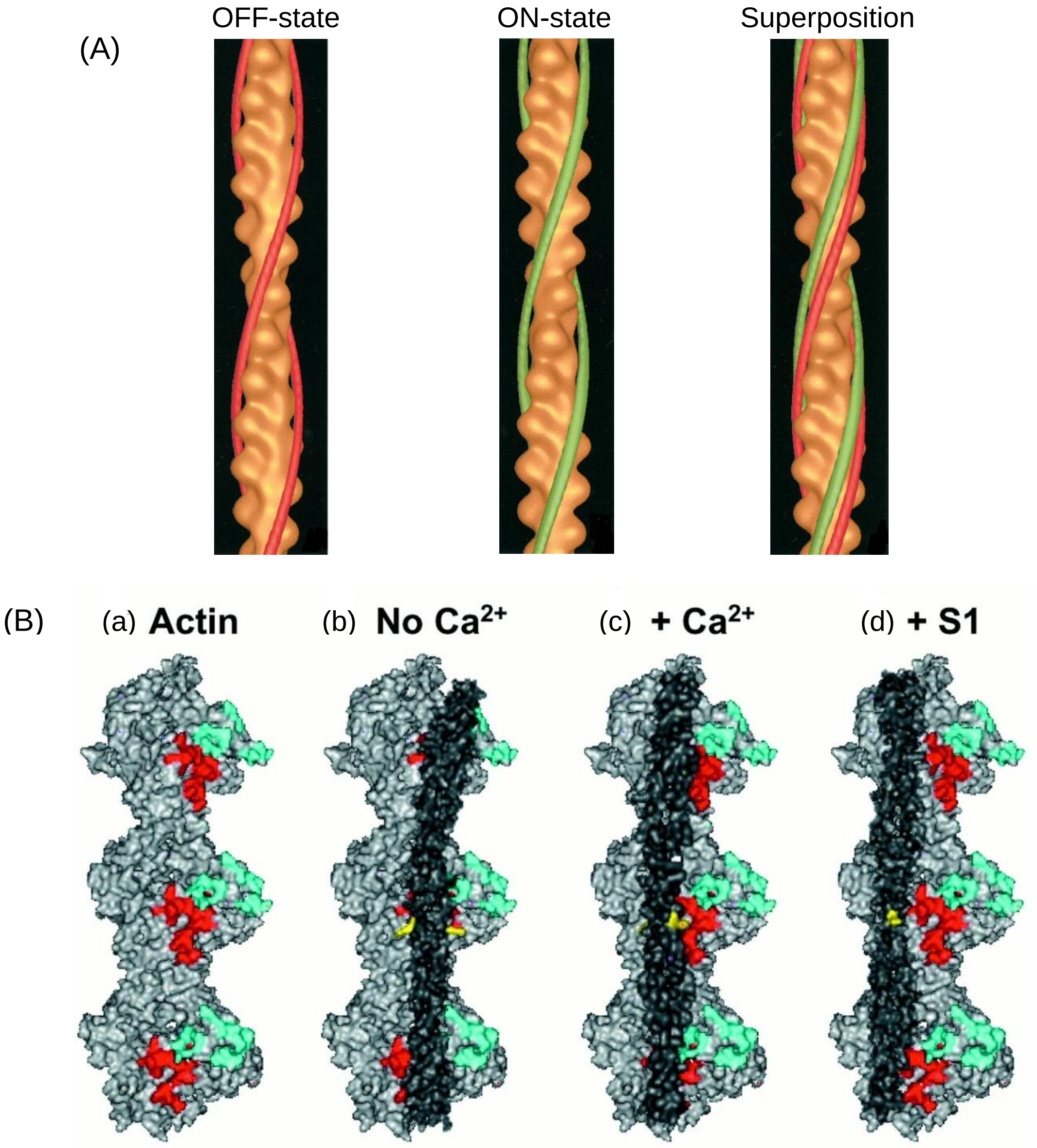

Figure 1.3.1: Movement of Tm over the surface of the actin filament. (A): Two-state model (Xu *et al*., 1999). From left to right: the Ca^{2+}-free (OFF) state (Tm in red), the Ca^{2+}-bound (ON) state (Tm in green) and a superposition of the two states. Actin filament is coloured in orange; (B): Three-state model (Gordon *et al*., 2001). (a): Major actin filament is shown in light grey, with weak and strong myosin binding sites in green and red, respectively; (b): In the absence of Ca^{2+}, Tm (dark grey) blocks both types of myosin binding sites (blocked state); (c): Upon Ca^{2+} binding to cTnC, Tm moves into a closed conformation to uncover some of the myosin binding sites (mostly for weak binding) to form weak binding cross-bridges (closed state); (d): Transition from weak to strong binding cross-bridges (S1) further displaces Tm, fully expose the strong myosin binding sites for the formation of more strong binding cross-bridges (open state).

As recently proposed by Sun and Irving (2010), relaxation may not be a simple reverse of the process in activation, implying the possibility of an additional “pre-relaxing” state after Ca^{2+} dissociate from cTnC. At this state, Ca^{2+} dissociation occurs before the detachment of cross-bridges. Thus the strong binding cross-bridges may still be able to generate force and hold Tm in the clear position even when cTnC is free of Ca^{2+}.

1.3.2.2 Cooperativity

Activation and relaxation of cardiac muscle is regulated by a narrow range of $[Ca^{2+}]_i$, i.e. the isometric steady-state force production is steeply dependent on $[Ca^{2+}]_i$. Small changes in $[Ca^{2+}]_i$ can produce functionally significant changes in force production, thus in cardiac output. The steep force-$[Ca^{2+}]$ relationship facilitates rapid and synchronous activation, and minimises the metabolic cost of Ca^{2+} cycling. Although in cardiac muscle, each Tn complex provides only one regulatory Ca^{2+} binding site, the steepness of the force-$[Ca^{2+}]$ relationship (denoted by Hill coefficient n_H, information regarding Hill equation is in 2.5.3) in skinned cardiac muscle (n_H = 3~4) is much higher than would be expected for the single Ca^{2+} binding site ($n_H = 1$), indicating highly cooperative Ca^{2+} regulation of muscle contraction. Over the years, the molecular basis underlying the cooperativity varies, including:

1. Binding of myosin heads to actin switches on thin filament activation, generates a positive feedback to the activation by promoting further binding of Ca^{2+} in neighbouring Tn complex and further formation of strong binding cross-bridges (Hofmann and Fuchs, 1988; Kobayashi et al., 2008; Razumova et al., 2000; Regnier et al., 2004).

2. Cooperativity is an intrinsic property of the thin filament. Initial Ca^{2+} binding enhances the Ca^{2+} binding affinity in adjacent regulatory units (RU, one Tn, one Tm and seven actin monomers), spread by the end-to-end coupling between adjacent Tm molecules (Sun and Irving, 2010; Sun et al., 2009).

The widely accepted former possibility bases on a well-established biochemical model in which myosin binding switches on the activation in rigor-like conditions (low [MgATP]) (Davis et al., 2007; Robinson et al., 2004; Rosenfeld and Taylor, 1985). However, trabecular studies in near-physiological conditions by inhibiting the formation of cross-bridges produced no significant change in the cooperativity, at variance with the first hypothesis (Sun *et al*., 2009). The downsides of the biochemical studies may be responsible for this discrepancy, such as the not well-reserved actomyosin interactions in the isolated proteins, and the lack of accurate force measurement in the biochemical studies. Sun and Irving (2010) concluded that although myosin heads binding switches on the thin filament activation in rigor conditions, it does not contribute significantly under physiological conditions, implying the effect of myosin binding in rigor is not a reliable model for its role in thin filament activation under physiological conditions.

If strong binding cross-bridges do not account for the Ca^{2+} cooperativity, the second hypothesis regarding the cooperative regulation as an intrinsic property of the thin filament has been considered. The Ca^{2+} binding signal originating from the Tn complex in one RU spreads along the surface of the thin filament to the neighbouring RUs containing Ca^{2+}-free (apo) troponins via the coupling between adjacent Tm molecules. Thus, the Ca^{2+} binding-induced impact on the conformation and/or position of the Tn and Tm molecules propagates along the thin filament to the adjacent RUs, exposing more myosin heads binding sites to form cross-bridges, thereby achieving a highly cooperative activation.

1.4 The Frank-Starling Relationship

The Frank-Starling relationship, also known as the Frank-Starling law of the heart, is a fundamental property of the myocardium, which describes a proportional relationship between the end-diastolic ventricular filling and the systolic output (stroke volume) in the heart on a beat-to-beat basis. First described by Otto Frank in Germany and Ernest Starling in England over a century ago, this relationship between ventricular filling and stroke volume has long been appreciated for its critical function in the regulation of cardiac output. During the time course of one heartbeat, increasing the volume of blood filling (known as preload) stretches the ventricular wall, leads to a greater, more forcefully contraction in the heart. It allows greater ejection volume, thus an enhancement of the heart's performance in the next beat (Figure 1.4.1).

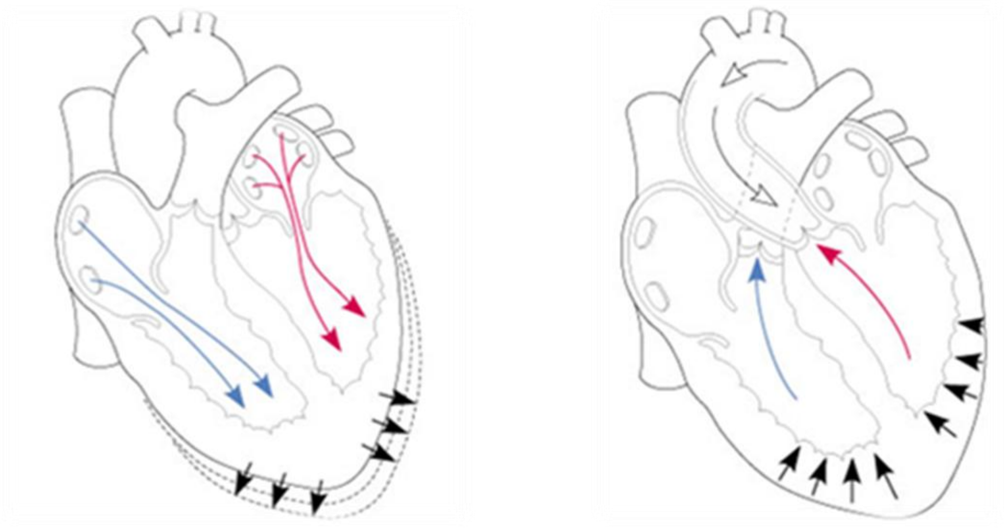

Figure 1.4.1: Cartoon representation of the Frank-Starling law of the heart. Red and blue arrows respectively denote the direction of blood flow in the left and right ventricle. Increasing ventricular filling (preload) stretches the ventricular wall (left figure), leads to more forcefully myocardium contraction (afterload) in the next heartbeat, resulting in more cardiac output from the ventricles to eject the additional preload (right figure). Figures from:https://www.studyblue.com/notes/note/n/bmsc-290-study-guide-2013-14-taylor/deck/8692093.

As described by Moss and Fitzsimons (2002), Frank-Starling relationship has an essential role in the synchronization between cardiac output and venous return. An increase in the venous return leads to a corresponding increase in the end-diastolic ventricular filling, which in turn induces greater stroke volume for the next heartbeat, such that more blood is pumped into arteries to accommodate the increased venous return from last circulation, thus the blood amount in the vasculature throughout the entire body can be maintained at equilibrium state in the circulation. Moreover, Frank-Starling relationship is an intrinsic property of the heart to adjust the ejection volume to meet the energy demands of the body tissues, completely separated from the central nervous system (Starling and Visscher, 1927). Studies have shown that in the patient with poor pump function or heart failure, the energy distribution by Frank-Starling relationship between supply and demand failed to function normally: increasing the ventricular volume resulted in a much smaller corresponding increase in the cardiac output. The output volume was inadequate to meet the demands of the body tissues, which would severely compromise organ system function and result in fluid build-up such as pulmonary oedema over time (Hanft *et al*., 2008). Therefore, despite the profound significance in the regulation of cardiac function, Frank-Starling relationship is also considered as a reference indicator of the physiological and pathophysiological features of the heart.

Generally, the relationship is named as the Frank-Starling law of the heart after the two physiologists Otto Frank and Ernest Starling who first described it, although opinions vary in terms of the novelty of who discovered the relationship, details concerning this topic can be found in reviews by Zimmer (2002).

Over the years, due to the great physiological significance of the Frank-Starling relationship in the regulation of cardiac function, the mechanism that underlies the enhancing cardiac contraction in response to the increasing ventricular filling on the cardiomyocyte level has been extensively investigated. A proportional relationship between myofilament SL and the maximum force generation, a phenomenon commonly referred to as the myofilament length dependent activation (LDA), is considered to be the main cellular basis of the Frank-Starling law of the heart (further explained in Section 1.6).

1.5 Myofilament Length Dependence Activation

1.5.1 The Cellular Basis of the Frank-Starling Relationship

The Frank-Starling relationship is an intrinsic regulatory mechanism in the heart that relates the diastolic ventricular filling with the systolic ejection volume. On the cellular level, an increase in the diastolic filling volume (preload) stretches the cardiomyocytes, leading to an increase in the SL. The increasing SL induces greater force development in the cardiac muscle contraction, which results in greater ventricular pressure at end-systole, and ultimately, more ejection volume. This direct proportionality between SL and force development, a phenomenon generally known as the myofilament length dependent activation (LDA), is the principle cellular basis that underlies the Frank-Starling modulation of cardiac output (Allen and Kentish, 1985; Jewell, 1977).

The speculation of active force as a proportional function of muscle length was first reported in skeletal muscle. Together with the sliding filament model of muscle contraction, this finding provides appealing explanation for the modulation of contractile force by muscle fibre length (Blix, 1894; Endo, 1972; Gordon *et al*., 1966). This was of particular interest to the cardiovascular investigations after the establishment of the Frank-Starling relationship, linking cardiac function to a fundamental property of the cardiomyocytes — the SL. Indeed, later study in isolated cardiac muscle has shown that the force production from sub-maximal Ca^{2+} activation is directly proportional to the SL (ter Keurs *et al*., 1980).

The force-length relationship in muscle contraction, presented as the length-tension curve, is a property of both skeletal and cardiac muscles that relates the strength of an isometric contraction to the resting length of the muscle fibre (skeletal) or the sarcomere (cardiac). A net length-tension curve is a combination of both the active and passive elements. Active tension is produced by the interactions between actin and myosin heads upon Ca^{2+}-induced activation, whilst passive tension (resting tension) is mostly the result of titin straining. As shown in Figure 1.5.1, there is an ideal fibre length or SL (L_0 in Figure 1.5.1) at which muscles operate with greatest active force. Thus in order to maximize the active force, the range of length at which muscle contraction occurs should remain on the peak of the curve. However, in cardiac muscle, instead of remaining on the peak of the curve, it is more likely to function on the ascending limb of the length-tension curve, reserving great force development potential that subject to the regulation by SL stretching as a result of more ventricular filling in the heart (Frank-Starling relationship).

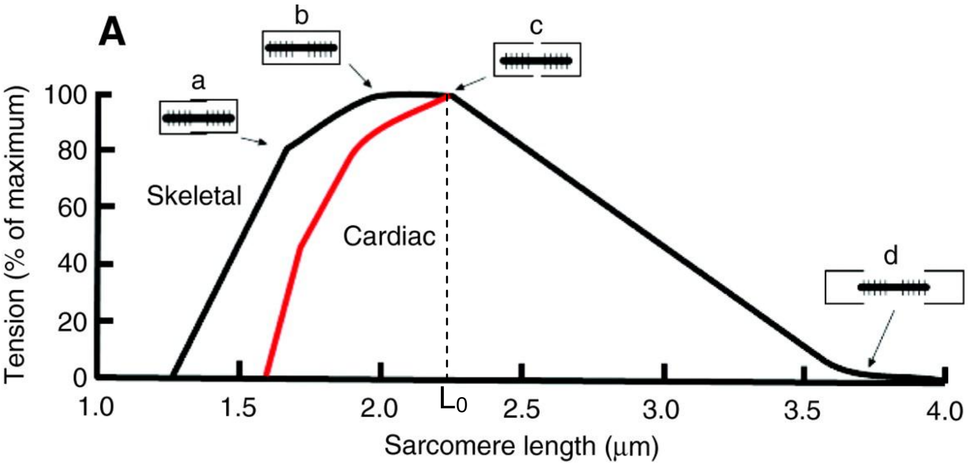

Figure 1.5.1: The length-tension curve for cardiac and skeletal muscle. The optimal SL (L_0) is the ideal length at which muscle operates with the maximum active force. Unlike skeletal muscle, cardiac muscle functions on the ascending limb, rather than the peak (platue) of the length-tension curve. The ascending limb of the length-tension curve is steeper in cardiac muscle. Figure was adapted from Shiels and White (2008).

In Gordon *et al*. (1966)'s experiments using frog fast-twitch skeletal muscle fibres, the shape of length-tension curve can be explained by the overlap between thick and thin filaments. Stretching muscle fibre towards the optimal length (the ascending limb) increases the optimal overlap between filaments, leading to increasing number of force-generating cross-bridges. As fibre is further stretched beyond the optimal length (across the plateau and descending limb), the number of cross-bridges decreases as a result of the decreasing filament overlap. However, this investigation was performed by the fully activation of skeletal fibres during isometric tetanic contraction.

In general, skeletal muscle contraction is separated into twitch and tetanic contraction according to the duration of electrical stimulation. A single stimulation causes a twitch muscle contraction, yet the duration is so short that the muscle begins relaxing even before reaching peak force. A period of multiple stimulations, on the other hand, is able to induce the contraction to reach maximum force and plateaus, resulting in a tetanic contraction. Yet cardiac muscle functions only as twitch muscle in which the Ca^{2+} activated contraction is generally sub-maximal (at most half-maximal) under physiological conditions (Fabiato, 1981), thus subjects to the modulation of many factors including SL. This explains the fact that cardiac muscle operates on the ascending limb (SL 1.7 to 2.3 μm in human heart) rather than the peak of the length-tension curve. Studies showed that the ascending limb of the length-tension curve in cardiac muscle becomes progressively steeper as the level of Ca^{2+} activation rises (Figure 1.5.2 A), indicating that factors such as the filament overlap become less dominant in cardiac muscle contraction when Ca^{2+} activation is sub-maximal, at variance with the optimal filament overlap theory (Allen et al., 1974; Lakatta and Jewell, 1977; ter Keurs et al., 1980).

As the cellular basis of the Frank-Starling relationship, it was initially assumed that the SL dependent modulation of the force production is determined on the molecular level by an increase in the amount of Ca^{2+} released to the myofibrils with increased SL. Early investigations by Fabiato and Fabiato (1975) suggested that there was indeed an increasing amount of Ca^{2+} released from the SR in response to increased SL in skinned ventricular cells, which might be responsible for the greater force production at longer SL. However, later investigations showed that upon changing muscle length, force development increased immediately and markedly, whereas the transient $[Ca^{2+}]$, which measured by a Ca^{2+}-sensitive photoprotein aequorin, did not change as fast and significant (Allen and Kurihara, 1982). Kentish *et al*. (1986) using skinned isolated cardiac muscle also demonstrated that over the ascending limb of the length-tension curve, the SL-induced maximum force increase was accompanied by the increasing Ca^{2+} sensitivity rather than the increasing Ca^{2+} supply (Figure 1.5.2 B). The Ca^{2+} sensitivity, indicates the level of $[Ca^{2+}]_i$ that required for 50% myofilament activation normalized to the maximum activation at saturating levels (Ruegg, 1998). Thus, the SL-dependent increase in the maximum force production is not due to the increasing $[Ca^{2+}]_i$, but the increasing Ca^{2+} sensitivity in response to increased SL. More force is generated at a given $[Ca^{2+}]_i$ as SL is increased. Therefore, with the increasing SL, the outcome of LDA has two aspects: the increasing maximum force production, and the increasing Ca^{2+} sensitivity.

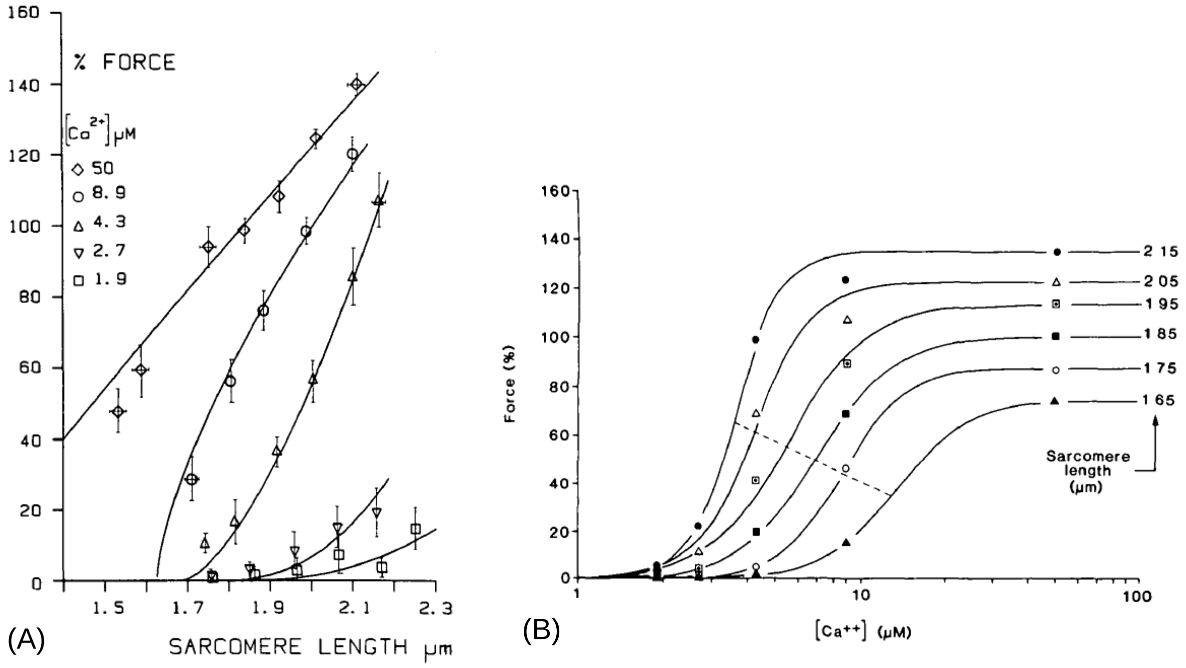

Figure 1.5.2: Kentish *et al*. (1986). (A): Ascending limb of the length-tension curve in cardiac trabeculae becomes progressively steeper with increasing [Ca^{2+}]. The active force-SL relationship was determined in five [Ca^{2+}] ranging from 1.9 μM to 50 μM between the threshold and saturating concentration; (B): Relationship between force generation and [Ca^{2+}]$_i$ at increasing SL from 1.65 μm to 2.15 μm. Increases in SL induce increases in the maximum Ca^{2+}-activated force as well as in the Ca^{2+} sensitivity. The latter is manifested by the rising dashed line which indicates the decreasing [Ca^{2+}] at half-maximum force production with increased SL.

1.5.2 Concepts regarding LDA

1.5.2.1 Two Phases

As the cellular basis of the Frank-Starling law of the heart, LDA describes an intrinsic property of the sarcomere in response to a change in length. Incidentally, investigations by sinusoidal SL alteration in skinned isolated cardiac muscle during activation have revealed two distinct phases of the SL-modulation of force development: an immediate twitch force response, which is largely due to the change in the Ca^{2+} sensitivity for force production as described above; and a slower force response that develops over the course of several minutes, which may results from alterations in the amount of Ca^{2+} released from SR (Allen and Kentish, 1985; Konhilas et al., 2002a). Later investigations by Campbell *et al*. (1993) in rabbit myocardium have suggested that the time constant for the latter phase (~100ms) was well correlated with the kinetics of cross-bridge cycling, suggesting the time course of LDA is relatively slow, accounting for ~25% of the time frame in one complete heartbeat. However, more recent studies by Mateja and de Tombe (2012) suggested that LDA describes the series of sarcomere lengthening-induced events that occur prior to the myofilament activation. Thus the latter delayed phase of force response, which may involve both LDA and its subsequent downstream processes including variations in the cycling of cross-bridges, is not a consistent indicator for the rate at which LDA develops. To measure the rate of LDA, Mateja and de Tombe (2012) compared the contraction kinetics (relaxation and activation) and force development in isolated guinea-pig myocardium at sub-maximal activation between steady-state SL and those after rapid ramp changes to the same SL before activation. Results showed that for the rapid ramp SL changes as fast as 5ms, neither contraction kinetics nor the sub-maximal force development was affected by the contraction modes (steady-state or rapid SL ramps), indicating almost instantaneous transduction of the signal from sarcomere lengthening to modulating the Ca^{2+} sensitivity in LDA (within 5ms), possibly due to the length-induced structural rearrangements of the sarcomeric proteins.

1.5.2.2 LDA in Skeletal Muscle vs Cardiac Muscle

Generally, LDA is a phenomenon applicable to all striated muscle, yet it is much more prominent in cardiac than skeletal muscle (Babu et al., 1988; Fabiato and Fabiato, 1975). Investigations by Konhilas *et al*. (2001) concluded the magnitude of SL modulated Ca^{2+} sensitivity change followed the order cardiac muscle> fast skeletal muscle (psoas)> slow skeletal muscle (soleus) in skinned rat muscle preparations. As described in 1.2.1, the major proteins that make up the sarcomere are important determinants in regulating sarcomeric function. Despite the fact that all striated muscle have identical type of sarcomeric proteins, the specific isoforms expression of these proteins varies between muscle types, which may explain the different magnitude of LDA.

As the Ca^{2+} binding subunit in Tn complex, TnC contains two types of Ca^{2+} binding sites: high affinity and low affinity. Both skeletal and cardiac TnCs have two high affinity Ca^{2+} binding sites, which are always occupied with Ca^{2+} and function as a structural component in anchoring TnC with the rest of Tn complex (Pan and Solaro, 1987). The activation of myofilament is triggered by the transient increase in $[Ca^{2+}]_i$ which binds to the low affinity binding sites of TnC. Studies showed skeletal muscle TnC provides two low affinity binding sites, whilst cTnC only has one (Holroyde et al., 1980; Potter and Gergely, 1975). In the absence of Ca^{2+}, the inhibitory region of TnI holds Tm in a position that covers the binding sites for myosin heads on actin, preventing the actomyosin interactions. Upon the binding of Ca^{2+} to the low affinity site(s) on TnC, a hydrophobic patch exposes in TnC to interact with TnI, thus removing the steric block for Tm on actin filament. However, the affinity of TnC/TnI interactions following Ca^{2+} binding is much greater in skeletal muscle than in cardiac muscle (Kobayashi et al., 2008; Kobayashi and Solaro, 2005). Also, the conformational changes in the N-lobe of TnC upon activation are substantially larger in skeletal muscle (Sun *et al*., 2006; Sun *et al*., 2009). These two phenomena may be related with the sub-maximal activation of cardiac muscle by Ca^{2+} binding, thus explain the more prominent regulation of myofilament activation by length observed in cardiac muscle compared to skeletal muscle (Konhilas *et al*., 2001).

Another study with regards to the impact of different isoforms expression of sarcomeric proteins on different magnitude of LDA in skeletal and cardiac muscle comes from the replacement of native cTnI with slow skeletal muscle TnI (ssTnI) in transgenic mice (Konhilas *et al*., 2003). The substitution with ssTnI in cardiac muscle reduced the SL-dependent difference in Ca^{2+} sensitivity, as expected for the blunted LDA observed in skeletal muscle, implying the critical role of TnI in determining the different impact of SL on skeletal and cardiac Ca^{2+} sensitivity. Despite the several deviations between cTnI and ssTnI isoforms, it was suggested that the key region underlies the signal transduction of sarcomere lengthening, and contributes to the various LDA in different muscle types may be located in the inhibitory domain of cTnI (de Tombe *et al*., 2010; Smith *et al*., 2003).

Additionally, as described in Section 1.3.2, the relationship between force and free [Ca^{2+}] is very steep in both skeletal and cardiac muscle, suggesting highly cooperative Ca^{2+} regulation of myofilament activation. Although the mechanism underlying this cooperativity differs from the positive feedback of myosin binding to the intrinsic property of thin filament, different isoforms of sarcomeric proteins in the different muscle types are surely not making the same contribution to the cooperativity, which presumably affects the modulation of Ca^{2+} sensitivity in response to SL change (Fuchs and Martyn, 2005; Gordon et al., 2001; Moss et al., 2004; Sun et al., 2009).

1.5.3 Current Hypotheses

As the cellular basis of the Frank-Starling relationship, the importance of LDA has been appreciated for a very long time, yet there is still no clear answer as for how the information concerning SL transmits to both the force production and the Ca^{2+} sensitivity. In the earlier investigations, the major determinants of LDA were divided into ‘physical’ factors and ‘activation’ factors (Allen and Kentish, 1985; Jewell, 1977). Physical factors mainly involve those transferring the sarcomere lengthening signal through spatial changes in the thick and thin filaments, such as filament overlap and interfilament spacing; whilst activation factors are the subsequent alterations in the signalling pathway following SL change, including cross-bridges cycling, Ca^{2+} binding to cTnC and protein-protein interactions. To investigate the molecular mechanisms underlying the signal pathway from sarcomere lengthening to increase the maximum force and the Ca^{2+} sensitivity is the main propose of this study. Current hypothesis include the role of the Ca^{2+}-binding protein cTnC, force-generating cross-bridges and cooperativity in terms of the activation factors; also, the effect of changes in filament overlap and interfilament spacing in terms of the physical factors.

1.5.3.1 cTnC

Contraction of the heart muscle is triggered by a rise in intracellular calcium ions, which bind to troponin on the actin-containing thin filaments, leading to structural changes in the thin filament that allows myosin heads to bind and generate force. As the Ca^{2+}-binding subunit, the cardiac troponin C (cTnC) has been proposed to play an important role in the regulation of Ca^{2+} sensitivity. cTnC has three Ca^{2+} binding sites: two high affinity Ca^{2+}/Mg^{2+} binding sites in the C-lobe of cTnC, and only one low affinity Ca^{2+} binding site in the N-lobe (Holroyde *et al*., 1980). Under physiological conditions, the high affinity sites are constantly occupied by Mg^{2+} or Ca^{2+} depending on the intracellular $[Ca^{2+}]$, thus the Ca^{2+} regulation of the cardiac contractility is mostly achieved by binding to the low affinity site on the N-lobe of cTnC, i.e. the regulatory head, which is considered to be the physiological Ca^{2+}-sensor. (Pan and Solaro, 1987; Takeda et al., 2003).

As described above, with the increasing SL, LDA has two outcomes: the increasing maximum force and the increasing Ca^{2+} sensitivity. Studies have shown that in association with the increasing Ca^{2+} sensitivity, there was an increasing Ca^{2+} binding affinity for the N-lobe of cTnC in response to SL elongation (Hofmann and Fuchs, 1987a; Hofmann and Fuchs, 1988; Wang and Fuchs, 1995). As the Ca^{2+} binding protein, the potential role of cTnC in LDA was initially hypothesised.

Investigations by Babu *et al*. (1988) replaced the native cTnC with skeletal TnC in skinned cardiac muscle. Substitution greatly compromised the enhancing Ca^{2+} sensitivity at longer SL, indicating the specific isoform of cTnC was able to regulate the Ca^{2+} sensitivity in LDA. However, further investigations using transgenic mice that express skeletal TnC instead of cTnC in cardiac muscle did not alter the SL-dependent difference in Ca^{2+} sensitivity compared to normal mice containing cTnC, vice versa (McDonald *et al*., 1995; Moss *et al*., 1991). Also, investigations using cTnC mutants L29Q and L48Q indicated the mutations on the Ca^{2+} sensor not only altered the Ca^{2+} sensitivity, but also affected the SL-dependent change in Ca^{2+} sensitivity (Korte *et al*., 2012; Li *et al*., 2013).Thus, the role of cTnC in transmitting the SL changing signal to regulate the Ca^{2+} sensitivity remains controversial.

On the other hand, *in vitro* studies have shown that Ca^{2+} binding opens the N-lobe of cTnC, exposes a hydrophobic patch that binds the switch peptide of cTnI, which leads to a further opening of the N-lobe (Li *et al*., 1999; Sia *et al*., 1997) (detailed description in Section 1.2.2). These global rearrangements in the troponin complex result in an azimuthal motion of the tropomyosin around the thin filament that exposes the myosin binding sites on actin monomers, which allows the interaction between actin and myosin, and drives force generation and muscle contraction. Our group's previous investigations have shown that the force generation in cardiac muscle contraction was coupled to the structural change of cTnC upon Ca^{2+} activation. Therefore, to investigate the possibility of cTnC in sensing the SL change to modulate maximum force and Ca^{2+} sensitivity is the first aspect in this study of the molecular basis of the Frank-Starling relationship (Chapter 4).

1.5.3.2 Force-generating Cross-bridges

The cellular basis of the Frank-Starling relationship between ventricular filling and pressure is the SL-dependent modulation of force production at a given $[Ca^{2+}]_i$. It was suggested that this SL-dependent force regulation largely depends on alterations in the number of the force-generating cross-bridges with varied SL (Allen and Kentish, 1985). Within the time course of one heartbeat, the formation of cross-bridges are determined by the degree of ventricular filling during diastole, and transferred from either blocked or weak binding non-force generating state to strong binding force-generating state during systole, results in the modulation of ventricular pressure development at end-systole.

In order to investigate the role of force-generating cross-bridges in the other outcome of LDA — the SL-dependent Ca^{2+} sensitivity, researchers have been focusing on the connection between strong-binding cross-bridges and Ca^{2+} sensitivity in cardiac muscle contraction. Over the years, the concept of cross-bridges switching on the regulatory system has been widely accepted, in which tropomyosin is held in a 'on' position by strong binding myosin heads, resulting in a higher Ca^{2+} affinity for troponin in adjacent RUs. Experiments using a phosphate analog vanadate to inhibit the strong binding of myosin to actin have suggested that, the strong binding of cross-bridges promoted further binding of Ca^{2+} to cTnC, in association with enhanced structural change in cTnC upon activation (Hofmann and Fuchs, 1987b; Martyn et al., 2001; Wang and Fuchs, 1994).

Recent studies also reported that the strong binding of myosin heads contributed partly in the structural changes of cTnC, and enhanced the Ca^{2+} affinity to cTnC as a consequence (Rieck *et al*., 2013; Zhou *et al*., 2012). It was suggested that the formation of force-generating cross-bridges stabilised the conformation change in cTnC by keeping the inhibitory regions of cTnI off actin, thus favouring the attachment of the switch peptide of cTnI to cTnC. The association of the switch peptide to the Ca^{2+}-induced hydrophobic patch in cTnC has been known to increase the Ca^{2+}-cTnC affinity substantially (Johnson *et al*., 1980). Thus, it is reasonable to assume the strong binding of myosin heads is involved in stabilizing the structural changes in cTnC, thus increasing the Ca^{2+} sensitivity upon activation.

The role of the force-generating cross-bridges in LDA has been investigated using experiments with modified actin-myosin interactions. Interventions which slow the rate of cross-bridges cycling and enhance the number of strong-binding cross-bridges, such as NEM-S1 (myosin subfragment-1 (S1) that was reacted with *N*-ethylmaleimide (NEM)), MgADP, reduced MgATP, increased both the maximum force and the Ca^{2+} sensitivity at short SL, yet reduced or even eliminated the SL-dependent difference in Ca^{2+} sensitivity (Adhikari et al., 2004; Fitzsimons and Moss, 1998; Fukuda et al., 2000). These results suggested at shorter SL before interventions, the formation of strong binding cross-bridges was less than at longer SL. The interventions enhanced the population of strong binding cross-bridges to a similar level as that formed at longer SL, which in turn reduced the Ca^{2+} sensitivity difference between short and long SL. Therefore, the SL-dependent variation in the number of the force-generating cross-bridges may be responsible for the length modulation of both maximum force and Ca^{2+} sensitivity.

However, all these investigations have been taken in rigor-like conditions. According to Sun *et al*. (2009), the impact of the rigor-binding myosin heads was distinct from that of the active-cycling myosin heads under physiological conditions. Thus, in order to re-evaluate the role of force-generating cross-bridges in the two outcomes of LDA, our next focus moved onto the thick filament, investigating the effect of cross-bridges in the SL-dependent maximum force and Ca^{2+} sensitivity by inhibiting the formation of them using a myosin binding inhibitor — blebbistatin (Chapter 5).

1.5.3.3 Cooperativity

As described in Section 1.3.2, the steepness of the force-$[Ca^{2+}]_i$ relationship is much greater than would be expected from the equilibrium Ca^{2+} binding to the single binding site on cTnC, indicating highly cooperative Ca^{2+} regulation (Shiner and Solaro, 1984). Over the years, the mechanisms underlying this cooperativity vary: it might be modulated by strong myosin heads binding, or it might be the intrinsic property of the thin filament. The former possibility has been considered more likely at first due to the widely accepted concept of myosin heads binding switching on the regulatory system. Thus, in the investigations slowing the cycling kinetics and enhancing the population of strong binding cross-bridges (applying NEM-S1, adding MgADP, or reducing MgATP), it was assumed that the increasing Ca^{2+} sensitivity at longer SL might result from a cooperative rising in the number of the force-generating cross-bridges at longer SL.

However, studies in our laboratory (Sun *et al*., 2009) have shown that the force-generating cross-bridges can only switch on thin filaments in rigor-like conditions (low [MgATP]), not under physiological conditions. Inhibition of active force by blebbistatin did not affect the steepness of the force-$[Ca^{2+}]_i$ relationship, indicating the highly cooperative Ca^{2+}-activation was not due to the positive feedback from myosin heads binding, but an intrinsic property of the thin filaments. In physiological conditions, the information of Ca^{2+} binding to one RU spreads to adjacent RUs via coupling between Tm molecules, promoting further binding of Ca^{2+} and formation of cross-bridges in those adjacent units. Investigations by Farman *et al*. (2010) indicated that the coupling between adjacent units increased with SL, such that less Ca^{2+}

binding was required to achieve activation at longer SL. Thus, at longer SL, upon the same amount of Ca^{2+} binding, the Ca^{2+} cooperativity was enhanced to transit more of the neighbouring RUs from the “blocked” state to the “closed” state via stronger coupling, which increased Ca^{2+} sensitivity. Interestingly, in an earlier study by Dobesh *et al*. (2002), the SL-dependent increase in Ca^{2+} sensitivity was not accompanied by an increase in cooperativity. Thus, the role of cooperativity in transmitting the signal from sarcomere lengthening to affect the Ca^{2+} sensitivity remains controversial and subject to further investigation.

1.5.3.4 Double Overlap Hypothesis

The impact of SL change on the number of force-generating cross-bridges was initially hypothesized to be due to the SL-induced change in filament overlap. The length of a sarcomere is defined by the distance between two Z-lines and ranges from 1.7 μm to 2.3 μm in human heart under physiological conditions, corresponding to the ascending limb of the length-tension curve. Over the SL range 1.7 to 2.1 μm, the combined length of the thin filaments extended from each side of the sarcomere is longer than SL, suggesting double overlap of the oppositely polarized actin filaments. The double overlap was assumed to interference with the normal interactions between actin and myosin heads, thus reduce the formation of force-generating cross-bridges at given [Ca^{2+}], leading to down-regulation of the Ca^{2+} sensitivity (Gordon et al., 1966; Hofmann and Fuchs, 1988).

However, studies in terms of the geometry of double overlap suggested that within the SL range 1.7 μm to 2.3 μm, the SL shorten-induced variation in the amount of double overlap is very small, involving a maximum of less than 25% of the cross-bridges that switches from the single overlap zone to the double overlap zone, which may account for the modest reduction in force development (Gordon *et al*., 1966). Yet the force-length relationship is too steeply and too variably dependent on [Ca^{2+}] to be fully explained by such a mechanism. Moreover, Fabiato and Fabiato (1978) reported increased Ca^{2+} sensitivity on the descending limb of the cardiac length-tension curve, where both the amount of double overlap and the potential for cross-bridge formations are diminished, suggesting the filament overlap-induced change in the number of cross-bridges is not sufficient to make a contribution to the SL-dependent change in either force generation or Ca^{2+} sensitivity.

1.5.3.5 Interfilament Spacing Hypothesis

Another popular hypothesis of the LDA proposes that it is the corresponding change in the radial distance between the thick and thin filament (the interfilament spacing, IS) that determines the impact of SL in LDA — the interfilament spacing theory. As shown by X-ray diffraction studies (Millman, 1998; Rome, 1972), the intact myofilament sarcomere is an isovolumic system that is able to maintain close to constant volume upon SL variation. Changes in lattice spacing are inversely related to changes in SL in isolated cardiac muscle (Irving *et al*., 2000). Thus, an increase in SL is expected to lead to a corresponding reduction in the lattice spacing between thick and thin filaments (Figure 1.5.3). The closer proximity between myosin heads and actin enhances the formation of cross-bridges and thereby enhances force development at a given concentration of Ca^{2+} (Fuchs and Smith, 2001; Godt and Maughan, 1981; McDonald and Moss, 1995).

Although the constant volume behaviour is not exhibited in skinned muscle preparations due to the loss of osmotic constraint by cell membrane, the amounts of reduction in the IS upon the same sarcomere lengthening are very similar between intact and skinned preparations, indicating changes in IS inversely related to changes in SL regardless of the preparations (Irving *et al*., 2000). The correlation between SL and IS is mostly mediated by titin (Figure 1.5.3). The interactions with both thick and thin filaments allow titin to produce a radial force which pulls the myofilaments together upon SL increasing (Cazorla et al., 1999; Cazorla et al., 2001; Fukuda and Granzier, 2005).

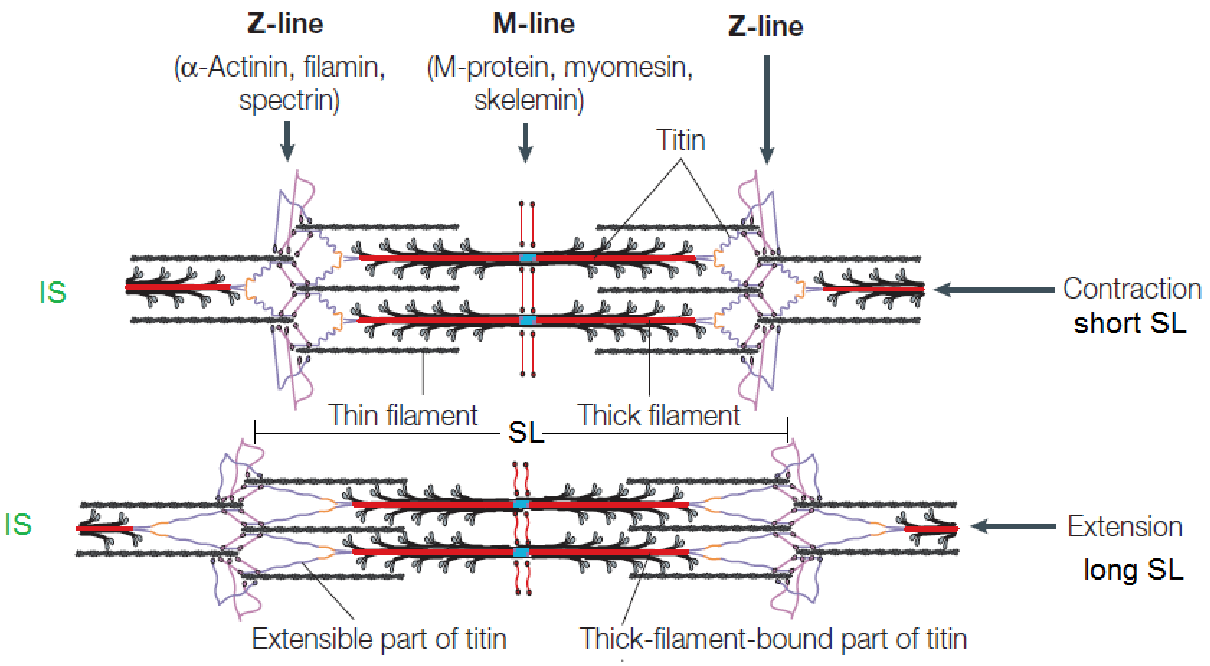

Figure 1.5.3: Schematic illustration of the reduction in interfilament spacing (IS) upon SL elongation. From upper to lower: increasing SL results in a closer proximity of the thick and thin filaments within the sarcomere, allowing a more favourable disposition of myosin heads to interact with actin. The correlation between SL and IS is mostly mediated by the extensible region of titin. Figure adapted from Tskhovrebova and Trinick (2003).

To evaluate the interfilament spacing hypothesis, osmotic compression of the myofilaments by high molecular weight molecule — dextran, which cannot enter the myofilament lattice structure, was used to mimic the SL-induced reduction in IS without changing SL.

At first, fibre width was measured as an indicator of the changes in IS. Studies by McDonald and Moss (1995) showed compression of the rat cardiomyocytes using 2.5% dextran at SL 1.85 µm led to an increase in Ca^{2+} sensitivity which matched that induced by increasing SL to 2.25 µm, indicating that the effect of SL elongation on Ca^{2+} sensitivity could be largely accounted for by mimicking the SL-induced changes in IS. Wang and Fuchs (1995) demonstrated similar conclusions using 5% dextran to compress bovine cardiac muscle bundle. At SL 1.7 µm, upon compression, there was an increase in Ca^{2+} sensitivity coupled with a reduction in fibre width, which were both equivalent to those produced by increasing SL to 2.3 μm. In the subsequent investigations by Fuchs and Wang (1996), demembranated bovine cardiac muscle bundles at SL ranging from 1.7 μm to 2.3 μm were exposed to varied concentrations of dextran (0-5%). Applying certain amount of dextran to maintain a relatively constant interfilament spacing among all the SLs essentially eliminated the length dependent change in Ca^{2+} sensitivity. Their results showed that changes in the Ca^{2+} sensitivity have closer correlation with changes in the IS than changes in the SL, agrees with the IS theory.

However, the evidence presented above came entirely from the experiments in which the extent of osmotic compression on interfilament spacing was estimated from the reduction in fiber width, based on the assumption that the changes in fibre width are proportional to the changes in lattice spacing. X-ray diffraction measurements have confirmed this assumption in skinned rabbit psoas muscle fibres. However, Kawai *et al*. (1993) argued that the close proportionality between muscle width and interfilament spacing might not apply to other muscle types which have a high mitochondrial content (cardiac and slow skeletal muscle). More recent investigations challenged this proportionality between fibre width and IS by direct measurement of the IS using X-ray diffraction. Konhilas *et al*. (2002b) reported that dextran treatment compressed the fibre width to a greater extent than IS, implying measurement of fibre width is not a consistent indicator of changes in interfilament spacing, questioning the supporting conclusions of the hypothesis obtained previously.

Since then, researchers have been trying to seek for a more accurate relationship between the actual IS and the Ca^{2+} sensitivity to prove the IS hypothesis. Konhilas *et al*. (2002b) measured the IS and the Ca^{2+} sensitivity in rat cardiac trabeculae under varying degrees of osmotic compression (0, 3% or 6% dextran) at three SLs — 1.95 μm, 2.15 μm and 2.25 μm. They found that the addition of 3% dextran remarkably increased Ca^{2+} sensitivity by a similar amount at all three SLs. However, further compression with 6% dextran did not show an additional significant effect on Ca^{2+} sensitivity. Although the outcome of 3% dextran compression was consistent with the interfilament spacing hypothesis, a further reduction in lattice spacing without a further increase in Ca^{2+} sensitivity could not be fully explained by such a theory, indicating the possibility of a saturated state in the impact of osmotic compression on Ca^{2+} sensitivity. It was suggested that lattice compression with more than 5% dextran might have no effect on Ca^{2+} sensitivity and over-compression with more than 10% dextran might even reduce the myofilament Ca^{2+} sensitivity (Ford et al., 1991; Wang and Fuchs, 1995; Zhao et al., 1993). As reported by Adhikari and Fajer (1996), a possible explanation for the saturation of osmotic compression was that, due to the distance between thick and thin filaments were too close by over-compression, normal cross-bridge motion was likely to be interrupted, resulting in a reduction in the number of strong binding cross-bridges and the Ca^{2+} sensitivity.

Their research also showed that the SL-induced increase in Ca^{2+} sensitivity was not affected by either 3% or 6% dextran treatment, whereas the reductions in interfilament spacing corresponding to SL elongation were significantly decreased upon the compression with 3% or 6% dextran. Moreover, moderate compression with 1% dextran, which decreased the lattice spacing equivalent to that induced by SL stretching from 2.02 μm to 2.19 μm in uncompressed trabeculae, did not show an increase in Ca^{2+} sensitivity, in contrast to the significant increase reported in SL elongation. These results suggested that the alteration in lattice spacing may not always be the primary mechanism that underlies SL's effect in Ca^{2+} sensitivity. However, later investigations by Martyn *et al*. (2004) held different point of view in terms of the null effect of 1% dextran on Ca^{2+} sensitivity. They argued that the change in lattice spacing with 1% dextran compression (measured by X-ray diffraction) was too minor to be detected, thus it produced no change in Ca^{2+} sensitivity. The discrepancy between the two studies is not clear, although it may be related to the different temperatures used in each measurement (5°C in Martyn *et al*. (2004) *vs* room temperature in Konhilas *et al*. (2002b)).

Above investigations have shown variable relationships between changes in IS and changes in Ca^{2+} sensitivity, depending on the degree of osmotic compression and the SL. There may be other mechanisms in LDA that can operate independent of changes in IS. The role of IS in LDA is further investigated in Chapter 6.

1.5.3.6 Other Hypotheses

In addition, it has been hypothesised that the giant elastic protein titin may be the primary length-sensing element in the myofilament sarcomere which underlies the LDA. Indeed, several studies have revealed a correlation between the amount of titin-based passive tension and the amount of LDA, indicating a possible role of titin in correlating its passive tension production with the signal transmission of SL change in LDA. Also, investigations in which the native cTnI was replaced by the slow skeletal isoform (ssTnI), which lacks one protein kinase A (PKA) target site, have provided insights of the role of cTnI, together with the phosphorylation of cTnI in the regulation of LDA.

1.6 Aims and Strategy of the Project

The aim of the project is to understand the molecular mechanisms underlying the Frank-Starling relationship in the heart, which is to a large extent determined by the molecular mechanisms of the LDA in the cardiomyocytes. Despite extensive research efforts over many years, there is no certain answer yet. In response to the increasing SL, the outcome of LDA has two aspects: the increasing maximum force and the increasing Ca^{2+} sensitivity. So this project mainly focused on the molecular mechanisms underlying the signal pathway from sarcomere lengthening to increase the maximum force and Ca^{2+} sensitivity. We investigated whether the two outcomes of LDA are correlated with each other and from the same mechanism.

The technique that was used in this project — Fluorescence for *In Situ* Structure (F*IS*S), offers a powerful new approach to test these hypotheses. This approach examines the dynamic conformations of proteins in real time in a working muscle cell using fluorescence polarization measurements and correlates the structure of sarcomeric proteins (in this case, the Ca^{2+} binding protein-cTnC) with their functions in the regulation of cardiac muscle activation. With F*IS*S, the force development and the *in situ* structural changes in cTnC upon Ca^{2+} binding can be determined simultaneously under various experimental conditions during the physiological activation of the heart in the cardiomyocyte environment. More importantly, it enables us to evaluate Ca^{2+} sensitivity and cooperativity under complete force inhibition by following the structural changes in Tn.

The native cTnC residues in demembranated trabeculae from rat ventricle were replaced by cTnC mutants with bifunctional rhodamine (BR) probes attached along either the C-helix of cTnC in the regulatory head, or the E- helix of cTnC in the IT arm, to determine the *in situ* orientation of the two major domains of the Tn complex. The dependence of isometric force and cTnC helix orientation changes on $[Ca^{2+}]$ were fitted to the Hill equation:

$$Y = 1/(1 + 10^{n_H(pCa - pCa_{50})})$$

where n_H measures the cooperativity of Ca^{2+} activation, and pCa_{50} represents Ca^{2+} sensitivity.

To perform our investigations in terms of the molecular basis underlying the SL-dependent Ca^{2+} sensitivity using the fluorescence polarization technique, a new experimental set-up was required to obtain the polarized fluorescence intensities emitted from the BR probes. Building the set-up was the very first step in this project. Detailed information concerning F*IS*S and the experimental set-up is in Chapters 2 and 3, respectively.

The investigations in this study (Chapters 4~6) can be summarised below:

1. Firstly, we tested the role of the Ca^{2+} binding protein cTnC on the thin filament, which has been recognised as an important mediator of the Ca^{2+} sensitivity. We investigated whether cTnCis primarily responsible for regulating the maximum force and the Ca^{2+} sensitivity with increased SL.
2. Secondly, it was suggested that the increasing maximum force production is the result of more force-generating cross-bridges formed at longer SL. But the effect of cross-bridges on the Ca^{2+} sensitivity at longer SL still remains controversial. So we then examined the role of the force-generating cross-bridges in the SL-dependent Ca^{2+} sensitivity by inhibiting the formation of them using blebbistatin.

3. Last, we examined one of the most popular hypothesis of LDA — the interfilament spacing theory. It assumes that the critical length-sensing function may be relying on the spatial factor, which is the radial distance between the thick and thin filaments in the sarcomere (the interfilament spacing).

The results will help us understand the molecular mechanisms underlying the Frank-Starling relationship in the heart, and lead to more effective drug designs and therapeutic strategies for improving heart’s pumping function and for cardiac diseases.

Chapter 2

Methods and Materials

2.1 Chemicals and Solutions

For the chemicals and solutions used in the preparation of rat cardiac trabeculae, see Section 2.2 for details. Composition of the solutions used in experiments is listed in Table 2.1. Activation of trabeculae was performed in activating solution after a 2-min bathing in pre-activating solution where no calcium was added and only 0.2 mM of EGTA was present. The immersion in pre-activating solution allowed most of the EGTA to diffuse out of the fibre prior to activation.

The concentrations are shown in mM. Ionic strength was adjusted to 200mM with potassium propionate (KPr). pH of all solutions have been adjusted to 7.1 at room temperature (~20°C). 0.1% protease inhibitor cocktail (Sigma, P8340) was added into all solutions to prevent proteolytic cleavage of proteins in the fibre. The purity of EGTA was 98.5% according to the manufacturer's analysis. The concentration of free Ca^{2+} was calculated using the program Maxchelator: Ca-Mg-ATP-EGTA Calculator v1.0 (http://www.stanford.edu/~cpatton/downloads.htm), and expressed on a logarithmic scale, as $pCa = -\log_{10}[Ca^{2+}]$ (Table 2.2). The calculated free $[Ca^{2+}]$ was in the range pCa 9.0 to pCa 4.5 (1 nM to 33 μM). It could be obtained by mixing relaxing (pCa 9.0) and activating (pCa 4.5) solutions according to the calculated ratios showed in Table 2.2.

When required, 25 μM blebbistatin (Sigma, B0560) was added from a 25 mM stock solution in DMSO, and 1% or 4% (w/v) Dextran (Sigma, 31392) was added to osmotically compress the demembranated trabeculae.

Table 2.1: Composition of experimental solutions (in mM) used in fluorescence polarization measurements. Ionic strength was adjusted to 200 mM with potassium propionate; pH was 7.1 at 20 °C. Na_2CrP, disodium creatine phosphate; KPr, potassium propionate; Na_2ATP, disodium adenosine-5'-triphosphate; K_2EGTA, dipotassium ethylene glycol tetra acetic acid; DTT, 2',2'-Dithiothreitol.

(mM)	Imidazole	Na_2CrP	KPr	Na_2ATP	$MgCl_2$	$CaCl_2$	K_2EGTA	DTT
Relaxing	25	15	78.4	5.65	6.8	0	10	1
Pre-activating	25	15	108.2	5.65	6.3	0	0.2	1
Activating	25	15	58.7	5.65	6.3	10	10	1

Table 2.2: Composition of pCa solutions — Ratio of activating solution. For the desired pCa (free [Ca^{2+}]) from 9.0 to 4.5 (1 nM to 33 μM), the total [Ca^{2+}] (calculated using "Maxchelator" program with 10 mM EGTA) indicates the fraction of activating solution in each pCa solution, the last two columns showed the composition of pCa solutions.

pCa	Free [Ca^{2+}] (M)	Total [Ca^{2+}] (M)	pCa 4.5 (ml)	pCa 9.0 (ml)
9.0	1.00E-09	3.50E-05	0.00	10.00
7.0	1.00E-07	2.55E-03	2.55	7.45
6.7	2.00E-07	4.04E-03	4.04	5.96
6.4	3.98E-07	5.72E-03	5.72	4.28
6.2	6.30E-07	6.77E-03	6.77	3.23
6.0	1.00E-06	7.80E-03	7.80	2.20
5.8	1.60E-06	8.40E-03	8.40	1.60
5.6	2.50E-06	8.85E-03	8.85	1.15
5.5	3.20E-06	9.04E-03	9.04	0.96
5.4	4.00E-06	9.20E-03	9.20	0.80
5.2	6.30E-06	9.44E-03	9.44	0.56
5.0	1.00E-05	9.60E-03	9.60	0.40
4.5	3.32E-05	1.00E-02	10.00	0.00

2.2 Fluorescence for *In Situ* Structure (F*IS*S)

Contraction of cardiac muscle is triggered by the reversible binding of Ca^{2+} to the N-terminal regulatory lobe of cTnC, initiating conformational changes in the filament proteins which allow the interactions between thick and thin filaments to form cross-bridges and generate force (Gordon *et al*., 2000; Tobacman, 1996). Although the structures of most major proteins in the sarcomere have been characterized by crystallography or NMR spectroscopy at near-atomic level, their conformational changes and cellular functions under physiological conditions are difficult to study (Sun *et al*., 2009). The heterogeneity of biochemical states and the flexibility of protein conformations *in vitro* have been contributed to this difficulty. The dynamic interactions between macromolecular complexes which may influence protein conformations cannot be reproduced *in vitro*. Therefore in this project, a technique called Fluorescence for *In Situ* Structure (F*IS*S) was used to measure orientation changes in protein domains during physiological activation of the heart muscle cells in the cellular environment, in which the native structural relationships and interactions between sarcomeric proteins in the regulatory system are preserved.

This approach examines the dynamic conformations of proteins in real time in a working muscle cell using fluorescence polarization measurements. Fluorescence polarization techniques have been widely used to study both cardiac and skeletal muscle contractility (Ferguson *et al*., 2003; Julien *et al*., 2007; Knowles *et al*., 2012; Sun *et al*., 2006; Sun *et al*., 2009). It requires double cysteine residues introduced into a protein domain at sites chosen from its static structure to cross-link with the bifunctional rhodamine (BR) dye (Ferguson *et al*., 2003; Sun *et al*., 2009). The bifunctional rhodamine reagent (Bis-iodoacetamidorhodamine, $BR\text{-}I_2$) contains a central rhodamine fluorophore flanked by two flexible linkers, each terminating in an iodoacetamido group (Corrie *et al*., 1998). When these groups react with the two suitably placed cysteine residues, the average orientation of the probe dipole, which is aligned with the long axis of the three coplanar rings of the fluorophore, is expected to be parallel to a line joining the cysteines (Corrie *et al*., 1999). The BR-labelled protein is then exchanged into its native environment, where the fluorescence polarization data from the BR probe can be used to determine the orientaion of the probe dipole, and thereby, determine the conformational changes of the chosen protein domain. This method correlates the structure of sarcomeric proteins with their functions in the regulation of cardiac muscle activation. Specifically, it has been applied to investigate the Ca^{2+} dependent structural changes of troponin C that are involved in muscle regulation (Ferguson *et al*., 2003; Sun *et al*., 2006; Sun *et al*., 2009). A schematic overview of this method is shown in Figure 2.1.

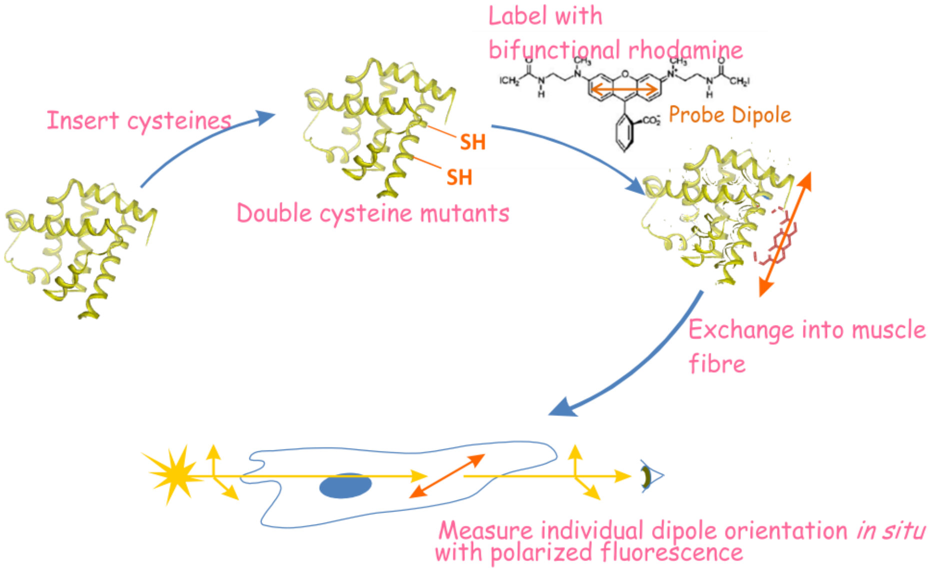

Figure 2.1: Schematic of the general work-flow of F*I*SS. A full description is in the text. Site-specific introduction of double cysteines allows the bifunctional rhodamine dye to cross-link with their β-carbons. Therefore, the probe dipole is parallel to the line joining the two cysteines, thus to the α-helix of the protein to which it was attached. After exchange the BR-labelled protein into muscle fibre, the orientation of the dipole can be determined by polarized fluorescence. With data from more than one probe, the orientation of the main domains in desire protein can be determined *in situ.*

In this project, to study the Ca^{2+} dependent structural changes in cTnC, the bifunctional fluorescent probes were attached along either the C-helix, adjacent to the regulatory Ca^{2+} binding site, or the E-helix, in the IT arm of the troponin complex (Figure 2.2). The labelling sites were chosen using the high resolution structures of isolated troponin components and engineered by expressing human cardiac TnC (hcTnC) mutants with double cysteine residues at the chosen sites (details in Section 2.3) (Takeda *et al*., 2003).Thus the two probes used here report conformational changes in the two major domains of the troponin core complex in the cellular environment — the N terminal regulatory lobe and the IT arm.

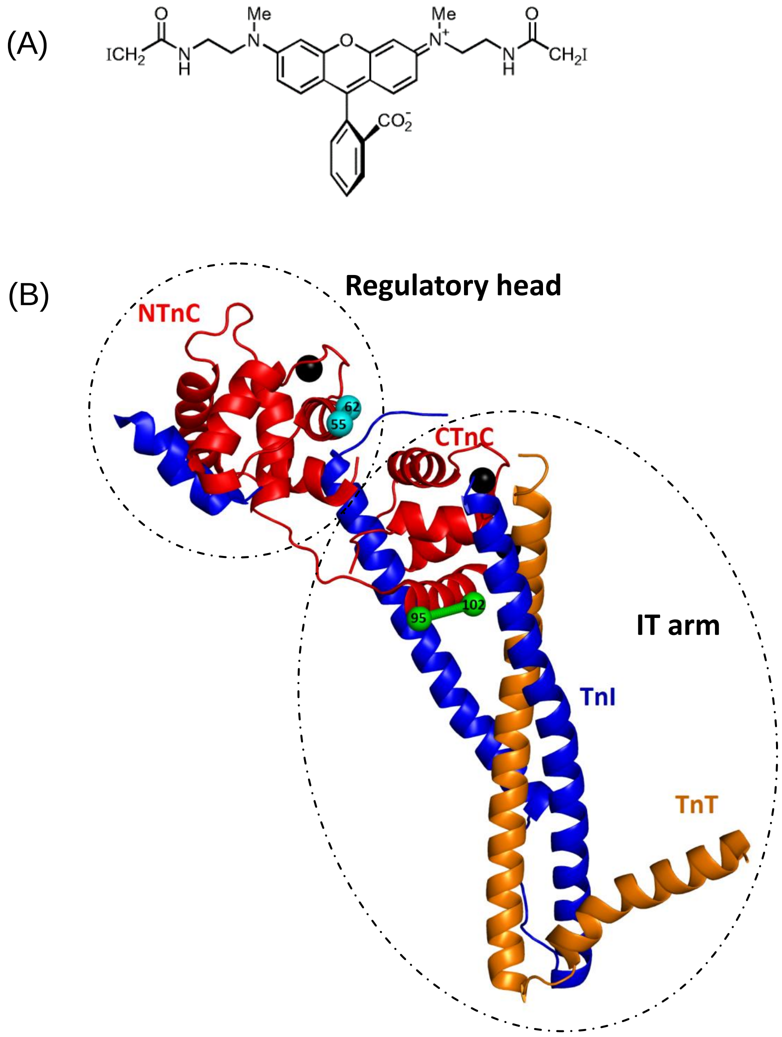

Figure 2.2: Bifunctional Rhodamine labelling of cTnC. (A) Structure of the bifunctional rhodamine reagent (BR-I_2). (B) Structure of the core domain of cardiac troponin complex in the Ca^{2+}-saturated form (Takeda *et al*., 2003) (PDB 1J1D), containing cTnC in red, part of cTnI in blue and cTnT in gold, showing the two pairs of cysteine residues: 55 and 62 along the C-helix in the regulatory head of Tn, or 95 and 102 along the E-helix in the IT arm were cross-lined with BR probes.

2.3 Preparation of Demembranated Cardiac Trabeculae

2.3.1 Dissection and Permeabilizing Cardiac Trabeculae from Rat

Wistar rats (male, 200-250g) were stunned and culled by cervical dislocation (Schedule 1 humane killing procedure in accordance with UK Animal Scientific Procedure Act, 1986). The hearts were removed immediately and rinsed free of blood in Krebs-Henseleit solution (Sigma, K3753) containing: NaCl 118 mM, $NaHCO_3$ 24.8 mM, Na_2HPO_4 1.18 mM, $MgSO_4$ 1.18 mM, KCl 4.75 mM, $CaCl_2$ 2.54 mM, glucose 10 mM; bubbled with 95% O2–5% CO_2; pH7.4 at 20°C. Suitable trabeculae (see Figure 2.3) (free running, unbranched, diameter ≤ 250 μm) were dissected from both the left and right ventricles in Krebs solution containing 25 mM 2,3-butanedione-monoxime (to inhibit spontaneous contraction). Isolated trabeculae were then permeabilized in relaxing solution (Table 2.1) containing 1% Triton X-100 for 60 min on ice and stored in relaxing solution containing 50% (v/v) glycerol at -20 °C for experiments, or incubated in exchange solution containing 0.5 mg/ml BR-hcTnC mutants (see Section 2.3.3 for details) on ice overnight. Prepared trabeculae were used within three days of dissection.

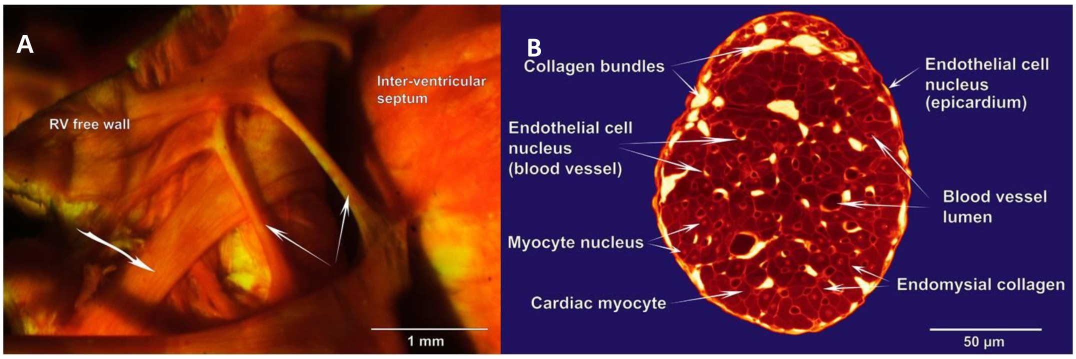

Figure 2.3: Cardiac Trabeculae. (A) Photomicrograph of a Bouin’s-fixed picrosirius red–stained rat right ventricle. The two narrow arrows point to thin, free–running trabeculae (similar to the specimen used for fluorescence polarization experiments). (B) Confocal image of the cross–sectional area of fixed, picrosirius red (PSR)–stained trabecula showing its cellular organization. Pictures were taken from Goo *et al*. (2009).

2.3.2 Preparation of BR-labelled hcTnC mutants

In order to attach bifunctional rhodamine probe along a helix on hcTnC, a pair of cysteine residues was introduced into the chosen site. The double cysteine mutants E55C/ D62C and E95C/ R102C of hcTnC in the Pet3a expression vector were obtained by site-directed mutagenesis and expressed in *E. coli.* (Sun *et al*. (2009). Residues 55 and 62 are on the C-helix in the regulatory lobe of TnC and residues 95 and 102 on the E-helix of TnC in the IT arm. The native cysteines C35 and C84 were replaced by serines. The hcTnC mutants were expressed, purified and labelled by the protocol from Ferguson *et al*. (2003). The cysteines were cross-linked with BR probe to form 1:1 BR:TnC conjugates TnC-BR$_{55\text{-}62}$ and TnC-BR$_{95\text{-}102}$. The BR probe was synthesized and provided by Corrie *et al*. (1999). The conjugates were then purified to more than 95% homogeneity by reverse-phase HPLC, and the confirmation of the labelling stoichiometry and specificity was performed by electrospray mass spectrometry. All the BR-cTnCs have the expected molecular weights; the measured mass of TnC-BR$_{55\text{-}62}$ was 18858.5 ± 0.9Da (calculated mass of 18858.6Da) and that of TnC-BR$_{95\text{-}102}$ was 18817.9 ± 0.8Da (calculated mass 18817.3Da). Labelled hcTnCs were then aliquoted and stored at -80°C in exchange buffer (10 mM Tris pH 7.5, 100 mM NaCl, 1 mM $MgCl_2$). Both TnC-BR$_{55\text{-}62}$ and TnC-BR$_{95\text{-}102}$ (1.8 mg/ml) have been previously produced in the lab and were available for this study. It has been shown that neither the mutagenesis nor the subsequent labelling is likely to affect the structure of the labelled domains of cTnC (Ferguson *et al*., 2003), although the presence of BR probe on either the C- or E-helix reduces the Ca^{2+} affinity of the regulatory site with no significant effect on the cooperativity of Ca^{2+} regulation (Sun *et al*., 2009).

2.3.3 Exchange of BR-hcTnCs into Permeabilized Rat Cardiac Trabeculae

Each BR-hcTnC was separately exchanged for the native cTnC of the permeabilized trabeculae from rat ventricle, using a passive exchange protocol. Previous experiments in the lab were using trifluoperazine (TFP) protocol (20-25 cycles of incubation) to extract about two thirds of the native cTnC from trabeculae (Sun *et al*., 2009). Although passive exchange does not involve cTnC extraction, it has been shown to achieve the same degree of exchange. For example, substitution of whole troponin (Brenner *et al*., 1999; Kohler *et al*., 2003; She *et al*., 2000; Sumandea *et al*., 2003; Tachampa *et al*., 2007) or cTnC (Farman *et al*., 2010) at room temperature for two hours achieved ~95% replacement. In addition, TFP protocol is not specific to cTnC extraction — it has also been used in studies that extract regulatory light chain (RLC) and essential light chain (ELC). Thus, TFP protocol is likely to remove more than just cTnC from trabecula. In order to avoid the downsides of TFP extraction, passive exchange was used in all experiments presented in this project.

After permeabilization, the trabeculae were incubated in 100µl relaxing solution containing 0.5 mg/ml TnC-BR$_{55\text{-}62}$ or TnC-BR$_{95\text{-}102}$ overnight on ice, to passively exchange the native cTnC for BR-hcTnCs. Subsequent preparation of the fibre (i.e. attachment of T-clips) and *in situ* fluorescence polarization measurements were performed the following day. The extent of reconstitution using the above exchange protocol was calculated by immunoblot analysis with a monoclonal anti-cTnC antibody. It was estimated that the percentage of BR-labelled cTnCs with respect to total cTnCs was about 77 ± 2% (± SEM, n = 3). This procedure was performed by Dr. Ivanka Sevrieva in the lab. Maximum Ca^{2+}-activated force in exchanged trabeculae was about 95 ± 10% (± SEM, n = 10) compared with that in un-exchanged trabeculae from separate batch of trabeculae, indicating the incorporation of BR-labelled cTnC produced no significant effect on cTnC function (unpaired t-test, $p = 0.477$).

2.3.4 Polarized Fluorescence Measurements

Permeabilized trabeculae were mounted via the attachment of two aluminium T-clips, between a force transducer (SI-KG7, World Precision Instruments, INC., USA) and a fixed hook in a 70 µl glass trough containing relaxing solution (details of troughs in Section 3.2.3). Trabeculae were bathed in relaxing solution containing 50% (v/v) glycerol on ice during the attachment of T-clips. The experimental temperature was 20-22°C (room temperature).

The BR dye on the fibre was illuminated by 532 nm incident light polarized either parallel or perpendicular to the fibre axis. The illuminating beam was either below the fibre (X-illuminating pathway) or from behind (Y-illuminating pathway). The emitted fluorescence was collected in line with the illuminating pathway and separated into parallel and perpendicular components. The measured intensities were then used to calculate three independent orientation order parameters: $<P_2>$, $<P_4>$ and $<P_{2d}>$, which describe the distribution of the angle between probe dipole and fibre axis over slower timescales (Dale *et al*., 1999). The orientation of the probe dipole, as the orientation of the helix to which it was attached, was estimated for a folded Gaussian orientation distribution model (see Section 2.4 for details). The polarized fluorescence measurements were undertaken using a self-built experimental set-up, a schematic diagram of which is shown in Figure 2.4. A full description for the design and building of the experimental apparatus is in Chapter 3.

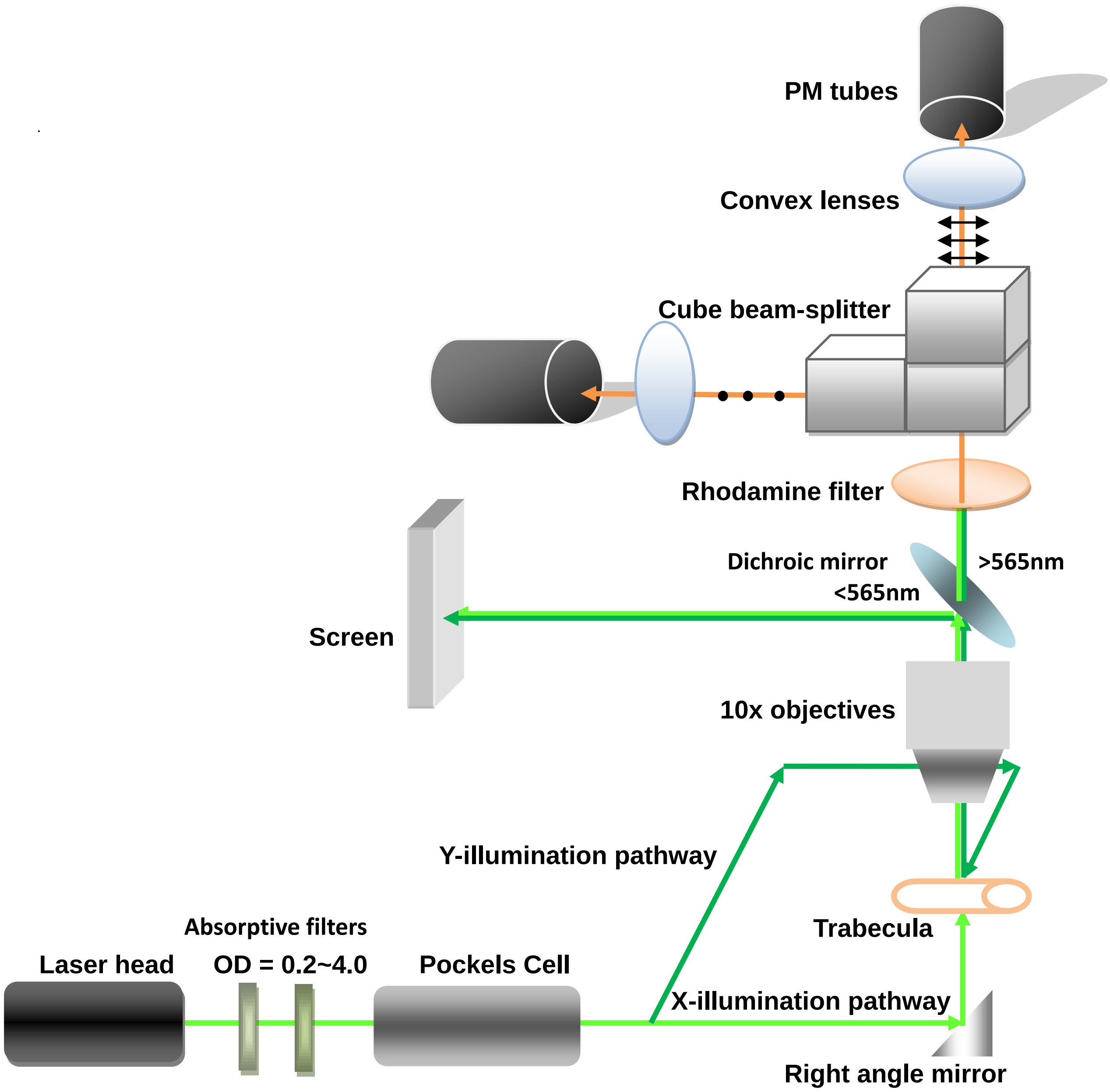

Figure 2.4: Schematic diagram of the fluorescence polarization set-up. A full description of the set-up is in the text. Trabecula was mounted in the glass trough with its long axis parallel with the transmission direction of initial incident light. Pale and dark green arrows respectively represent the light from X- and Y-illumination pathway, and orange light is the rhodamine fluorescence. PM tubes: photomultiplier tubes.

2.4 Interpretation of F*IS*S Measurements

2.4.1 Analysis of Fluorescence Intensity Data

The orientation of the BR fluorescence dipole, and thus of the cTnC helix to which it was attached, was determined from the polarized fluorescence intensities. Eight fluorescence intensities were measured from X- and Y-illumination pathway: ${}_{\parallel}{}^{x}I_{\perp}$, ${}_{\parallel}{}^{x}I_{\parallel}$, ${}_{\perp}{}^{x}I_{\perp}$ and ${}_{\perp}{}^{x}I_{\parallel}$ from X-pathway and ${}_{\parallel}{}^{y}I_{\perp}$, ${}_{\parallel}{}^{y}I_{\parallel}$, ${}_{\perp}{}^{y}I_{\perp}$ and ${}_{\perp}{}^{y}I_{\parallel}$ from Y-pathway (see Figure 2.5 for pictorial description).

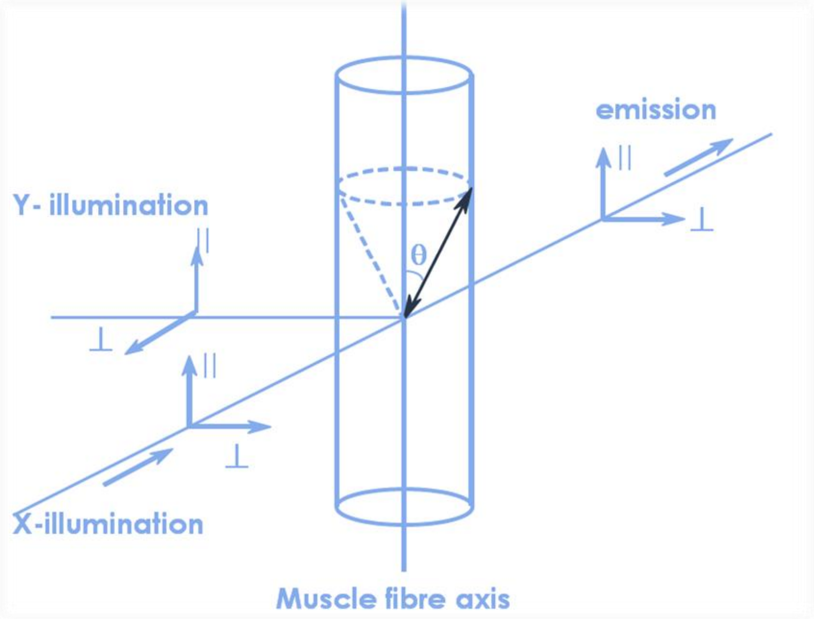

Figure 2.5: The propagation of the excitation and emission pathway. Incident light polarized either parallel or perpendicular to the fibre axis illuminates trabecula from X- and Y-illumination pathway. The angle between probe dipole and trabecular axis is probe angle θ. The emitted fluorescence light from the probe is collected in-line with X-illumination pathway, and separated into parallel and perpendicular polarized components.

The first (${}_{m}I$) and second subscript (I_{n}) denote the excitation and emission polarization respectively, where $\parallel$ and $\perp$ represent the parallel and perpendicular polarization with respect to the trabecular axis, whilst x and y indicate the different illumination pathway. However, in this study, Y-illumination pathway was used only in the measurements of SL (details in Section 2.5.1), although it was designed for the second illumination (more details of the experimental apparatus in Chapter 3), and the difference between the measured fluorescence intensities from X- and Y- illumination can be used to determine the fast motion of the probe (see Section 2.4.2 for details).

The measured fluorescence intensities are affected by the differential transmittance of parallel and perpendicular components in excitation and emission light. In order to eliminate these effects, a rhodamine slide — made by embedding a sample of iodoacetamidotetramethylrhodamine (IATR) in epoxy resin on a glass slide under a cover slip — was used to obtain correction for the excitation (${}^{x}g = \perp/{}^{\parallel}$) and emission (${}^{x}k = \perp/{}^{\parallel}$) transmission factors in X-pathway (since it was the only pathway used in this project to take the fluorescence polarization measurements). Since for an isotropic rhodamine sample, ${}_{\parallel}^{x}I_{\parallel} = {}_{\perp}^{x}I_{\perp}$ and ${}_{\parallel}^{x}I_{\perp} = {}_{\perp}^{x}I_{\parallel}$, the X-pathway correction factors could be calculated using the measured intensities of the rhodamine slide:

If the real fluorescence intensities are: ${}_{\parallel}^{x}I_{\parallel}$, ${}_{\parallel}^{x}I_{\perp}$, ${}_{\perp}^{x}I_{\parallel}$ and ${}_{\perp}^{x}I_{\perp}$

And the measured intensities from rhodamine slide are: ${}_{\parallel}^{x}j_{\parallel}$, ${}_{\parallel}^{x}j_{\perp}$, ${}_{\perp}^{x}j_{\parallel}$ and ${}_{\perp}^{x}j_{\perp}$

To calculate the correction factors: ${}_{\parallel}^{x}j_{\parallel} = {}_{\parallel}^{x}I_{\parallel}$, ${}_{\parallel}^{x}j_{\perp} = {}_{\parallel}^{x}I_{\perp}{}^{x}k$, ${}_{\perp}^{x}j_{\parallel} = {}_{\perp}^{x}I_{\parallel}{}^{x}g$, ${}_{\perp}^{x}j_{\perp} = {}_{\perp}^{x}I_{\perp}{}^{x}g{}^{x}k$

Rhodamine slide was considered as an isotropic sample: ${}_{\parallel}^{x}I_{\parallel} = {}_{\perp}^{x}I_{\perp}$ and ${}_{\parallel}^{x}I_{\perp} = {}_{\perp}^{x}I_{\parallel}$

Therefore: ${}_{\parallel}^{x}j_{\parallel} = {}_{\perp}^{x}j_{\perp}/{}^{x}g{}^{x}k$ and ${}_{\parallel}^{x}j_{\perp}/{}^{x}k = {}_{\perp}^{x}j_{\parallel}/{}^{x}g$

$${}^{x}g = \surd{}_{\perp}^{x}j_{\perp} * {}_{\perp}^{x}j_{\parallel} / {}_{\parallel}^{x}j_{\parallel} * {}_{\parallel}^{x}j_{\perp}$$

$${}^{x}k = \surd{}_{\perp}^{x}j_{\perp} * {}_{\parallel}^{x}j_{\perp} / {}_{\parallel}^{x}j_{\parallel} * {}_{\perp}^{x}j_{\parallel}$$

In the polarized fluorescence measurements of the trabeculae, the corrected intensities can be calculated from the measured intensities (${}_{\parallel}^{x}F_{\parallel}$, ${}_{\parallel}^{x}F_{\perp}$, ${}_{\perp}^{x}F_{\parallel}$ and ${}_{\perp}^{x}F_{\perp}$) and the correction factors: ${}_{\parallel}^{x}I_{\parallel} = 1*{}_{\parallel}^{x}F_{\parallel}$, ${}_{\parallel}^{x}I_{\perp} = {}_{\parallel}^{x}F_{\perp}/{}^{x}k$, ${}_{\perp}^{x}I_{\parallel} = {}_{\perp}^{x}F_{\parallel}/{}^{x}g$ and ${}_{\perp}^{x}I_{\perp} = {}_{\perp}^{x}F_{\perp}/{}^{x}g{}^{x}k$.

The corrected intensities from the fibre were then used to obtain polarization ratios, which provide the orientation distribution information of the probe dipole without influenced by brightness of the illumination, size of the fibre, extent of labelling or protein exchange and efficiency of fluorescence collection etc.

Polarization ratios: ${}^{x}P_{\parallel} = ({}_{\parallel}^{x}I_{\parallel} - {}_{\parallel}^{x}I_{\perp})/({}_{\parallel}^{x}I_{\parallel} + {}_{\parallel}^{x}I_{\perp})$

${}^{x}P_{\perp} = ({}_{\perp}^{x}I_{\perp} - {}_{\perp}^{x}I_{\parallel})/({}_{\perp}^{x}I_{\perp} + {}_{\perp}^{x}I_{\parallel})$

In principle, if the parallel and perpendicular components of the excitation and emission light were equally transmitted, and the rhodamine was completely isotropic and immobile with absorption and emission dipoles collinear, the ${}^{x}P_{\parallel}$ calculated from the corrected intensities of the rhodamine slide would be 0.50. However, the polarization ratio obtained in the X-illumination pathway was 0.43 in this study, the deviation from 0.50 could be the result of incomplete immobilization of the IATR in the epoxy or instrumental imperfections.

Even though cross-linked with two residues, the BR probes are not completely immobilized on the protein. This may due to the wobble of BR probes with respect to the trabeculae or to the dynamic native environment of the fibre itself. If probes change orientation on a rapid timescale (nanosecond) compared to the fluorescence lifetime, the orientation of the dipole can be different between the absorption moment and emission moment. Fluorescence polarization ratios are very sensitive to the motion of the fluorophores, and this motion decreases the observed polarization ratios. Therefore, it is necessary to understand the extent of the fast probe mobility and distinguish it from the orientation change of the protein to which it is attached. By assuming the rapid probe motion is cylindrically symmetrical about the average orientation, like wobbling in a cone, the extent of this wobbling can be characterized by the semi-cone angle δ or the order parameter $<P_{2d}>$ (the amplitude of the fast motion, defined in Section 2.4.2), and calculated from the difference between the fluorescence intensities obtained from X- and Y-illumination pathways. Nonetheless, angle δ and $<P_{2d}>$ are constant values for a given probe ($\delta \approx 20°$, $<P_{2d}> \approx 0.8$), thus the measurements from Y-illumiantion pathway was not necessary for this purpose (Dale *et al*., 1999; Irving, 1996).

2.4.2 Orientation Distribution of the Probe

Shown in Figure 2.5, the angle between the probe dipole and the trabecular axis (θ) was used to describe the probe orientation with respect to the fibre axis during different experimental conditions. Due to the cylindrically symmetrical property of the trabeculae, the top and bottom of the cylinder were impossible to differentiate, thereby, θ was the only angle we obtained for a given probe. Moreover, even though the probe labelling sites on cTnC were precisely designed to crosslink between two specific atoms, the orientation of each probe is not likely to be at exactly the same angle. Due to the intrinsic disorder of the probes, and/or since the cTnC molecules are probably not all in precisely the same conformation, and are likely to adopt two or more different conformations simultaneously, the orientation of the probe and the protein domain must be described as a distribution of angles rather than a single angle. The distribution of all probe angles on the trabeculae, mathematically written as f(θ), was used to indicate the possibility of finding a probe at angle θ.

Legendre showed that any angular distribution f(θ) can be represented by the summation of a set of functions, now called Legendre polynomials — $P_j(\cos\theta)$:

$$f(\theta) = \sum_{j=1}^{k} < Pj > Pj(cos\theta)$$

where j is an integer showing the rank of the polynomials. $P_j(\cos\theta)$ denotes a standard set of functions with the terms of cosθ, $\cos^2\theta$, $\cos^3\theta$, and so on in response to rank j. $<P_j>$ is the order parameter and is the average value of $P_j(\cos\theta)$ over the normalized distribution f(θ). With fluorescence from a cylindrically symmetrical system like a muscle fibre, only the two first even-ranked order parameters: second-rank $<P_2>$ and fourth-rank $<P_4>$ can be obtained to describe the shape of the angular distribution of BR probes. The corresponding second and fourth Legendre polynomials:

$$P_2(\cos\theta) = 0.5(3\cos^2\theta-1)$$

$$P_4(\cos\theta) = (35\cos^4\theta-30\cos^2\theta+3)/8.$$

Thus, $<P_2>$ and $<P_4>$ represent the average of the corresponding Legendre polynomial functions over the probe orientation distribution. They imply the similarity of shapes between the general dipole distribution and these two even-rank polynomial functions (see Figure 2.6). The values of them depend on both the average orientation and dispersion of the probe population with respect to the fibre axis, and they are always between +1 and -0.5. Furthermore, they are both 0 when the probe orientations are isotropic. As shown in Figure 2.6, a positive $<P_2>$ indicates a parallel preference of the average probe orientation relative to the fibre axis, whilst a negative $<P_2>$ shows a perpendicular preference. Therefore, an increase or decrease of $<P_2>$ indicates the axial angle θ has become more parallel or more perpendicular. Likewise, the value of $<P_4>$ works in a similar way, except it gives higher resolution information - a positive $<P_4>$ shows a more preferable probe orientations around 0° or 90° rather than those near 50°.

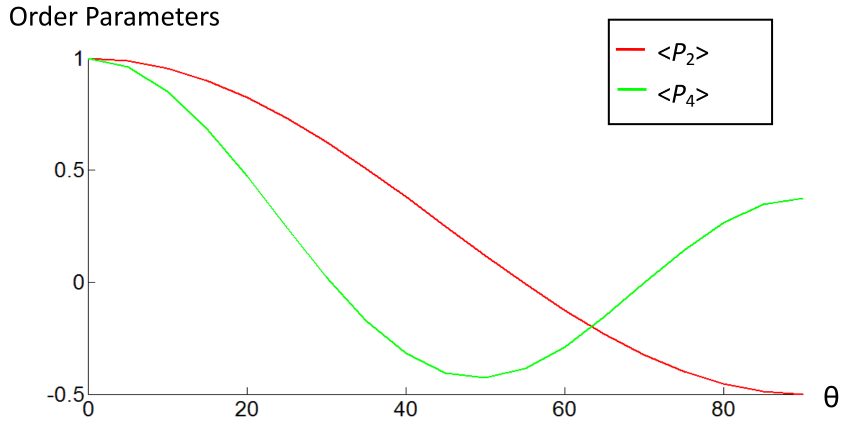

Figure 2.6: Second and forth rank Legendre polynomials. θ is the angle between probe dipole and trabecular axis. SInce a trabecula is cylindrically symmetrical around its axis, the limitation of θ is considered ranging from 0° to 90°. The second and forth rank Legendre polynomials are: $P_2(\cos\theta) = 0.5(3\cos^2\theta - 1)$ (in red) and $P_4(\cos\theta) = (35\cos^4\theta - 30\cos^2\theta + 3)/8$ (in green).

The fast probe motion mentioned above is an inevitable artefact that affects the values of the measured polarized intensities. This mobility of the probe can be accessed using another independent second-rank order parameter, $<P_{2d}>$, referred to as the $<P_2>$ for fast motion, indicating the amplitude of the rapid probe motion. It is a property of the BR probes attached to a specific site on a protein (Dale *et al*., 1999). Therefore in this study, $<P_{2d}>$ was considered constant for each probe (C- or E-helix probe), and both of them were obtained from our group's previous publications (Sun *et al*., 2009). Assuming the fluorophore moves within a symmetrical cylinder around its axis like wobbling in a cone on the timescale of fluorescence lifetime (ca 4ns), the semi angle of this cone (δ) can be used to describe the average amplitude of this wobbling and determine the value of $<P_{2d}>$:

$$<P_{2d}> = \cos\delta\,(1 + \cos\delta)/2$$

The value of $<P_{2d}>$ ranges from 0 to 1.0, indicating two extreme conditions of the probe, unlimited rapid wobble as well as completely immobile.

As the effect of the fast probe motion has been factored out by $<P_{2d}>$, $<P_2>$ and $<P_4>$ can describe the average orientation distribution of angle θ between fluorophore dipole and trabecular axis independently. Also, they are linearly related with the probe populations within muscle cell (Sun *et al*., 2006). If a fraction f of probes have the orientation shown by order parameter $<P_{2a}>$, and a fraction (1-f) of probes have another orientation with order parameter $<P_{2b}>$, then the measured $<P_2>$ is simply f $<P_{2a}>$ + (1-f) $<P_{2b}>$.

Dale *et al*. (1999) showed that there was no specific form for either the orientation distribution or rapid motion of the probe, however some reasonable assumptions about the characteristics of the local probe motion has been taken into account to obtain these order parameters:

1. The orientation distribution of the BR probe dipole is cylindrically symmetrical to the trabecular axis.
2. The orientation distributions of the excitation and emission dipole moments are collinear.
3. The probe moves within a symmetrical cylinder around its axis like wobbling in a cone, and this motion is fast (sub-nanosecond) compared with the timescale of fluorescence lifetime (nanosecond).
4. The probe orientation is fixed within the protein, and the motions of a protein are trifling on the time scale of fluorescence lifetime.

In this study, the polarized fluorescence intensities measured with our experimental set-up (described in Chapter 3) were used to calculate these Legendre polynomial order parameters according to the equations described by Dale *et al*. (Dale *et al*., 1999). The value of $<P_{2d}>$ in this project has been determined by our group's previous publication — for C-helix probe $<P_{2d}>$ = 0.8625, for E-helix probe $<P_{2d}>$ = 0.9025 (Sun *et al*., 2009), therefore some modifications have been made to the original equations to calculate $<P_2>$ and $<P_4>$ from polarized intensities recorded using only X-illumination pathway, the modified equations were provided by Dr. Luca Fusi (King’s College London) and Dr. Elisabetta Brunello (University of Florence).

$$<P_2> = S_d/<P_{2d}>$$

$$<P_4> = 5\ (G_0+G_2)/(3<P_{2d}>^2)-2/3$$

where S_d is the second-rank order parameter for the axial angle θ between probe dipole and fibre axis, whilst G is the correlation function for θ. They can be determined from the four corrected polarized fluorescence intensities obtained from the X-illumination pathway of the experimental set-up: ${}_{\parallel}^{x}I_{\parallel}$, ${}_{\parallel}^{x}I_{\perp}$, ${}_{\perp}^{x}I_{\parallel}$ and ${}_{\perp}^{x}I_{\perp}$.

$$S_d = 1-3(I/2-{}_{\parallel}^{x}I_{\parallel}/2-{}_{\perp}^{x}I_{\parallel})/I$$

$$G_0 = 3(I/2+{}_{\parallel}^{x}I_{\parallel}/2-{}_{\parallel}^{x}I_{\perp}-{}_{\perp}^{x}I_{\parallel})/2I-1/2$$

$$G_2 = 3(2{}_{\perp}^{x}I_{\perp}-I/2+{}_{|}^{x}I_{\parallel}/2+{}_{\parallel}^{x}I_{\perp}+{}_{\perp}^{x}I_{\parallel})/2I$$

$$I = (15\,{}_{\parallel}^{x}I_{\parallel}+42{}_{\parallel}^{x}I_{\perp}+42{}_{\perp}^{x}I_{\parallel}+72{}_{\perp}^{x}I_{\perp}+12\,{}_{\parallel}^{x}I_{\parallel}<P_{2d}>+24{}_{\perp}^{x}I_{\parallel}<P_{2d}>)$$

Notice that the normalized changes in $<P_2>$ and $<P_4>$ had the same Ca^{2+} dependence in all conditions studied in this project, and detail results are presented only for $<P_2>$, which can be measured with greater signal-to-noise ratio (Sun *et al*., 2006).

2.4.3 Modelling the orientation distribution of cTnC C- and E-helix

Due to the dynamic property of the protein orientation in a symmetrical system like trabeculae, every cTnC in the fibre is not expected to adopt exactly the same angle relative to the fibre axis. Therefore, the orientation distribution of the probe dipole with respect to the fibre axis was estimated from $<P_2>$ and $<P_4>$ by fitting model orientation distributions with a Gaussian shape (Ferguson *et al*., 2003).

Assuming f(θ) has a Gaussian shape with a mean peak angle θ_g and a standard deviation σ about the distribution of probe orientations, i.e. $f(\theta) = \exp.\ -(\theta-\theta_g)^2/2\sigma^2$, where θ is the axial angle between probe dipole and trabecular axis. Unlike the previous models — “truncated Gaussians” which chop off the Gaussian shape at θ = 0° and 90° (Corrie *et al*., 1999; Ferguson *et al*., 2003; Hopkins *et al*., 2002), the present model — “folded Gaussians” was not truncated at 0° or 90° since there is no physical reason to exclude the negative and > 90° axial angles. The cylindrical symmetry of the trabecular system, the bipolar organization of sarcomeres and the dipole nature of the probes allow the Gaussian distributions outside the set limit $0° < \theta < 90°$ to be folded back into this region. The mean angle of the folded Gaussian distribution is θ_f, and it is not equal to θ_g (Julien *et al.*, 2007).

2.5 Experimental Protocols

2.5.1 Sarcomere Length Measurements

Sarcomere Length (SL) measurements were performed using the Y-illumination pathway of the experimental set-up (mentioned in Section 2.3.4 with full description in Chapter 3). The same laser was used as the light source for both the fluorescence polarization and SL measurements. SL was estimated from the position of the first-order laser diffraction pattern, and can be calculated according to the formula:

$$SL = \lambda/\sin(\arctan(d/h))$$

where λ represents the wavelength of illumination source in μm, d is the distance between the 1st order diffraction and the 0th order in cm, and h equals to the distance between the trabeculae and the screen where the image of the diffraction pattern is presented in cm.

With the trabeculae illuminated from behind by Y-illumination pathway, the sarcomere diffraction pattern was projected onto a “screen” mounted in front of the trabeculae. The screen used to show the diffraction pattern was made by paper card, with the 0th order marked in the middle. The position of the 1st order diffraction pattern corresponding to the SL from 1.9 μm to 2.5 μm at 0.1 μm intervals was calculated using the formula above, and marked on the screen. The image of the diffraction pattern on the screen was then used to set the desired SL (1.9 μm and 2.3 μm in this project). Additionally, when trabeculae showed faint or disordered diffraction pattern, a blocker was inserted in the illumination path before the screen to reduce the intensity of the 0th pattern on the screen to make the 1st order diffraction more visible.

2.5.2 Steady-state Measurements

Steady-state polarization measurements were performed on trabeculae with BR-labelled cTnC by immersing muscle fibres in different solutions or at different SLs. As described in Section 2.3.4, the permeabilized trabecula with BR-labelled cTnC was transferred into a 70 μl glass trough and immersed in relaxing solution. Fibre was mounted via two aluminium T-clips between a force transducer and a fixed hook (schematic picture in Figure 3.2). SL was measured by laser diffraction pattern as explained in last Section, and fibre length was adjusted to SL 1.9 μm by hook separation before first activation. Fibre diameter was measured on the graduated scale of a 64x objective (Stemi SV 8, Zeiss, Germany) and ocular microscope.

Force was measured and recorded by force transducer and, simultaneously, polarization fluorescence intensities were measured by illuminating trabeculae vertically from below with polarized laser light as described in Section 2.3.4. The processing and interpretation of the polarized fluorescence intensities were described in Section 2.4.

The trabecula was activated at SL 1.9μm in activating solution preceded by 2 min incubation in pre-activating solution at room temperature. It was necessary to induce fast Ca^{2+} diffusion into fibres. Maximal isometric force and fluorescence intensities were measured and recorded after steady-state force was established (<30s). The fibre was then transferred to relaxing solution followed by stretching the SL to 2.3 μm, and activated again. Force per cross-sectional area of the trabecula was calculated by dividing the obtained force (in mN) with the fibre cross-section area (in mm^2), assuming that the trabecula has an elliptical shape, whereby the width-to-depth ratio of the fibre (varied from 1~2) was measured before mounting. The fibre was discarded if it had a slow force development or low force generation (<20mN/mm^2). Polarized fluorescence intensities were used to obtain the order parameters and the Gaussian orientation distributions of the probe dipole with respect to the fibre axis.

When applicable, 1% or 4% Dextran was added into relaxing, pre-activating and activating solutions to investigate the effect of osmotic compression on trabecular force development (details see Chapter 6).

2.5.3 Ca^{2+} Titration Measurements

In order to determine whether different experimental conditions (i.e. changing SL, inhibiting active force, and osmotic compression of fibre diameter) altered the ability of cTnC to regulate contraction, the dependence of force and cTnC structure change (denoted by $\langle P_2 \rangle$ or θ_f, see Section 2.4 for details) on free [Ca^{2+}] was measured using Ca^{2+} titration measurements. All measurements were taken in the same trough — the activating trough to avoid variance of the trough, whilst the remaining troughs were used to switch solutions.

Similar to the steady-state measurements mentioned in previous section, each trabecula was first activated at SL 1.9µm in activating solution preceded by 2 min incubation in pre-activating solution to calculate the force per cross-sectional area, followed by a continuous activation of the fibre by step increments of [Ca^{2+}] from pCa 9.0 to pCa 4.5. The trabecula was then washed in relaxing solution, adjusted to SL 2.3 µm or changed to other experimental conditions, and activated again. The pCa solutions (listed in Table 2.2) were mixed up from the stock solutions on the day of experiment. Isometric force and fluorescence intensities were measured and recorded after steady-state force was established at each pCa. Typically, measurements were taken at least twice at each [Ca^{2+}] and averaged. Maximum activated force was recorded before and after each series of activations. If the maximum force decreased by ≥ 20% at the end of the Ca^{2+} titration experiment, the data were not used.

When applicable, 25 µM blebbistatin or 1% or 4% dextran was added into all solutions (including relaxing, pre-activating, activating and all pCa solutions). Trabeculae were incubated in the relaxing solution containing blebbistatin or dextran for 10min to 30min to allow the reagent to diffuse into the fibre, the titration experiments were then repeated in the presence of blebbistatin or dextran (details in Chapters 5 and 6).

The force and cTnC structure changes (represented by $<P_2>$ or θ_f) from each titration experiment were fitted to the Hill equation using non-linear least-squares regression:

$$Y = 1/(1 + 10^{n_H(pCa - pCa_{50})})$$

where pCa is the negative $\log_{10}$ of the free Ca^{2+} concentration — pCa = $-\log_{10}[Ca^{2+}]$, pCa_{50} is the pCa corresponding to half-maximum force production or cTnC structure changes, and n_H is the Hill coefficient representing the cooperativity of the Ca^{2+} regulated muscle contraction (Ferguson *et al*., 2003). All values presented in this study are given as mean ± SEM except where noted, with n representing the number of the trabeculae. Paired student’s t test (two-tailed) was used to estimate statistical significance.

Chapter 3

Experimental Apparatus

3.1 Introduction

In order to investigate the sarcomere length regulation of cardiac contractility, i.e. the Ca^{2+} dependence of troponin conformational change in response to sarcomere length change, an *in situ* fluorescence polarization approach, F*IS*S, has been used in this project. F*IS*S provides an effective way to measure the motions of cTn with respect to fibre axis during the contraction in single cardiac trabecula (details see Section 2.2). Bifunctional rhodamine probes were introduced into the regulatory head of cTn, cross-linking cysteines in the C-helix of cTnC, and into the IT arm, cross-linking cysteines in the E-helix of cTnC (Figure 2.2). The polarized fluorescence from the BR probes were then used to measure the orientation change of each helix when Ca^{2+} binds to the regulatory sites and/or when SL changes. Building a new experimental set-up for F*IS*S measurement was the first step in this project.

The basic design of the experimental apparatus was to excite BR probes with polarized incident light through two alternative excitation pathways — X- and Y-illumination. The emitted fluorescence was then separated into parallel and perpendicular components with respect to the muscle fibre axis by beam-splitters and the intensities were collected and measured by two photomultipliers. This newly built optical set-up was similar to that described by Hopkins *et al*. (1998) which consists of two orthogonal illumination pathways to obtain additional information about the probe orientational distribution.

It has been reported that the BR probe, even though attached with two points along a helix, is not completely rigid on the protein. It typically exhibits rapid orientational motion ("wobble") with respect to the protein backbone. The timescale of the motion is fast (sub-nanosecond) compared with the fluorescence lifetime of rhodamine (~ 5-nanosecond). Therefore probe dipole orientation could be different between the moments of absorption and emission. Assuming the probe motion is cylindrically symmetrical about its average position, like wobbling in a cone, the extent of wobbling can be described by the semi angle δ of the cone (Irving, 1996) (see

Section 2.4.1 for details). To estimate the extent of this probe motion, i.e. the estimation of δ, polarized fluorescence intensities were measured using excitation light propagating perpendicular to the emission axis — Y-illumination pathway in addition to the one in-line with the emission axis — X-illumination pathway. The addition of a second illumination pathway allows the measurement of fluorescence intensities with different angle between the excitation and emission pathway. The estimation assumes that the probe has equal possibility to sample any angular position within the cone defined by the semi cone angle δ during the ~ 5-ns lifetime of rhodamine and that the protein domain to which it is attached has relatively slower inter-domain motion than the probe (Hopkins *et al*., 1998).

Additionally, the new set-up was different to the fluorescence polarization microscope described by Brack *et al*. (2004) which had two orthogonal emission pathways instead of two illumination pathways to collect the parallel and perpendicular polarization simultaneously. The new set-up has been proved to give the same information as the previous one, but less expensive and difficult in terms of set-up building and maintenance (further discussed in Section 3.4). Figure 3.1 shows both the schematic representation and photograph of the new fluorescence polarization set-up. It consists of two parts: excitation optics, which allow the generation and modulation of linearly polarized laser light, and collecting optics, which allow the recording of the emitted polarized fluorescence.

The acquired polarized fluorescence intensities were then used to obtain order parameters of the probe dipoles using the equations from Dale *et al*. (1999) to describe the orientation changes of the two major domains of the troponin core complex — the regulatory lobe and the IT arm, with respect to the actin axis on Ca^{2+} regulation and subsequent SL change.

(A)

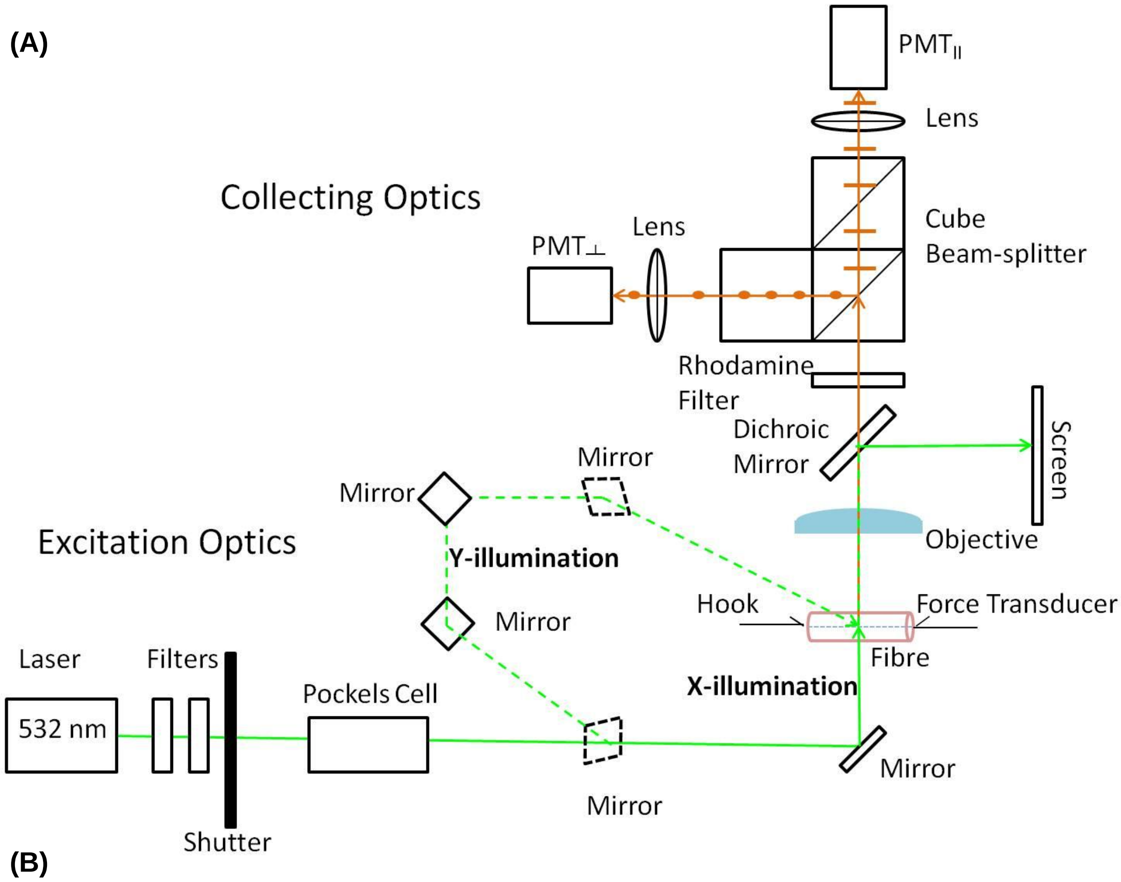
PMT$_{II}$
Lens
Collecting Optics
Lens
PMT$_{\perp}$
Cube
Beam-splitter
Rhodamine
Filter
Dichroic
Mirror
Screen
Mirror
Mirror
Excitation Optics
Y-illumination
Objective
Hook
Force Transducer
Mirror
Fibre
Laser
Filters
X-illumination
532 nm
Pockels Cell
Mirror
Mirror
Shutter

(B)

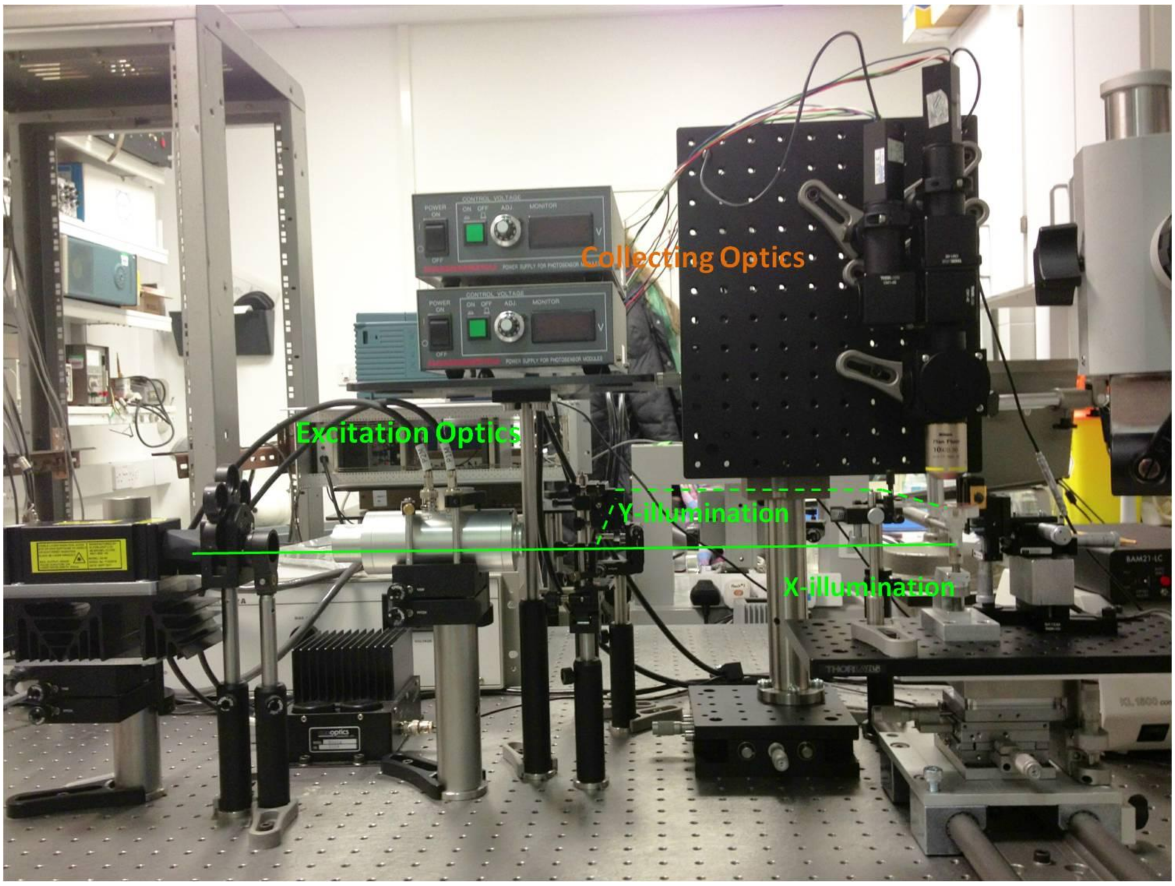
Collecting Optics
Excitation Optics
Y-illumination
X-illumination

Figure 3.1: Fluorescence polarization set-up designed and built for the project. (A): Schematic diagram of the set-up. Excitation optics (Green) allow 532 nm laser light to illuminate the fluorophores on the BR-labelled fibre from below (X-illumination, solid) or from behind (Y-illumination, dashed). Dashed mirrors are inserted in the pathway for Y-illumination. The muscle fibre was mounted between a force transducer (right) and a fixed hook (left) under a binocular microscope. Collection optics (orange) collect the emitted fluorescence in-line with X-illumination, parallel and perpendicular components were separated by beam-splitters and each component was measured with the photomultiplier. (B): Photograph of the set-up showing the actual geometry. A full description of the set-up is in the text.

3.2 Design and Building the Experimental Set-up

3.2.1 Excitation Optics

A continuous diode pumped solid state laser light (class G4, power 75 mW, model G4-60, Elforlight, UK) with the wavelength of 532 nm was used to illuminate the fluorophores in the trabeculae. It was initially polarized parallel to the fibre axis. Two heatsinks (Thermal Resistance 1.3°C/W, RS components, UK) were mounted underneath the laser head to remove waste heat (maximum 15W). To avoid reaching the photomultiplier tube saturation limit, the intensity of laser beam was attenuated by a set of absorptive filters and the gain factor of the photomultiplier was adjusted accordingly (explained in Section 3.2.2). Absorptive filters were mounted on a manually rotated filter wheel which provides a selection from six filters with the optical density (O.D.) value ranging from 0.2 to 4.0. Additionally, a second absorptive filter (O.D. = 2.0) was inserted in the pathway after the wheel when needed. For a typical BR-cTnC exchanged trabecula used in the project, an O.D. value of 2.0-3.0 was sufficient for achieving strong output fluorescence intensities without saturating the photosensors. The O.D. value of the filters is the negative of the common logarithm of the transmission coefficient (O.D. = $-\log_{10}(I_1/I_0)$, where I_1 is the intensity of transmitted radiation and I_0 is the intensity of the incident radiation) and it describes the reduction of intensity by reflecting or absorbing a portion of the radiation. A manually controlled, electronic shutter was inserted after the filters. It was opened only during data recording to minimise photobleaching.

The polarization of the laser light was modulated by a Pockels Cell optical modulator (model M370, Conoptics, Danbury, CT, USA), which modulates the direction of polarization between parallel and perpendicular with respect to the trabecular axis through voltage control. The Pockels cell contains a static polarizer and a birefringent crystal. It was positioned in the pathway so the laser beam was centred on the input and the exit crystal faces to assure no deviation from its previous path. The principal axis of the Pockels cell polarizer was aligned with the initial polarization of the laser light. Therefore, there was neither polarization change (i.e. parallel to the fibre axis) nor any retardation in the laser beam while no voltage signal was applied. Voltage control of the Pockels cell was manipulated using a computer software program Labview 2011 (National Instruments, Texas, USA) to generate a square wave analog output voltage signal to the birefringent crystal (details of Labview programs in Section 3.2.4). When switched between -1V to +1V at 100 kHz, the voltage signal altered the optical properties of the crystal. The crystal then acted as a half-wave plate to switch the polarization of the resultant light between parallel and perpendicular relative to the fibre axis. Precise linear alignment of the laser light and the Pockels cell was critical for the fully functioning of the set-up, failure to do so would lead to the incomplete separation of parallel and perpendicular polarizations by the beam-splitter prisms in the collecting path (defined in Section 3.2.2).

The illumination pathway was divided into two orthogonal directions, i.e. X- and Y-illumination pathways. The transformation between each pathway was achieved by a flip mount (FM 90, Thorlabs, UK) which held a silver right angle prism mirror (5mm, Thorlabs, UK). The mirror was inserted for the Y-illumination pathway and removed for the X-illumination pathway (Figure 3.1). An isolated trabecula was then illuminated with a laser beam size approximately 300*60 µm either from below (X-illumination) or from behind (Y-illumination), as shown in Figure 3.2. The addition of Y-pathway was necessary in the determination of rapid probe motion (i.e. the semi cone angle δ or $<P_{2d}>$). However, for a given probe, no significant changes in $<P_{2d}>$ were observed during isometric contraction as suggested in previous studies (Ferguson *et al*., 2003). For the two probes used in this project, $<P_{2d}>$ has already been determined from our group's previous work — for the C-helix probe, $<P_{2d}> = 0.8625$; for the E-helix probe, $<P_{2d}> = 0.9025$, suggesting the amplitude of such a motion is small (Sun *et al*., 2009). Provided the knowledge of $<P_{2d}>$, polarized intensities were only recorded with X-illumination pathway, although Y-pathway was fully functional and used for SL measurement and future experiment.

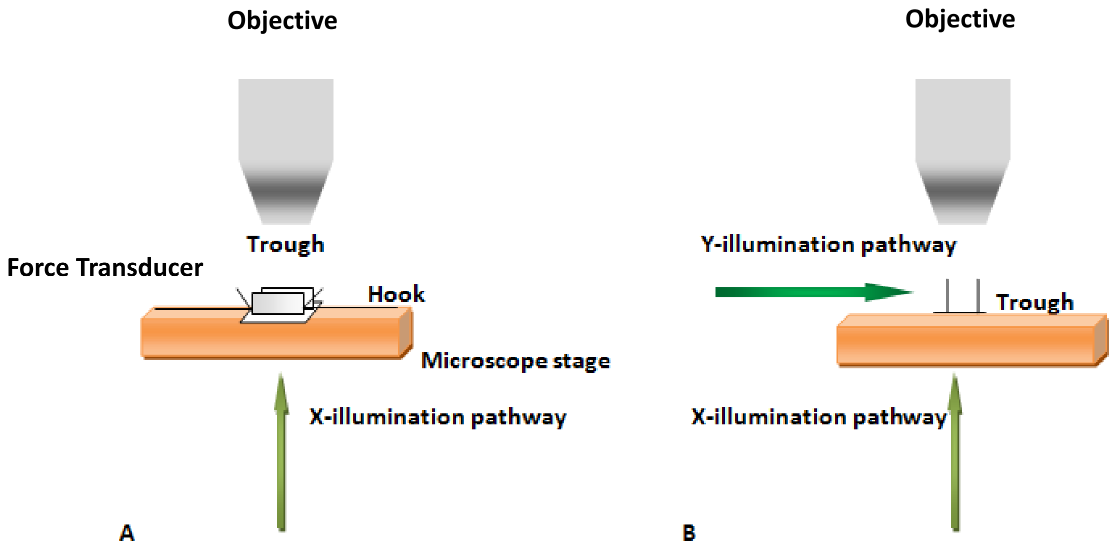

Figure 3.2: Schematic representation of illumination pathways. Cardiac trabecula was mounted in the glass trough via the connection between force transducer and fixed hook. A: Viewed from the front of the set-up, showing the X-pathway illuminated the fibre from below. B: Viewed from the side of the set-up, showing fibre was illuminated from two orthogonal directions.

3.2.2 Collecting Optics

After the BR fluorophores in the trabecula were excited by the polarized laser light from below (X-illumination), the emitted fluorescence was propagated vertically and was collected directly on top of the fibre in-line with the exciting light via a 10x objective (0.3 N.A., 16 mm working distance, Nikon). A dichroic mirror (565 nm, Long pass, Chroma technology, USA) was then inserted in the collecting pathway to divert a fraction of the emission light (wavelength under 565nm) to produce an image of the fibre on a screen for accurate alignment and positioning. Whilst the light transmitted through the dichroic mirror (> 565nm) passed a rhodamine emission filter (605-70 nm bandpass, Chroma technology, USA) above to selectively transmit the rhodamine fluorescence. Above the rhodamine filter, three broadband polarizing cube beam-splitters (25.4mm, 420-680 nm, Newport Corporation, UK), each fitted inside a 4-port prism cage cube mount (30mm cage system cube, Thorlabs, UK), were used to separate the emitted fluorescence into parallel and perpendicular polarized components.

After the emission beam entered the first cube prism, it was split into P-polarized light (transmitted) and S-polarized light (reflected). P light was polarized parallel to the incident plane (the plane spanned by the surface normal and the propagation vector of the incoming radiation) whilst S light was perpendicular, as shown in Figure 3.3. Ideally, the incident light would be split into two orthogonal, linearly and fully polarized outgoing beams. However, for the beam-splitter, only the transmitted component (P light) is fully polarized, the reflected one (S light) contains a mixture of polarization states. At least two beam-splitters were therefore necessary for the complete separation of the two components — a second cube mounted on the side of the first one was to purify the reflected S light (perpendicular) to a similar ratio as the transmitted P light (parallel). The third cube beam-splitter mounted above the first one in this set-up was inserted for the equivalent and accuracy of the experiments (Figure 3.1).

A convex lens (focal length 50mm, N-BK7 Bi-Convex Lens, Thorlabs, UK) was placed 5cm in front of each photomultiplier (PM) tube (H5784-20, Hamamatsu, Japan). It was used to focus the emission fluorescence of both components to a small dot on the PM window to minimize the artefact of small movements in the fluorescence pathway. It was necessary since different regions of the PM window had different sensitivity — it's decreasing towards the edge of the PM window.

The fluorescence intensities of each component were then detected by the two PM tubes. Photomultipliers converted the electrical current signal of the polarized fluorescence into a voltage signal for analysis and processing with Labview (details in Section 3.2.4). Three independent order parameters $<P_2>$, $<P_4>$ and $<P_{2d}>$ were then calculated from the measured intensities, representing the distribution of the orientational changes of the BR probes.

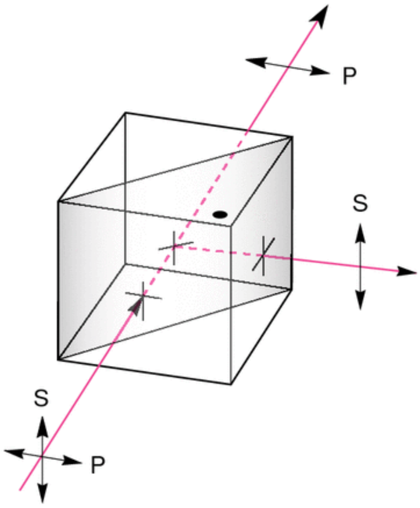

Figure 3.3: Beam-splitter separates incident light into two orthogonal polarizations simultaneously — P-polarized light (transmitted) and S-polarized light (reflected). Only P light is fully polarized, whilst S light contains a mixture of polarization states. For fully separation of the two components, three beam-splitters were used in the project.

3.2.3 The Microscope Stage

As shown in Figure 3.4, the central part of the set-up where the muscle fibre was mounted is the microscope stage. It holds five glass troughs, a force transducer and a fixed holder. Changing of solutions during measurement was achieved by rotating glass troughs on the stage.

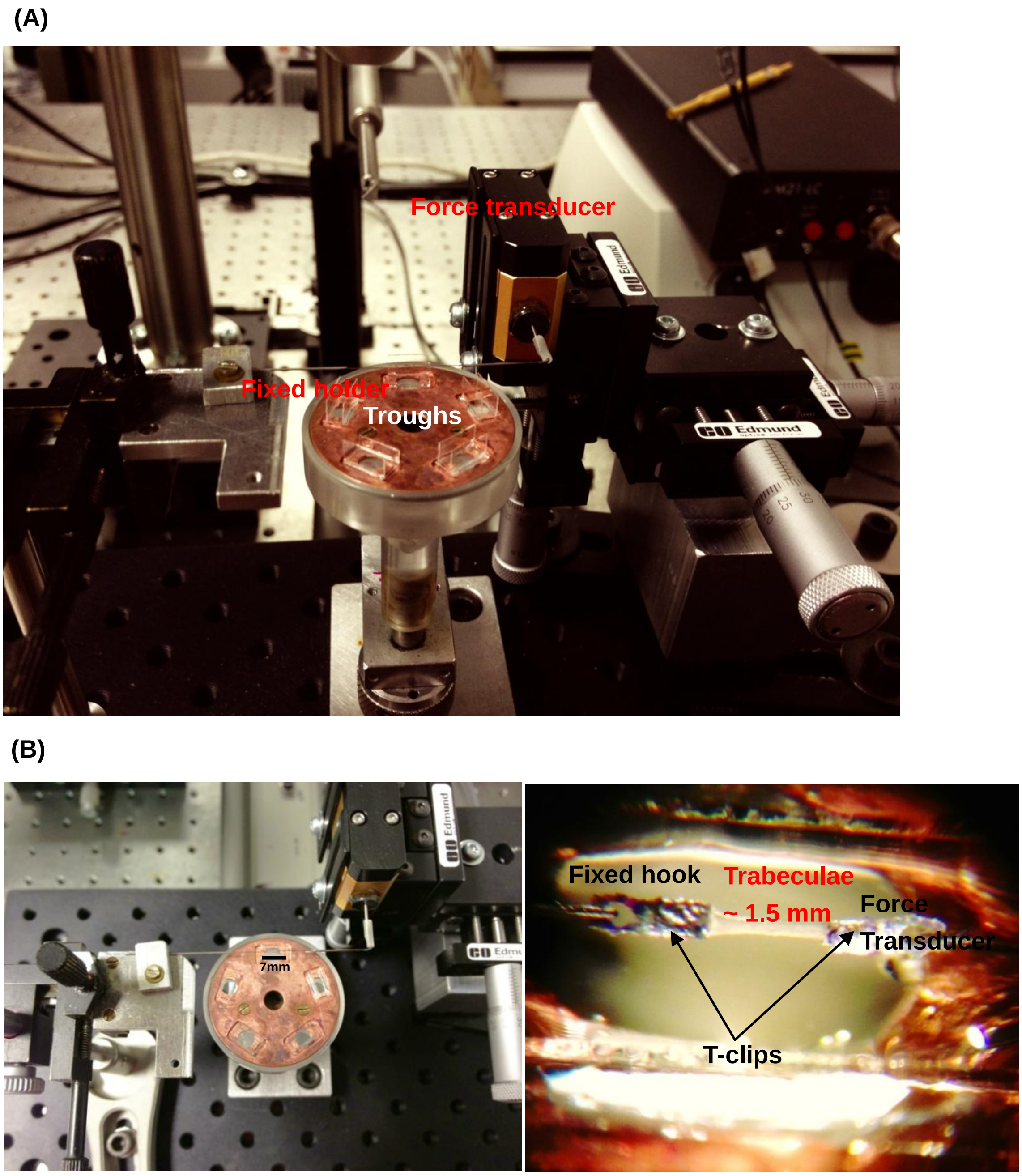

Figure 3.4: Photographs of the microscope stage. (A): Five glass troughs on a copper plate were used to hold experimental solutions. Manually rotate trough stage to switch solutions. Fixed holder and force transducer were mounted on stages that can be adjusted by xyz translation stages. (B): The muscle fibre was mounted in one of the troughs via T-clips between a fixed end and a force transducer.

3.2.3.1 Muscle fibre mounting

After incorporating BR labelled hcTnC mutants into the permeabilized ventricular trabeculae (details in Section 2.3.3), aluminium T-clips were attached to both ends in relaxing solution (Table 2.1) containing 50% (v/v) glycerol on a cooling stage under a 50x binocular microscope (Stemi SV 6, Zeiss, Germany). The dimension of the fibre was measured prior to the mounting. Trabeculae are not typically cylindrical, therefore the width and depth of the fibre were measured and used to calculate the fibre’s width/depth ratio.

As described in Section 2.5.2, the fibre was then transferred into one of the five glass troughs– the loading trough on a manually rotated stage (details see next section). The trabecula was mounted via the connection between T-clips and hooks in relaxing solution. The trabecula was attached to a fixed hook at one end and to a strain gauge force transducer (250Hz resonance frequency, SI-KG7, World Precision Instruments, INC., USA) at the other end (Figure 3.2). In order to align the fibre, the microscope stage, the fixed hook and the force transducer can be adjusted individually in x, y, z directions by translation stages.

Hooks were prepared by bending the sharp tip of JH pin to approximate 50°-60° with respect to the pin axis, then inserting the other end of the bended pin into a 30 gauge needle (0.3x13mm, microlance 3, Becton Dickinson), which served as the lever of the hook. The two hooks were carefully aligned under a 64x binocular microscope (Stemi SV 8, Zeiss, Germany) to make sure the fibre axis was perpendicular to the optical axes. Separation of the hooks was used to set the sarcomere length of the fibre. The sarcomere length was measured by laser diffraction pattern, as explained in Section 2.5.1. In this study, the initial sarcomere length of the fibre was set to 1.9µm as it was just above the slack length of the fibre in relaxation. The width of the fibre was then read on the graduated scale of the 64x microscope, together with the width/depth ratio, to calculate the cross-sectional area.

3.2.3.2 Troughs

The microscope stage contains five glass troughs on a copper plate, each holds different experimental solutions. The fibre was immersed into a solution by manually rotating the plate. Each of the five troughs has glass base and walls with the same size (7*4 mm) and was marked according to their usage – holding relaxing, pre-activating and activating solution. Each trough had a space of 2.5 mm between each wall to immerse the fibre (trough volume 70µl); whilst the loading trough has a distance of 3mm, more space makes handling fibre easier during mounting.

For changing the solution, the plate was lowered, rotated and raised to immerse the stationary fibre in a different trough containing the required solution. The trabecula was in air for less than 2s. When measurements were taken, a glass cover slip was placed on top of the trough so the top surface was optically flat. During experiments, an electronic suction (12V) was used to clean the trough.

3.2.3.3 Force Transducer

The isolated trabecula was mounted in the trough via the connection between T-clips and two hooks. One of the hooks was attached to a strain gauge force transducer by a heat shrink tubing (3:1 shrink ratio, HIS-3, HellermannTyton, UK). During experiments, the force development of the fibre was measured by a force transducer. The SI-KG7 force transducer used in this set-up is shown in Figure 3.5. An amplifier (SI-BAM21-LC, World Precision Instruments, INC., USA) was connected to the force transducer to output analog voltage signal to communicate with Labview (see next section for details). The output signal was proportional to the force that applied to the force transducer. It was buffered and multiplied by a factor of 1, 2, 5 or 10 to provide a better resolution for a minimal change in applied force, depending on the front panel gain switch setting. In this study, the x10 setting was often used since the tension signals were usually small. The force transducer was regularly calibrated before measurements to assure accurate performance, as described in Section 3.3.

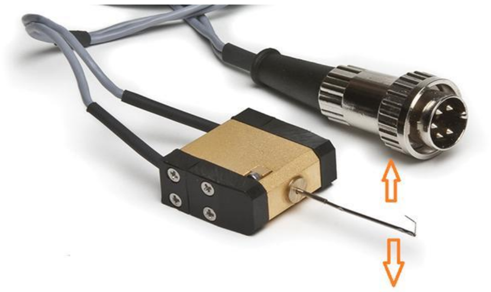

Figure 3.5: Direction of force detecting in SI-KG7 force transducer (orange arrows). For measurement of muscle fibre force development in this project, force transducer was mounted vertically with sensing direction horizontal (parallel with fibre axis).

3.2.4 Data Generation and Acquisition – Labview Programs

Computer software programs using Labview 2011 were written in-house to control the data acquisition (DAQ) board PCI-6251 (National Instruments, Texas, USA) which was installed in the computer to communicate with the Pockels Cell, photomultipliers and force transducer. A 68-pin shielded desktop connector block (SCB-68, National Instruments, USA) was used to provide analog input and output channels to connect the DAQ device and the instruments. Output channel ao 0 was used to generate analog voltage signals to switch the polarization direction of the incident light by the Pockels Cell. Input channels ai 0, ai 1 and ai 2 were used to acquire force and fluorescence intensities simultaneously from the force transducer and two photomultipliers, respectively.

3.2.4.1 Pockels Cell Calibration

To obtain a complete separation of the parallel and perpendicular polarized excitation light, the calibration of Pockels cell was performed on a daily basis. A ramp voltage signal ranging from -1 V to +1 V with a precision of 0.002V was generated using LabView to drive the Pockels cell, thus 1000 data points were generated to alter the polarization of the excitation light. Acquisition of intensities from the two photomultipliers was performed at the same time. The sampling rate of each channel (number of data points collected per second per channel) was 100 kHz. The maximum and minimum intensities collected from both photomultipliers, together with the corresponding voltage signals generated to drive the Pockels cell, were measured and recorded. The voltages at which the photomultipliers detected the maximum parallel intensity and minimum perpendicular intensity were averaged (recorded as $V_{\parallel}$) and considered to provide a maximum extinction ratio $I_{\parallel}\mathrm{max}{:}I_{\perp}\mathrm{min}$ for the parallel excitation light. Similarly, $V_{\perp}$ (the averaged voltage at which the photomultipliers detected the maximum parallel intensity and minimum perpendicular intensity) was recorded to obtain the maximum extinction ratio $I_{\perp}\mathrm{max}{:}I_{\parallel}\mathrm{min}$ in perpendicular excitation polarization. The $V_{\parallel}$ and $V_{\perp}$ were then used to form a square wave signal to drive the Pockels cell, enabling the switching between parallel and perpendicular polarizations of the excitation light.

3.2.4.2 General Measurements

After the determination of $V_{\parallel}$ and $V_{\perp}$, another Labview program produced a 200 Hz square wave voltage signal to the birefringent crystal of the Pockels cell to alter its optical properties. For the first half of a square wave cycle, the voltage input to the Pockels cell was $V_{\parallel}$ and the polarization of the excitation light was parallel relative to the fibre axis; and for the second half of the cycle, the input voltage was $V_{\perp}$, switching the polarization to perpendicular.

Meanwhile, the polarized fluorescence intensity data were simultaneously collected from the two photomultipliers — the parallel photomultiplier ($PMT_{\parallel}$) for the emitted fluorescence polarized parallel to the fibre axis and the perpendicular photomultiplier ($PMT_{\perp}$) for the perpendicular polarization. The fluorescence from each photomultiplier was separated into two groups according to the polarization of the excitation light — the parallel and perpendicular excitation. The extractions were then averaged to obtain the fluorescence intensities: ${}_{\parallel}^{x}I_{\parallel}$ and ${}_{\perp}^{x}I_{\parallel}$ from the parallel photomultiplier, and ${}_{\parallel}^{x}I_{\perp}$ and ${}_{\perp}^{x}I_{\perp}$ from the perpendicular photomultiplier. The first (${}_{m}I$) and second subscript (I_{n}) denote the excitation and emission polarization respectively. The background signals were obtained prior to the measurements with the illumination pathway blocked by a shutter (mentioned in Section 3.2.1). After subtracting the background signal and applying the correction factors explained in Section 2.4.1, the corrected fluorescence intensities were used to calculate order parameters to determine the orientation distribution of the BR probes (details in Section 2.4).

Additionally, force development data was collected from the force transducer through channel ai 0 continuously for 0.5s in the same program. The average value — Mean Tension, together with the fluorescence intensities were shown in the front panel of the program. The program front panel and the description of the workflow are shown in Figure 3.6.

(A)

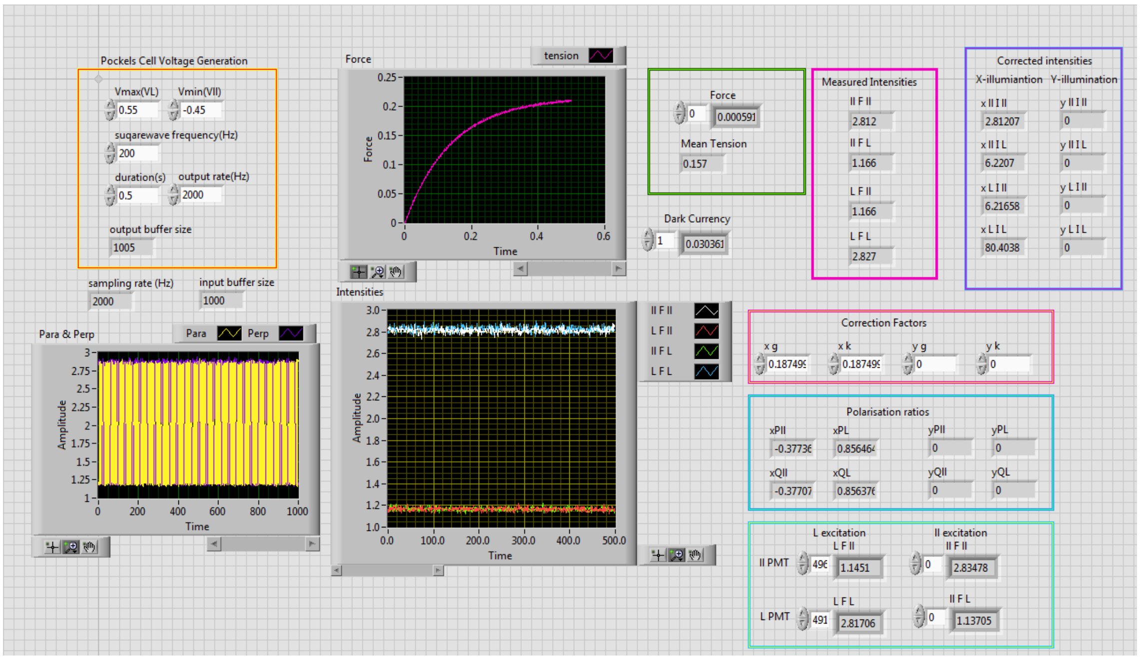

Pockels Cell Voltage Generation

Vmax(VL) 0.55

Vmin(VII) -0.45

suqarewave frequency(Hz) 200

duration(s) 0.5

output rate(Hz) 2000

output buffer size 1005

sampling rate (Hz) 2000

input buffer size 1000

Force 0 0.000591

Mean Tension 0.157

Dark Currency 1 0.030361

Measured Intensities

II F II 2.812

II F L 1.166

L F II 1.166

L F L 2.827

Corrected intensities

X-illumiantion		Y-illumination	
x II I II	2.81207	y II I II	0
x II I L	6.2207	y II I L	0
x L I II	6.21658	y L I II	0
x L I L	80.4038	y L I L	0

Correction Factors

x g 0.18749

x k 0.18749

y g 0

y k 0

Polarisation ratios

xPII -0.3773

xPL 0.85646

yPII 0

yPL 0

xQII -0.37707

xQL 0.85637

yQII 0

yQL 0

	L excitation	II excitation
II PMT	L F II 496 1.1451	II F II 0 2.83478
L PMT	L F L 491 2.81706	II F L 0 1.13705

(B)

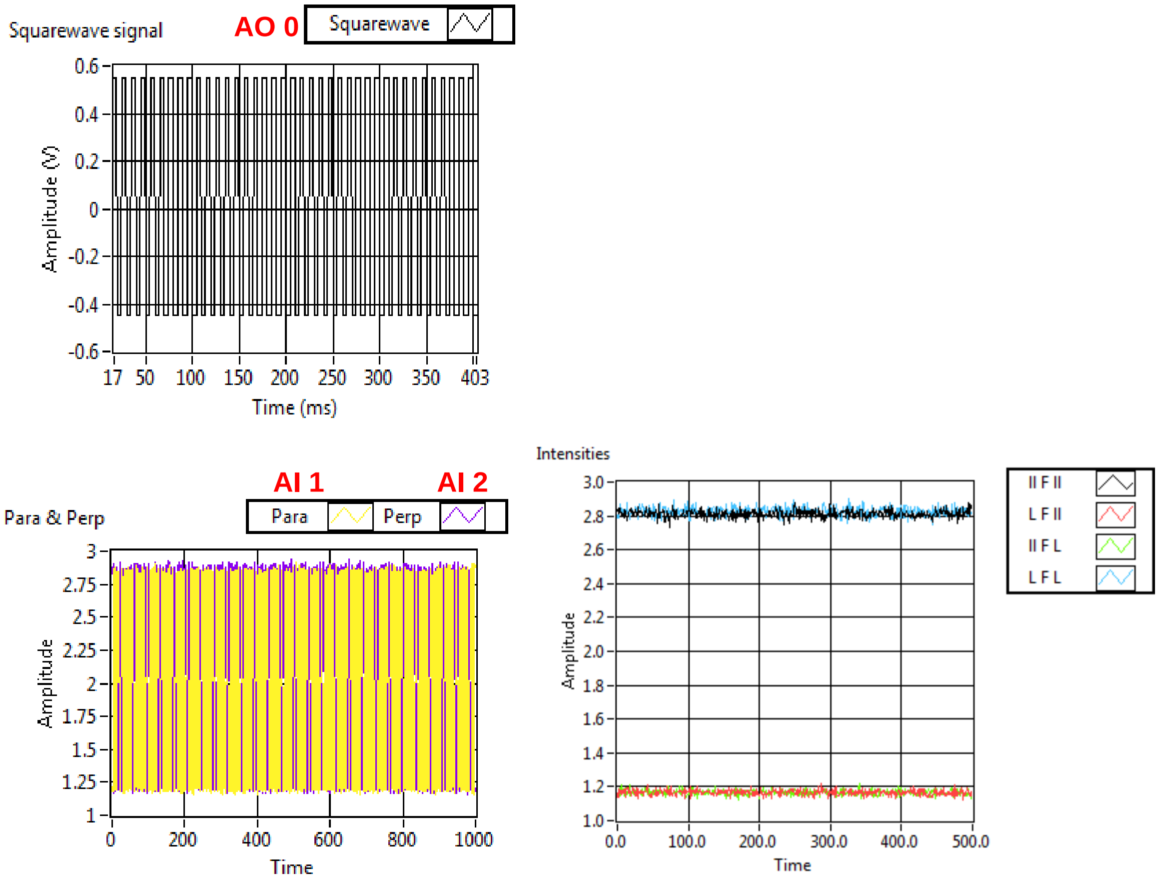

Figure 3.6: Labview program for force and fluorescence intensity measurements. (A): Front panel of the program. Firstly, input $V_{\parallel}$ and $V\perp$ values for the square wave generation, then choose the illumination pathways and measure background signal (Dark currency), followed by opening the shutter, measuring fluorescence intensities ($_{m}F_{n}$) and calculating the corrected intensities ($_{m}I_{n}$). Mean tension measured from force transducer is recorded simultaneously with the fluorescence intensities. All values are shown in the front panel. (B): Workflow of the program. Channel ao 0 generates a square wave voltage signal ranging from $V_{\parallel}$ to $V\perp$, whilst fluorescence intensity signals output from channel ai 1 ($PMT_{\parallel}$) and ai 2 ($PMT\perp$) are extracted into four groups of signals according to the polarization of excitation. The signals from each group were averaged to acquire $_{\parallel}{}^{x}F_{\parallel}$ and $\perp^{x}F_{\parallel}$ from parallel photomultiplier and $_{\parallel}{}^{x}F\perp$ and $\perp^{x}F\perp$ from perpendicular photomultiplier.

3.2.4.3 Force Measurements

An additional program for the continuous detection of force development was written using only the force transducer-connected channel ai 0. There was no time limitation in the program. It was used to record the force trace of muscle activation in steady-state measurements (Figure 3.7). The calibration of the force transducer was regularly performed using this program (details in next section).

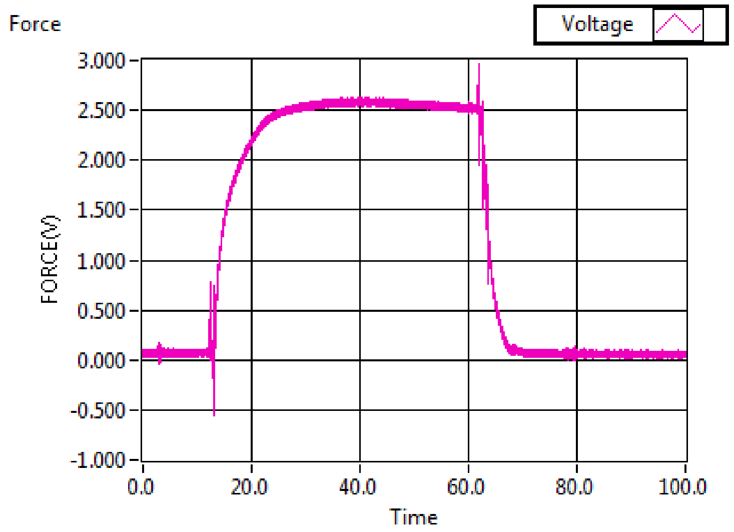

Figure 3.7: Force trace recording of typical trabecula activation at pCa 4.5 using Labview program. Force is presented as the output voltage (V) from force transducer, further calculation to convert into mN is needed.

3.3 Force Transducer Calibration

Before taking measurements, the force transducer and its amplifier were calibrated by applying different known mass weights to correlate the loaded force with its voltage output. In order to perform the calibration, the force transducer was unmounted from the stage (Figure 3.2), and mounted temporally on another stage to hold the force transducer in a position that allowed the lever and the hook to be vertically downward (Figure 3.8). In this way, when the weights were hung on the hook, the force sensing direction was the same as that in the steady-state measurements.

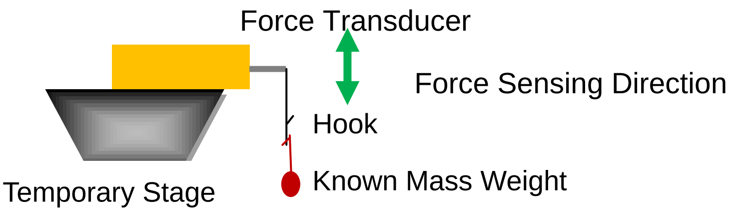

Figure 3.8: Mounting of force transducer for calibration. The force transducer was unmounted from its original stage on the set-up (with force sensing horizontal) and mounted on a temporary stage, which senses force vertically. Green arrows show the direction of force sensing. Five weights were used for calibration. Output voltage was recorded after the weight became motionless.

The force transducer was calibrated for all four gain switches (x1, x2, x5 and x10). At each factor, a baseline reference point was set when the force transducer was un-loaded. Five weights with different mass (listed in Table 3.1) were suspended on the hook respectively. After the suspended weight became motionless, output voltage was measured and recorded using Labview program mentioned in 3.2.4.2. Each amplification factor was tested with the five mass three times to eliminate the error, the averaged output voltages were listed in Table 3.1. A linear relationship between force and output voltage was then established in each gain factor for calculation of force development (Figure 3.9).

Table 3.1: Force transducer calibration with five mass weights at gain factors x1, x2, x5 and x10. Force was calculated by F = ma (mass times acceleration 9.8m/s^2). Baseline point at each amplification factor was obtained before the weight was added. The output voltages of x2, x5 and x10 factors are approximately two, five and ten times of the value recorded in the x1 gain switch.

No.	Mass (mg)	Force (mN)	Voltage (V) x1	Voltage (V) x2	Voltage (V) x5	Voltage (V) x10
0	0	0	0	0	0	0
1	95	0.931	0.294	0.589	1.452	2.903
2	190	1.862	0.593	1.179	2.910	5.816
3	272	2.666	0.843	1.682	4.153	8.288
4	351	3.440	1.093	2.185	5.391	9.273
5	458	4.488	1.419	2.847	6.998	9.317

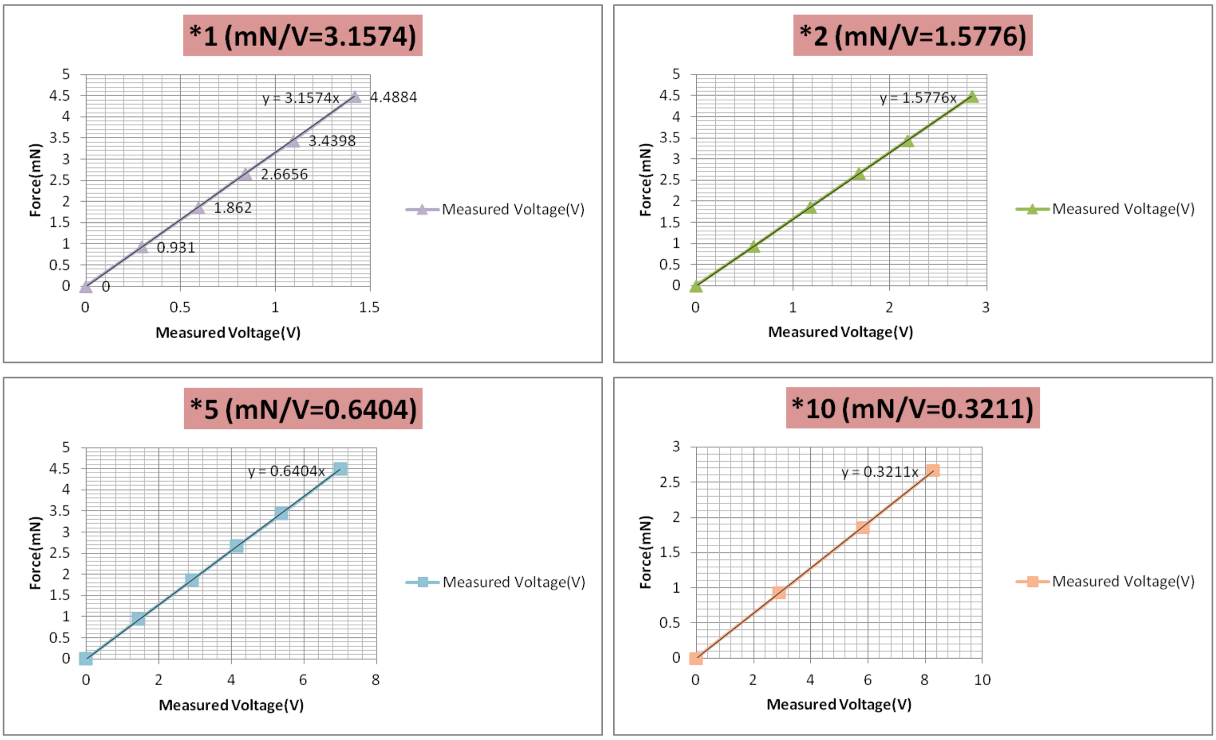

Figure 3.9: The correlation between weights and output voltages for each amplification factor of the force transducer. Data were averaged from three repetitions at each amplification factor. The value of the slope (mN/V) was used for calculation of force development. In the study, x10 was most often used as the force signals from cardiac trabeculae were relatively small.

3.4 Performance of the Experimental Set-Up

3.4.1 Alignment of the Optical Pathway

The alignment of the optical pathway and polarization axis was critical for the performance of the experimental set-up in F*I*SS measurements. Imperfect alignment would result in light deviation, incomplete separation of the parallel and perpendicular excitations, unequal detection of the polarized fluorescence intensities etc.

First, the laser beam was aligned horizontally with the initial polarization parallel to the fibre axis. The Pockels cell was positioned into the pathway to make sure there was no deviation of the laser light. The principal axis of the Pockels cell polarizer was aligned with the initial polarization of the laser light. Thus no polarization was switched in the laser light when no voltage applied to the Pockels cell. The optical devices were then inserted into the illumination and emission pathways one by one to assure the light that passed through was not deviated.

The microscope stage where the muscle fibre was mounted was able to be moved in xyz directions using translation stages. Thus the fibre could be positioned and aligned to allow the excitation light to illuminate it from below, whilst the emission light to reach the objectives and other collecting optics in the centre. All the optics and PM tubes in the emission pathway were mounted on a stage and could be adjusted as one unit for accurate positioning. Once the alignment was completed, any movement in the illumination or emission pathway (except for the microscope stage) would require a precise re-alignment of the whole system. To test the performance of the set-up after alignment, calibration of the Pockels cell and optical pathway were performed on a daily basis.

3.4.2 Calibration of the Pockels Cell

To ensure complete separation of the parallel and perpendicular excitations, the Pockels cell calibration was performed regularly. Using the Labview program described in Section 3.2.4.1, a ramp voltage signal ranging from -1 V to +1 V was delivered to the Pockels cell to obtain the voltages at which the maximum and minimum parallel and perpendicular fluorescence intensities were recorded. The Pockels cell ratio ($I_{\parallel}$max:$I_{\parallel}$min, $I_{\perp}$max:$I_{\perp}$min) varied between parallel and perpendicular components — about 180:1 in the parallel PM tube and 65:1 in the perpendicular. The reason for this differentiation was likely due to the alignment of the pathway after splitting the fluorescence was not equally precise. On the older set-up described by Brack *et al*. (2004), the typical Pockels cell ratio was 40:1. Therefore both ratios obtained here indicated a well aligned Pockels cell to achieve the maximum separation of the parallel and perpendicular excitations.

Due to the factory setting for the Pockels cell, the input voltage signals below -0.6 V or above + 0.6V were cut-off, although the whole range of -1 V to +1 V signal was generated by DAQ device. Therefore, the fluorescence intensity output from each photomultiplier was not a complete sine wave (Figure 3.10), although it did not affect obtaining the maximum and minimum intensities from both photomultipliers.

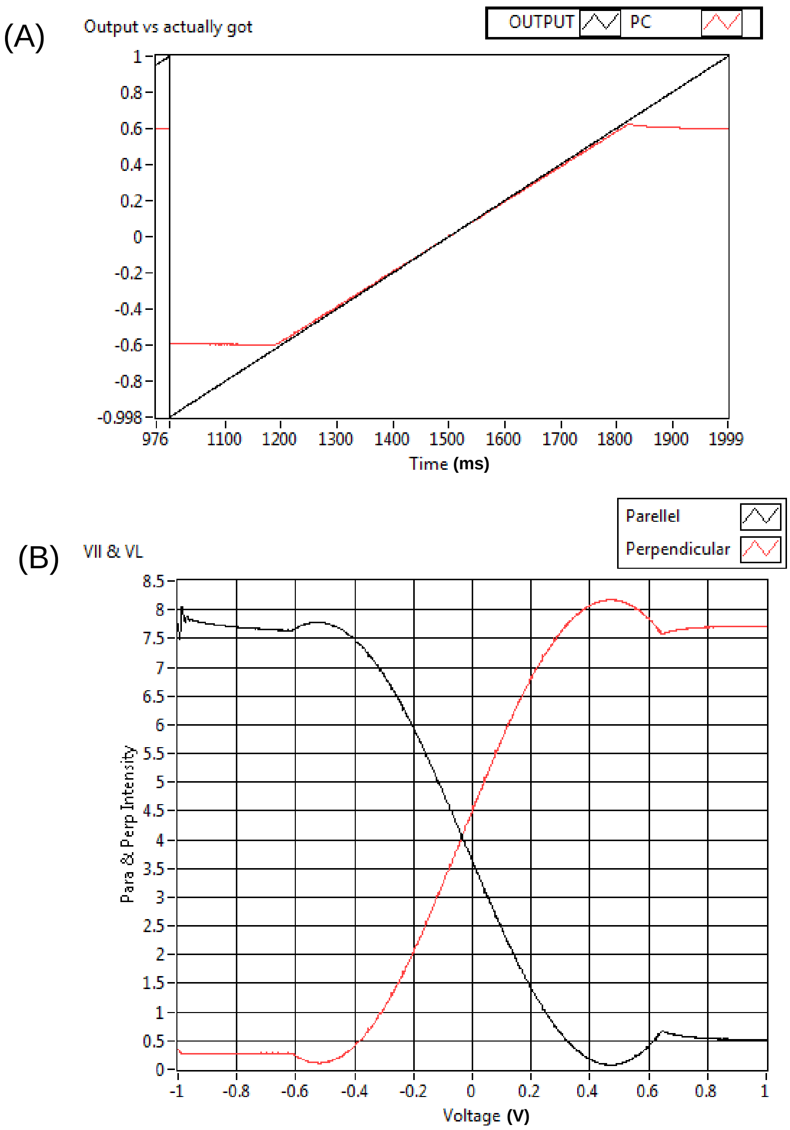

Figure 3.10: Calibration of the Pockels cell. (A): voltage signals output from DAQ device (black) verses what Pockels cell received (red). The input -1 V~+1 V ramp signal was cut off due to the factory setting of the Pockels cell to -0.6 V~+0.6 V. (B): The fluorescence intensity curves output from PMT$_{\parallel}$ (black) and PMT$_{\perp}$ (red), corresponding to the incomplete signal (x-axis) of the Pockels cell. Although both curves are not complete, maximum and minimum intensities from each photomultiplier could be obtained at the same time by adjusting bias.

3.4.3 Calibration of the Optical Pathway

A daily calibration of the optical pathway was performed to correct for the differential transmittance of the exciting and emission light and the differences in photomultiplier sensitivity. A rhodamine slide (used to get the correction factors, explained in Section 2.4) was used to measure the polarized fluorescence intensities to obtain the polarization ratio — $^{x}P_{||}$. Polarization ratio would be 0.50 if the set-up had equal transmittance for parallel and perpendicular excitation and emission light, and the rhodamine on the slide was completely isotropic and immobile.

Using the Labview program described in 3.2.4.2, $V_{||}$ and $V_{\perp}$ (determined from Pockels cell calibration), a square wave signal was delivered to perform polarization switch in the excitation light, and four fluorescence intensities were measured from illuminating the rhodamine slide. The polarization ratio from the rhodamine slide on the new set-up was 0.430. The lower signal in the ratio compared with that from the older set-up described by Brack *et al*. was possibly due to instrumental imperfections, incomplete immobilisation or anisotropic orientation of the rhodamine, or imperfect alignment of the pathway. However, the polarization ratio was similar to that obtained by group members from another set-up (0.446). Additionally, the order parameter $\langle P_2 \rangle$ obtained from muscle fibre experiments on the new set-up were in good agreement with our group’s previous data on other set-up (Sevrieva, 2014), indicating the new set-up was in a condition to provide reliable results in the measurements, and that the Pockels cell ratio was sufficient to separate the parallel and perpendicular excitations.

After the removal of the rhodamine slide, the background calibration was also performed mainly to examine the transparency of the optical pathway, i.e. whether there was stain on the trough or whether the mirror was clean etc. The ideal intensity in the background calibration would be 0.

3.5 Discussion

The new set-up was built differently from the older one in the group described by Brack *et al*. (2004), which had two orthogonal emission pathways: X-emission — in-line with the illumination pathway, and Y-emission — at 90° with the excitation light.

As described in Section 3.1, the reason of adding Y-pathway was to estimate the amplitude of the fast probe motion (δ or $<P_{2d}>$) experimentally (Hopkins *et al*., 1998). For a cylindrically symmetric model like cardiac trabecula, the measured fluorescence polarization intensities that have at least one parallel polarization (${}_{\parallel}I_{\parallel}$, ${}_{\parallel}I_{\perp}$ and ${}_{\perp}I_{\parallel}$) are identical for X- and Y-pathway, the only difference is ${}_{\perp}I_{\perp}$. As shown in Figure 2.5, among the eight intensities that can be obtained from X- and Y-illumination pathway, only ${}_{\perp}{}^{y}I_{\perp}$ has the excitation and emission polarization in orthogonal direction. According to the equations by Irving (1996), ${}_{\perp}{}^{x}I_{\perp}$ and ${}_{\perp}{}^{y}I_{\perp}$ are independent intensities. The difference between these two can be used to estimate the semi-angle of the probe wobble — δ. Therefore, to describe the fast probe motion, fluorescence intensity measurements need to be taken with different angles between the excitation and emission pathway. Either Y-illumination or Y-emission can provide this information.

Compared with the addition of Y-emission pathway, Y-illumination was preferred in the new set-up for two main reasons. Firstly, it was more durable, efficient and affordable. Instead of mounting another collecting optics, Y-illumination was comprised by a series of right angle mirrors. Secondly, even though in this project it was not necessary to determine the value of $<P_{2d}>$ (obtained from our group's previous publication), Y-illumination was also used as the light source for SL measurement using first-order diffraction pattern. Since switching between the X- and Y-illumination pathways was performed by a manually controlled mirror bearer, the measurements from both pathways could not be taken simultaneously. Therefore repeated measurements were needed.

Chapter 4

Effects of Sarcomere Length on Force Development and cTnC Orientation

4.1 Introduction

Contraction of heart muscle is triggered by a rise in intracellular calcium ions. Ca^{2+} binding to cTnC leads to a series of structural rearrangements in the thin filament that allows myosin heads to bind and generate force. Our group's previous investigations (Sun *et al*., 2009) on the molecular mechanism of Ca^{2+} regulation have reported that the Ca^{2+} activation-induced structural changes in the C- and E-helix of cTnC have the same Ca^{2+} dependence as force production, indicating the force production was linearly related to the structural change in cTnC upon activation. The C- and E-helices of cTnC are located in the regulatory head and the IT arm of the cTn complex, respectively. Thus the combination of the orientation changes from both helices represents the structural change in cTn complex upon Ca^{2+} binding (Sun *et al*., 2009). The similar force-[Ca^{2+}] and troponin structural change-[Ca^{2+}] relationships indicated similar Ca^{2+} sensitivity for both force and cTnC structural change in Ca^{2+} activation.

As the Ca^{2+} binding protein, cTnC has long been considered a significant modulator of the Ca^{2+} sensitivity. Therefore, the coupling between force production and cTnC structural change, together with that between the Ca^{2+} sensitivity for force and cTnC structural change might imply the impact of cTnC in cardiac muscle regulation.

As the cellular basis of the Frank-Starling relationship, both maximum force production and the Ca^{2+} sensitivity for force increase with increased SL. Thus, it is reasonable to assume that these two outcomes of LDA are regulated by the SL-dependent changes in cTnC.

Therefore, in this study, we first investigated the possibility of cTnC in sensing the SL change to modulate maximum force and the Ca^{2+} sensitivity. Here, we used a polarized fluorescence technique called F*IS*S (Section 2.2) on an experimental set-up (Chapter 3) that was built for the project to study the role of the thin filament protein cTnC in LDA. The advantage of this method is that it allows simultaneous measurements of force and cTnC structural change in the native environment of a working heart muscle cell on the timescale of a heartbeat. The investigations were performed through the continuous activation of the cardiac trabeculae by step-wise increased [Ca^{2+}] at two different SLs — 1.9 and 2.3 μm.

4.2 Effect of SL on Force Development

4.2.1 Effect of SL on Resting and Maximum Ca^{2+}-activated Force

The effect of SL on force development was investigated by steady-state force measurements in permeabilized cardiac trabeculae from rat ventricle at SLs ranging from 1.9 μm to 2.3 μm. The SLs were chosen according to the working length in the ascending limb of the cardiac length-tension curve (see Section 1.5.1). SL 1.9 μm and 2.3 μm represent lengths just above slack and optimally stretched, respectively. The SL was carefully set by adjusting the separation between two hooks according to laser diffraction pattern (Section 2.5.1). At each SL, force was measured and recorded after it was steadily established at relaxation and maximal Ca^{2+} activation. Thus, both resting tension (passive tension) and maximum Ca^{2+}-activated force were obtained at each SL. Maximum Ca^{2+}-activated force was defined as the difference between maximum force level and resting tension, indicating the actual force development upon Ca^{2+}-activation. SL was measured before and after each activation to ensure the resting tension and maximum activated force were obtained at the same SL. Force per cross-sectional area (mN/mm^2) was calculated to minimise the individual variation (i.e. fibre size and shape). For comparison, both resting and maximum Ca^{2+}-activated force at different SLs were normalized to the maximum activated force produced at initial SL (1.9 μm) in each trabecula. The averaged data were used to plot force-SL relationships to illustrate the impact of SL elongation on force production (Figure 4.1).

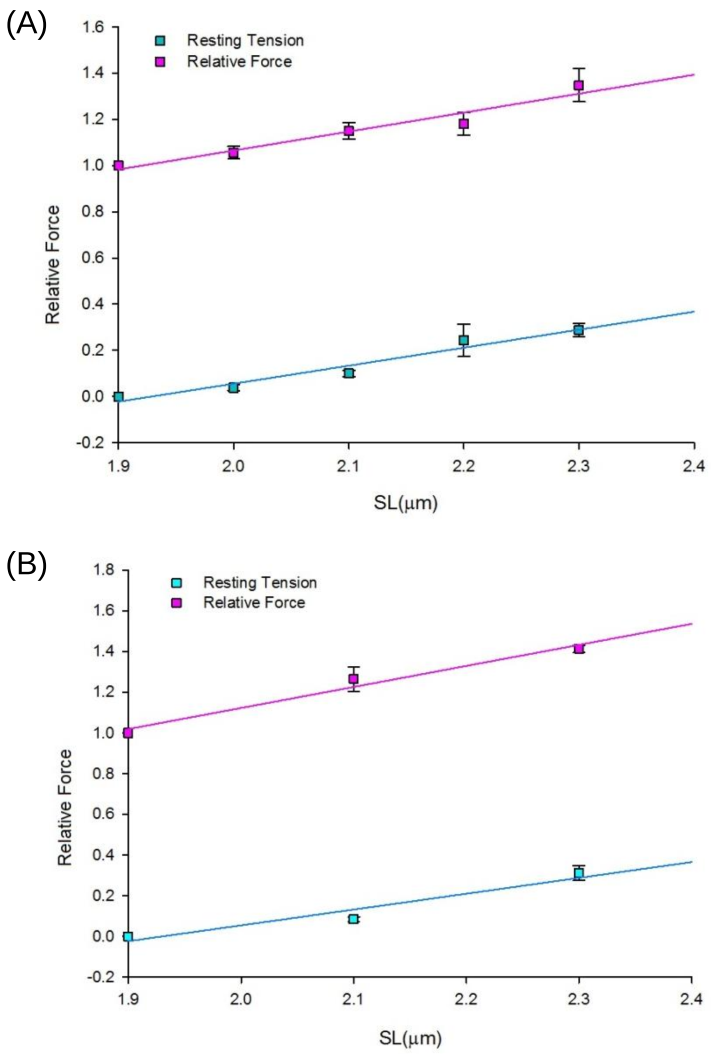

Figure 4.1: Effect of SL on force development. Relative force is the difference between measured force and resting tension, represents the active force (the maximum Ca^{2+}-activated force in this case) developed upon Ca^{2+}-activation. (A): unexchanged trabeculae, n = 6, force was normalised to the maximum force produced at 1.9 μm. Blue squares represent resting tension, purple squares are relative force. Force development of unexchanged fibre was measured and recorded from SL 1.9 μm to 2.3 μm at 0.1 μm intervals. (B): BR-cTnC exchanged trabeculae, n = 8, data were pooled from both C- and E-helix probes exchanged preparations (data from each helix probe were not significantly different, details see Table 4.2). Force was normalised to the relative force produced at 1.9 μm. Blue squares denote resting tension, purple squares are relative force.

To determine the influence of cTnC reconstitution, steady-state force measurements were performed on both unexchanged and BR-cTnC exchanged trabeculae. For unexchanged trabeculae, measurements were taken at SL 1.9 μm to 2.3 μm at 0.1 μm intervals. As shown in Figure 4.1 (A), both resting and maximum Ca^{2+}-activated tensions are linearly proportional to the SL within the physiological working range of cardiac sarcomeres. At SL 2.3 μm, maximum Ca^{2+}-activated force increased 35 ± 7% (± SEM, n = 6) compared to that at 1.9 μm, whilst resting tension increased to 29 ± 3% (± SEM, n = 6) of the active force level at 1.9 μm (see Table 4.1 A). The increasing resting tension upon stretching may be due to the regulation of the giant protein titin (Granzier and Irving, 1995; Wu et al., 2000).

Unlike unexchanged trabeculae, the steady-state force measurements on the exchanged fibres, where the native cTnCs were reconstituted with BR-labelled hcTnC-C or –E, were performed at SL 1.9 μm, 2.1 μm and 2.3 μm (Figure 4.1 (B)). Similarly, both resting tension and relative force increased linearly in response to SL stretching, with a total increasing of 31 ± 4% (± SEM, n = 8) in resting tension and 41 ± 2% (± SEM, n = 8) in relative force from SL 1.9 μm to 2.3 μm (see Table 4.1 B). These values were not significantly different from those in unexchanged fibres, indicating the incorporation of BR-labelled cTnCs does not affect the SL dependent force increase. The force-SL relations in Figure 4.1 (B) was plotted using data from both C- and E-helix probes; the separate data are shown in Table 4.2. At SL 2.3 μm, resting tension increased 29 ± 5% (± SEM, n = 6) for the C-helix probe and 36 ± 3% (± SEM, n = 2) for the E-helix probe, whilst maximum Ca^{2+}-activated force showed an increase of 40 ± 2% (± SEM, n = 6) and 47 ± 2% (± SEM, n = 2) for the C- and E-helix probes, respectively. Results from BR-cTnC-C and -E did not show significant difference compared either with each other or with measurements in unexchanged trabeculae, indicating the SL dependence of force is not affected by either BR-cTnCs reconstitution or BR labelling site.

.

Table 4.1: Steady-state force measurement parameters for (A): unexchanged trabeculae, n = 6; (B): BR-cTnC exchanged trabeculae, n = 8 (n = 6 for BR-cTnC-C and n = 2 for BR-cTnC-E). Measurements in exchanged fibres were performed at 1.9, 2.1 and 2.3 μm. Active force describes the maximum Ca^{2+}-activated force produced in addition to the resting tension at each SL. Both resting and active tensions were normalized to the maximum Ca^{2+}-activated force produced at SL 1.9 μm for each trabecula. Both force per cross-sectional area and normalization were presented. Mean ± SEM. Comparison: paired two-tailed student t-test (force at 1.9 μm *vs* at 2.3 μm) (statistical significance *p<0.05). Unpaired t-test between unexchanged and exchanged data was not significant (not shown).

(A)

Unexchanged fibre (n = 6)	**Resting Tension**		**Active Force**	
SL(μm)	**mN/mm^2**	**Normalised**	**mN/mm^2**	**Normalised**
1.9	0	0	29.3 ± 5.3	1.00 ± 0.00
2.0	0.9 ± 0.3	0.04 ± 0.01	31.5 ± 6.1	1.06 ± 0.03
2.1	2.9 ± 0.7	0.10 ± 0.01	34.1 ± 6.7	1.15 ± 0.04
2.2	7.2 ± 3.3	0.24 ± 0.07	34.4 ± 6.3	1.18 ± 0.05
2.3	8.6 ± 1.6	0.29 ± 0.03	40.8 ± 7.6	1.35 ± 0.07
Δ	**29 ± 3%***		**35 ± 7%***	

(B)

Exchanged fibre ($C+E^{\#}$, n = 8)	**Resting Tension**		**Active Force**	
SL (μm)	**N/mm^2**	**Normalised**	**mN/mm^2**	**Normalised**
1.9	0	0	25.5 ± 2.3	1.0 ± 0.0
2.1	2.1 ± 0.3	0.1 ± 0.0	32.3 ± 3.5	1.3 ± 0.1
2.3	7.9 ± 1.4	0.3 ± 0.0	35.9 ± 3.1	1.4 ± 0.0
Δ	**31 ± 4%***		**41 ± 2%***	

[#] For separate C- and E-helix probe data, see Table 4.2.

Table 4.2: Steady-state force measurement parameters for (A): C-helix and (B): E-helix BR-probes. Active force describes the maximum Ca^{2+}-activated force generated in addition to the resting tension at each SL. Force was normalized to the maximum Ca^{2+}-activated force produced at SL 1.9 µm for each trabecula. Both force per cross-sectional area and normalization were presented. Mean ± SEM. Comparison: paired two-tailed student t-test (*p<0.05).

(A)

C-helix (n = 6)	**Resting Tension**		**Active Force**	
SL (µm)	**mN/mm^2**	**Normalised**	**mN/mm^2**	**Normalised**
1.9	0	0	26.7 ± 2.9	1.0 ± 0.0
2.1	1.9 ± 0.4	0.1 ± 0.0	35.0 ± 4.1	1.3 ± 0.1
2.3	8.0 ± 1.9	0.3 ± 0.0	37.2 ± 3.9	1.4 ± 0.0
Δ	**29 ± 5%***		**40 ± 2%***	

(B)

E-helix (n = 2)	**Resting Tension**		**Active Force**	
SL (µm)	**mN/mm^2**	**Normalised**	**mN/mm^2**	**Normalised**
1.9	0	0	21.7 ± 1.9	1.0 ± 0.0
2.1	2.4 ± 0.6	0.1 ± 0.0	24.3 ± 1.2	1.1 ± 0.0
2.3	7.8 ± 0.1	0.4 ± 0.0	31.8 ± 3.1	1.5 ± 0.0
Δ	**36 ± 3%***		**47 ± 2%***	

Together with the data from unexchanged fibres, results showed linear relationship between SL and force development in cardiac muscle. In response to SL elongation from 1.9 μm to 2.3 μm, the maximum Ca^{2+}-activated force increased ~40% of that at 1.9 μm (P_0), whilst passive tension increased by ~30% P_0. Incorporation of BR-labeled cTnCs had no effect on this relationship. This was in good agreement with the previous studies on LDA (Dobesh et al., 2002; Kentish et al., 1986; Martyn and Gordon, 2001)

Additionally, force traces from a steady-state measurement of force development at SL 1.9 μm and 2.3 μm are shown in Figure 4.2. Figure was directly exported from Labview program where the force signal was detected from the force transducer, thus represented by voltage values. Resting tension was recorded in relaxing solution before activation. Stretching SL from 1.9 μm to 2.3 μm increased resting tension from 0.120 V to 0.230 V, which can be converted to an increase from 2.2 mN/mm^2 to 4.3 mN/mm^2 (cross-sectional area 17275 $μm^2$) according to the calibration of the force transducer x10 gain prior to the measurements (details in Section 3.3). Maximum Ca^{2+}-activated force was calculated as the difference between the maximum measured force and the resting tension. The maximum Ca^{2+}-activated force of the representative fibre in Figure 4.2 increased about 28% (from 1.13 V to 1.455 V, equals to 21.0 mN/mm^2 to 27.0 mN/mm^2) upon SL increasing from 1.9 μm to 2.3 μm. The increasing was slightly smaller compared to the results above and it was likely due to fibre variation.

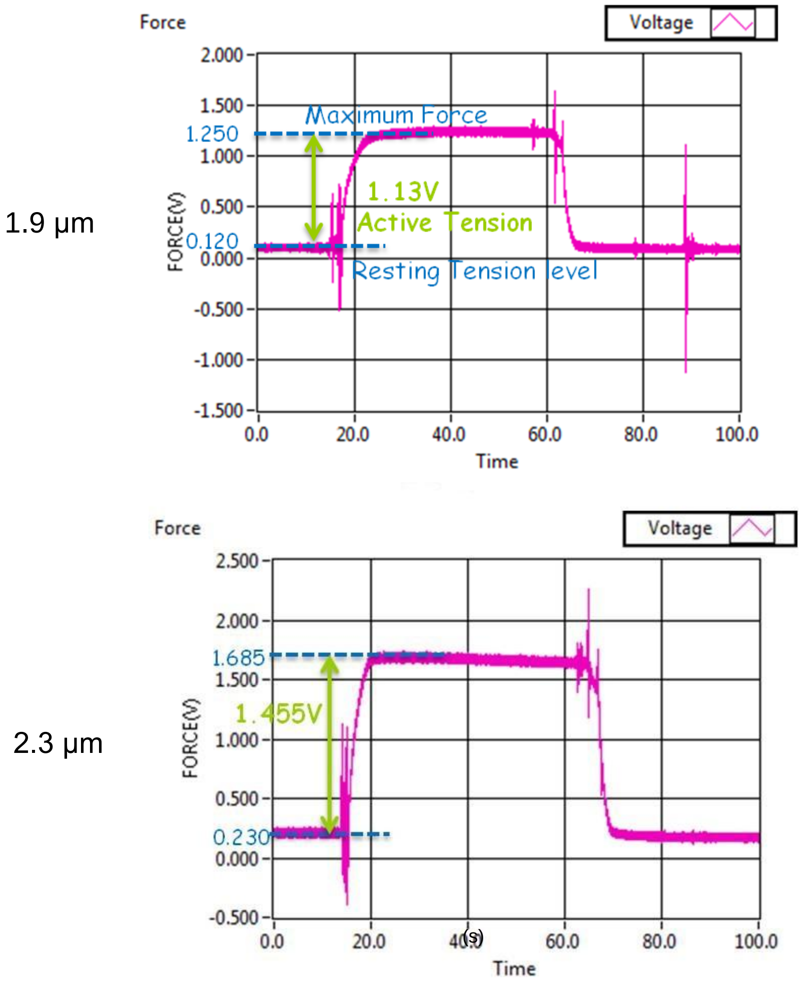

Figure 4.2: Force traces from the steady-state measurement of a representative fibre at SL 1.9 µm and 2.3 µm. Trabecula reconstituted with BR-cTnC-C was activated at SL 1.9 µm and 2.3 µm. Trace recording started after setting SL and finished after maximal activation. Resting tension was developed by stretching the fibre, and maximum Ca^{2+}-activated force (active tension in the figure) was indicated by the difference between maximum force level and resting tension (green arrow). Force traces were directly exported from Labview program, thus force signal was described as voltage signal. Force values in mN/mm^2 can be found in the text.

4.2.2 Effect of SL on the Ca^{2+} Dependence of Force Development

To determine the effect of SL variation on the Ca^{2+} dependence of force development, Ca^{2+} titration experiments were performed in skinned trabeculae at the two SLs described above — 1.9 µm and 2.3 µm. Permeabilization allows the control of free

[Ca^{2+}] using EGTA buffers. Free [Ca^{2+}] was expressed on a logarithmic scale, as pCa = -$\log_{10}$[Ca^{2+}]. Trabecula reconstituted with either BR-cTnC-C or BR-cTnC-E was continuously activated by a stepwise increase in [Ca^{2+}] (from pCa 9.0 to maximum activated at pCa 4.5) at SL 1.9 μm (as the control group) and 2.3 μm, respectively. The SL was carefully set according to diffraction pattern and was checked before and after each series of continuous activation. At each SL, Ca^{2+}-activated force was measured after steady-state was established at each pCa, and plotted as a function of free [Ca^{2+}]. Ca^{2+}-activated force was calculated as the force production above the resting tension. It was then normalized to the maximum Ca^{2+}-activated force at each SL to reduce the biological variation (i.e. shape, size of the fibre) between trabeculae. Maximum Ca^{2+}-activated force was recorded at maximal Ca^{2+} activation (pCa 4.5) at each SL. Data from individual fibres at each SL were fitted by modified Hill relationship — $Y = 1/(1+10^{n\mathrm{H(pCa-pCa50)}})$, where pCa_{50} (corresponding to the pCa at half maximum force) describes the Ca^{2+} sensitivity and Hill coefficient-n_H (the steepness of the force-pCa relationship) describes the cooperativity of Ca^{2+} regulation. The average parameters are summarized in Table 4.3.

After stretching SL from 1.9 μm to 2.3 μm, maximum force increased 31 ± 6% (± SEM, n = 5) and 24 ± 3% (± SEM, n = 5), respectively, for trabeculae reconstituted with BR-cTnC-C and BR-cTnC-E (Table 4.3), inducing a leftward shift of the force-pCa curve (Figure 4.3). This is consistent with the previous studies, for example, Dobesh *et al*. (2002), which reported an average increase of 9% of the maximum Ca^{2+}-activated force in response to per 0.1 μm SL elongation within the physiological range. Results were also in agreement with the maximum force measurements described in Section 4.2.1, suggesting the development of maximum activated force is proportional to SL in cardiac muscle, although the SL dependent force increases in titration experiments were smaller than that in Fmax measurements (~30% in Ca^{2+} titration vs ~40% in Fmax measurements). This may be the result of some minor damage to the fibre caused by continuous activation during titration experiment.

Table 4.3: Hill parameters for the effect of SL on the Ca^{2+} dependence of force development. (A). C-helix probe experiments; (B). E-helix probe experiments. Mean ± SEM of the parameters obtained by fitting parameters for each trabecula at each SL. F_{max} indicates the force per cross-sectional area of the maximum Ca^{2+}-activated force. Δ describes the difference between two SLs. Comparison: paired two-tailed student t-test between SL 1.9 and 2.3 µm (statistical significance * p<0.05, ** p<0.01, *** p<0.001).

(A)

	Mean ± SEM	**1.9 µm**	**2.3 µm**	**Δ**
C-helix	**F_{max} (mN/mm^2)**	24 ± 1	32 ± 2	31 ± 6%*
	pCa_{50}	5.37 ± 0.04	5.50 ± 0.03	0.12 ± 0.01***
	n_H	4.01 ± 0.19	4.29 ± 0.24	0.27 ± 0.08*
	n	5		

(B)

	Mean ± SEM	**1.9 µm**	**2.3 µm**	**Δ**
E-helix	**F_{max} (mN/mm^2)**	22 ± 5	27 ± 6	24 ± 3%*
	pCa_{50}	5.37 ± 0.02	5.49 ± 0.03	0.11 ± 0.02**
	n_H	4.05 ± 0.24	4.45 ± 0.26	0.40 ± 0.07**
	n	5		

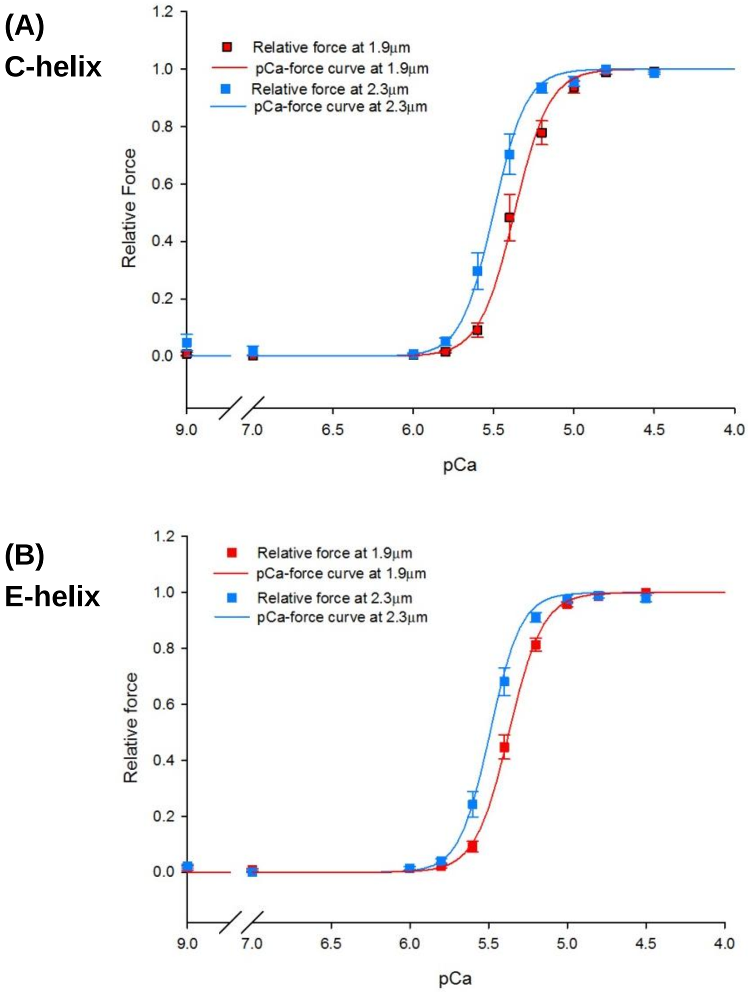

Figure 4.3: Effect of SL on the Ca^{2+}-dependence of force development. Force was plotted as a function of pCa at SL 1.9 μm (red solid squares) and 2.3 μm (blue solid squares) for (A). C-helix probe; (B). E-helix probe. Red and blue lines indicate the fittings by Hill equation at SL 1.9 μm and 2.3 μm, respectively. Error bars denote S.E.M. Trabeculae number n = 5 for both C- and E-helix probes (Hill parameters are provided in Table 4.3).

Increasing SL in fibres reconstituted with BR-cTnC-C resulted in a leftward shift of the force-calcium relationship (Figure 4.3 A), indicated by an increasing in pCa_{50} (the pCa at half-maximum force) from 5.37 ± 0.04 to 5.50 ± 0.03 (± SEM, n = 5). The steepness of the Ca^{2+} dependence (n_H), increased by 0.27 ± 0.08 (± SEM, n = 5) when the SL was increased (Table 4.3 A). However, the increase in n_H was quite small when compared with the highly cooperative Ca^{2+} regulation, denoted by a Hill coefficient close to 4.

A similar situation was also observed for BR-cTnC-E. Increasing SL from 1.9 μm to 2.3 μm induced a leftward shift of the force-pCa curve (Figure 4.3 B), indicated by a significant increase in pCa_{50} from 5.37 ± 0.02 to 5.49 ± 0.03 (± SEM, n = 5) (Table 4.3 B). The cooperativity of the Ca^{2+}-dependent change in force (n_H) was increased by 0.40 ± 0.07 (± SEM, n = 5) at longer SL (Table 4.3 B).

Taken together, as SL was increased, both the maximum Ca^{2+}-activated force and the Ca^{2+} sensitivity for force were increased. The increase in Ca^{2+} sensitivity upon SL stretching was similar for both labelled helices (~0.11pCa units, Table 4.3), indicating a similar length dependent behaviour in the force-[Ca^{2+}] relationship in the two major domains of cTn complex.

4.3 Effect of SL on cTnC orientation

4.3.1 Effect of SL on *In Situ* Orientation of cTnC

Investigations were then focused on the physiological Ca^{2+}-sensor — cTnC. Measurements were taken simultaneously in the same set of ventricular trabeculae as that in force-[Ca^{2+}] measurements, where the native cTnC was reconstituted with BR-labelled hcTnC-C or hcTnC-E. The native structural relationships between the full complement of proteins in the regulatory system are preserved (Sun *et al*., 2009). The orientation of the BR probes, thus of the C- or E-helix of cTnC to which it was attached, was determined by polarised fluorescence (see Section 2.2). As mentioned in Chapter 2, the C- and E- helix probes were used to report changes in the orientation of the two major domains of the troponin core complex in the regulation of Ca^{2+}-dependent activation — the regulatory head and the IT arm.

The *in situ* orientation changes of the C- and E-helix of cTnC were determined during relaxation (pCa 9.0) and maximal Ca^{2+} activation (pCa 4.5) at SL 1.9 μm and 2.3 μm, respectively. The Ca^{2+}-induced orientation changes in cTnC are thought to be primarily associated with the movement of B and C helices away from the N, A and D helices in response to the Ca^{2+}binding and the switch peptide of cTnI binding to the N-lobe of cTnC (Sun *et al*., 2006; Sun *et al*., 2009). The order parameters $<P_2>$ and $<P_4>$ were calculated from the fluorescence polarization to describe the orientation distribution of the BR dipoles with respect to the fibre axis. A Gaussian model was used to acquire the peak angle θ_f and standard deviation σ_g of these dipole orientation distributions (Julien *et al*., 2007) (data reported in Table 4.4. For details about order parameters and Gaussian model, see Section 2.4).

At SL 1.9 µm, the C-helix had a more parallel orientation with respect to the fibre axis at relaxation (θ_f = 51.9 ± 0.4°, ± SEM, n = 5) compared with at maximum activation (θ_f = 55.5 ± 0.2°), corresponding to the $<P_2>$ values 0.104 ± 0.004 and 0.028 ± 0.004 at relaxation and maximum activation (Table 4.4 A). Stretching to a longer SL at 2.3 µm slightly reduced C-helix's axial angle θ_f during both relaxation (~51.9° at 1.9 µm *vs* ~51.3° at 2.3 µm) and activation (~55.5° at 1.9 µm *vs* ~55.0° at 2.3 µm) by shifting towards more parallel conformations, although the shifting of the relaxing orientation was not statistically significant. Yet the overall orientation changes of the C-helix from pCa 9.0 to pCa 4.5 were not significantly affected by SL alteration, indicated either by $\Delta<P_2>$ (0.076 ± 0.006 at SL 1.9 µm, 0.075 ± 0.006 at 2.3 µm) or $\Delta\theta_f$ (3.6° ± 0.2° at both SLs). Figure 4.4 A gives a more direct comparison of the *in situ* orientation of the C-helix during relaxation and maximum activation at both SLs. Although these orientation changes were small, they were highly reproducible. Additionally, there was no significant change in the probe dispersion σ_g upon either Ca^{2+} activation or SL elongation.

Table 4.4: Parameters for the effect of SL on cTnC *in situ* orientation change. A. C-helix probe experiments; B. E-helix probe experiments. Order parameters <P_2> and <P_4> were obtained during relaxation and maximum activation. θ_f and σ_g indicate the peak angle and standard deviation of the Gaussian orientation distribution of the probe angle with respect to the fibre axis, respectively (indicated in the text and Section 2.4). Mean ± SEM. Δ is the difference of each parameter between pCa9.0 and pCa4.5. n = 5 for both BR-cTnC-C and -E. Comparison: paired two-tailed student t-test between SL 1.9 and 2.3 µm (statistical significance * $p<0.05$, ** $p<0.01$).

(A)

C-helix	**1.9 µm**				**2.3 µm**			
	<P_2>	**<P_4>**	**Θ_f (°)**	**σ_g (°)**	**<P_2>**	**<P_4>**	**Θ_f (°)**	**σ_g (°)**
pCa 9.0	0.104 ± 0.004	-0.132 ± 0.028	51.9 ± 0.4	18.8 ± 1.4	0.111 ± 0.006	-0.168 ± 0.025	51.3 ± 0.3	16.8 ± 1.2
pCa 4.5	0.028 ± 0.004	-0.145 ± 0.022	55.5 ± 0.2	17.7 ± 1.2	0.036 ± 0.003*	-0.158 ± 0.028	55.0 ± 0.2*	17.1 ± 1.5
Δ	0.076 ± 0.006	0.013 ± 0.019	-3.6 ± 0.2		0.075 ± 0.006	-0.010 ± 0.006	-3.6 ± 0.2	
n	5							

(B)

E-helix	**1.9 µm**				**2.3 µm**			
	<P_2>	**<P_4>**	**Θ_f (°)**	**σ_g (°)**	**<P_2>**	**<P_4>**	**Θ_f (°)**	**σ_g (°)**
pCa 9.0	0.259 ± 0.008	-0.155 ± 0.046	44.4±0.4	15.9 ± 2.1	0.277 ± 0.009*	-0.207 ± 0.034*	43.8 ± 0.3*	13.1 ± 1.6*
pCa 4.5	0.182 ± 0.007	-0.205 ± 0.038	47.9±0.3	14.7 ± 1.8	0.208 ± 0.008**	-0.232 ± 0.028	46.8 ± 0.3**	13.2 ± 1.3
Δ	0.077 ± 0.010	0.050 ± 0.010	-3.6±0.5		0.069 ± 0.005	0.025 ± 0.008	-3.0 ± 0.2	
n	5							

The orientation of the E-helix had a more parallel preference compared with the C-helix (Table 4.4 B). Similarly, at SL 1.9 μm, maximum activation shifted E-helix towards a slightly more perpendicular conformation: decreasing $<P_2>$ by 0.077 ± 0.010 (± SEM, n = 5), or increasing θ_f by 3.6 ± 0.5° (± SEM, n = 5). However, increasing SL to 2.3 μm induced a small but significant increase in $<P_2>$ values at both pCa 9.0 (from ~0.259 to ~0.277) and pCa 4.5 (from ~0.182 to ~0.208), indicating a more parallel conformation of the E-helix at longer SL at both relaxed and activated state. Interestingly, the net angular change from relaxation to maximum activation at each SL ($\Delta<P_2>$ or $\Delta\theta_f$, see Table 4.4 B and Figure 4.4 B) was very similar (Table 4.4 A). It was not affected by SL either, as in the case of the C-helix probe. The standard deviation of the E-helix probe σ_g decreased slightly at pCa 9.0 after stretching, but did not show significant change at pCa 4.5. The slightly bigger standard error in $<P_2>$ values for the E-helix probe was likely due to a greater fibre to fibre variation in the $<P_2>$ of BR-cTnC-E, thus a bigger spread in the mean, while $\Delta<P_2>$ remained relatively constant.

Although increasing SL caused small changes in the orientation of both C- and E-helix of cTnC at either relaxation or maximum activation state, the results above reported no significant impact of SL alteration on the amplitude of cTnC orientation change upon Ca^{2+} activation. The results indicate that as one of the two outcomes of LDA, the SL-dependent increase of maximum force is not likely due to more cTnC structural change upon Ca^{2+} activation.

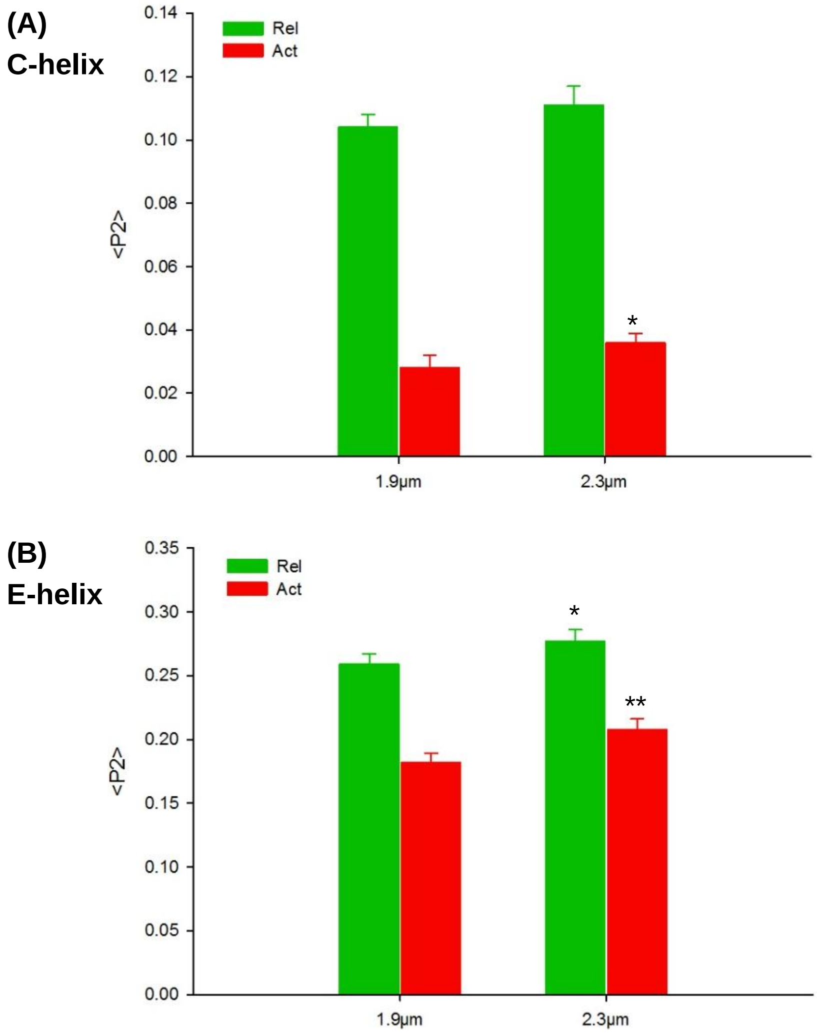

Figure 4.4: Effect of SL change on cTnC *in situ* orientation. Bar Charts show $<P_2>$ upon activation and SL alteration. (A): C-helix probe; (B): E-helix probe. Green and red bars in each set represent $<P_2>$ value at relaxation (pCa 9.0) and maximum activation (pCa 4.5), respectively. First set in each graph is at SL 1.9 µm, second at 2.3 µm. Error bars denote SEM. n = 5 for each probe. Statistical significance of differences between values from two SLs for each probe was assessed using paired two-tailed student t-test: $*p < 0.05$, $**p<0.01$ ($<P_2>$ values are presented in Table 4.4).

4.3.2 Effect of SL on the Ca^{2+} Dependence of cTnC Orientation

In order to determine the effect of SL on the Ca^{2+} dependence of cTnC orientation change, *in situ* orientation of either C- or E-helix of cTnC was measured simultaneously with isometric force development in the Ca^{2+} titration experiments described in Section 4.2.2. The SL was set to 1.9 µm and 2.3 µm for the continuous activation in each permeabilized trabecula. In situ orientation was determined from the fluorescence polarization of the BR dipole attached along C- or E-helix of cTnC using F*IS*S, and was described by the order parameter $<P_2>$, which gives the same relationship to $[Ca^{2+}]$ as that of the mean axial angle θ_f (Figure 4.5). $<P_2>$ from each titration was recorded and plotted as a function of free $[Ca^{2+}]$, which was represented by pCa ($-\log_{10}[Ca^{2+}]$). $<P_2>$-pCa relationship was fit by Hill equation for each fibre at each SL, the curve was set through the maximum and minimum of $<P_2>$ values, while pCa_{50} and n_H were acquired from the average of each individual fitting (reported in Table 4.5).

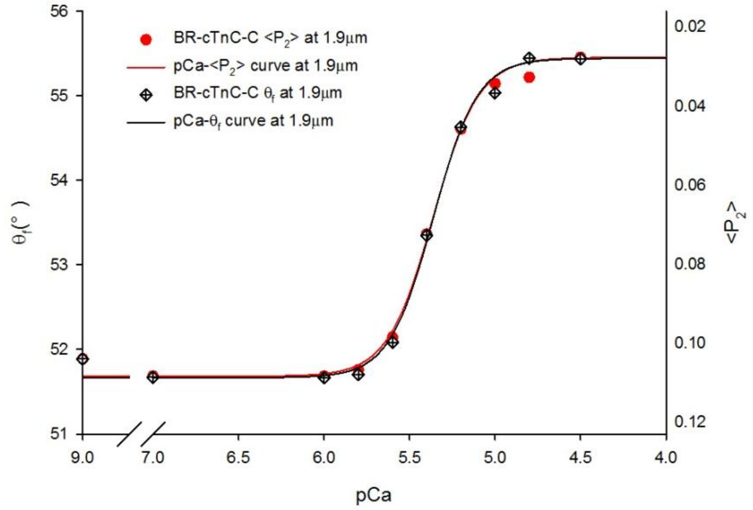

Figure 4.5: The Ca^{2+}-dependent C-helix orientation change at SL 1.9 µm, showing the consistency of θ_f (left axis, cross in the circle) and $<P_2>$ (right axis, red circles) in terms of representing the *in situ* orientation changes in cTnC. Black and red lines are the Hill fit of pCa-θ_f and pCa-$<P_2>$ curve respectively. Error bars are omitted here for clarity. n = 5.

The stretching of the SL in skinned trabeculae reconstituted with BR-cTnC-C from 1.9 µm to 2.3 µm induced a shift of the $<P_2>$-pCa curve (Figure 4.6 A). As described above, although stretching to a longer SL slightly increased $<P_2>$ value at pCa 4.5, the overall orientation change of the C-helix was not significantly affected by SL increasing, indicated by the similar amplitude of the $<P_2>$-pCa relationship at both

SLs (Δ<P_2 > ~0.076 at 1.9 μm *vs* ~0.075 at 2.3 μm, Table 4.4 A and Table 4.5 A). When SL increased from 1.9 μm to 2.3 μm, the Ca^{2+} sensitivity for C-helix orientation change increased from pCa_{50} 5.37 ± 0.02 to 5.48 ± 0.01, showing a ΔpCa_{50} of 0.11 ± 0.02 (± SEM, n = 5), which is similar to what was observed for the force development (ΔpCa_{50} = 0.12 ± 0.01, ± SEM, n = 5, see Table 4.3 A). Although there was a tendency to increase the cooperativity of the Ca^{2+}-dependent C-helix orientation change upon stretching (Δn_H = 0.10 ± 0.19, ± SEM), it was not statistically significant as that in the force-pCa relationship (Δn_H = 0.27 ± 0.08, ± SEM) (Table 4.3 A and Table 4.5 A). The <P_2>-pCa relationship was less steep than what was observed for the force-pCa relationship at both SLs. The reduction in n_H for <P_2> was found in the E-helix probe experiments as well. Detailed comparison of force-pCa and <P_2>-pCa relationship for the E-helix probe is presented in next section.

Unlike BR-cTnC-C, the <P_2>-pCa relationship for BR-cTnC-E had a small additional component in the subthreshold of pCa, which was similar in both SLs (Figure 4.6 B) (for details in terms of the additional orientation component of the E-helix, see next Section 4.3.3). The major component of the E-helix orientation change upon pCa<6.0 was fitted to the Hill equation. Increasing SL to 2.3 μm showed an increase in the <P_2> values over the whole range of pCa (Figure 4.6 B). Although there was an increase in <P_2> at both pCa 9.0 and 4.5, SL elongation had no significant effect on the amplitude of E-helix's orientation change during activation (Δ<P_2> ~0.077 at 1.9 μm *vs* ~0.069 at 2.3 μm, see Table 4.4 B and 4.5 B). As anticipated, stretching SL increased the Ca^{2+} sensitivity for E-helix orientation change by increasing pCa_{50} from 5.34 ± 0.02 to 5.45 ± 0.02, with a overall ΔpCa_{50} of 0.11 ± 0.03 (± SEM, n = 5) (Table 4.5 B). The increase in Ca^{2+} sensitivity corresponds well to that observed for force development in the same set of trabeculae (Table 4.3 B), and to that for the C-helix probe experiments (Table 4.5 A). However, the increased SL appeared to show a tendency towards reduced cooperativity for the Ca^{2+}-dependent change in the E-helix orientation (Δn_H = -0.36 ± 0.41, ± SEM, n = 5), opposite to the increasing Hill coefficient for the C-helix probe, although these changes of n_H in response to stretching observed in the <P_2>-pCa relationship for both C- and E-helix probes were not statistically significant (Table 4.5).

Table 4.5: Hill parameters for the effect of SL on the Ca^{2+} dependence of cTnC orientation change. (A): C-helix probe experiments; (B): E-helix probe experiments. Parameters were obtained by fitting data for each trabecula at each SL. $\Delta\langle P_2\rangle$ represents the orientation change from relaxation to maximum activation. Mean ± SEM. n = 5 for both BR-cTnC-C and –E exchanged trabeculae. Δ indicates the difference in each parameter from SL 1.9 to 2.3 μm. Comparison: paired two-tailed student t-test between two SLs (statistical significance * p<0.05, ** p<0.01).

(A)

	C-helix			
		1.9 μm	**2.3 μm**	**Δ**
Orientation	**$\langle P_2\rangle$ pCa 9.0**	0.104 ± 0.004	0.111 ± 0.006	
	$\langle P_2\rangle$ pCa 4.5	0.028 ± 0.004	0.036 ± 0.003*	
	$\Delta\langle P_2\rangle$	0.076 ± 0.006	0.075 ± 0.006	
	pCa_{50}	5.37 ± 0.02	5.48 ± 0.01**	0.11 ± 0.02**
	n_H	3.26 ± 0.15	3.36 ± 0.17	0.10 ± 0.19
	n	5		

(B)

	E-helix			
		1.9 μm	**2.3 μm**	**Δ**
Orientation	**$\langle P_2\rangle$ pCa 9.0**	0.259 ± 0.008	0.277 ± 0.009*	
	$\langle P_2\rangle$ pCa 4.5	0.182 ± 0.007	0.208 ± 0.008**	
	$\Delta\langle P_2\rangle$	0.077 ± 0.010	0.069 ± 0.005	
	pCa_{50}	5.34 ± 0.02	5.45 ± 0.02*	0.11 ± 0.03*
	n_H	3.61 ± 0.29	3.25 ± 0.18	-0.36 ± 0.41
	n	5		

(A)
C-helix

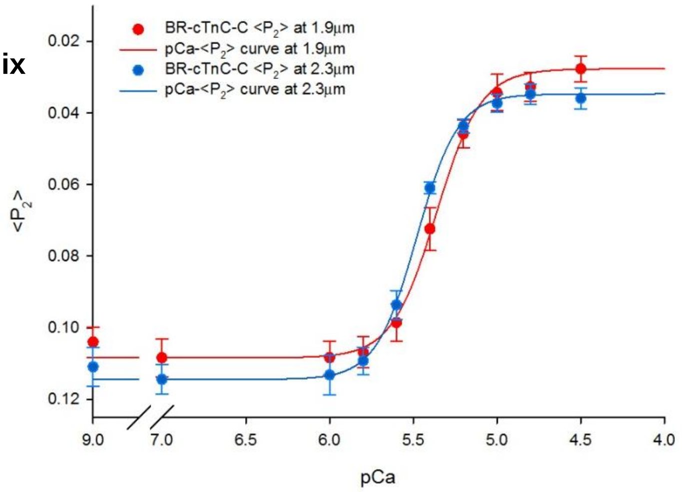

(B)
E-helix

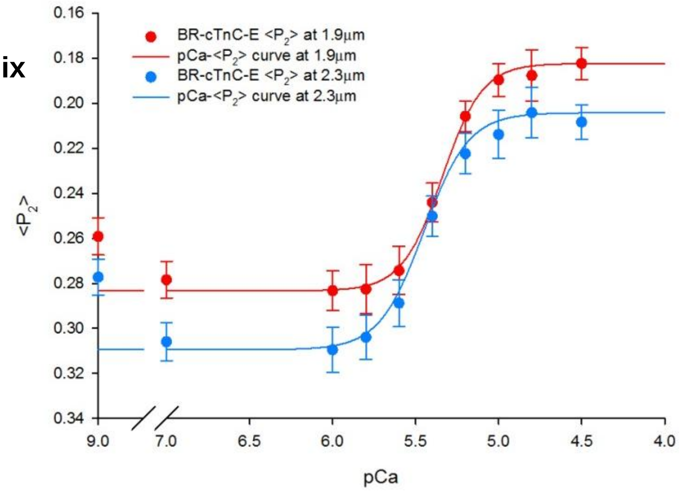

Figure 4.6: Effect of SL change on the Ca^{2+} dependence of cTnC orientation change. $<P_2>$ values were plotted as functions of pCa at SL 1.9 μm (red circles) and 2.3 μm (blue circles), respectively. (A): C-helix probe; and (B): E-helix probe. Red and blue lines indicate the fitting by Hill equation for 1.9 μm and 2.3 μm, respectively. Error bars denote SEM. Trabeculae number n = 5 for each helix probe. (Hill parameters are provided in Table 4.5).

4.3.3 Ca^{2+} Regulation of Force and cTnC Orientation

As mentioned above, the Ca^{2+}-dependence of force and cTnC orientation were investigated simultaneously in the same set of trabeculae using Ca^{2+} titration experiments, where the force development, together with the orientation change in either helices were measured and plotted as functions of pCa. As shown in Figure 4.7, force and <P_2> from averaging individual fibre were fitted to Hill equation. Since <P_2> is inversely related to force, in order to compare the force development and orientation change from the same trabeculae, <P_2>-pCa was plotted inversely and the scale was adjusted accordingly in the second graph of each group in Figure 4.7 and all <P_2>-pCa curves in this thesis. Force was normalised to the one produced at maximal Ca^{2+}-activation, whilst the <P_2>-pCa curve was set through the maximum and minimum of <P_2> values. pCa_{50} and n_H were determined from the mean of each individual fitting.

As mentioned in last section, for BR-cTnC-E, unlike the Ca^{2+}-dependent force development, the orientation change had an additional component in the lower range of [Ca^{2+}], i.e. pCa 9.0 to pCa 6.0, where the changes in <P_2> was at opposite direction compared with in the higher [Ca^{2+}] (pCa 6.0 to pCa 4.5) (Figure 4.7). The additional orientation component has been previously observed for the E-helix probe and mono-functional probes on Cys-84 of cTnC (Bell *et al*., 2006; Sun *et al*., 2009). Of the three Ca^{2+} binding sites on cTnC, two high affinity sites (Ca^{2+}/Mg^{2+}) are in the C-lobe of cTnC, whilst one low affinity site is in the N-lobe and specific for Ca^{2+} (details in Section 1.2.2.3). Possibly, the additional component is associated with Ca^{2+} binding to the Ca^{2+}/Mg^{2+} sites in the C-lobe near the E-helix. According to the Ca^{2+} binding affinities for the cTnC sites calculated by Kobayashi and Solaro (2005), the majority of Ca^{2+}-Mg^{2+} exchange (~85%) at high affinity sites occurs between pCa 9.0 and pCa 7.0 (Bell *et al*., 2006), which could be partly responsible for the offset between the Ca^{2+} dependence of the E-helix orientation change and force development.

The similar shape of force-pCa and <P_2>-pCa curves in each group suggests similar Ca^{2+} sensitivity (pCa_{50}) and cooperativity (n_H) in the Ca^{2+} dependence of force development and cTnC orientation change, indicating that the orientation change in cTnC upon Ca^{2+} binding, together with the subsequent force development, have essentially the same Ca^{2+} dependence. SL variation did not affect this similarity between force and cTnC. Thus, there is a simple relationship between cTnC orientation change and force development — with the increasing [Ca^{2+}], force is linearly related to the Ca^{2+}-induced orientation changes in cTnC at each SL. This is in agreement with previous investigations (Sun *et al*., 2009), suggesting that force development is proportional to the fraction of cTnC molecules in the Ca^{2+}-binding state. However, the SL-dependent increase in maximum force was not accompanied by the increasing amplitude of cTnC structural change upon activation. More importantly, the results showed similar increase in the Ca^{2+} sensitivity for both force and cTnC structural change in response to SL elongation, suggesting the SL-dependent increase in the Ca^{2+} sensitivity for force is very likely modulated by cTnC on the thin filament through increasing the Ca^{2+} sensitivity for cTnC structural change.

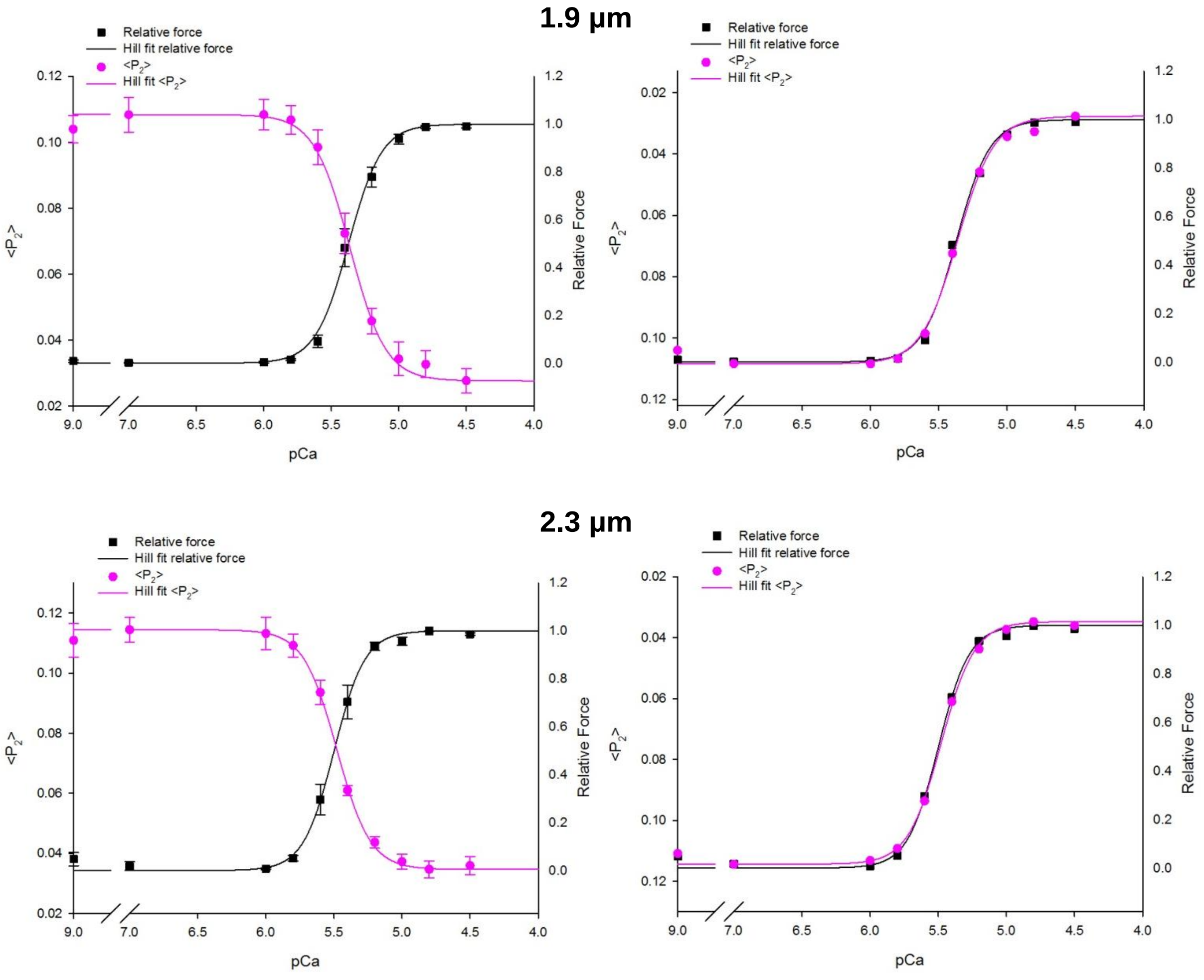

C-helix

1.9 µm

2.3 µm

Figure 4.7 (to be continued)

E-helix

1.9 µm

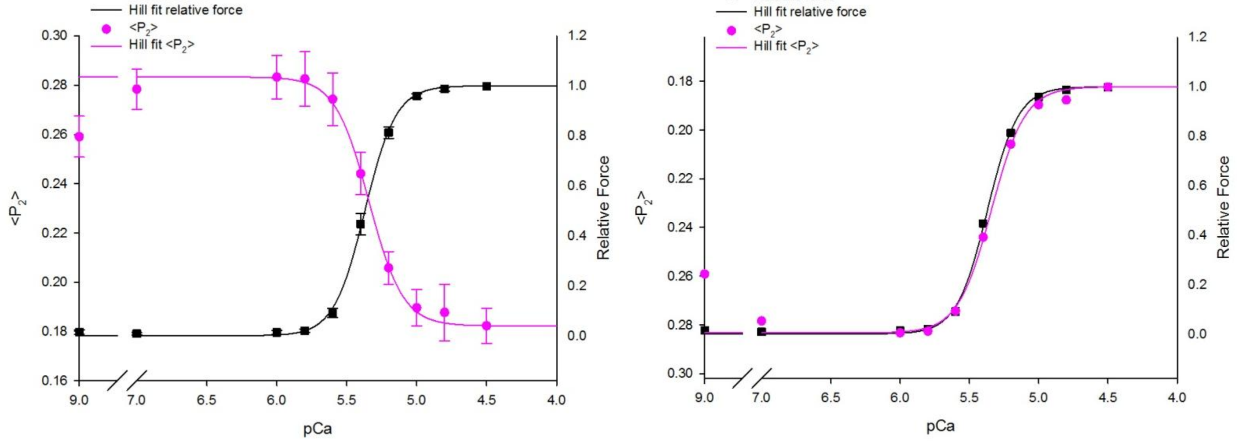

2.3 µm

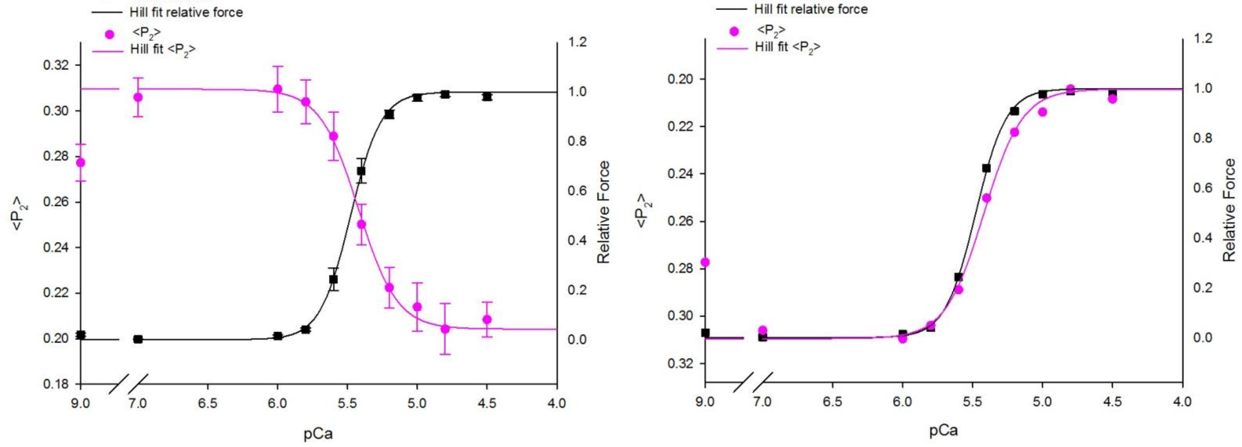

Figure 4.7: The Ca^{2+} dependence of force and structural changes in cTnC at two SLs. Force (solid black squares) and orientation changes (solid purple circles) for the C- or E-helix probe from the same set of trabeculae (n = 5 for both probes) were plotted as functions of pCa at two SLs — 1.9 µm and 2.3 µm. Black and purple lines are fits of the Hill equation to force and $<P_2>$ respectively. Relative force was normalised to the maximum Ca^{2+}-activated force at each SL in each fibre. Error bars denote S.E.M. for n = 5 trabeculae for each helix probe. In the 2nd figure of each group, $<P_2>$ values were plotted inversely and the scale was adjusted accordingly so the $<P_2>$-pCa relationship follows the force-pCa relationship very closely. Error bars are omitted in the 2nd figures for clarity.

4.4 Discussion

4.4.1 Role of cTnC in LDA

In this chapter, we investigated the role of the Ca^{2+} binding protein cTnC in the two outcomes of LDA — the SL-dependent maximum force and Ca^{2+} sensitivity. Increasing SL from 1.9 μm to 2.3 μm caused ~40% increase in the maximum Ca^{2+}-activated force in skinned cardiac trabeculae. No significant difference was observed in the SL-dependent force increase between BR-cTnC exchanged and unexchanged fibres (Table 4.1), nor between BR-cTnC-C and BR-cTnC-E exchanged trabeculae (Table 4.2). The resting tension increased ~30% upon SL increasing from 1.9 μm to 2.3 μm, which was largely regulated by the elastic titin. Titin spans the full half of the sarcomere and it has interactions with both the thick and thin filaments. The increased resting tension suggests the increased titin strain might be correlated with positioning cross-bridges, so as to increase the probability of myosin heads binding at longer SL, thus increase the maximum Ca^{2+}-activated force.

However, the ~40% maximum force increase at SL 2.3 μm was not accompanied by the increasing amplitude of cTnC structural change upon activation. Structural changes in cTnC upon Ca^{2+} activation were reported by BR probes on the C- and E-helix of cTnC, corresponding to the changes in the angle θ_f between each helix and the trabecular axis. Although increasing SL showed small effect on the orientation of each helix with respect to the fibre axis, the net orientation change upon maximum activation (represented by either $\Delta\langle P_2\rangle$ or $\Delta\theta_f$) was independent of SL change, suggesting the SL-dependent increase in the maximum activated force was not due to the increased structural changes in cTnC. However, the small effect on the orientation of each helix upon SL stretching may imply the possibility of a reorientation of cTnC on the thin filament, inducing a closer proximity with the switch peptide of cTnI. In this way, the increasing cTnC/cTnI interactions at longer SL may result in an increasing Ca^{2+} sensitivity. The amplitude of each helix's orientation change upon activation was

~3.6° at both SL 1.9 and 2.3 μm (Table 4.4). It was smaller than previously reported (~5°) (Sun *et al*., 2009), possibly due to the difference in the exchange and titration protocols between studies.

As mentioned above, the additional component of E-helix orientation change observed in the subthreshold range of [Ca^{2+}] at both SLs may be associated with Ca^{2+} binding to the Ca^{2+}/Mg^{2+} site in the C-lobe of cTnC near the E-helix. This independent motion of the C-lobe of cTnC at lower [Ca^{2+}] altered the relative conformation between the two lobes of cTnC. It may be related to the system preparing for the interactions between cTnC and cTnI prior to the Ca^{2+} binding to the N-lobe and the subsequent Ca^{2+}-induced structural change in troponin.

Titration experiments on the Ca^{2+} dependence of force and cTnC structural change showed an almost identical leftward shift of the force-pCa and $<P_2>$-pCa curves upon SL changing from 1.9 μm to 2.3 μm, indicative of a similar SL-dependent change in pCa$_{50}$ (Ca^{2+} sensitivity) and n_H (Ca^{2+} cooperativity) of force and orientation change for both C- and E-helix probes. Increasing SL increased the Ca^{2+} sensitivity for force and both C- and E-helix orientation change by a similar amount of 0.11 pCa units (Table 4.3 & Table 4.5). Thus, it is reasonable to conclude that the mechanism underlying the SL-dependent Ca^{2+} sensitivity for force and cTnC structural change is the same.

Additionally, current experiments showed that the steepness (n_H) of the force-pCa relationship had a small increase in response to SL increasing, whereas that of the cTnC structural change-pCa relationship did not change significantly. As described before, the cooperativity of Ca^{2+} regulation is not driven by the feedback of cross-bridge attachment, rather, it is more likely to be the intrinsic property of the thin filament itself. Ca^{2+} binding cooperatively induces Tm movement in adjacent RUs, leads to the structural change of neighbouring cTnC, and exposes more sites for myosin heads to bind and generate force.

Based on this theory, Farman *et al*. (2010) reported that it was the number of the RUs able to bind Ca^{2+} that most affects LDA. Their findings indicated the coupling between neighbouring RUs upon Ca^{2+} binding was enhanced at longer SL, thus allowing the impact of Ca^{2+} binding to propagate further along the thin filament with the assistance by weak binding cross-bridges, which ultimately transmit to the strong binding and generate force. Presumably, the influence of SL would have the same effect on the Ca^{2+} cooperativity of force production and cTnC structural change by stronger coupling of the adjacent RUs. However, titin may also play a role in the SL-dependent regulation of cooperativity. As increasing SL strains the titin molecule, the straining may affect the relative conformation between myosin heads and actin monomers which favours the weakly attached heads. It has been suggested that the fully open conformation of cTnC was stabilized by strong-binding cross-bridges. In this case, the opening in cTnC will not be as substantial as that induced by the cooperative coupling of RU. The effect of cooperativity to couple the structural change of cTnC in adjacent RUs may not be as efficient as to couple the formation of cross-bridges in neighbouring sites. Yet the weak binding cross-bridges are capable of further shifting towards the strongly bound force-generating conformation. Thereby, no significant increase was observed in the cooperativity for cTnC structural change upon SL increasing, by contrast to the small increase in that for force.

Therefore, the results in this chapter showed that, even though with the increasing [Ca^{2+}], force generation was still coupled to cTnC structural change at each SL, the SL-dependent increase in maximum force was not accompanied by the similar increase in the amplitude of cTnC structural change upon Ca^{2+} activation. However, the SL-dependent increase in the Ca^{2+} sensitivity was very similar for both force production and cTnC structural change, suggesting the two outcomes of LDA (increasing maximum force and Ca^{2+} sensitivity) are not both related with cTnC. While the SL-dependent Ca^{2+} sensitivity for force is very likely modulated through the Ca^{2+} sensitivity for cTnC structural change by cTnC, the SL-dependent maximum force is not. It was suggested that this SL-dependent increase in the maximum force was the result of an increasing number of force-generating cross-bridges formed at longer SL (Allen and Kentish, 1985; Wannenburg et al., 2000; Wannenburg et al., 1997), which leads us to the next investigation on the thick filament cross-bridges.

4.4.2 Comparison with Previous Studies

As the cellular basis of the Frank-Starling relationship, LDA describes the effects of sarcomere lengthening on both the maximum force production and the Ca^{2+} sensitivity on the level of cardiomyocytes. In this study, we found ~40% increase in the maximum force in response to SL increasing from 1.9 to 2.3 μm. The result was in good agreement with the previous studies, which concluded that: at a given $[Ca^{2+}]$, SL increasing was accompanied by significant increase in the force development; and it was the SL-dependent increase in the maximum force production that contributes to the rising ventricular pressure in the heart. For instance, the investigation by Kentish *et al*. (1986) has shown that the average maximum force increased ~87% as SL increased from 1.65 to 2.15 μm in skinned cardiac trabeculae experiments. Dobesh *et al*. (2002) reported the averaged maximum force development increased ~9% for each 0.1 μm increase in SL. The various amounts of force increase among different studies may be due to different experiment protocols applied in each study: force production at different SLs was determined from different groups of trabeculae in Kentish *et al*. (1986), whereas determined from the same group of trabeculae in Dobesh *et al*. (2002) and our study.

However, we found this SL-dependent increase in the maximum force was not accompanied by the similar increase in the amplitude of cTnC structural change upon activation, at variance with the previous conclusions that both force and activation-dependent changes in cTnC structure were influenced by SL (Martyn and Gordon, 2001). The results indicate that there may not be a certain relationship between force development and structural change in cTnC upon activation at different SLs. The SL-dependent maximum force increase is more likely to due to increasing number of force-generating cross-bridges than increasing extent of cTnC conformation change at longer SL.

A total angular change of only ~3.6° in each helix upon maximum Ca^{2+}-activation was reported in this study. This seems to be at variance with the measurements previously done on isolated cTnC, which demonstrated a change of 12° in the opening of the N-lobe on Ca^{2+} binding alone, and 34° after the subsequent binding of the cTnI switch peptide (Li *et al*., 1999; Sia *et al*., 1997). However, the two probes used here did not necessarily measure the extent of N-lobe opening. The small angular change with respect to the fibre axis does not exclude the possibility of an azimuthal motion around the axis, which may result in a substantial opening in the N-lobe. To characterise this, further investigation using probes on other sites of cTnC are needed.

The similar Ca^{2+} sensitivity for force production and cTnC structural change at either SL1.9 or 2.3 μm was consistent with our group's previous experiments (Sun *et al*., 2009), in which the $[Ca^{2+}]$ for half maximum force production and half cTnC structural change at SL 2.1 μm was not significantly different. The similarity was not affected by SL. The Ca^{2+} sensitivity for both force and cTnC structural change increased similar amounts as SL increased from 1.9 to 2.3 μm. Thus, with the increasing SL, the increased Ca^{2+} sensitivity for force, as one of the two outcomes of LDA, was linearly related to the increasing Ca^{2+} sensitivity for cTnC structural change.

In conclusion, the present results are to a large extent consistent with the previous studies of LDA. We have shown a ~40% increase in the maximum Ca^{2+}-activated force upon SL increasing from 1.9 μm to 2.3 μm, together with ~0.11 pCa units increase in the Ca^{2+} sensitivity for both force and cTnC structural change. The present results also showed that the SL-dependent increase in the maximum force was not due to the increase in the extent of cTnC structural change upon activation. Yet, the SL-dependent Ca^{2+} sensitivity was very likely to due to the modulation of the Ca^{2+} sensitivity for cTnC structural change in the thin filament. Further investigations in terms of the effect of thick filament in LDA by inhibiting the strong binding of cross-bridges are presented in next chapter.

Chapter 5

Role of Force-generating Cross-bridges in the Regulation of LDA

5.1 Introduction

Previous studies have shown that the SL-dependent modulation of maximum force production largely depends on alterations in the number of force-generating cross-bridges with varied SL (Allen and Kentish, 1985). The role of cross-bridges in the other outcome of LDA — the SL-dependent Ca^{2+} sensitivity, on the other hand, has been of particular interest for researchers lately, yet still remains controversial. Therefore, our next focus moved onto the thick filament, investigating the role of force-generating cross-bridges in the SL-dependent Ca^{2+} sensitivity, determining whether the two outcomes of LDA are regulated by the same mechanism through cross-bridges.

In our group's previous study (Sun *et al*., 2009), the formation of force-generating cross-bridges was inhibited using a myosin binding inhibitor — blebbistatin. The results have shown that the widely-accepted concept of myosin binding switching on the thin filaments (keeping Tm in the clear position, thus favouring a Tn conformation with higher Ca^{2+} affinity) only occurred in rigor-like conditions. Under physiological conditions, the thin filament activation is driven by Ca^{2+} binding-induced cTn structural change, which leads to Tm movement and cross-bridges formation. Also, inhibition of active force by blebbistatin slightly reduced the Ca^{2+} sensitivity, with no significant effect in the cooperativity of cTnC structural change and force production upon activation. These results suggested that the highly cooperative Ca^{2+} regulation of cardiac muscle contraction is not due to the force-generating cross-bridges, but an intrinsic property of the thin filaments — the coupling between Tm molecules in adjacent RUs along the thin filament. Thus, it showed that myosin binding does not contribute significantly in the Ca^{2+} regulation of cardiac contractility.

The conclusions were at variance with the previous ones, which suggested that force-generating cross-bridges play a dominant role in cooperatively regulating the Ca^{2+}-cTnC affinity through controlling the amount of cTnC structural change upon activation (Hofmann and Fuchs, 1987a; Martyn et al., 2001; Wang and Fuchs, 1994).

The discrepancies could be due to the different inhibitors applied in these studies: the 25 µM blebbistatin used in our group's study is a more specific inhibitor than the millimolar vanadate used in the previous studies (Hofmann and Fuchs, 1987a; Martyn et al., 2001; Wang and Fuchs, 1994). Blebbistatin binds to the actin-binding cleft of myosin with high affinity, preventing the strong binding of myosin heads to actin (Allingham *et al*., 2005; Straight *et al*., 2003), inhibiting the ATPase activity of actin-myosin interactions (Kovacs *et al*., 2004), thus inhibiting the active force development in cardiac muscle contraction (Dou *et al*., 2007; Farman *et al*., 2008) (Figure 5.1). Vanadate, on the other hand, has been reported to have non-specific effect on other sarcomeric proteins: it extracts TnC from skeletal muscle (Agianian *et al*., 2004; Allhouse *et al*., 1999), and extracts both cTnC and cTnI from cardiac muscle (Strauss *et al*., 1992). Thus, conclusions drawn from the previous studies using vanadate may not have been entirely due to the inhibition of myosin binding.

Therefore, in this chapter, in order to investigate the role of force-generating cross-bridges in the two outcomes of LDA, especially the SL-dependent Ca^{2+} sensitivity, we examined the Ca^{2+} dependence of cTnC structural change at two SLs — 1.9 and 2.3 µm after inhibiting active force by 25 µM blebbistatin.

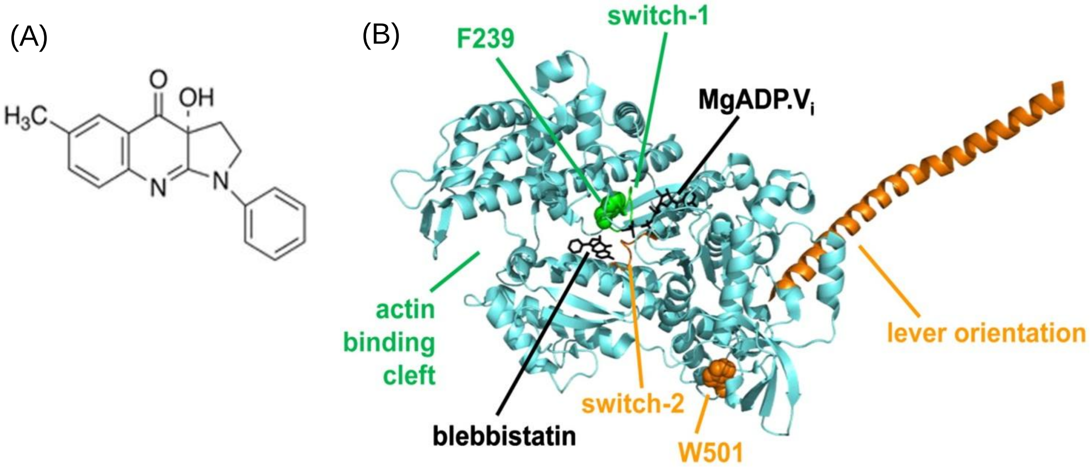

Figure 5.1: (A): Chemical structure of the myosin binding inhibitor — blebbistatin; (B): Protein structure of the location of blebbistatin in cardiac myosin. Figure has been taken from Takacs *et al*. (2010).

5.2 Effect of Force Inhibition on cTnC Orientation

In order to determine the role of force-generating cross-bridges on the orientation change of cTnC upon Ca^{2+} activation, skinned trabeculae exchanged with either BR-cTnC-C or BR-cTnC-E were bathed in experimental solutions with 25 µM blebbistatin to prevent the strong binding of myosin heads to actin. In this chapter, together with the Ca^{2+} dependence of cTnC structural change, the *in situ* orientation of cTnC at two extreme states — relaxation and maximum activation were acquired from the same set of Ca^{2+} titration experiment described in Section 2.5.3. Trabeculae were continuously activated from pCa 9.0 to 4.5 at SL 1.9 µm at first (as the control group). Followed by 30mins of incubation in relaxing solution containing 25 µM blebbistatin, the same fibre was then undergone a second round of Ca^{2+} titration in the presence of blebbistatin. Incubation allows the diffusion of blebbistatin into fibre. After incubation, the maximum activated force was reduced by 94 ± 1% (± SEM, n = 7) for BR-cTnC-C and by 95 ± 1% (± SEM, n = 8) for BR-cTnC-E compared to that in the absence of blebbistatin. As described in Chapter 4, the orientation changes of cTnC were determined from the fluorescence polarization of the BR dipole attached along C- or E-helix of cTnC using F*IS*S, and was described by order parameters $<P_2>$ and $<P_4>$. A Gaussian model was used to acquire the mean axial angle θ_f and standard deviation σ_g of these dipole orientation distributions (data reported in Table 5.1). $<P_2>$-pCa relationship was fit by Hill equation for each fibre with and without blebbistatin. The curve was set through the maximum and minimum of $<P_2>$ values.

5.2.1 Effect of Force Inhibition on the *In Situ* Orientation of cTnC

In agreement with the results from last chapter (Table 4.4), upon maximum activation, both the C- and E-helices of cTnC were slightly shifted towards more perpendicular conformations with respect to the trabecular axis at SL 1.9 µm. The orientation change was indicated by a decrease in $<P_2>$ value ($\Delta<P_2>$) of 0.076 ± 0.003 (± SEM, n = 7) for the C-helix probe and 0.089 ± 0.006 (± SEM, n = 8) for the E-helix probe. These reductions in $<P_2>$ values were consistent with the small increases in θ_f of 3.8 ± 0.2° (± SEM, n = 7) and 4.6 ± 0.4° (± SEM, n = 8) for the C- and E-helix probe, respectively (Table 5.1).

Inhibition of active force showed some non-significant effect on the orientation of the C-helix at either pCa 9.0 or pCa 4.5. The net angular change from relaxation to maximum activation was depressed after the addition of blebbistatin, indicated by a decrease in either $\Delta<P_2>$ from 0.076 ± 0.003 to 0.066 ± 0.004, or $\Delta\theta_f$ from 3.8 ± 0.2° to 3.3 ± 0.2° (± SEM, n = 7) (Table 5.1 A). The ~0.5° reduction in the total orientation change of the C-helix upon Ca^{2+}-activation after force inhibition was small but statistically significant, suggesting the strong-binding of myosin heads enhances the orientation change of the C-helix upon Ca^{2+}-activation. Additionally, the standard deviation of the Gaussian distribution σ_g for the C-helix probe showed no significant change either upon activation or in the presence of blebbistatin (Table 5.1 A).

Unlike the C-helix, the orientation of the E-helix has been reported to be more sensitive to the feedback from myosin heads binding (Sun *et al*., 2009). The conformation of the E-helix at both relaxation and maximum activation was perturbed by active force inhibition. As presented in Table 5.1 B, blebbistatin increased $<P_2>$ significantly at both pCa 9.0 and pCa 4.5 causing a decrease in θ_f from ~44° to ~43° at relaxing and from ~49° to ~47° at activating state. These results showed that the inhibition of myosin heads binding induced a shift in the E-helix towards a more parallel conformation with respect to fibre axis. The decrease in θ_f for the E-helix probe was consistent with the previous study by Sun *et al*. (2009). As in the case of the C-helix probe, the overall orientation change for the E-helix upon Ca^{2+}-activation was hindered by the presence of blebbistatin as well: $\Delta<P_2>$ was reduced from 0.089 ± 0.006 to 0.075 ± 0.004 (± SEM, n = 8), whilst $\Delta\theta_f$ decreased by about 0.8° to 3.8 ± 0.2°(± SEM, n = 8). Likewise, there was no significant change in the E-helix probe dispersion, σ_g, either.

Table 5.1: Parameters for the effect of force-generating cross-bridges on cTnC *in situ* orientation change. (A): C-helix probe experiments; (B): E-helix probe experiments. Order parameters <P_2> and <P_4> were obtained at pCa 9.0 and 4.5 using F*IS*S. θ_f and σ_g respectively indicate the peak angle and standard deviation of the Gaussian orientation distribution of the probe angle with respect to the fibre axis (indicated in the text and Section 2.4). Mean ± SEM. Δ is the difference of each parameter between pCa9.0 and pCa4.5. n is the number of trabeculae in experiments. Comparison: paired two-tailed student t-test between no blebbistatin and 25 µM blebbistatin (statistical significance * $p<0.05$, ** $p<0.01$, ***$p<0.001$, ****$p<0.0001$).

(A)

C-helix	**1.9 µm**				**1.9 µm+Blebbistatin**			
	<P_2>	**<P_4>**	**Θ_f (°)**	**σ_g (°)**	**<P_2>**	**<P_4>**	**Θ_f (°)**	**σ_g (°)**
pCa9.0	0.086 ± 0.002	-0.140 ± 0.018	52.7 ± 0.2	18.3 ± 0.9	0.081 ± 0.005	-0.147 ± 0.015	52.9 ± 0.3	17.9 ± 0.8
pCa4.5	0.010 ± 0.002	-0.138 ± 0.020	56.5 ± 0.3	17.9 ± 1.1	0.014 ± 0.002	-0.135 ± 0.015	56.2 ± 0.2	18.0 ± 0.8
Δ	0.076 ± 0.003	-0.002 ± 0.006	-3.8 ± 0.2		0.066 ± 0.004**	-0.011 ± 0.005	-3.3 ± 0.2*	
n	7							

(B)

E-helix	**1.9 µm**				**1.9 µm+Blebbistatin**			
	<P_2>	**<P_4>**	**Θ_f(°)**	**σ_g (°)**	**<P_2>**	**<P_4>**	**Θ_f(°)**	**σ_g (°)**
pCa9.0	0.258 ± 0.009	-0.073 ± 0.013	44.1 ± 0.5	20.0 ± 0.6	0.280 ± 0.010***	-0.080 ± 0.011	43.1 ± 0.5***	19.0 ± 0.5
pCa4.5	0.169 ± 0.007	-0.116 ± 0.010	48.7 ± 0.3	19.0 ± 0.5	0.205 ± 0.006****	-0.126 ± 0.012	46.9 ± 0.3****	18.1 ± 0.6
Δ	0.089 ± 0.006	0.043 ± 0.010	-4.6 ± 0.4		0.075 ± 0.004**	0.046 ± 0.009	-3.8 ± 0.2**	
n	8							

Thus, the results indicate that inhibiting the formation of force-generating cross-bridges significantly affects the net angular change in both helices of cTnC upon activation. In good agreement with the studies reported by Sevrieva (2014), these results highlight the important role of cross-bridges in stabilising the conformational change of cTnC. Investigations by Zhou *et al*. (2012) have shown the strong binding of myosin heads stabilised the association of the switch peptide of cTnI to the hydrophobic patch on cTnC by keeping the inhibitory region off of actin via pushing Tm, thus shifting the equilibrium towards an open conformation for the N-lobe of cTnC. Detailed data are summarised in Table 5.1. Figure 5.2 gives a more direct comparison of the *in situ* orientation transitions of the C and E-helix of cTnC from relaxation to maximal activation in the absence and presence of blebbistatin.

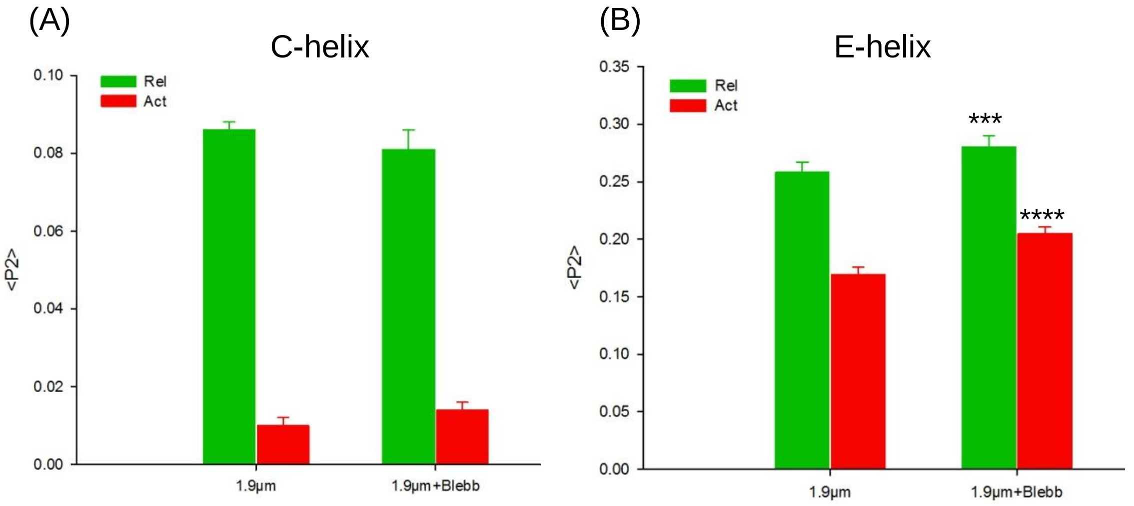

Figure 5.2: Effect of active force inhibition on cTnC *in situ* orientation. (A): C-helix probe; (B): E-helix probe. Green and red bar in each set represent $<P_2>$ value at relaxation (pCa 9.0) and maximum activation (pCa 4.5), respectively. First set in each graph is before the addition of blebbistatin, second is in the presence of blebbistatin. SL has been set to 1.9 µm in this experiment. Error bars denote SEM. n = 7 for BR-cTnC-C and n = 8 for BR-cTnC-E. Statistical significance of differences between the $<P_2>$ values in the absence and presence of blebbistatin for each helix probe was assessed using paired two-tailed student t-test: ***p< 0.001, ****p<0.0001 ($<P_2>$ values in Table 5.1).

5.2.2 Effect of Force Inhibition on the Ca^{2+} Dependence of cTnC Orientation

The Ca^{2+} dependence of cTnC orientation change was examined using the titration experiments. As shown in Figure 5.3 A, active force inhibition had a tendency of reducing $<P_2>$ value at the lower range of [Ca^{2+}] (pCa 9.0 to pCa 5.5), reflected in a small increasing in axial angle θ_f, whilst shifted the $<P_2>$-pCa curve slightly towards relaxed value at higher [Ca^{2+}] (pCa 5.4 to pCa 4.5). The difference in $<P_2>$ value in the presence of blebbistatin was minimised towards the middle [Ca^{2+}] of the titration. As described in the last section (Section 5.2.1), the overall amplitude of the $<P_2>$-pCa curve for the C-helix probe was diminished in the presence of blebbistatin (Table 5.1 A and Table 5.2 A). Additionally, blebbistatin reduced the Ca^{2+} sensitivity for the C-helix orientation change by decreasing pCa_{50} from 5.40 ± 0.01 to 5.35 ± 0.01, showing a ΔpCa_{50} of -0.06 ± 0.02 pCa units (± SEM, n = 7). There was a minor, but not statistically significant, propensity of reducing the cooperativity of the Ca^{2+}-dependent C-helix orientation change in the presence of blebbistatin. A similar situation was observed in the previous studies by Sun *et al*. (2009), and in the later investigations on BR-cTnC-E.

As explained in last chapter, there were similar additional components in the $<P_2>$-pCa relationship for BR-cTnC-E in both the absence and presence of blebbistatin at subthreshold pCa as well (Figure 5.3 B). The major component of the E-helix orientation change between pCa 6.7 and pCa 4.5 was fitted to the Hill equation.

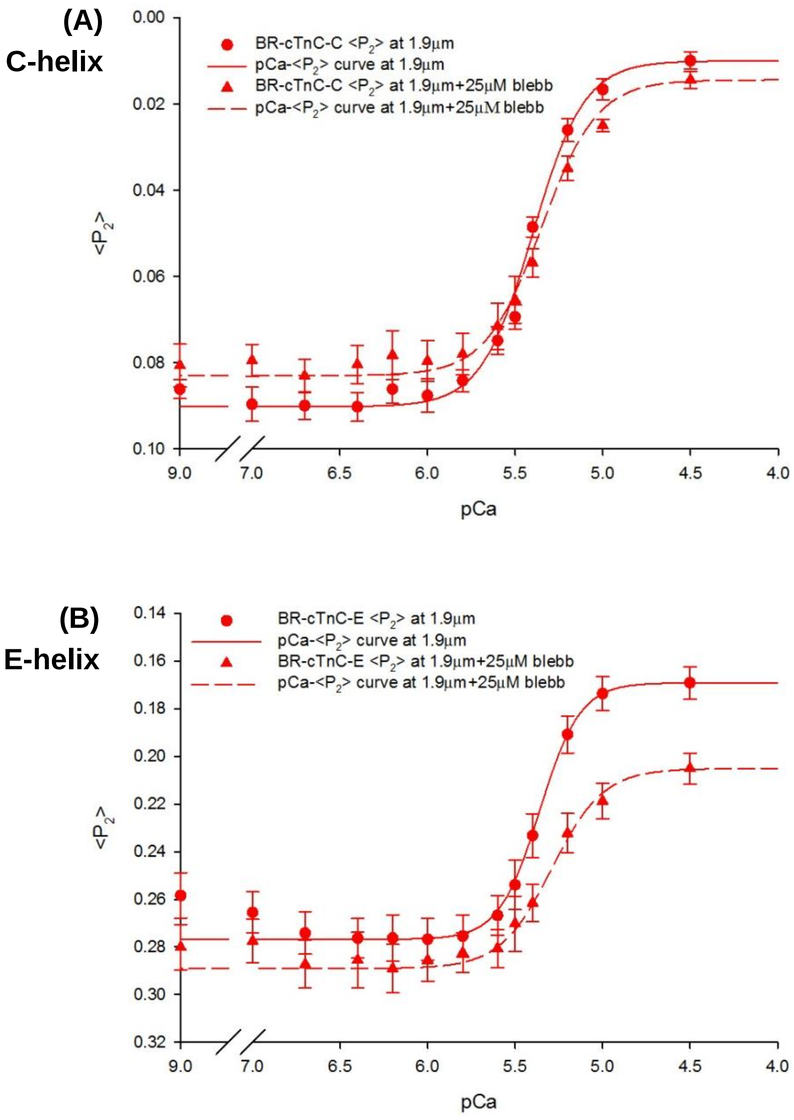

Figure 5.3: Effect of force inhibition on the Ca^{2+} dependence of cTnC orientation change. $<P_2>$ values were plotted as functions of pCa before the addition of blebbistatin (red circles) and in the presence of blebbistatin (red triangles) for A. C-helix; and B. E-helix probe. Red indicates the SL in this experiment has been set to 1.9 µm. Solid and dotted lines respectively indicate the fitting by Hill equation for 1.9 µm and 1.9 µm+25 µM blebbistatin. Since the cause of the additional component for BR-cTnC-E has not been identified, $<P_2>$-pCa curves for the E-helix probe were fitted by fixing the minimum $<P_2>$ to the lowest value. Error bars denote SEM. Trabeculae number n = 7 for the C-helix probe and n = 8 for the E-helix probe. (Hill parameters are provided in Table 5.2).

Table 5.2: Hill parameters for the effect of force inhibition on the Ca^{2+} dependence of cTnC orientation change. A. BR-cTnC-C; B. BR-cTnC-E. Parameters were obtained by individually fitting data for each trabecula in the absence and presence of blebbistatin. Δ<P_2> represents the overall orientation change from relaxation to maximum activation. Mean ± SEM. n is the number of trabeculae used in experiments. Δ indicates the difference in each parameter after adding 25 µM blebbistatin. Comparison: paired two-tailed student t-test before and after adding blebbistatin (statistical significance *p<0.05, ** p<0.01,***p<0.001, ****p<0.0001).

(A)

		C-helix		
		1.9 µm	**1.9 µm+Blebb**	**Δ**
Orientation	**<P_2> pCa9.0**	0.086 ± 0.002	0.081 ± 0.005	
	<P_2> pCa4.5	0.010 ± 0.002	0.014 ± 0.002	
	Δ<P_2>	0.076 ± 0.003	0.066 ± 0.004**	
	pCa$_{50}$	5.40 ± 0.01	5.35 ± 0.01*	-0.06 ± 0.02*
	n_H	2.96 ± 0.27	2.74 ± 0.33	-0.22 ± 0.19
	n	7		

(B)

		E-helix		
		1.9 µm	**1.9 µm+Blebb**	**Δ**
Orientation	**<P_2> pCa9.0**	0.258 ± 0.009	0.280 ± 0.010***	
	<P_2> pCa4.5	0.169 ± 0.007	0.205 ± 0.006****	
	Δ<P_2>	0.089 ± 0.006	0.075 ± 0.004**	
	pCa$_{50}$	5.36 ± 0.02	5.29 ± 0.03***	-0.07 ± 0.01***
	n_H	3.77 ± 0.30	2.96 ± 0.27	-0.81 ± 0.43
	n	8		

The effect of active force inhibition was more pronounced on the orientation of the E-helix. Blebbistatin increased $<P_2>$ significantly over the whole range of pCa, and the increase became more dramatic near the maximum activation ($<P_2>$ increased from 0.258 ± 0.009 to 0.280 ± 0.010 at pCa 9.0 and from 0.169 ± 0.007 to 0.205 ± 0.006 at pCa 4.5, ± SEM, n = 8) (Table 5.2 B). The $<P_2>$-pCa curve shifted downward in the presence of blebbistatin, corresponding to a reduction in the axial angle θ_f by 1°~2° over the whole pCa, consistent with the previous studies by Sun *et al*. (2009). As shown in Figure 5.3 B, the amplitude of the $<P_2>$-pCa curve was decreased by the addition of blebbistatin, as in the case of the C-helix probe, suggesting the important effect of myosin heads binding on the Ca^{2+}-dependent cTnC structural change. Additionally, the Ca^{2+} sensitivity (pCa_{50}) for the E-helix orientation change reduced a similar amount after force inhibition as that of the C-helix probe — ΔpCa_{50} = -0.07 ± 0.01 for BR-cTnC-E (± SEM, n = 8), and ΔpCa_{50} = -0.06 ± 0.02 for BR-cTnC-C (± SEM, n = 7). Similarly, a small and non-significant reduction in the steepness of the $<P_2>$-pCa relationship in the presence of blebbistatin was obtained in the E-helix probe as well.

The present results showed a decrease in the Ca^{2+} sensitivity for structural change when the strong binding of myosin heads was disrupted. This is in agreement with the conclusion that the formation of force-generating cross-bridges would enhance the Ca^{2+} sensitivity of thin filaments (Gordon and Ridgway, 1993; Pan and Solaro, 1987). Although the molecular mechanisms are not yet fully understood, an important role of cross-bridges in driving the movement of tropomyosin into the “open state” by stabilising the Ca^{2+}-sensitizing cTnI/cTnC interaction has been proposed to be involved in this effect (Zhou *et al*., 2000; Zhou *et al*., 2012). In agreement with the investigations by Sun *et al*. (2009), there was no significant change (only a minor tendency towards a reduction, see Table 5.2) in the steepness of $<P_2>$-pCa relationships in both helices. These results indicate that the force-generating cross-bridges are not responsible for the cooperativity of the Ca^{2+}-dependent cTnC structural change, suggesting a dominant role of troponin in switching on the thin filaments cooperatively upon Ca^{2+} binding.

5.3 Effect of Force Inhibition on LDA

In order to determine the role of force-generating cross-bridges in LDA, a third round of Ca^{2+} titration was performed at SL 2.3 μm in the presence of blebbistatin. Measurements were taken in the same set of trabeculae as described in previous section, where the native cTnC was exchanged with either BR-cTnC-C or BR-cTnC-E. 25 μM blebbistatin was added in all experimental solutions throughout the titrations to prevent the strong binding of myosin heads to actin. After the 30mins incubation within relaxing solution containing blebbistatin, trabecula was activated continuously from pCa 9.0 to 4.5 in the presence of blebbistatin at SL 1.9 μm (as the control group), followed by another set of Ca^{2+} titration at SL 2.3 μm, to investigate the impact of active force inhibition on the SL dependent changes in cTnC. SL was set before each titration by laser diffraction, and was checked after each series of activation to avoid inadequate measurement due to the deterioration of the diffraction pattern at high [Ca^{2+}].

Overall, three rounds of titration experiments were taken in the permeabilized trabeculae used in this chapter — at SL 1.9 μm without blebbistatin, the addition of blebbistatin at SL 1.9 μm, and at SL 2.3 μm in the presence of blebbistatin. Although multiple activations would cause irreversible damage to the fibre, the inhibition of active force by blebbistatin from the second round of titration should minimise this effect.

5.3.1 Role of Force-generating Cross-bridges in SL's Effect on cTnC *In Situ* Orientation

In the presence of blebbistatin, at both SL 1.9 and 2.3 μm, maximum Ca^{2+}-activation shifted the C-helix towards a more perpendicular conformation with respect to the fibre axis, indicated by a decrease in $<P_2>$ ($\Delta<P_2>$) by 0.066 ± 0.004 at 1.9 μm and

0.059 ± 0.002 (± SEM, n = 7) at 2.3 μm. The reduction in <P_2> equals to a rise in the axial angle θ_f from 52.9 ± 0.3° to 56.2 ± 0.2° ($\Delta\theta_f$ = 3.3° ± 0.2°) at 1.9 μm and from 52.8 ± 0.2° to 55.7 ± 0.1° ($\Delta\theta_f$ = 2.9 ± 0.1°) at 2.3 μm. As shown in Table 5.3 A, while increasing SL from 1.9 μm to 2.3 μm in the presence of blebbistatin did not significantly affect C-helix's orientation at pCa 9.0, it affected the orientation at pCa 4.5 by shifting towards the relaxing value. That is, at maximum activation, <P_2> was increased from 0.014 ± 0.002 to 0.022 ± 0.003 (± SEM, n = 7) in response to SL increasing, corresponding to a small decrease in θ_f by ~0.5°. The present results were similar compared to the earlier investigations in the effect of SL on the C-helix orientation without blebbistatin (Table 4.4 A). However, the amplitude of orientation change from relaxation to maximum activation for the C-helix probe was significantly depressed at SL 2.3 μm after the inhibition of active force, indicated either by Δ<P_2> (from 0.066 ± 0.004 at 1.9 μm to 0.059 ± 0.002 at 2.3 μm) or $\Delta\theta_f$ (from 3.3 ± 0.2° to 2.9 ± 0.1°) (± SEM, n = 7). Interestingly, as observed in the measurements without blebbistatin, SL change alone did not affect the overall orientation change of the C-helix upon Ca^{2+}-activation (Table 4.4 A). Current results therefore indicated that the smaller conformational change in the regulatory head of cTn upon maximum activation at longer SL was likely to be the result of inhibiting the formation of force-generating cross-bridges. Thus, it is reasonable to conclude that certain change in strong-binding myosin heads occurs with SL variation, which interferes with the Ca^{2+}-induced structural change in cTnC. Additionally, no significant change was observed in the standard deviation (σ_g) of the C-helix probe on either maximum activation or SL alteration in the presence of blebbistatin.

Table 5.3: Parameters for the role of force-generating cross-bridges in the effect of SL on cTnC *in situ* orientation. (A): C-helix probe experiments; (B): E-helix probe experiments. Order parameters $<P_2>$ and $<P_4>$ were obtained at pCa 9.0 and 4.5 using F*I*SS. θ_f and σ_g respectively indicate the peak angle and standard deviation of the Gaussian orientation distribution of the probe angle with respect to the fibre axis (indicated in the text and Section 2.4). Mean ± SEM. Δ is the difference of each parameter between pCa 9.0 and pCa 4.5. n is the number of trabeculae in experiments. Comparison: paired two-tailed student t-test between SL 1.9 and 2.3 μm in the presence of blebbistatin (statistical significance $^*p<0.05$, $^{**}p<0.01$).

(A)

C-helix	**1.9 μm+Blebbistatin**				**2.3 μm+Blebbistatin**			
	$<P_2>$	$<P_4>$	Θ_f (°)	σ_g (°)	$<P_2>$	$<P_4>$	Θ_f (°)	σ_g (°)
pCa 9.0	0.081 ± 0.005	-0.147 ± 0.015	52.9 ± 0.3	17.9 ± 0.8	0.081 ± 0.004	-0.157 ± 0.010	52.8 ± 0.2	17.3 ± 0.5
pCa 4.5	0.014 ± 0.002	-0.135 ± 0.015	56.2 ± 0.2	18.0 ± 0.8	0.022 ± 0.003*	-0.147 ± 0.010	55.7 ± 0.1*	17.4 ± 0.5
Δ	0.066 ± 0.004	-0.011 ± 0.005	-3.3 ± 0.2		0.059 ± 0.002*	-0.010 ± 0.002	-2.9 ± 0.1*	
n	7							

(B)

E-helix	**1.9 μm+Blebbistatin**				**2.3 μm+Blebbistatin**			
	$<P_2>$	$<P_4>$	Θ_f (°)	σ_g (°)	$<P_2>$	$<P_4>$	Θ_f (°)	σ_g (°)
pCa 9.0	0.280 ± 0.010	-0.080 ± 0.011	43.1 ± 0.5	19.0 ± 0.5	0.284 ± 0.008	-0.100 ± 0.012*	43.2 ± 0.4	17.9 ± 0.6*
pCa 4.5	0.205 ± 0.006	-0.126 ± 0.012	46.9 ± 0.3	18.1 ± 0.6	0.227 ± 0.006**	-0.127 ± 0.012	45.9 ± 0.3**	17.7 ± 0.6*
Δ	0.075 ± 0.004	0.046 ± 0.009	-3.8 ± 0.2		0.057 ± 0.005**	0.027 ± 0.005*	-2.7 ± 0.3**	
n	8							

The E-helix in the IT arm of troponin had a more parallel orientation with respect to the fibre axis (smaller axial angel θ_f) compared to the C-helix under all conditions (relaxation and maximum activation at both SLs) (Table 5.3). At both SL 1.9 and 2.3 µm in the presence of blebbistatin, maximum Ca^{2+}-activation decreased $<P_2>$ value ($\Delta<P_2>$) by 0.075 ± 0.004 at 1.9 µm and 0.057 ± 0.005 (± SEM, n = 8) at 2.3 µm. The reduction in $<P_2>$ can be translated to an increase in θ_f ($\Delta\theta_f$) by 3.8 ± 0.2° at 1.9 µm and 2.7 ± 0.3° (± SEM, n = 8) at 2.3 µm, as a result of the perpendicular shifting of the E-helix upon activation (Table 5.3 B). Increasing SL to 2.3 µm in the presence of blebbistatin induced a small but significant change in the active orientation of the E-helix — decreased θ_f at pCa 4.5 from 46.9 ± 0.3° to 45.9 ± 0.3° (± SEM, n = 8), indicating the perpendicular shifting of the E-helix upon maximum activation was reduced at longer SL. On the other hand, the relaxed orientation of the E-helix did not appear to change with SL. As a consequence, increasing SL in the presence of blebbistatin perturbed the amplitude of E-helix orientation change from pCa 9.0 to pCa 4.5 by decreasing $\Delta<P_2>$ significantly from 0.075 ± 0.004 to 0.057 ± 0.005 (or $\Delta\theta_f$ from 3.8 ± 0.2° to 2.7 ± 0.3°, ± SEM, n = 8), similar with the situation obtained for BR-cTnC-C. Previous measurements in the absence of blebbistatin have shown the net angular change of the E-helix was not affected by SL change either, as in the case of BR-cTnC-C (Table 4.4 B). Thus, it must be the inhibition of active force that compromises the structural change in cTnC corresponding to SL increasing. Moreover, probe dispersion σ_g for BR-cTnC-E had a minor decrease at both relaxation and maximum activation in response to sarcomere lengthening in the presence of blebbistatin, which might be the reason of a slightly more stabilised conformation of the E-helix at longer SL. Figure 5.4 gives a more direct view of the *in situ* orientation change in cTnC during relaxation and maximal activation at both SLs in the presence of blebbistatin.

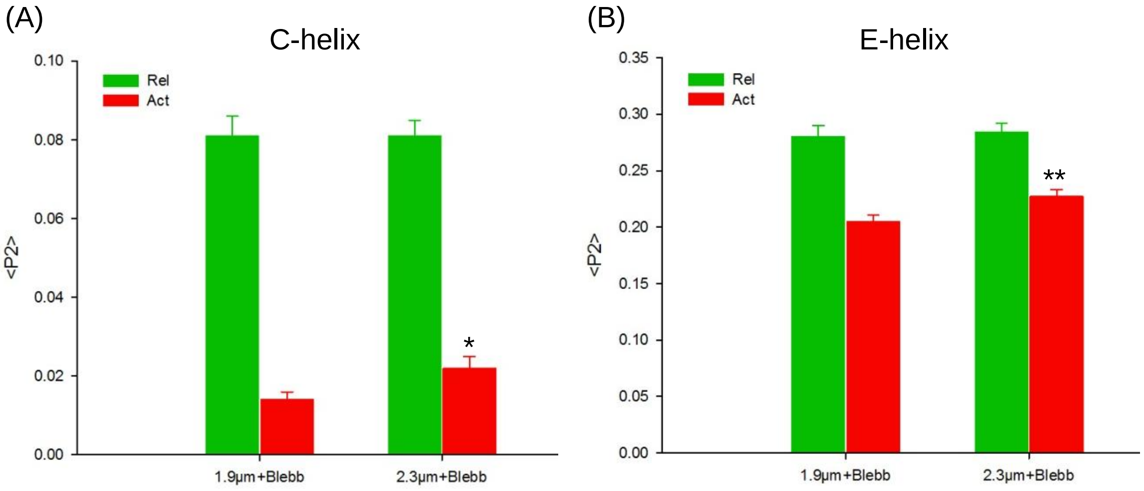

Figure 5.4: Role of force-generating cross-bridges in SL's effect on cTnC *in situ* orientation. (A): BR-cTnC-C; (B): BR-cTnC-E. Green and red bar in each set respectively represent $<P_2>$ value at relaxation (pCa 9.0) and maximum activation (pCa 4.5). First set in each graph is at SL 1.9 µm, second one at 2.3 µm, both in the presence of blebbistatin. Error bars denote SEM. n = 7 for the C-helix probe and n = 8 for the E-helix probe. Statistical significance of differences between the $<P_2>$ values from two SLs in the presence of blebbistatin for each helix probe was assessed using paired two-tailed student t-test: *p< 0.05, **p<0.01 ($<P_2>$ values are presented in Table 5.3).

5.3.2 Role of Force-generating Cross-bridges in the SL-dependent Ca^{2+}-regulation

The effect of SL variation on the Ca^{2+} dependence of cTnC orientation change in the presence of blebbistatin was investigated using the same two sets of Ca^{2+} titration experiments described above — SL 1.9 µm+blebbistatin and SL 2.3 µm+blebbistatin. The data were described by individual Hill fitting, and the $<P_2>$-pCa curve was set through the maximum and minimum $<P_2>$ values, whilst pCa_{50} and n_H were obtained from the average of each individual fitting (Table 5.4).

Table 5.4: Hill parameters for the role of force-generating cross-bridges in the SL-dependent Ca^{2+} regulation. (A): C-helix probe experiments; (B): E-helix probe experiments. Parameters were obtained by individually fitting data for each trabecula at SL 1.9 μm and 2.3 μm respectively in the presence of blebbistatin. $\Delta\langle P_2 \rangle$ represents the overall orientation change in cTnC from relaxation to maximum activation. Mean ± SEM. n is the number of trabeculae used in experiments. Δ indicates the difference in each parameter from SL 1.9 to 2.3 μm in the presence of blebbistatin. Comparison: paired two-tailed student t-test between two SLs in the presence of blebbistatin (statistical significance * $p<0.05$, ** $p<0.01$).

(A)

	C-helix			
		1.9 μm+Blebb	**2.3 μm+Blebb**	**Δ**
Orientation	**$\langle P_2 \rangle$ pCa 9.0**	0.081 ± 0.005	0.081 ± 0.004	
	$\langle P_2 \rangle$ pCa 4.5	0.014 ± 0.002	0.022 ± 0.003*	
	$\Delta\langle P_2 \rangle$	0.066 ± 0.004	0.059 ± 0.002*	
	pCa_{50}	5.35 ± 0.01	5.42 ± 0.02*	0.07 ± 0.02*
	n_H	2.74 ± 0.33	2.22 ± 0.17	-0.52 ± 0.27
	n	7		

(B)

	E-helix			
		1.9 μm+Blebb	**2.3 μm+Blebb**	**Δ**
Orientation	**$\langle P_2 \rangle$ pCa 9.0**	0.280 ± 0.010	0.284 ± 0.008	
	$\langle P_2 \rangle$ pCa 4.5	0.205 ± 0.006	0.227 ± 0.006**	
	$\Delta\langle P_2 \rangle$	0.075 ± 0.004	0.057 ± 0.005**	
	pCa_{50}	5.29 ± 0.03	5.36 ± 0.02**	0.07 ± 0.02**
	n_H	2.96 ± 0.27	2.70 ± 0.24	-0.26 ± 0.24
	n	8		

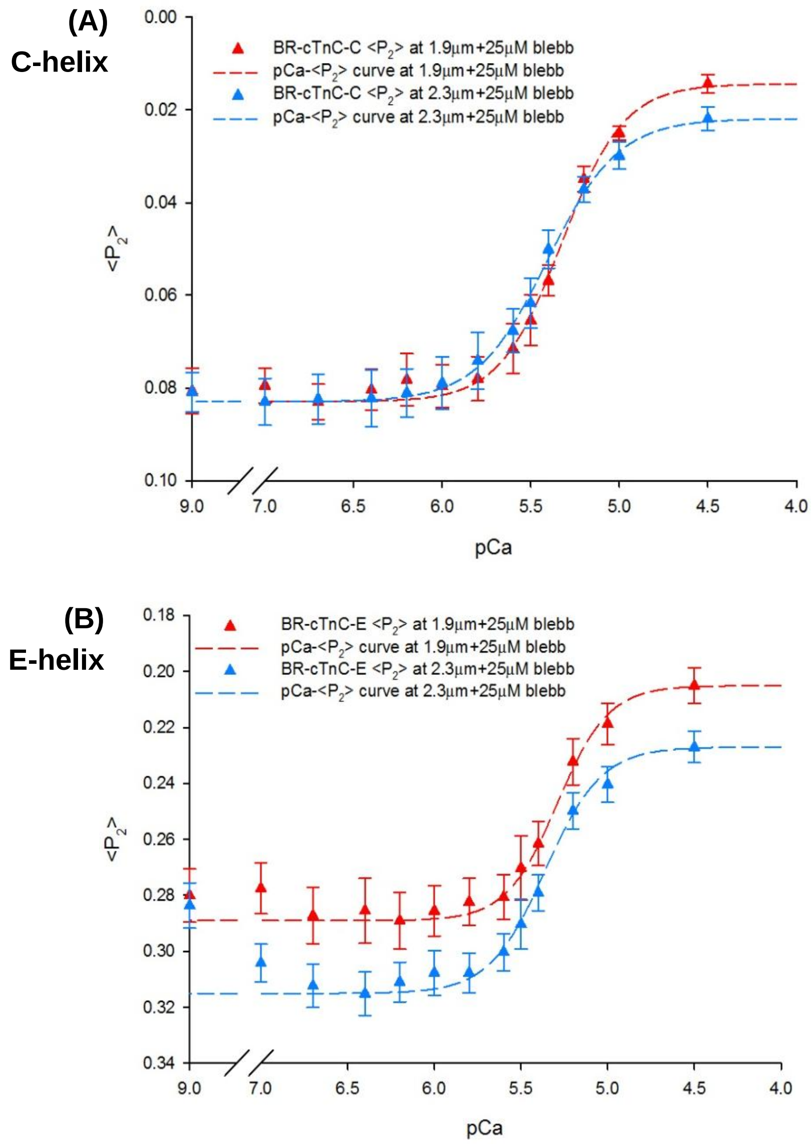

Figure 5.5: Effect of force inhibition on the Ca^{2+} dependence of cTnC orientation change. $<P_2>$ values were plotted as functions of pCa at SL 1.9 µm (red triangles) and 2.3 µm (blue triangles) in the presence of blebbistatin for A. C-helix; and B. E-helix probe. Dotted lines indicate the Hill fitting after adding blebbistatin. Error bars denote SEM. Trabeculae number n = 7 for BR-cTnC-C and n = 8 for BR-cTnC-E. (Hill parameters are provided in Table 5.4).

As shown in Figure 5.5 A, both curves had similar baselines at the lower range of $[Ca^{2+}]$, whilst the difference became biggest at pCa 4.5, indicating that stretching SL from 1.9 µm to 2.3 µm in the presence of blebbistatin shifted the curve towards more relaxed conformation at pCa 4.5 with no significant effect at pCa 9.0. Unlike in the absence of blebbistatin, SL elongation in the presence of blebbistatin depressed the overall orientation change of the C-helix probe from relaxation to maximum activation (as demonstrated in last section, see Table 5.3 A and 5.4 A). Additionally, the present results showed a significant increase in the Ca^{2+} sensitivity for C-helix orientation change with the increasing SL, indicated by an increase in the pCa_{50} from 5.35 ± 0.01 at 1.9 µm to 5.42 ± 0.02 at 2.3 µm, with a ΔpCa_{50} of 0.07 ± 0.02 pCa units (± SEM, n = 7) in response to SL elongation after active force inhibition (Table 5.4 A). Our results showed that the SL-dependent increase in the Ca^{2+} sensitivity could still happen, even without the presence of cross-bridges, though this increase was smaller than that in the absence of blebbistatin (~0.11 pCa units, Table 4.5 A). Moreover, there was a small, but not significant, tendency of reducing the cooperativity of the Ca^{2+} regulation at longer SL in the presence of blebbistatin (Δn_H = -0.52 ± 0.27, ± SEM, n = 7).

Similar to the measurements described previously for BR-cTnC-E, an additional component was observed here for the orientation change of the E-helix in the subthreshold range of pCa (pCa 9.0 to 6.7) (Figure 5.5 B). This small component of the $<P_2>$-pCa relation for the E-helix probe was found at both SLs in the presence of blebbistatin. To ease analysis, the major component of the E-helix orientation change between pCa 6.7 and 4.5 was fitted to the Hill equation.

As shown in Figure 5.5, stretching SL from 1.9 µm to 2.3 µm in the presence of blebbistatin had a more pronounced effect on the E-helix of cTnC — $<P_2>$ value was increased significantly over the whole range of pCa (pCa 7.0 to 4.5), shifting the $<P_2>$-pCa curve downward. Although SL elongation in the presence of blebbistatin shifted the curve towards bigger $<P_2>$ value at each pCa, the relaxed orientation of the E-helix at pCa 9.0 was not affected (Table 5.3 B and 5.4 B). The net $<P_2>$ change from relaxation to maximum activation ($\Delta <P_2>$) decreased upon SL stretching, different from what has been seen in the absence of blebbistatin. Additionally, stretching SL in the presence of blebbistatin increased the Ca^{2+} sensitivity for the E-helix orientation change pCa_{50} from 5.29 ± 0.03 to 5.36 ± 0.02 (ΔpCa_{50} = 0.07 ± 0.02, ± SEM, n = 8, Table 5.4 B). The SL-dependent increase in the Ca^{2+} sensitivity for the E-helix orientation change was almost identical to the ΔpCa_{50} reported above for the C-helix probe (ΔpCa_{50} = 0.07 ± 0.02 pCa units (± SEM, n = 7, Table 5.4 A)), which was less than that in the absence of blebbistatin (~0.11 pCa units, see Table 4.5). These results suggested that the force-generating cross-bridges might not be an essential component in the SL-dependent Ca^{2+} sensitivity in LDA. It might be involved in increasing the Ca^{2+} sensitivity with increased SL as a positive feedback factor. Moreover, there was a tendency towards reducing the cooperativity of the Ca^{2+} dependent E-helix orientation change (Table 5.4 B). However, it was not statistically significant.

Taken together, the present results showed that the inhibition of active force disturbed the effect of SL elongation on both cTnC *in situ* orientation and the Ca^{2+} dependence of cTnC orientation. Increasing SL in the presence of blebbistatin decreased the amplitude of cTnC orientation change by shifting the active orientation slightly towards the relaxed state. The effect was in support of the theory that the formation of the force-generating cross-bridges stabilizes the conformational changes in cTnC upon maximum Ca^{2+}-activation by favouring the attachment of the switch peptide of cTnI to cTnC. More importantly, blebbistatin decreased the SL-dependent increase in the Ca^{2+} sensitivity for both helices' orientation change from ~0.11 pCa units to ~0.07 pCa units, implying the importance of force-generating cross-bridges in the regulation of LDA. However, the present results also showed that even without force-generating cross-bridges, there was still SL-dependent Ca^{2+} sensitivity in the thin filament, indicating that strongly bound myosin heads might not be the essential component in the length dependent Ca^{2+} sensitivity in LDA. The thin filament, on the other hand, is more likely to be the centre of transmitting the signal of sarcomere lengthening to regulate the Ca^{2+} sensitivity for force production in LDA.

5.4 Discussion

5.4.1 Impact of Force-generating Cross-bridges on Ca^{2+} regulation

Strong cross-bridge attachment has long been considered to be the primary mediator of Ca^{2+} binding properties through switching on the thin filament activation (Bremel and Weber, 1972). It was suggested that the actomyosin interaction was able to hold Tm in a position where the high Ca^{2+} binding affinity to cTnC was favoured. Yet its dominant role has been challenged in more recent investigations, which suggested such a mechanism can only occur in rigor conditions, not under physiological conditions (Sun *et al*., 2009). Under physiological conditions, the thin filament activation is driven by Ca^{2+} binding-induced cTn structural change, which leads to Tm movement and cross-bridges formation.

In this chapter, we first examined the impact of force-generating cross-bridges on the Ca^{2+}-regulated activation by inhibiting the formation of them at SL 1.9 μm. We used the myosin binding inhibitor — blebbistatin to prevent the strong binding of myosin heads to actin and reduced the active force development by ~94%. Active force inhibition depressed the orientation change in the C-helix of cTnC from relaxation to maximum activation by ~0.5°, with the effect being slightly bigger in the E-helix (~0.8°). Although these net angular reductions were small, they were significant and highly reproducible. The reduction in the amplitude of cTnC structural change after active force inhibition were in good agreement with the previous investigations by our group members (Sevrieva, 2014; Sun *et al*., 2009), implying an impact of the force-generating cross-bridges on the structural change of cTnC upon Ca^{2+}-activation. The addition of blebbistatin also reduced the Ca^{2+} sensitivity for both helices' orientation change by a similar amount (~0.07 pCa units), suggesting the force-generating cross-bridges may be involved in modulating the Ca^{2+} sensitivity through interfering with the structural change in cTnC upon activation.

As reported by Zhou *et al*. (2012), the strong binding of myosin heads to actin stabilized the interaction between the switch peptide of cTnI and the N-lobe of cTnC. The attachment of the switch region of cTnI to cTnC is known to further open the N-lobe of cTnC from studies in isolated cTnC (Li *et al*., 1999; Sia *et al*., 1997). Thus, the strong cross-bridge attachments may be necessary to support the fully open conformation of cTnC by keeping cTnI off of actin and stabilizing the cTnI/cTnC interaction. According to Johnson *et al*. (1980), attachment of the switch peptide of cTnI to cTnC substantially increased the Ca^{2+} binding affinity to cTnC. Therefore, the reduction in the Ca^{2+} sensitivity and the structural change of cTnC after inhibiting the formation of cross-bridges may be due to the fewer cTnI/cTnC interactions, as a result of lacking support from strong binding cross-bridges.

In addition, no significant difference was observed in the cooperativity of the Ca^{2+} regulation (indicated by n_H) after force inhibition, consistent with the results in Sun *et al*. (2009), which recognised the cooperative Ca^{2+} regulation is not due to the force-generating cross-bridges, but an intrinsic property of the thin filaments.

5.4.1.1 Comparison with Previous Studies

The molecular mechanisms linking the myosin heads binding with the Ca^{2+} sensitivity modulation have been investigated extensively over these years. Our current conclusion, that the force-generating cross-bridges may be involved in regulating the Ca^{2+} sensitivity through stabilizing the structural change in cTnC upon activation, was in agreement with the previous studies.

Experiments by Hofmann and Fuchs (1987b) used a phosphate analog vanadate to inhibit the strong binding of myosin to actin. Their results showed that the amount of Ca^{2+} binding to cTnC was a function of not only the $[Ca^{2+}]_i$, but also the force development. Active force inhibition by vanadate reduced Ca^{2+} binding, i.e. Ca^{2+}-cTnC affinity, significantly. Subsequent study by Martyn *et al*. (2001) showed that this strong binding cross-bridges-induced Ca^{2+}-cTnC affinity change was accompanied by changes in cTnC conformation. Both the amplitude of cTnC structural change and the Ca^{2+} sensitivity were reduced after inhibiting actomyosin interaction. These studies indicated the importance of force-generating cross-bridges in modulating Ca^{2+} binding properties, possibly through modulating the structural changes in cTnC upon Ca^{2+}-activation.

However, the results from Martyn *et al*. (2001) have shown that inhibition of force generation caused both the structural change and the Ca^{2+} sensitivity for this structural change to decrease in the N-lobe of cTnC, while only the Ca^{2+} sensitivity decreased for the C-lobe, with no significant change in the structure. These were at variance with our conclusions that force inhibition decreased the amplitude of both the C- and E-helix orientation change. The main difference between our present work and Martyn *et al*. (2001) is that we used bifunctional probes to label specific cTnC helices to measure the structural change in cTnC, whilst they used monofunctional probes. Bifunctional probe cross-links with two cysteine residues at sites chosen from the static structure. The averaged orientation of the probe dipole is expected to be parallel to a line joining the two cysteines. Whilst with monofunctional probe, the orientation and motion of the probe with respect to the attached protein domain is unknown, and different results were obtain with different probe sites (Martyn *et al*., 2001; Putkey *et al*., 1997). Therefore, experiment results from bifunctional probes are likely to be more reliable.

Additionally, in the studies carried out by Lehrer (1994); McKillop and Geeves (1993), three thin filament states, associated with two cross-bridges states, have been proposed to explain the role of the cross-bridges in the thin filament activation. Although the movement of Tm is initially determined by Ca^{2+} binding to cTnC, the model postulates that the isomerisation transition from weak to strong cross-bridge attachments pushes Tm further into the groove of the actin filament, allowing the formation of more force-generating cross-bridges. It was suggested that the second dislocation of Tm driven by strong-binding cross-bridges was highly cooperative via the propagation by neighbouring RUs, which promoted further Ca^{2+} binding to the adjacent cTnCs, along with increasing conformational changes in cTnC (Fuchs and Martyn, 2005; Regnier et al., 2002). However, both our current results and those from our group's previous publications have shown no significant difference in the n_H for the Ca^{2+} dependence of cTnC structural change after inhibiting the strong-binding of myosin to actin by blebbistatin. These results provided strong evidence that even if the force-generating cross-bridge did push Tm to move further along the actin filament, they are not responsible for the cooperativity of Ca^{2+} binding, which must be intrinsic to the thin filaments.

Current results promote a link between the force-generating cross-bridges and the Ca^{2+} dependence of cTnC structural change. Disruption of strong binding cross-bridges hindered the Ca^{2+}-induced cTnC structural change and the Ca^{2+} sensitivity for this structural change without interfering with the cooperativity. Thus, the formation of strong binding cross-bridges may be involved in regulating the Ca^{2+} sensitivity through stabilising the Ca^{2+}-sensing cTnI/cTnC interactions, which in turn, stabilises the conformational change in cTnC in Ca^{2+}-activation.

5.4.2 Role of Force-generating Cross-bridges in LDA

Our results presented in Chapter 4 have shown a ~40% increase in the maximum force production in response to SL increasing from 1.9 to 2.3 μm, which was not due to an increase in the amplitude of cTnC structural change upon activation. Over the years, the molecular basis that underlies the increasing force production upon increased SL has been focused on the effect of force-generating cross-bridges. Studies with skinned cardiac fibres showed that the increase in force development was accompanied by a SL-dependent increase in the number of force-producing cross-bridges in the sarcomere (Allen and Kentish, 1985; Wannenburg et al., 2000; Wannenburg et al., 1997). Yet the role of the cross-bridges in the other outcome of LDA — the SL-dependent Ca^{2+} sensitivity, still remained controversial.

In our results reported in Chapter 4, we concluded that with the increasing SL, the increasing Ca^{2+} sensitivity for force was very likely to be modulated by increasing the Ca^{2+} sensitivity for cTnC structural change. In this chapter, we focused on investigating the role of the force-generating cross-bridges in LDA, especially the SL-dependent Ca^{2+} sensitivity, by increasing SL from 1.9 to 2.3 μm in the presence of the myosin-binding inhibitor — blebbistatin.

Unlike in the absence of blebbistatin, after active force inhibition, there was a decrease in the amplitude of cTnC structural change in response to SL increasing, together with a reduced SL-dependent difference in the Ca^{2+} sensitivity between short and long SL (~0.07 pCa units in the presence of blebbistatin *versus* ~0.11 pCa units without blebbistatin). About one third of the length-dependent Ca^{2+} sensitivity increase was hindered after myosin binding inhibition, suggesting the force-generating cross-bridges may be partly involved in mediating the Ca^{2+} sensitivity with SL. More importantly, our results showed that the SL-dependent modulation of the Ca^{2+} sensitivity can still happen even without the presence of the force-generating cross-bridges, indicating that cross-bridges may not be the essential component in the length-dependent Ca^{2+} sensitivity in LDA.

Our results from the last chapter have shown that the total amplitude of cTnC structural change was not affected by SL. Thus, the reduction in cTnC conformational change reported here—at SL 2.3 μm in the presence of blebbistatin, indicated the strong binding of myosin to actin was fairly important to hold the structural change in cTnC to be not affected by SL variation. As discussed in last section, the interaction of myosin heads to actin stabilizes the conformational change in cTnC upon activation by favouring the attachment of cTnI to cTnC (Zhou *et al*., 2012). Therefore, without the support from the force-generating cross-bridges, SL alteration may indirectly affect the opening conformation in cTnC, probably through the interactions between titin and the thin filament. In turn, the less conformational change in cTnC caused by cross-bridges disruption may be the reason of the reduced Ca^{2+} sensitivity difference between SLs. Our results suggested that the strong binding cross-bridges may be partly involved in the mediation of Ca^{2+} sensitivity through the feedback from stabilising the conformational change in cTnC.

In conclusion, increasing SL after the disruption of the force-generating cross-bridges caused a small but significant decrease in the total amplitude of cTnC structural change upon activation, in association with reduced SL-dependent Ca^{2+} sensitivity. Our results suggested the effect of strong myosin binding may play a role, but not essential, in modulating the SL-dependent Ca^{2+} sensitivity. The SL-dependent

Ca^{2+} sensitivity can still occur even without the presence of force-generating cross-bridges. Therefore, we conclude that the two outcomes of LDA are very likely due to two independent pathways: the control centre for regulating the SL-dependent Ca^{2+} sensitivity locates on the thin filament by cTnC, and that for regulating the SL-dependent maximum force located on the thick filament by force-generating cross-bridges. In the meantime, the thick filament cross-bridges may provide a positive feedback to support the increasing Ca^{2+} sensitivity with increasing SL, possibly by stabilizing the structural change in cTnC upon Ca^{2+}-activation.

5.4.2.1 Comparison with Previous Studies

The role of force-generating cross-bridges in LDA has been investigated for a very long time. Although it has been well-established that the SL-dependent change in the cross-bridges (either the increasing number or the increasing capacity for force generation) is mostly responsible for the SL-dependent increase in maximum force, whether cross-bridges play a part in the SL-dependent Ca^{2+} sensitivity still remained debatable over years.

In this study, we found that in the presence of blebbistatin, the SL-dependent increase in the Ca^{2+} sensitivity still happened, although this increase was smaller than what we have reported in the previous experiments without blebbistatin. We concluded that the force-generating cross-bridges may not be the essential component in the SL-dependent Ca^{2+} sensitivity. The strong binding of myosin to actin may provide a positive feedback to support the increasing Ca^{2+} sensitivity with increased SL by stabilizing the structural change in cTnC upon activation. The present conclusion is at variance with that from the previous studies, which suggested that myosin binding is essential in changing the Ca^{2+} sensitivity with SL.

In the investigations carried out by Hofmann and Fuchs (1987a), suppressing the actomyosin interaction with 1.0mM vanadate eliminated the SL-dependent Ca^{2+} binding to cTnC. They showed that the SL-dependent Ca^{2+} sensitivity in LDA was associated with a SL-dependent binding affinity of the Ca^{2+} to cTnC. This SL-dependent Ca^{2+} binding disappeared when myosin binding was inhibited by pre-treatment with vanadate. Their results indicated that it was the length-dependent number of cross-bridges, not the SL *per se*, that determines the SL-dependent Ca^{2+} sensitivity. In the current study, we found the SL-dependent Ca^{2+} sensitivity still existed after active force inhibition, though it reduced about one third compared to that in the presence of attached cross-bridges.

The main difference between our study and the one presented above is the various myosin-binding inhibitors applied in the experiments (25mM blebbistatin in this study *vs* 1.0mM vanadate in Hofmann and Fuchs (1987a)). As described in Section 5.1, compared to the non-specific effect of vanadate may have on other sarcomeric proteins, blebbistatin is a more potent inhibitor that binds to the actin-binding cleft of myosin specifically. Thus, the effects of vanadate reported in the previous studies may not have been solely due to its inhibition of attachment of cross-bridges.

There was an alternative theory in terms of the role of force-generating cross-bridges in LDA, which suggested the strong binding of myosin to actin was secondary to the SL-dependent modulation of the Ca^{2+} sensitivity. Thus even if the number of cross-bridges does increase with SL, it does not mediate the length-dependent Ca^{2+} sensitivity (Farman *et al*., 2010). Blebbistatin was also used to inhibit the force-generating cross-bridges in this study. Their results showed the addition of blebbistatin had no effect on the SL-dependent modulation of either the Ca^{2+} sensitivity or the cooperativity. Despite the fact that they were consistent with our results in terms of the cooperativity, the lack of change in the SL-dependent Ca^{2+} sensitivity was not in agreement with our finding.

In Farman *et al*. (2010), skinned trabeculae were incubated in 1.0 μM blebbistatin overnight, which was quite a modest amount compared to the 25 μM in our experiments. Consequently, the reduction in active force was not comparable as well — ~61% in Farman's versus ~94% in ours. Thus, it seems reasonable to argue that the inhibition of cross-bridge attachments by 1.0 μM blebbistatin may be incomplete, that large number of myosin heads may still be able to bind with actin under this circumstance. Their results cannot rule out the possibility that the remaining cross-bridge attachments in the presence of 1.0 μM blebbistatin were sufficient to function in mediating Ca^{2+} sensitivity with SL.

Additionally, recent investigations suggested the variation in the number of the weak binding cross-bridges, or the orientational disordering of the myosin heads in resting muscle, may be important determinants in transmitting the changes in SL to affect the Ca^{2+} sensitivity as well. Details are not considered further in this study (see Farman *et al*. (2010) and Farman *et al*. (2011) for detailed description).

In this chapter, we investigated whether there was a link between force-generating cross-bridges and the Ca^{2+} sensitivity with varied SL. To characterise the step prior to that, i.e. how cardiac sarcomere transmits the signal from lengthening to the variation in strong binding cross-bridges, is elucidated in next chapter.

Chapter 6

Role of Lattice Spacing in the Regulation of LDA

6.1 Introduction

The SL-dependent modulation of maximum force production and Ca^{2+} sensitivity in cardiac muscle contraction are known as the cellular basis of the Frank-Starling relationship of the heart. Our results from the last two chapters suggest that force-generating cross-bridges are partly involved in transmitting the information of SL change in LDA. The increasing number of myosin heads binding at longer SL results in the SL-dependent increase in maximum force. Although cross-bridges may not be the essential component in the SL-dependent Ca^{2+} sensitivity in LDA, myosin heads binding may provide a positive feedback to support the increasing Ca^{2+} sensitivity with increased SL. In this chapter, we focused on how sarcomere lengthening affects force-generating cross-bridges.

We examined one of the most popular hypothesis — the interfilament spacing (IS) theory. The hypothesis basically proposes that it is the corresponding change in the radial distance between the thick and thin filament (the interfilament spacing) that determines the effect of SL in LDA. Increasing the SL is expected to cause a corresponding reduction in the IS, this closer distance between the myosin heads and actin filament enhances the possibility of cross-bridges formation, which in turn increases the Ca^{2+} sensitivity .

For the time-being, the theory has been investigated quite thoroughly. However, more and more recent findings have shown that there may be no certain relationship between the changes in IS and the changes in Ca^{2+} sensitivity (Section 1.5.3). These results implied that changes in IS alone may not be a primary determinant in LDA, which disagrees with the IS hypothesis. So the main purpose of our experiments in this chapter was more like to confirm the disagreement of the IS theory, and more importantly, to discover the impact of different degrees of osmotic compression on thin filament activation, i.e. the Ca^{2+} dependence of force and cTnC structure.

According to Konhilas *et al*. (2002b), neither the SL-induced nor the osmotic compression-induced reduction in muscle width was in proportion to the reduction in

IS in cardiac trabeculae (Figure 6.1). Both SL change and dextran compression have different impacts on muscle width and IS. They showed that much less dextran is needed to mimic the SL-induced changes in IS than in muscle width. So in my study, 1% and 4% dextran were chosen to respectively mimic the reductions in IS and muscle width as those induced by SL stretching from 1.9 to 2.3 μm without changing SL. The experiments were performed in the skinned cardiac trabeculae at SL 1.9 μm. The choice of the two concentrations were based on the calculations from previous studies (Farman et al., 2006; Fuchs and Wang, 1996; Irving et al., 2000; Konhilas et al., 2002b; Wang and Fuchs, 1995).

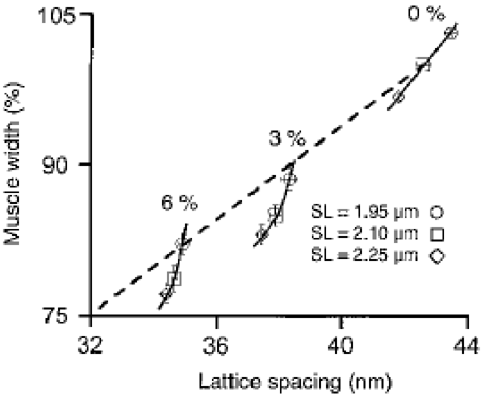

Figure 6.1: Different impacts of SL change and dextran concentration on muscle width (measured by microscopy) and IS (measured by X-ray diffraction) (Konhilas *et al*., 2002b). Muscle width and lattice spacing were determined at 3 SLs (1.95 μm, 2.10 μm, and 2.25 μm) with 0%, 3%, or 6% dextran in the solutions. The dotted line is the predicted relationship if IS were directly proportional to fibre width; normalized to SL 2.10 μm with 0% dextran.

6.2 Effect of Osmotic Compression on the Ca^{2+}-regulated Force Development

In order to investigate the impact of osmotic compression on the Ca^{2+} sensitivity for force development, Ca^{2+} titration measurements were performed in permeabilized rat trabeculae exchanged with either BR-cTnC-C or -E, using dextran T-500 at either 1% or 4% (weight/volume, g/100ml). Dextran T-500 (Sigma-Aldrich) is a high molecular weight molecule which cannot enter the myofilament lattice structure, thus is able to shrink the distance between thick and thin filaments via osmotic compression. As mentioned above, 1% and 4% were chosen based on previous studies (Farman et al., 2006; Fuchs and Wang, 1996; Irving et al., 2000; Konhilas et al., 2002b; Wang and Fuchs, 1995) to mimic the corresponding changes induced by increasing SL (from 1.9 μm to 2.3 μm) in IS and fibre width, respectively. The skinned trabecula was first activated continuously from pCa 9.0 to pCa 4.5 at SL 1.9 μm (as the control group), followed by 10mins incubation in relaxing solution containing either 1% or 4% dextran. The trabecula was then activated for a second round of Ca^{2+} titration in the presence of either 1% or 4% dextran. Dextran was prepared as a stock solution before adding into pCa solutions on the day of experiment. SL was set and checked according to laser diffraction pattern (Section 2.5.1) prior to, and after each series of activations. Isometric force was measured after steady force was established at each pCa. The force was normalized to the maximal Ca^{2+}-activated force at pCa 4.5 in each found of titration and plotted as function of pCa. Data from individual fibre in each titration were fitted to the Hill equation, pCa_{50} (Ca^{2+} sensitivity) and n_H (cooperativity) were determined from each individual fitting. The average parameters are summarized in Tables 6.1 (1% dextran) and 6.3 (4% dextran).

6.2.1 Osmotic Compression with 1% Dextran

In this study, 1% dextran was used to compress the interfilament spacing of cardiac trabeculae at SL 1.9 μm to match that at 2.3 μm. As shown in Table 6.1, 1% dextran reduced the maximum Ca^{2+}-activated force, with the effect being statistically significant only in BR-cTnC-E (-18 ± 4% (± SEM, n = 5)). However, current results are at odds with the previous studies that showed that the moderate compression of cardiomyocytes by less than 10% dextran increased maximum force production (Wang and Fuchs, 1995).

Table 6.1: Hill parameters for the effect of 1% dextran on the Ca^{2+} dependence of force development. (A). C-helix probe experiments; (B). E-helix probe experiments. Mean ± SEM. The parameters were obtained by fitting data from each trabecula, with or without 1% dextran. SL was set to 1.9 µm in this study. F$_{max}$ is the maximum Ca^{2+}-activated force. Δ indicates the difference in each parameter caused by 1% dextran compression. Comparison: paired two-tailed student t-test (* $p<0.05$).

(A)

		1.9 µm	**1.9 µm+1%Dex**	**Δ**
C-helix	**F$_{max}$ (mN/mm^2)**	21.9 ± 2.5	20.1 ± 3.2	-10 ± 5%
	pCa$_{50}$	5.46 ± 0.03	5.45 ± 0.03	-0.01 ± 0.02
	n_H	3.63 ± 0.50	4.21 ± 0.41	0.58 ± 0.20
	n	4		

(B)

		1.9 µm	**1.9 µm+1%Dex**	**Δ**
E-helix	**F$_{max}$ (mN/mm^2)**	28.3 ± 5.2	23.4 ± 4.7*	-18 ± 4%*
	pCa$_{50}$	5.49 ± 0.02	5.50 ± 0.02	0.01 ± 0.01
	n_H	3.62 ± 0.47	3.49 ± 0.42	-0.13 ± 0.23
	n	5		

In this set of experiments, the maximum force production was measured at the end of the titration. Fibre deterioration from multiple activations might result in a decreased maximum activated force at the end of each titration measurement. To determine the effect of dextran (1% and 4%) alone on force generation, steady-state measurements of maximum force development with and without osmotic compression were performed on another batch of trabeculae (Table 6.2). Each fibre was maximally activated at 1.9 µm in the absence of dextran and in the presence of 1% or 4% dextran. Results showed no significant effect of dextran on force generation. The relative changes in maximal Ca^{2+}-activated force are -3 ± 5% for 1% dextran and -11 ± 6% for 4% dextran (± SEM, n = 9). These changes were not statistically significant. Hence, the F$_{max}$ reductions observed in the titration experiments were not due to the addition of dextran (Table 6.1), and are most likely to be the result of fibre damage by multiple activations.

Table 6.2: Steady-state measurements for the effect of 1% or 4% dextran on maximal Ca^{2+}-activated force (F_{max}). Each trabecula was fully activated three times: control, added 1% dextran, and added 4% dextran. Measurements were performed at SL 1.9 µm. Fmax was normalised to the one produced in control group without dextran. Both force per cross-sectional area and normalization were presented. n is the number of trabeculae. Mean ± SEM. Comparison: paired two-tailed student t-test — control *vs* 1% dextran (not significant) and control *vs* 4% dextran (not significant).

n = 9	Control	1% DEX	4% DEX
F_{max} (mN/mm^2)	17.5 ± 2.4	16.9 ± 2.1	15.5 ± 2.1
Normalized (%)	1.00	0.97 ± 0.05	0.89 ± 0.06
Δ (%)	/	-3 ± 5	-11 ± 6

As illustrated in Figure 6.2 A, the force-pCa curve for the trabeculae reconstituted with the C-helix probe of cTnC after osmotic compression by 1% dextran was almost identical to that in control conditions. Lattice spacing shrinkage with 1% dextran at 1.9 µm did not affect the Ca^{2+} sensitivity for force development. The pCa_{50} for force was 5.46 ± 0.03 in the control and 5.45 ± 0.03 (± SEM, n = 4) in the presence of 1% dextran (Table 6.1 A). There was a tendency of increased cooperativity for the Ca^{2+} dependence of force after the addition of 1% dextran (Δn_H = 0.58 ± 0.20 (± SEM, n = 4)), although the opposite situation was observed in the n_H for BR-cTnC-E (Δn_H = -0.13 ± 0.20 (± SEM, n = 5)), neither of them were significant according to the paired t-test.

Trabeculae reconstituted with BR-cTnC-E exhibited the same behaviour as with BR-cTnC-C in response to osmotic compression with 1% dextran (Figure 6.2 B). The pCa_{50} for force was altered slightly from 5.49 ± 0.02 to 5.50 ± 0.02 (± SEM, n = 5) after compression with 1% dextran (Table 6.1 B).

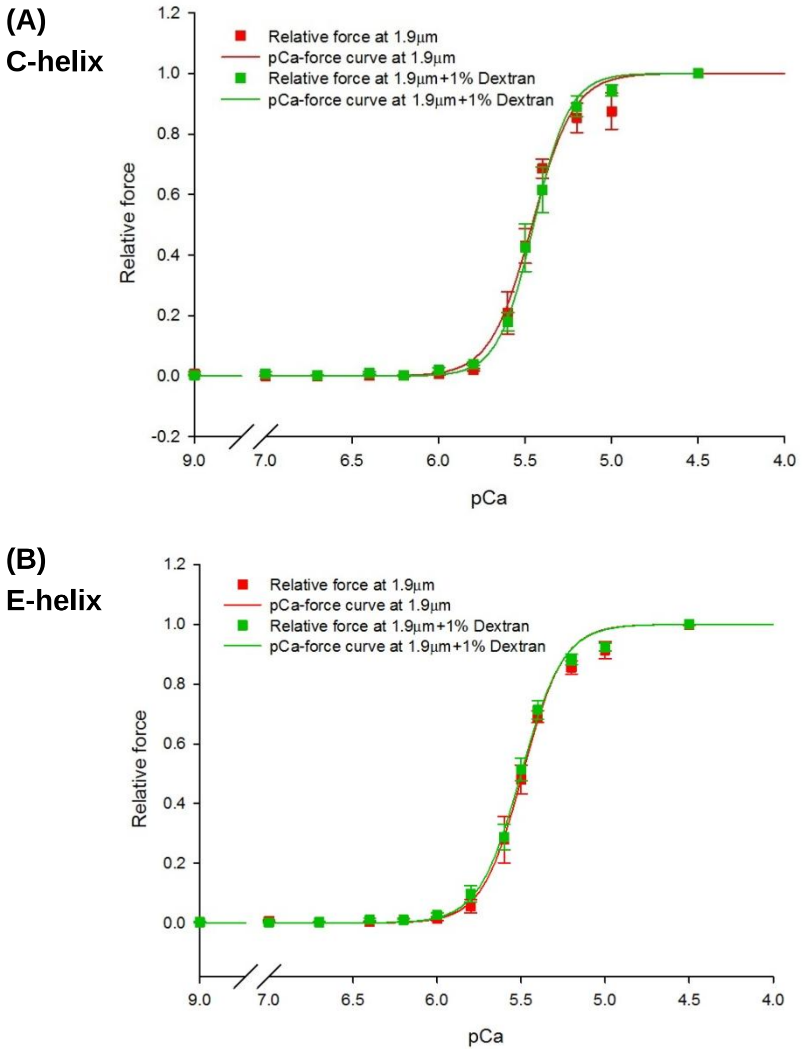

Figure 6.2: Effect of 1% dextran on the Ca^{2+} dependence of force development. Force was normalized to the maximum force at pCa4.5 and plotted as a function of pCa at SL 1.9 μm (red squares) and at 1.9 μm with 1% dextran (green squares). (A). BR-cTnC-C; (B). BR-cTnC-E. Red and green lines indicate the fittings by Hill equation for control and 1% dextran, respectively. Error bars denote S.E.M. Trabeculae number n = 4 for the C-helix probe and n = 5 for the E-helix probe. (Hill parameters are provided in Table 6.1).

The above results showed no significant effect of 1% dextran on the Ca^{2+} sensitivity for force production when SL was unchanged. Given the osmotic compression with 1% dextran was supposed to reduce the IS at short SL to match that at long SL without actually changing SL, an increase in myofilament Ca^{2+}

sensitivity similar to that in response to SL elongation was expected. However, in comparison with our results in Chapter 4, where SL was increased from 1.9 μm to 2.3 μm (Table 4.3), the difference in the Ca^{2+} dependence of force upon 1% dextran compression was in no way comparable with that obtained by actual SL increasing. However, our current results were consistent with a similar study carried out by Konhilas *et al*. (2002b), where the Ca^{2+} sensitivity at short SL did not increase by 1% dextran treatment.

6.2.2 Osmotic Compression with 4% Dextran

4% dextran was added to experimental solutions to osmotically compress the fibre at SL 1.9 μm to mimic the fibre width reduction when SL was increased to 2.3 μm. With no change in the SL (remained 1.9 μm), 4% dextran showed much more pronounced effect on the Ca^{2+} dependence of force compared to 1% dextran.

Osmotic compression with 4% dextran induced a leftward shift of the force-pCa curve for the trabeculae reconstituted with the C-helix probe (Figure 6.3 A), similar to that induced by increasing SL from 1.9 to 2.3 μm (Figure 4.3 A). In contrast to the findings with 1% dextran, 4% dextran remarkably increased pCa_{50} for force at SL 1.9 μm from 5.37 ± 0.02 to 5.51 ± 0.03 for BR-cTnC-C, with a total increase (ΔpCa_{50}) of 0.14 ± 0.03 pCa units (± SEM, n = 4) (Table 6.3 A).

Similarly, the addition of 4% dextran increased the Ca^{2+} sensitivity for force development in trabeculae reconstituted with BR-cTnC-E by a similar amount from 5.53 ± 0.03 to 5.67 ± 0.02, with a ΔpCa_{50} of 0.14 ± 0.02 pCa units (± SEM, n = 6) (Table 6.3 B and Figure 6.3 B). Like the addition of 1% dextran, there was no effect of the compression on the cooperativity (n_H) for the Ca^{2+} dependence of force by 4% dextran (Table 6.3).

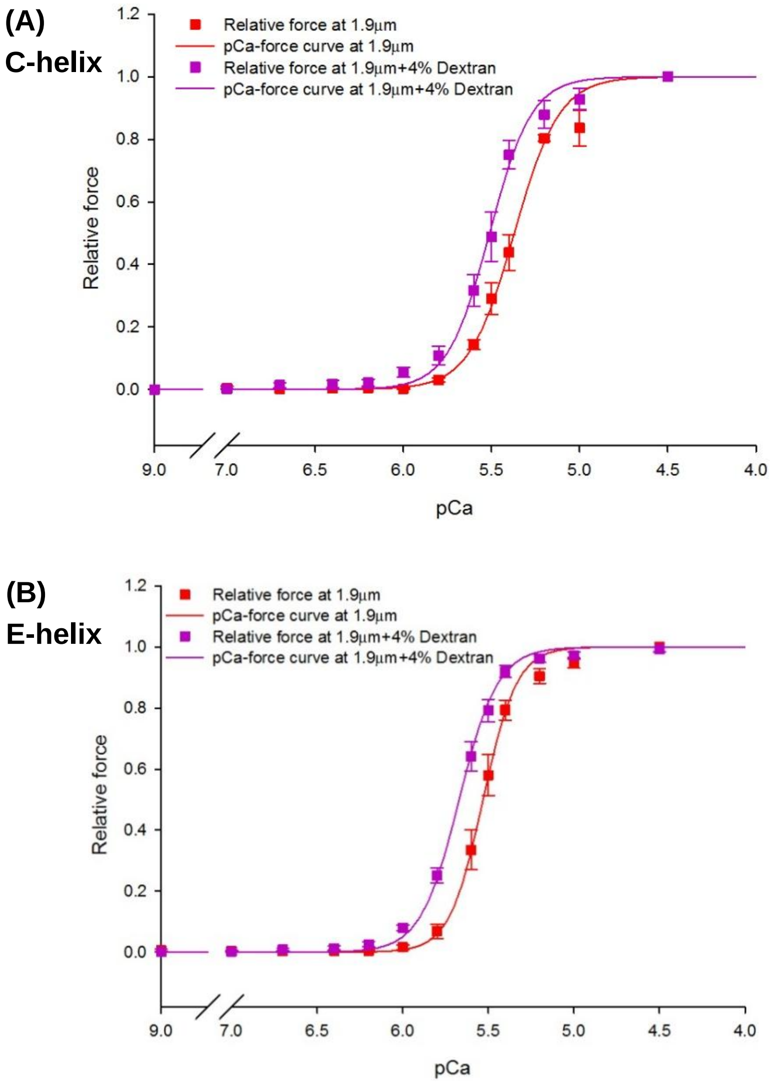

Figure 6.3: Effect of 4% dextran on the Ca^{2+} dependence of force development. Force was normalized to the one produced at maximum activation and plotted as a function of pCa at SL 1.9 μm (red solid squares) and at 1.9 μm with 4% dextran (purple solid squares) for (A). BR-cTnC-C; (B). BR-cTnC-E. Red and purple lines respectively indicate the Hill fitting for control and 4% dextran. Error bars denote S.E.M. Trabeculae number n = 4 for BR-cTnC-C and n = 6 for BR-cTnC-E. (Hill parameters are provided in Table 6.3).

Table 6.3: Hill parameters for the effect of 4% dextran on the Ca^{2+} dependence of force development. (A). C-helix probe; (B). E-helix probe. Mean ± SEM of the parameters obtained by individual fitting data for each trabecula. SL was set to 1.9 µm in this study. F_{max} indicates the maximum Ca^{2+}-activated force. Δ describes the difference in each parameter that brought by 4% dextran. Comparison: paired two-tailed student t-test — before and after 4% dextran compression (* $p<0.05$, *** $p<0.001$).

(A)

		1.9 µm	**1.9 µm + 4%Dex**	**Δ**
C-helix	**F_{max} (mN/mm^2)**	24.0 ± 6.8	20.3 ± 5.1	-14% ± 5%
	pCa_{50}	5.37 ± 0.02	5.51 ± 0.03*	0.14 ± 0.03*
	n_H	3.41 ± 0.24	3.66 ± 0.41	0.25 ± 0.49
	n	4		

(B)

		1.9 µm	**1.9 µm + 4%Dex**	**Δ**
E-helix	**F_{max} (mN/mm^2)**	21.7 ± 4.3	19.8 ± 3.6	-8% ± 4%
	pCa_{50}	5.53 ± 0.03	5.67± 0.02***	0.14 ± 0.02***
	n_H	4.45 ± 0.41	3.86 ± 0.32	-0.59 ± 0.31
	n	6		

In conclusion, compression of the trabeculae by 1% dextran to mimic the reduction in IS in response to SL increase did not reproduce the SL-dependent increase in the Ca^{2+} sensitivity. However, 4% dextran did increase the myofilament Ca^{2+} sensitivity by a similar amount as that induced by SL elongation. The current results suggested the impact of mimicking the SL-induced change in lattice spacing on Ca^{2+} sensitivity was not as pronounced as mimicking the change in fibre width. However, this does not necessarily imply that fibre width is the primary determinant of LDA. These results indicated the impact of different degrees of osmotic compression on the Ca^{2+} sensitivity for force production.

6.3 Effect of Osmotic Compression on the Ca^{2+}-regulated cTnC *In Situ* Orientation Change

In Chapter 4, we showed that the elongation of SL had similar effects on the Ca^{2+} dependence of force development and cTnC orientation change in both the C- and E-helix of cTnC. In order to investigate the impact of osmotic compression with dextran on cTnC orientation change-pCa relationship, the *in situ* orientation of the C- or E-helix was measured simultaneously with isometric force in the same batch of skinned trabeculae exchanged with either BR-cTnC-C or -E. In this chapter, the *in situ* orientation of cTnC and its Ca^{2+} dependence were determined in the same set of titration experiments described in the last section. As described in Chapter 4, orientation change was determined from the fluorescence polarization of the BR dipole attached along C- or E-helix of cTnC using F*IS*S, and was described by order parameters $<P_2>$ and $<P_4>$. Gaussian model was used to acquire the mean axial angle θ_f and standard deviation σ_g of these dipole orientation distributions at relaxation and maximum activation state (data reported in Table 6.4 and 6.6). $<P_2>$-pCa data were fit by the Hill equation for each fibre with and without compression. The fitting was set through the maximum and minimum of $<P_2>$ values and the averaged pCa_{50} and n_H were shown in Table 6.5 and 6.7.

6.3.1 Osmotic Compression with 1% Dextran

As demonstrated in Table 6.4, at SL 1.9 μm, both the C- and E-helix of cTnC had a more parallel conformation with respect to the trabecular axis at pCa 9.0 than at pCa 4.5. Maximum Ca^{2+} activation shifted cTnC towards a more perpendicular conformation, indicated by $\Delta\theta_f = 4.7 \pm 0.8°$ for the C-helix probe (± SEM, n = 4) and 4.1 ± 0.6° for the E-helix probe (± SEM, n = 5).

Table 6.4: Parameters for the effect of 1% dextran on cTnC *in situ* orientation change. (A). C-helix probe; (B). E-helix probe. Order parameters $\langle P_2 \rangle$ and $\langle P_4 \rangle$ were obtained at relaxation and maximum activation using F*I*SS. θ_f and σ_g respectively indicates the peak angle and standard deviation of the Gaussian orientation distribution of the probe angle with respect to the fibre axis. Mean ± SEM. Δ is the difference of each parameter between pCa 9.0 and pCa 4.5. n = 4 for the C-helix probe and n = 5 for the E-helix probe. Comparison: paired two-tailed student t-test — no dextran *vs* 1% dextran (statistical significance * $p<0.05$, ** $p<0.01$, *** $p<0.001$). Changes in $\langle P_4 \rangle$ upon 1% dextran compression for BR-cTnC-C had a p value of 0.0536.

(A)

C-helix	**1.9 µm**				**1.9 µm + 1% Dextran**			
	$\langle P_2 \rangle$	$\langle P_4 \rangle$	Θ_f (°)	σ_g (°)	$\langle P_2 \rangle$	$\langle P_4 \rangle$	Θ_f (°)	σ_g (°)
pCa9.0	0.096 ± 0.005	-0.085 ± 0.021	52.5 ± 0.1	21.4 ± 1.3	0.091 ± 0.001	-0.135 ± 0.026**	52.5 ± 0.2	18.5 ± 1.4***
pCa4.5	0.005 ± 0.007	-0.107 ± 0.029	57.2 ± 0.7	19.7 ± 1.6	0.013 ± 0.005	-0.131 ± 0.027*	56.4 ± 0.5	18.3 ± 1.5*
Δ	0.091 ± 0.010	0.022 ± 0.008	-4.7 ± 0.8		0.078 ± 0.004	-0.004 ± 0.003 (p=*0.0536*)	-3.9 ± 0.3	
n	4							

(B)

E-helix	**1.9 µm**				**1.9 µm + 1% Dextran**			
	$\langle P_2 \rangle$	$\langle P_4 \rangle$	Θ_f (°)	σ_g (°)	$\langle P_2 \rangle$	$\langle P_4 \rangle$	Θ_f (°)	σ_g (°)
pCa9.0	0.250 ± 0.012	-0.120 ± 0.033	44.7 ± 0.6	17.8 ± 1.7	0.242 ± 0.011	-0.176 ± 0.024*	45.3 ± 0.5	15.2 ± 1.1*
pCa4.5	0.164 ± 0.004	-0.159 ± 0.022	48.8 ± 0.2	17.0 ± 1.0	0.164 ± 0.010	-0.199 ± 0.018*	48.8 ± 0.5	15.1 ± 0.8*
Δ	0.085 ± 0.012	0.039 ± 0.015	-4.1 ± 0.6		0.078 ± 0.010	0.023 ± 0.013**	-3.5 ± 0.5	
n	5							

As shown in Table 6.4 A, the <P_2> values for the C-helix probe at both relaxation (pCa 9.0) and maximum activation (pCa 4.5) were not significantly affected by osmotic compression with 1% dextran, neither was the amplitude of C-helix's orientation change upon maximum activation — Δ<P_2>. Similarly, 1% dextran did not affect the corresponding changes in the mean axial angle θ_f. Interestingly, another order parameter <P_4>, which reports higher resolution information about the orientation change of the BR probes, was reduced significantly both at pCa 9.0 (from -0.085 ± 0.021 to -0.135 ± 0.026) and at pCa 4.5 (-0.107 ± 0.029 to -0.131 ± 0.027), giving a total reduction in Δ<P_4> from 0.022 ± 0.008 to -0.004 ± 0.003 (± SEM, n = 4) upon 1% dextran compression. However, the difference in Δ<P_4> between the absence and presence of 1% dextran reported in Table 6.4 A was only nearly significant according to the paired two-tailed student t-test with a statistical significance p value equals to 0.0536. More direct comparison of the *in situ* orientation of both the C- and E-helix of cTnC during relaxation and maximum activation, with and without 1% dextran, is illustrated in Figure 6.4.

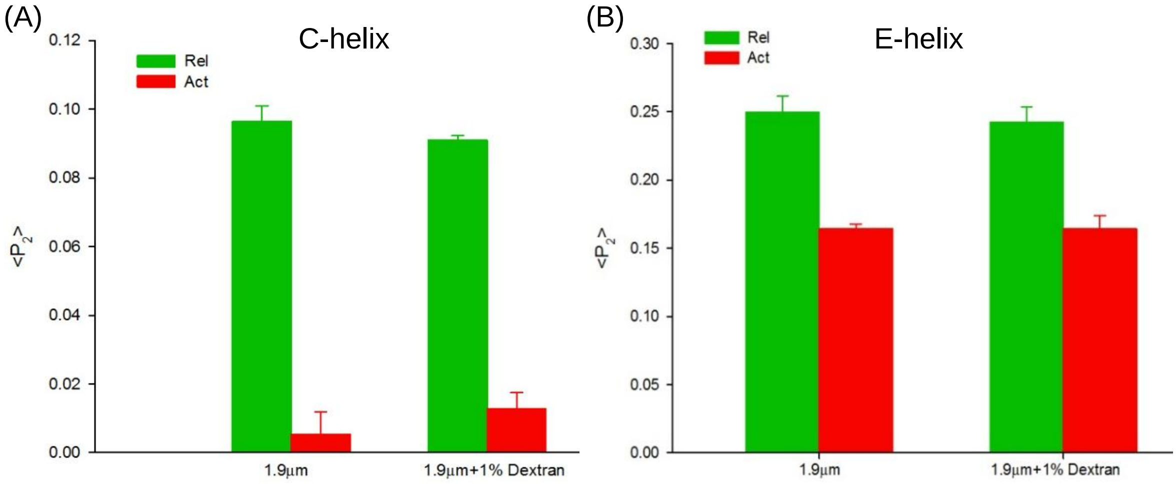

Figure 6.4: Effect of 1% dextran on cTnC *in situ* orientation. Bar Charts show changes in <P_2> upon maximum activation and addition of 1% dextran for A. C-helix probe; and B. E-helix probe. Green and red bar in each set respectively represent <P_2> value at relaxation (pCa 9.0) and maximum activation (pCa 4.5). First set in each graph is the control group, second is with 1% dextran. Error bars denote SEM. n = 4 for BR-cTnC-C and n = 5 for BR-cTnC-E. (<P_2> values are presented in Table 6.4).

On the other hand, in spite of an additional component in the $<P_2>$ values at higher pCa (9.0 to 6.0), the main part of $<P_2>$-pCa curve of the C-helix probe did not shift upon compression with 1% dextran (Figure 6.5 A). The Ca^{2+} sensitivity (pCa_{50}) was 5.46 ± 0.02 and 5.45 ± 0.03, respectively, for control and in 1% dextran, with ΔpCa_{50} being 0.01 ± 0.01 pCa units (± SEM, n = 4, not significant) (Table 6.5 A). The changes in n_H showed a tendency towards increased cooperativity for the Ca^{2+}-dependent change in C-helix orientation upon compression ($\Delta n_H = 0.52 \pm 0.65$, $p = 0.0836$). These results were consistent with those obtained from the force-pCa relationship (Table 6.1 A).

Similar to that for BR-cTnC-C, $\Delta<P_2>$ and $\Delta\theta_f$ were also unaltered upon the treatment with 1% dextran in the E-helix probe experiments (Table 6.4 B). Likewise, in response to the osmotic compression with 1% dextran, $<P_4>$ was significantly decreased from -0.120 ± 0.033 to -0.176 ± 0.024 at relaxation, and from -0.159 ± 0.022 to -0.199 ± 0.018 at maximum activation (± SEM, n = 5). The overall changes in $<P_4>$ between pCa 9.0 and 4.5 ($\Delta<P_4>$) were significantly reduced from 0.039 ± 0.015 to 0.023 ± 0.013 (± SEM, n = 5).

Similar to the previous measurements of BR-cTnC-E in the presence of 1% dextran, there was an additional component in the $<P_2>$-pCa relationship for the E-helix probe at subthreshold pCa (pCa 9.0 to 6.2) (Figure 6.5 B). To simplify the analysis, the major component of the E-helix orientation change below pCa 6.2 was fitted to the Hill equation. As illustrated in Figure 6.5 B, $<P_2>$-pCa curves were similar between the control and in the presence of 1% dextran, indicating a similar Ca^{2+} dependence. The Ca^{2+} sensitivity for the $<P_2>$-pCa relationship for the E-helix probe was not significantly changed in response to the shrinkage of IS by 1% dextran, indicated by pCa_{50} = 5.46 ± 0.02 in control and 5.46 ± 0.02 (± SEM, n = 5) with addition of 1% dextran. n_H was not affected by 1% dextran significantly either ($\Delta n_H = -0.12 \pm 0.16$, $p = 0.916$). The results were comparable with those from the Ca^{2+} dependence of force (Table 6.1 B).

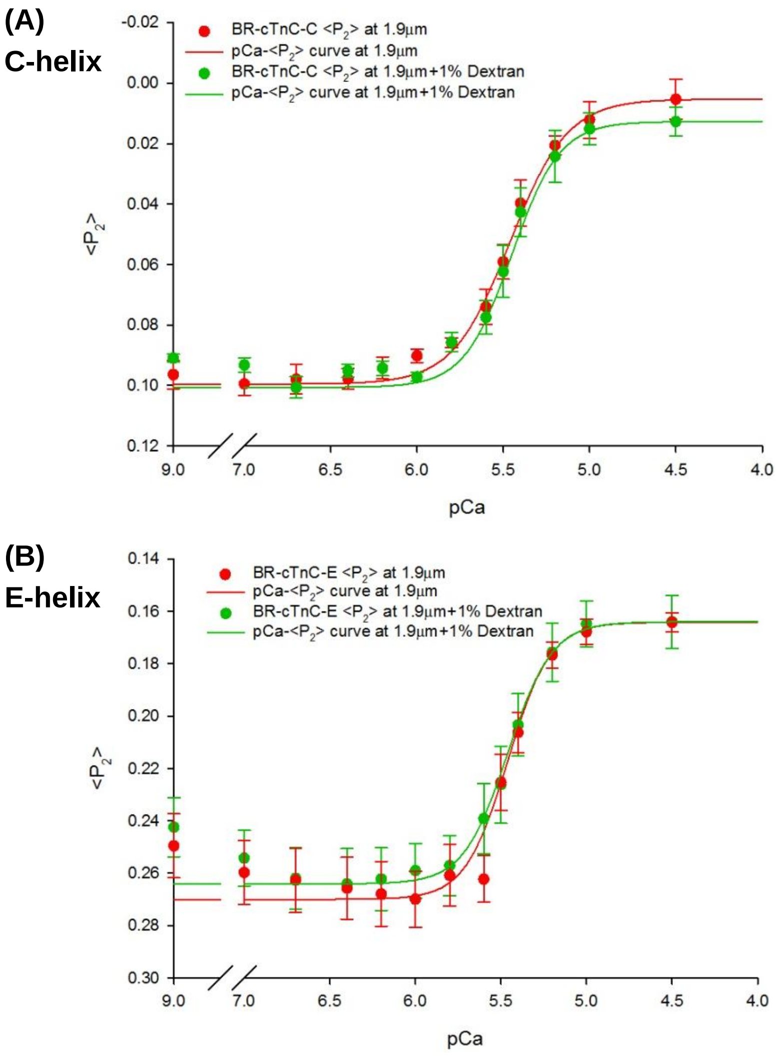

Figure 6.5: Effect of 1% dextran on the Ca^{2+} dependence of cTnC orientation change. $<P_2>$ values were plotted as functions of pCa at SL 1.9 μm (red circles) and at 1.9 μm with 1% dextran (green circles) for A. C-helix probe; and B. E-helix probe. Red and green lines respectively indicate the Hill fitting for control and with 1% dextran. Error bars denote SEM. n = 4 for the C-helix labelled trabeculae and n = 5 for the E-helix labelled ones. (Hill parameters are provided in Table 6.5).

Table 6.5: Hill parameters for the effect of 1% dextran on the Ca^{2+} dependence of cTnC orientation change. (A). C-helix probe experiments; (B). E-helix probe experiments. Parameters were obtained by individually fitting data for each trabecula with and without 1% dextran. Δ<P_2> represents the orientation change from relaxation to maximum activation. Mean ± SEM. n = 4 for the C-helix probe and n = 5 for the E-helix probe. Δ indicates the difference in each parameter after adding 1% dextran. Comparison: paired two-tailed student t-test before and after 1% dextan compression (not significant).

(A)

		C-helix		
		1.9 µm	**1.9 µm + 1%Dex**	**Δ**
Orientation	**<P_2> pCa 9.0**	0.096 ± 0.005	0.091 ± 0.001	
	<P_2> pCa 4.5	0.005 ± 0.007	0.013 ± 0.005	
	Δ<P_2>	0.091 ± 0.010	0.078 ± 0.004	
	pCa_{50}	5.46 ± 0.02	5.45 ± 0.03	-0.01 ± 0.01
	n_H	2.62 ± 0.38	3.15 ± 0.28	0.52 ± 0.65
	n	4		

(B)

		E-helix		
		1.9 µm	**1.9 µm + 1%Dex**	**Δ**
Orientation	**<P_2> pCa 9.0**	0.250 ± 0.012	0.242 ± 0.011	
	<P_2> pCa 4.5	0.164 ± 0.004	0.164 ± 0.010	
	Δ<P_2>	0.085 ± 0.012	0.078 ± 0.010	
	pCa_{50}	5.46 ± 0.02	5.46 ± 0.02	0.00 ± 0.01
	n_H	3.51 ± 0.31	3.38 ± 0.39	-0.12 ± 0.16
	n	5		

Additionally, the standard deviation σ_g for both C- and E-helix probes decreased slightly in response to dextran treatment, implying a less dispersion of probe distribution in the presence of dextran.

The results so far showed that the Ca^{2+} sensitivity for both force and cTnC structural change were unaffected by 1% dextran, suggesting that the SL-dependent Ca^{2+} sensitivity in LDA is not determined by the corresponding changes in IS. There must be other mechanisms linking the information of SL to the myofilament Ca^{2+} sensitivity.

6.3.2 Osmotic Compression with 4% Dextran

At SL 1.9 μm, the orientation of both the C- and E-helix of cTnC showed a parallel preference with respect to the fibre axis at relaxation state compared to the maximum activation state (Table 6.6). The similar slight perpendicular shift of cTnC conformation upon activation was found in previous experiments. Although there were small discrepancies among data reported in each study, it was very likely due to the variance in many factors, such as daily calibration of the experimental apparatus, different batches of trabeculae and solutions, etc.

Osmotic compression with 4% dextran significantly affected the orientation of the C-helix at pCa 9.0 by decreasing $<P_2>$ from 0.079 ± 0.006 to 0.072 ± 0.006, resulting to a small increase in the axial angle θ_f from 53.5 ± 0.4° to 53.6 ± 0.3° (± SEM, n = 4) (Table 6.6 A). At the same time, the other order parameter $<P_4>$, which describes the orientation of the BR probe with higher resolution information, also changed significantly in relaxation upon 4% dextran treatment. The significant effect of compression on the C-helix orientation at relaxing state has not been seen in the presence of 1% dextran (Table 6.4 A). However, there was no further impact of 4% dextran on the orientation of the C-helix either at pCa 4.5 or the overall change upon maximum activation ($\Delta<P_2>$ or $\Delta\theta_f$), similar to that for 1% dextran. In addition, a lower standard deviation σ_g in the presence of 4% dextran was observed for the C-helix probe at relaxation state (21.6 ± 0.6° in control, 19.8 ± 0.7° in 4% dextran (± SEM, n = 4)). The comparisons of the *in situ* orientation of the C- and E-helix, at relaxation and maximum activation, in control and in 4% dextran, are presented in Figure 6.6.

Table 6.6: Parameters for the effect of 4% dextran on cTnC *in situ* orientation change. (A). C-helix probe experiments; (B). E-helix probe experiments. Order parameters $\langle P_2 \rangle$ and $\langle P_4 \rangle$ were obtained at relaxation and maximum activation using F*IS*S. θ_f and σ_g respectively indicates the peak angle and standard deviation of the Gaussian orientation distribution of the probe with respect to the fibre axis. Mean ± SEM. Δ is the difference of each parameter between pCa 9.0 and pCa 4.5. n = 4 for the C-helix probe and n = 6 for the E-helix probe. Comparison: paired two-tailed student t-test — no dextran *vs* 4% dextran (statistical significance * $p<0.05$, ** $p<0.01$).

(A)

C-helix	**1.9 µm**				**1.9 µm + 4% Dextran**			
	$\langle P_2 \rangle$	$\langle P_4 \rangle$	Θ_f (°)	σ_g (°)	$\langle P_2 \rangle$	$\langle P_4 \rangle$	Θ_f (°)	σ_g (°)
pCa 9.0	0.079 ± 0.006	-0.089 ± 0.010	53.5 ± 0.4	21.1 ± 0.6	0.072 ± 0.006*	-0.109 ± 0.012**	53.6 ± 0.3*	19.8 ± 0.7**
pCa 4.5	-0.004 ± 0.000	-0.079 ± 0.010	58.1 ± 0.2	21.3 ± 0.7	-0.002 ± 0.004	-0.094 ± 0.007	57.7 ± 0.3	20.3 ± 0.4
Δ	0.083 ± 0.007	-0.010 ± 0.005	-4.6 ± 0.4	/	0.074 ± 0.010	-0.016 ± 0.006	-4.0 ± 0.6	/
n	4							

(B)

E-helix	**1.9 µm**				**1.9 µm + 4% Dextran**			
	$\langle P_2 \rangle$	$\langle P_4 \rangle$	Θ_f (°)	σ_g (°)	$\langle P_2 \rangle$	$\langle P_4 \rangle$	Θ_f (°)	σ_g (°)
pCa 9.0	0.219 ± 0.013	-0.094 ± 0.010	55.4 ± 0.7	19.5 ± 0.5	0.218 ± 0.016	-0.121 ± 0.014*	46.3 ± 0.8	18.1 ± 0.7*
pCa 4.5	0.131 ± 0.009	-0.127 ± 0.007	60.6 ± 0.4	18.7 ± 0.4	0.134 ± 0.009	-0.147 ± 0.012*	50.3 ± 0.5	17.7 ± 0.6*
Δ	0.088 ± 0.005	0.033 ± 0.008	-5.2 ± 0.3	/	0.084 ± 0.008	0.026 ± 0.007	-4.0 ± 0.4	/
n	6							

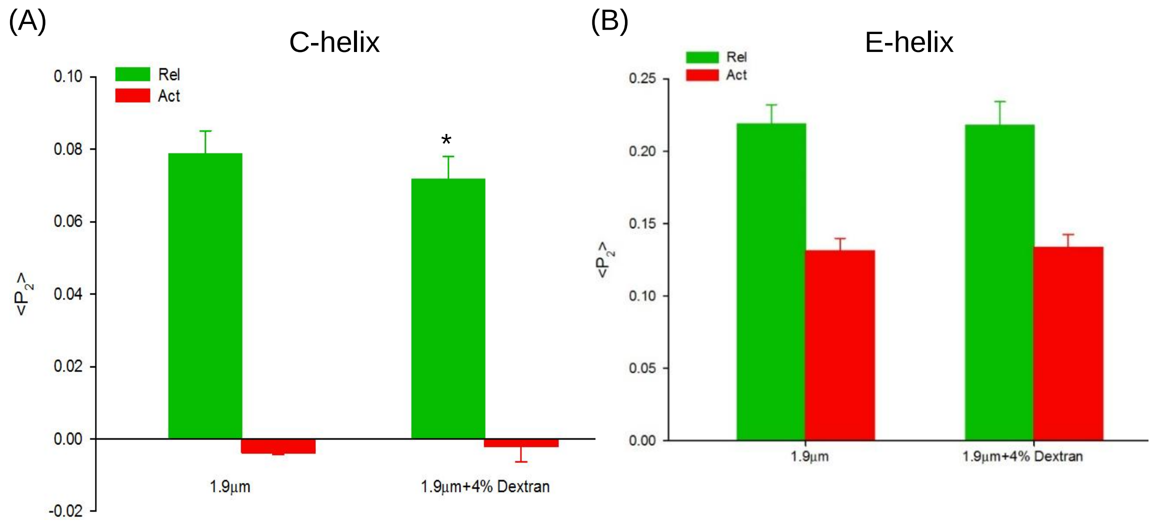

Figure 6.6: Effect of 4% dextran on cTnC *in situ* orientation. Bar Charts show changes in $<P_2>$ upon activation and addition of 4% dextran for A. C-helix probe; and B. E-helix probe. Green and red bar in each set represent $<P_2>$ value at relaxation (pCa 9.0) and maximum activation (pCa 4.5), respectively. First set in each graph is the control group, second is with 4% dextran. Error bars denote SEM. n = 4 for BR-cTnC-C and n = 6 for BR-cTnC-E. Statistical significance of the differences in the $<P_2>$ values between 0% dextran group and 4% dextran group for each helix probe was assessed using paired two-tailed student t-test: $*p< 0.05$. ($<P_2>$ values are presented in Table 6.6).

As illustrated in Figure 6.7 A, the $<P_2>$ values fluctuated in the higher range of pCa. In this study, the Hill fitting was set through the maximum and minimum $<P_2>$ values in each condition. Figure 6.7 A showed the impact of 4% dextran on $<P_2>$ was over a very large range of pCa and became smaller near the maximum [Ca^{2+}]. The Ca^{2+} sensitivity increase upon compression was indicated by an increase in pCa_{50} from 5.41 ± 0.02 to 5.51 ± 0.02 (± SEM, n = 4) (Table 6.7 A). Also, there was no significant change in the cooperativity for the Ca^{2+}-regulation of the C-helix orientation in the presence of 4% dextran. Current results were in agreement with the impact of 4% dextran on the Ca^{2+} dependent force development reported in Table 6.3 A

(A)
C-helix

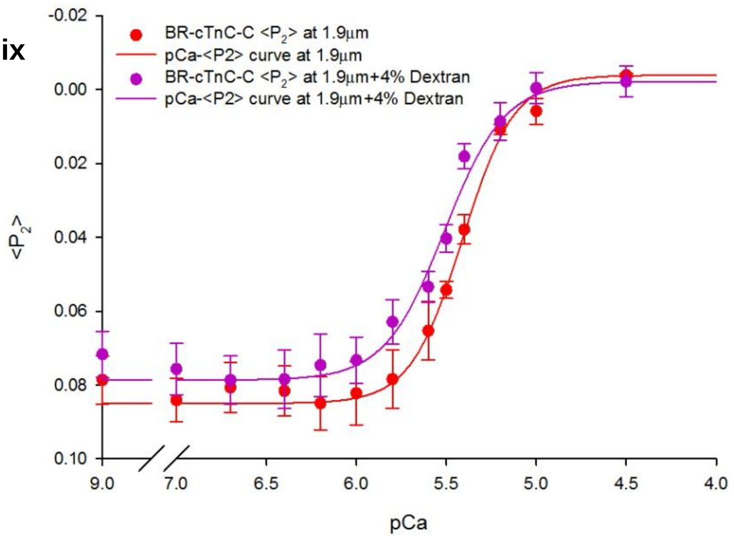

(B)
E-helix

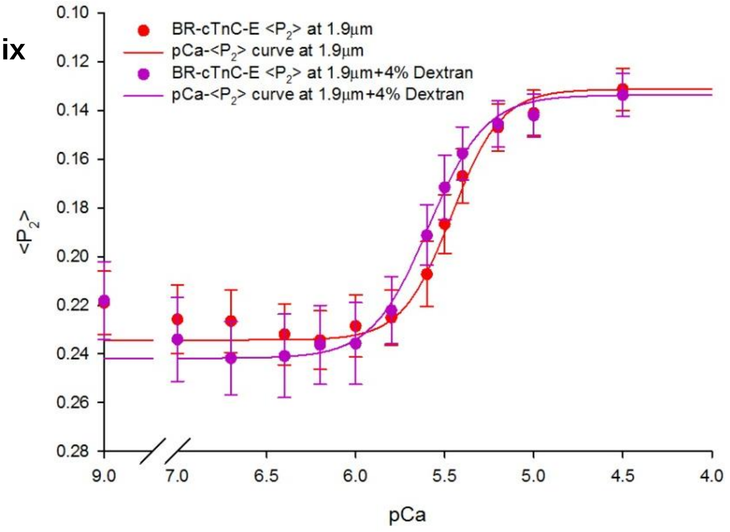

Figure 6.7: Effect of 4% dextran on the Ca^{2+} dependence of cTnC orientation change. $<P_2>$ values were plotted as functions of pCa at SL 1.9 µm (red circles) and at 1.9 µm with 4% dextran (purple circles) for A. C-helix probe; and B. E-helix probe. Red and purple lines indicate the Hill fitting for control and with 4% dextran, respectively. Error bars denote SEM. n = 4 for BR-cTnC-C and n = 6 for BR-cTnC-E. (Table 6.7).

For BR-cTnC-E, there were no significant changes in $<P_2>$ and θ_f in response to compression with 4% dextran. On the other hand, $<P_4>$ was significantly reduced from -0.094 ± 0.010 to -0.121 ± 0.014 at pCa 9.0 and from -0.127 ± 0.007 to -0.147 ± 0.012 at maximum activation at pCa 4.5(± SEM, n = 6) (Table 6.6 B). However, no significant difference in $\Delta<P_4>$ between pCa 9.0 and pCa 4.5 was observed after adding 4% dextran. Additionally, during both relaxation and maximum activation, there were reductions in the standard deviation σ_g for the E-helix probe in 4% dextran, similar to those in the presence of 1% dextran, suggesting a decrease in the dispersion of the orientation distribution for the BR probe by osmotic compression.

As described previously, the orientation changes of the E-helix in 4% dextran showed an additional component in the subthreshold range of pCa (pCa 9.0 to 6.7) (Figure 6.7 B). The major component between pCa 6.7 and pCa 4.5 was then fitted to the Hill equation. Unlike the C-helix, the orientation of the E-helix, indicated by $<P_2>$, was not significantly affected by 4% dextran at either relaxed or maximum activated state (Table 6.7 B, Figure 6.7 B). However, the compression by 4% dextran did increase the Ca^{2+} sensitivity for the E-helix orientation change significantly. The pCa_{50} was increased from 5.46 ± 0.03 to 5.59 ± 0.02 with a ΔpCa_{50} of 0.13 ± 0.02 pCa units (± SEM, n = 6). Similar to those in the force measurement and the C-helix probe experiment, there was no significant change in the cooperativity (n_H) for the Ca^{2+} dependence of the E-helix orientation.

The present results showed that the amplitude of orientation changes in both C and E helices of cTnC upon activation were not affected by osmotic compression, similar to that observed in increasing SL from 1.9 to 2.3 μm reported in Chapter 4. However, only in the presence of 4% dextran, there were increases in the Ca^{2+} sensitivity for both the force production and cTnC structural change (~0.14 pCa units). 1% dextran did not affect the Ca^{2+} sensitivity significantly. Moreover, the increase in the Ca^{2+} sensitivity upon 4% dextran treatment reported here was largely comparable with that induced by SL increasing from 1.9 μm to 2.3 μm in Chapter 4 (~0.11 pCa units) (Table 4.3 & 4.5). Thus, mimicking the SL-induced changes in fibre width using 4% dextran was able to reproduce a similar change of the Ca^{2+} sensitivity as SL elongation.

Table 6.7: Hill parameters for the effect of 4% dextran on the Ca^{2+} dependence of cTnC orientation. (A). C-helix probe experiments; (B). E-helix probe experiments. Parameters were obtained by fitting data from each trabecula with and without 4% dextran. $\Delta\langle P_2 \rangle$ represents the orientation change from pCa 9.0 to pCa 4.5. Mean ± SEM. n = 4 for BR-cTnC-C and n = 6 for BR-cTnC-E. Δ indicates the difference in each parameter after adding 1% dextran. Comparison: paired two-tailed student t-test before and after 4% dextran compression (* p<0.05, *** p<0.001).

(A)

		C-helix		
		1.9 μm	**1.9 μm + 4%Dex**	**Δ**
Orientation	**$\langle P_2 \rangle$ pCa 9.0**	0.079 ± 0.006	0.072 ± 0.006*	
	$\langle P_2 \rangle$ pCa 4.5	-0.004 ± 0.000	-0.002 ± 0.004	
	$\Delta\langle P_2 \rangle$	0.083 ± 0.007	0.074 ± 0.010	
	pCa_{50}	5.41 ± 0.02	5.51 ± 0.02*	0.10 ± 0.02*
	n_H	3.01 ± 0.57	2.62 ± 0.21	-0.39 ± 0.40
	n	4		

(B)

		E-helix		
		1.9 μm	**1.9 μm + 4%Dex**	**Δ**
Orientation	**$\langle P_2 \rangle$ pCa 9.0**	0.219 ± 0.013	0.218 ± 0.016	
	$\langle P_2 \rangle$ pCa 4.5	0.131 ± 0.009	0.134 ± 0.009	
	$\Delta\langle P_2 \rangle$	0.088 ± 0.005	0.084 ± 0.008	
	pCa_{50}	5.46 ± 0.03	5.59 ± 0.02***	0.13 ± 0.02***
	n_H	3.13 ± 0.17	2.73 ± 0.11	-0.40 ± 0.22
	n	6		

6.4 Discussion

6.4.1 Role of Interfilament Spacing in LDA

Our results from the last two chapters have suggested that the LDA was likely controlled via two signalling pathways. The SL-dependent Ca^{2+} sensitivity was mainly regulated by the thin filament, while the SL-dependent maximum force generation was controlled by the thick filament. Yet how the signal of sarcomere lengthening transmits to affect both myofilaments is still an issue of discussion. One of the most popular hypothesis — the interfilament spacing theory, relates the radial distance between the thick and thin filaments to the SL-dependent regulation in LDA.

In this chapter, we first re-examined the role of IS in LDA. We investigated the relationship between changes in IS and the changes in maximum force/Ca^{2+} sensitivity without changing SL. The experiments were performed by osmotically compressing the myofilament lattice at SL 1.9 μm using 1% or 4% dextran to mimic the IS or fibre width change as induced by increasing SL to 2.3 μm. However, the amount of neither IS nor fibre width change was measured directly in this study. Our results also showed the effect of different degrees of osmotic compression on the Ca^{2+}-regulated thin filament activation.

As shown in the present study, the addition of either 1% or 4% dextran did not have significant effect on the maximum force development. This was not consistent with the previous reports, which showed the osmotic compression with less than 10% dextran increased the maximum force production markedly (Konhilas et al., 2002b; Wang and Fuchs, 1995). Our results disagreed with the IS theory, that the closer distance between the thick and thin filaments brought by osmotic compression enhances the probability of cross-bridges formation. However, as elucidated by Konhilas et al. (2002b), the osmotic compression-induced change in the IS depends on both the applied dextran concentration and the SL of the fibre. Therefore, one possible explanation for the different impacts of lattice compression on the maximum force production amongst these studies, may be due to the different amounts of IS changes caused by various [dextran] and SL. On the other hand, we argued that, instead of increasing the number of force-generating cross-bridges, the osmotic compression-induced shrinkage of the myofilament lattice may have a structural impact on the myofilaments, especially on the relatively loose structure of the thick filament. The thick filament has a relatively loose structure as it contains parallel-organised and electrostatic interactions-aligned myosin molecules (Farman et al., 2006; McLachlan and Stewart, 1982). The structural impact of osmotic compression on the thick filament may include changes in the mobility, orientation, and position of the myosin heads, together with variations in the interactions with other sarcomeric proteins, either of them may affect Ca^{2+} sensitivity indirectly.

In this study, we showed that the Ca^{2+} sensitivities for both force development and cTnC structural change were not affected by 1% dextran. The present results suggested that, under moderate compression with 1% dextran, there was no direct correlation between changes in the IS and the Ca^{2+} sensitivity. Mimicking the SL increasing-induced reductions in IS with 1% dextran did not reproduce the SL-dependent increase in Ca^{2+} sensitivity, disagreed with the IS theory.

However, osmotic compression with 4% dextran significantly increased the Ca^{2+} sensitivity for both force and cTnC structural change. The increasing Ca^{2+} sensitivity was comparable with that induced by sarcomere lengthening from 1.9 μm to 2.3 μm. Although our current study showed that the SL-dependent Ca^{2+} sensitivity did not correlate with changes in the IS as well as with the fibre width, it did not necessarily imply a role of muscle width instead of lattice spacing as a determinant of SL change in LDA. Under physiological conditions, SL variation may have additional impacts on the extra-sarcomeric structures in addition to inducing inverse changes in IS. Therefore in our current results, osmotic compression with 1% dextran might only be sufficient to shrink the IS to match that at longer SL, yet the impact of SL elongation on the entire trabecula is more appropriately imitated by larger degree of compression with 4% dextran.

Together with the results from 1% dextran, our results suggested there was no simple relationship between the changes in the IS and the changes in the Ca^{2+} sensitivity. Osmotic compression at a short SL was not functionally equivalent to sarcomere lengthening. Our results suggested the effect of dextran treatment on Ca^{2+} sensitivity may be independent of changes in IS, indicating that changes in IS alone may not be a primary determinant in LDA. The different effects of 1% and 4% dextran compression on the Ca^{2+} sensitivity implied the existence of an osmotic compression-sensitive mechanism, by which the Ca^{2+} sensitivity is modulated independent of changes in the IS.

6.4.2 Comparison with Previous Studies

As the molecular basis of the Frank-Starling relationship, the two outcomes of LDA are regulated via two signalling pathways — the thick filament-regulated SL-dependent maximum force, and the thin filament-regulated SL-dependent Ca^{2+} sensitivity. In investigating how sarcomere lengthening transmits to affect both the thick and thin filaments, one particular hypothesis — the IS theory, has gained considerable experimental supports over the years. It proposes that it is the corresponding change in the radial distance between the thick and thin filament (the IS) that determines the effect of SL in LDA. The evaluations of the IS hypothesis have been performed by osmotically compression the myofilament lattice at short SL using high molecular weight molecule, dextran, to mimic the IS reduction induced by SL increasing.

In this study, we found osmotic compression with either 1% or 4% dextran had no significant effect on maximum force production, which was not in agreement with the previous studies (Konhilas et al., 2002b; Wang and Fuchs, 1995). In the experiments by Wang and Fuchs (1995), compressing skinned cardiac fibre at SL 1.7 μm increased the force production at pCa 5.0 (maximum activation) of ~8%. Similarly, Konhilas *et al*. (2002b) found that the application of 1%, 3%, and 6% dextran at SL 2.2 μm increased maximum force production by 13.3%, 12.2%, and 11.9%, respectively, compared with that in the absence of dextran. Our results in this study therefore challenge the role of IS in determining the SL-dependent maximum force production. Our current conclusion implies that the reduction of IS is more likely to affect the structure of myosin-containing thick filaments than the number of force-generating cross-bridges. There is a possible structural effect of osmotic compression on potentially all components in the sarcomere, especially on the relatively loose composition of the thick filaments.

The present experiments also showed the Ca^{2+} sensitivity for both force and cTnC structural change did not change significantly upon 1% dextran compression. The results were not in supportive of the earlier studies of the hypothesis, which concluded that the effect of SL on Ca^{2+} sensitivity in LDA could be largely accounted for by mimicking the SL-induced changes in IS (Fuchs and Wang, 1996; McDonald and Moss, 1995; Wang and Fuchs, 1995). However, this conclusion came almost entirely from the experiments in which the changes in IS were estimated from the reductions in muscle width, based on the assumption that the the changes in muscle width were proportional to the changes in IS. The assumption has been proved invalidate in cardiac muscle by the direct measurement of IS with X-ray diffraction. In contrast with the earlier studies using muscle width as an indicator of IS, our results were more consistent with that by Konhilas *et al*. (2002b), in which the actual IS was measured by X-ray diffraction. They showed that moderate compression with 1% dextran, which reduced the IS equivalent to that induced by SL increasing from 2.02 μm to 2.19 μm in uncompressed trabeculae, did not increase the Ca^{2+} sensitivity significantly.

Further compression with 4% dextran markedly increased the Ca^{2+} sensitivity by ~0.14 pCa units. Our results showed no constant relationship between the changes in the IS and the changes in the Ca^{2+} sensitivity. Changes in the IS alone may not determine the effect of changing SL in LDA. More importantly, the various effects of 1% and 4% dextran compression on the Ca^{2+} sensitivity may rely on other mechanisms, such as the optimal IS theory, or the osmotic pressure-sensitive mechanism (explained below).

It was suggested that there was an optimal lattice spacing between cardiac myofilaments at which the position and formation of the cross-bridges was ideal to participate in the regulation of the Ca^{2+} sensitivity. An interfilament spacing smaller or larger than the optimal distance would result in imperfect attachments of myosin heads (Farman *et al*., 2006). In agreement with this theory, Konhilas *et al*. (2002b) showed that the relationship between IS and the Ca^{2+} sensitivity was highly non-linear. There was only a narrow range of IS within which the formation of cross-bridges, along with the changes in Ca^{2+} sensitivity were best correlated with the changes in IS. As described previously, the effect of osmotic compression on the myofilament lattice depends on both the concentration of dextran and SL. Thus, if the distance between myosin heads and actin is too far away from the optimal value (short SL), a small degree of compression would produce little or no change in the Ca^{2+} sensitivity (Cazorla *et al*., 2001). Therefore, at SL 1.9 μm in this study, 1% dextran might not be sufficient to reduce the IS into the narrow range of optimal IS. On the other hand, 4% dextran compression might produce a IS much closer to the ideal distance than that with 1% dextran (Fuchs and Martyn, 2005; Konhilas et al., 2002b). In such a case, myosin heads were able to interact with actin in a more optimal and efficient manner, resulting in an increase in the Ca^{2+} sensitivity.

Additionally, studies by Farman *et al*. (2006) implied the existence of a osmotic pressure-sensitive mechanism, through which the Ca^{2+} sensitivity was regulated largely by the changes in the external osmotic pressure, independent of the changes in the IS. The mechanism assumes the Ca^{2+} sensitivity is regulated by osmotic pressure through the structural effect of compression on myosin heads. In their experiments, Farman *et al*. (2006) showed that there was a narrow range of osmotic pressure (0.24~0.38kPa, corresponding to 0.7%~1.0% dextran T-500) in which the Ca^{2+} sensitivity, together with the relative position of myosin heads, increased substantially upon compression. Further compression with higher osmotic pressure up to 6.7kPa (6% dextran) did not further increase either the Ca^{2+} sensitivity or the disposition of myosin heads, suggesting a switch-like mechanism in the regulation of Ca^{2+} sensitivity that highly depends on the extent of external osmotic compression rather than the alterations in the IS. It should be noted that these experiments were performed at SL 2.2 μm, longer than the 1.9 μm employed in our investigations. Because the required osmotic compression to induce the switch-like activation depends on both SL and dextran concentration, the critical range of osmotic pressure that switches on the regulation of Ca^{2+} sensitivity in our current study might be reached by the addition of dextran between 1 and 4% at SL 1.9 μm.

In conclusion, mimicking the SL-induced alterations in IS with 1% dextran did not reproduce the SL-dependent increase in the Ca^{2+} sensitivity, whereas further compression with 4% dextran significantly enhanced the Ca^{2+} sensitivity for both force and cTnC structural change. These results suggest that there is no simple relationship between the IS and the Ca^{2+} sensitivity. The different impacts of 1% and 4% dextran compression on the Ca^{2+} sensitivity may be due to the following mechanisms.

Firstly, compression with 4% dextran that mimics the changes of fibre width as produced by stretching SL from 1.9 to 2.3 μm might lead to an IS much closer to the optimal one to which the myosin heads and the Ca^{2+} sensitivity are most sensitive; Secondly, changing SL may not only affect IS, but also alter interactions between the extra-sarcomeric proteins which consequently affect fibre width more than IS. Thus, mimicking changes in fibre width with 4% dextran might better reproduce the impact of SL stretching from 1.9 μm to 2.3 μm; moreover, there may be an osmotic pressure-sensitive mechanism in the regulation of Ca^{2+} sensitivity that depends on the extent of compression in a narrow range rather than the IS. In this study at SL 1.9 μm, 4% dextran may draw the compression into the critical range.

Chapter 7

Conclusions and Future Work

7.1 Conclusions and Future Work

The Frank-Starling relationship describes an important regulatory system in the heart which correlates the amount of cardiac output with the amount of diastolic ventricular filling. During the time course of a heartbeat, increasing the blood filling in the ventricle stretches the ventricular wall, and leads to a stronger contraction in the heart. The stronger heart muscle contracts, the greater the ventricular pressure during systole, and ultimately, the more ejection volume. At its basis, the Frank-Starling relationship in the heart is caused by a phenomenon called LDA on the level of a cardiac muscle cell. Increasing the diastolic ventricular filling in the heart stretches the SL in the cardiomyocytes, leads to greater force production in the cardiac muscle contraction, which results in an enhancement of the heart's performance in the next beat. It was suggested that this SL-dependent increase in the force production was not due to the increasing Ca^{2+} supply but the increasing Ca^{2+} sensitivity with increased SL. Therefore, in response to the increasing SL, the outcome of LDA has two aspects: the increasing maximum force production, and the increasing Ca^{2+} sensitivity.

In the scope of this thesis, the primary goal was to investigate the potential determinants and/or major events in LDA. As the cellular basis of the Frank-Starling relationship, the importance of LDA has been appreciated for a very long time. However, despite the extensive research regarding the molecular mechanisms underlying this length dependence in cardiomyocytes, no definite answer has yet to be produced. So this project mainly focused on the molecular mechanisms in sensing sarcomere lengthening and transmitting the signal to increase the maximum force generation and the Ca^{2+} sensitivity.

Early investigations have suggested that in a typical event of LDA, associated with the increased Ca^{2+} sensitivity for force, there was also an increased Ca^{2+} binding affinity for cTnC as SL increased (Hofmann and Fuchs, 1987a; Hofmann and Fuchs, 1988; Wang and Fuchs, 1995). Our group's previous studies have shown that the force development in cardiac muscle contraction was linearly related to the structural change in cTnC upon Ca^{2+} activation, implying similar Ca^{2+} dependent behaviour in force and cTnC structural change (Sun *et al*., 2009). As the Ca^{2+}-binding protein, cTnC has long been considered as an important modulator of the Ca^{2+} sensitivity. Therefore, our first investigation focused on the possibility of cTnC in sensing the SL change to modulate the maximum force and the Ca^{2+} sensitivity.

In this study, we used a fluorescence polarization technique, F*I*SS, on a specific experimental set-up to examine some of the most promising hypotheses that may contribute to the signal transmission from sarcomere lengthening to increase the maximum force and the Ca^{2+} sensitivity. It allows us to measure the force development and cTnC structural change simultaneously, and to correlate the structure with the function of cTnC in the native environment of a working cardiac muscle cell on the timescale of a heartbeat.

As described before, cardiac muscle functions on the ascending limb of the length-tension curve under physiological conditions, corresponding to SL 1.7 μm to 2.3 μm in human hearts (Hibberd and Jewell, 1982; Kentish et al., 1986). Within this working SL range, the contraction of the generally sub-maximally activated cardiomyocyte has large contractile reserve which is primarily subject to the regulation by SL change at a given [Ca^{2+}] (Fabiato, 1981). In our experiments, in order to investigate the possible underlying mechanisms of the steep SL dependence in cardiac muscle contraction, we examined the alterations in some of the sarcomeric properties upon sarcomere lengthening from 1.9 μm to 2.3 μm in demembranated ventricular trabeculae from rat. The two SLs were chosen to represent lengths just above slack and optimally stretched, respectively, and each was set carefully by laser diffraction before activation (Section 2.5.1). As reported by Kentish et al. (1986), maximum Ca^{2+}-activation at high SL caused an irreversible deterioration of the diffraction pattern. Even though the pattern could recovery after the muscle was slacked and relaxed, the pattern in subsequent contractions was compromised. For this reason, we investigated the impact of SL change on myofilament activation by stretching the trabeculae from SL 1.9 μm to 2.3 μm, instead of shortening them in the opposite direction, to leave the high [Ca^{2+}] high SL condition at the end of the experiment and minimise the muscle deterioration.

The key results of this project are concluded below.

1. The role of cTnC

In evaluating the possible role of cTnC in transmitting the information concerning SL variation to modulate the maximum force and the Ca^{2+} sensitivity for force, we found almost identical leftward shifts of the force-[Ca^{2+}] and cTnC structural change-[Ca^{2+}] relationships as SL increased from 1.9 to 2.3 μm, indicating similar SL-dependent increases in the Ca^{2+} sensitivity for both force and cTnC structural change. We have shown a ~40% increase in the maximum Ca^{2+}-activated force upon SL increasing from 1.9 μm to 2.3 μm, together with ~0.11 pCa units increase in the Ca^{2+} sensitivity for force and cTnC structural change. However, the amplitude of orientation changes in either the C-helix in the regulator lobe of cTnC or the E-helix in the IT arm upon Ca^{2+}-activation were not affected by SL increasing. That is, the SL-dependent increase in the force production was not accompanied by the increasing extent of structural changes in cTnC. Thus, we concluded, of the two outcomes of LDA, while the SL-dependent Ca^{2+} sensitivity for force is very likely modulated through the Ca^{2+} sensitivity for cTnC structural change by cTnC, the SL-dependent maximum force is not. It was suggested that this SL-dependent increase in the maximum force was the result of an increasing number of force-generating cross-bridges formed at longer SL (Allen and Kentish, 1985; Wannenburg et al., 2000; Wannenburg et al., 1997), thus leads us to the next investigation on the thick filament cross-bridges.

2. The role of force-generating cross-bridges

As the cellular basis of the Frank-Starling relationship between ventricular volume and pressure, the SL-dependent modulation of the force development at a given [Ca^{2+}] largely depends on alterations in the number of the force-generating cross-bridges (Allen and Kentish, 1985). In order to investigate the role of force-generating cross-bridges in the other outcome of LDA — the SL-dependent Ca^{2+} sensitivity, our next focus moved onto the thick filament. We determined whether the SL-dependent variation in the number of the strong cross-bridge attachments may be responsible for the length modulation of not only the maximum force development, but also the Ca^{2+} sensitivity. In our experiments, active force inhibition by blebbistatin depressed the amplitude of cTnC structural change upon activation in both the regulatory head and the IT arm, with the effect being stronger in the IT arm. The results indicate an important role of the force-generating cross-bridges on the structural changes of cTnC upon activation, possibly, by keeping the inhibitory region of cTnI off the actin and stabilizing the Ca^{2+}-sensitizing cTnI/cTnC interactions. The inhibition of force-generating cross-bridges also reduced the Ca^{2+} sensitivity for cTnC structural changes, but had no significant effect on the cooperativity. Thus, the formation of strong binding cross-bridges may be involved in regulating the Ca^{2+} sensitivity through stabilising the Ca^{2+}-sensing cTnI/cTnC interactions, which in turn, stabilises the conformational change in cTnC in Ca^{2+}-activation.

To further investigate the role of the force-generating cross-bridges in LDA, we examined the impact of cross-bridges inhibition on the SL-dependent Ca^{2+} sensitivity by increasing SL from 1.9 to 2.3 μm in the presence of blebbistatin. We found that stretching SL after the inhibition of the force-generating cross-bridges still produced an increase in the Ca^{2+} sensitivity, although to a less degree as that without force inhibition. That is, even without force-generating myosin cross-bridges, there was still SL-dependent Ca^{2+} sensitivity in the thin filament. These results suggested that, even though the force-generating cross-bridges modulated the myofilament Ca^{2+} sensitivity in certain ways, they were not essential for the SL-dependent Ca^{2+} sensitivity in LDA. The two outcomes of LDA are very likely due to two independent pathways: the control centre for regulating the SL-dependent Ca^{2+} sensitivity locates on the thin filament by cTnC, and that for regulating the SL-dependent maximum force locates on the thick filament by force-generating cross-bridges. In the meantime, the thick filament cross-bridges may provide a positive feedback to support the increasing Ca^{2+} sensitivity with increasing SL, possibly by stabilizing the structural change in cTnC upon Ca^{2+}-activation.

3. The role of interfilament spacing

Lastly, we examined one of the most popular hypotheses of LDA — the interfilament spacing theory. It has been suggested that the SL increasing-induced closer approximation of the myosin heads and actin favours more actomyosin interactions, thereby enhances the probability of cross-bridges formation, and may in turn increase the Ca^{2+} sensitivity. The role of IS in LDA has been tested in this study. High molecular weight molecule dextran was used to osmotically compress the skinned cardiac trabeculae at a short SL (1.9 μm) to mimic the impact of stretching to a long SL (2.3 μm) on thin filament activation. According to the different impact of dextran compression on the IS and fibre width, two concentrations of dextran, 1% and 4%, were chosen to mimic the corresponding reductions in the IS and fibre width as those induced by SL increasing from 1.9 to 2.3 μm, respectively.

The results showed that mimicking the SL increasing-induced reductions in the IS with 1% dextran did not reproduce the SL-dependent increase in the Ca^{2+} sensitivity. However, further compression with 4% dextran did increase the Ca^{2+} sensitivity significantly. Our results suggested there was no simple relationship between the changes in the IS and the changes in the Ca^{2+} sensitivity. Osmotic compression at a short SL was not functionally equivalent to sarcomere lengthening. Consistent with the recent findings from other researchers, our investigations disagreed with the hypothesis, indicating that change in IS was not completely responsible for the SL-dependent Ca^{2+} sensitivity in LDA.

The different impact of 1% dextran and 4% dextran compression on the Ca^{2+} sensitivity may be due to various factors, including: the existence of an optimal IS at which the regulation of Ca^{2+} sensitivity is most sensitive to the change in IS; the additional impacts of SL variation on the entire trabeculae in addition to inducing inverse change in IS; and a possible osmotic pressure-sensitive effect of compression in the regulation of Ca^{2+} sensitivity that depends on the extent of compression in a narrow range rather than the IS.

From our current findings we know that the two outcomes of LDA come from two independent signally pathways: the thin filament-regulated Ca^{2+} sensitivity and the thick filament-regulated maximum force. This specifies the direction for the future investigations of the signal pathway in LDA. Next task on the list would be to investigate how the signal of sarcomere lengthening is transmitted to affect both the thick and thin filaments, is there a primary length sensing component in LDA or is the effect of multiple protein networks in the sarcomere? Further considerations should focus on the giant protein titin and cMyBP-C, as the two proteins have interactions with both filaments. Also, the structural impact of LDA on other sarcomeric proteins that involved in the cardiac muscle contraction could provide insights in the molecular mechanisms of LDA as well. Using more BR-probes on various sites and proteins in the sarcomere is desired.

7.2 Limitations and Future Improvements of F*IS*S

In this study, fluorescence for *in situ* structure was used to study the orientation changes in the two major domains, the regulatory head and the IT arm in the Tn complex, and their relationships with [Ca^{2+}]. This approach measures the orientation distributions of all labelled proteins. Thus, the accuracy of F*IS*S is largely dependent on the normal structure and function of the target protein domain after labelling and reconstitution. Previous studies using NMR spectroscopy have shown that neither the mutagenesis nor the BR labelling substantially altered the structure of the labelled domain (Mercier *et al*., 2003). However, current studies cannot exclude the possibility that these modifications may affect the *in situ* interactions between cTnC and other sarcomeric proteins. The force recovery after reconstitution with each BR-cTnC was similar compared to that obtained for unlabelled recombinant cTnC, indicating that the functional properties of cTnC were not significantly affected by BR probes either. Previous studies show that the presence of BR probe on either the C- or E-helix of cTnC did reduce the Ca^{2+} affinity of the regulatory site of cTnC with no significant effect on the cooperativity of Ca^{2+} regulation (Sun *et al*., 2009). The orientation information obtained by the fluorescence polarization measurement in this study has limitations, including the limited orientational resolution obtained from the first two order parameters and the lack of the information in the azimuthal orientation distribution of the probe dipole around the symmetric actin filament axis.

Further development of the fluorescence polarization technique for *in situ* measurements of protein structure may focus on the above limitations in various ways, e.g. increasing the number of probe labelling sites on the desired protein, in combination with using pulsed rather than continuous excitation, may help improve the resolution of the orientation measurements, also allow the measurement of azimuthal motions in the labelled-domain (Bell *et al*., 2002; Cone, 1972; van der Heide *et al*., 2000).

7.3 Other Limitations

The conclusions we drew in this study were based on experiments performed with skinned preparations of the rat cardiac trabeculae. Permeabilization allows easy access and control of the free [Ca^{2+}], MgATP and other small molecules in the trabeculae, direct measurement of the Ca^{2+} binding, and the replacement and modification of the sarcomeric proteins for mechanistic studies (Sun and Irving, 2010). However, demembranation of muscle fibres has a number of downsides compared to the intact cells, such as the non-constant myofilament volume which results in the greater interfilament spacing at a given SL. Also, the experimental temperature was lower than the physiological one. Moreover, in terms of the impact of skinning on SL, Kentish et al. (1986) reported an increasing intensity with a decreasing dispersion of the first order diffraction pattern upon the skinning procedure. Initially, it seemed not only did the permeabilization not interfere with the measurement of SL, but made it even easier due to the increasing intensity and decreasing dispersion. However, as described previously, the first order diffraction pattern deteriorated during activations at high [Ca^{2+}] and high SLs in the skinned fibres, whilst remained constant in the intact cardiac muscle. It is therefore necessary to seek for an effective solution to elucidate the mechanisms and events underlying the LDA under more realistic physiological conditions in the living heart in the future.

Additionally, it may be argued that the measurements of the force-pCa and cTnC structural change-pCa relationships in this study were under activation conditions, whereas the SL was set under relaxing conditions prior to the activation. Although the SL was checked after each series of continuous activation to make sure it did not deviate from the original setting, it was not measured during activation due to technical difficulties and the deterioration of the laser diffraction pattern after maximum Ca^{2+}-activation. Therefore, the relationships reported in the current experiments between myofilament Ca^{2+} sensitivity and SL under various conditions actually included some uncertainty about SL. Further experiments are still in need for assessing the quantitive relationships between SL and myofilament activation during contraction more specifically. Powerful techniques as to simultaneously measure the SL during continuous activation are highly demanded.

Bibliography

Adhikari, B.B., and P.G. Fajer. 1996. Myosin head orientation and mobility during isometric contraction: effects of osmotic compression. *Biophys. J.* 70:1872-1880.

Adhikari, B.B., M. Regnier, A.J. Rivera, K.L. Kreutziger, and D.A. Martyn. 2004. Cardiac length dependence of force and force redevelopment kinetics with altered cross-bridge cycling. *Biophys. J.* 87:1784-1794.

Agianian, B., U. Krzic, F. Qiu, W.A. Linke, K. Leonard, and B. Bullard. 2004. A troponin switch that regulates muscle contraction by stretch instead of calcium. *EMBO J.* 23:772-779.

Allen, D.G., B.R. Jewell, and J.W. Murray. 1974. The contribution of activation processes to the length-tension relation of cardiac muscle. *Nature*. 248:606-607.

Allen, D.G., and J.C. Kentish. 1985. The cellular basis of the length-tension relation in cardiac muscle. *J. Mol. Cell. Cardiol.* 17:821-840.

Allen, D.G., and S. Kurihara. 1982. The effects of muscle length on intracellular calcium transients in mammalian cardiac muscle. *J Physiol*. 327:79-94.

Allhouse, L.D., J.D. Potter, and C.C. Ashley. 1999. A novel method of extraction of TnC from skeletal muscle myofibrils. *Pflugers Arch.* 437:695-701.

Allingham, J.S., R. Smith, and I. Rayment. 2005. The structural basis of blebbistatin inhibition and specificity for myosin II. *Nat Struct Mol Biol*. 12:378-379.

Anson, M., M.A. Geeves, S.E. Kurzawa, and D.J. Manstein. 1996. Myosin motors with artificial lever arms. *EMBO J.* 15:6069-6074.

Babu, A., E. Sonnenblick, and J. Gulati. 1988. Molecular basis for the influence of muscle length on myocardial performance. *Science*. 240:74-76.

Bell, M.G., R.E. Dale, U.A. van der Heide, and Y.E. Goldman. 2002. Polarized fluorescence depletion reports orientation distribution and rotational dynamics of muscle cross-bridges. *Biophys. J.* 83:1050-1073.

Bell, M.G., E.B. Lankford, G.E. Gonye, G.C. Ellis-Davies, D.A. Martyn, M. Regnier, and R.J. Barsotti. 2006. Kinetics of cardiac thin-filament activation probed by fluorescence polarization of rhodamine-labeled troponin C in skinned guinea pig trabeculae. *Biophys. J.* 90:531-543.

Blix, M. 1894. Die Länge und die Spannung des Muskels1. *Skandinavisches Archiv Für Physiologie*. 5:173-206.

Brack, A.S., B.D. Brandmeier, R.E. Ferguson, S. Criddle, R.E. Dale, and M. Irving. 2004. Bifunctional rhodamine probes of Myosin regulatory light chain orientation in relaxed skeletal muscle fibers. *Biophys. J.* 86:2329-2341.

Bremel, R.D., and A. Weber. 1972. Cooperation within actin filament in vertebrate skeletal muscle. *Nat New Biol*. 238:97-101.

Brenner, B., T. Kraft, L.C. Yu, and J.M. Chalovich. 1999. Thin filament activation probed by fluorescence of N-((2-(iodoacetoxy)ethyl)-N-methyl)amino-7-nitrobenz-2-oxa-1,3-diazole-labeled troponin I incorporated into skinned fibers of rabbit psoas muscle. *Biophys. J.* 77:2677-2691.

Brown, J.H., Z. Zhou, L. Reshetnikova, H. Robinson, R.D. Yammani, L.S. Tobacman, and C. Cohen. 2005. Structure of the mid-region of tropomyosin: bending and binding sites for actin. *Proc. Natl. Acad. Sci. U. S. A.* 102:18878-18883.

Campbell, A.P., and B.D. Sykes. 1991. Interaction of troponin I and troponin C. Use of the two-dimensional nuclear magnetic resonance transferred nuclear Overhauser effect to determine the structure of the inhibitory troponin I peptide when bound to skeletal troponin C. *J. Mol. Biol.* 222:405-421.

Campbell, K.B., H. Taheri, R.D. Kirkpatrick, T. Burton, and W.C. Hunter. 1993. Similarities between dynamic elastance of left ventricular chamber and papillary muscle of rabbit heart. *Am. J. Physiol.* 264:H1926-1941.

Cazorla, O., G. Vassort, D. Garnier, and J.Y. Le Guennec. 1999. Length modulation of active force in rat cardiac myocytes: is titin the sensor? *J. Mol. Cell. Cardiol.* 31:1215-1227.

Cazorla, O., Y.M. Wu, T.C. Irving, and H. Granzier. 2001. Titin-based modulation of calcium sensitivity of active tension in mouse skinned cardiac myocytes. *Circ. Res.* 88:1028-1035.

Cone, R.A. 1972. Rotational diffusion of rhodopsin in the visual receptor membrane. *Nat New Biol*. 236:39-43.

Cooke, R. 1997. Actomyosin interaction in striated muscle. *Physiol. Rev.* 77:671-697.

Corrie, J.E., B.D. Brandmeier, R.E. Ferguson, D.R. Trentham, J. Kendrick-Jones, S.C. Hopkins, U.A. van der Heide, Y.E. Goldman, C. Sabido-David, R.E. Dale, S. Criddle, and M. Irving. 1999. Dynamic measurement of myosin light-chain-domain tilt and twist in muscle contraction. *Nature*. 400:425-430.

Corrie, J.E., J.S. Craik, and V.R. Munasinghe. 1998. A homobifunctional rhodamine for labeling proteins with defined orientations of a fluorophore. *Bioconjug. Chem.* 9:160-167.

Craig, R., K.H. Lee, J.Y. Mun, I. Torre, and P.K. Luther. 2014. Structure, sarcomeric organization, and thin filament binding of cardiac myosin-binding protein-C. *Pflugers Arch.* 466:425-431.

Dale, R.E., S.C. Hopkins, U.A. an der Heide, T. Marszalek, M. Irving, and Y.E. Goldman. 1999. Model-independent analysis of the orientation of fluorescent probes with restricted mobility in muscle fibers. *Biophys. J.* 76:1606-1618.

Davis, J.P., C. Norman, T. Kobayashi, R.J. Solaro, D.R. Swartz, and S.B. Tikunova. 2007. Effects of thin and thick filament proteins on calcium binding and exchange with cardiac troponin C. *Biophys. J.* 92:3195-3206.

de Tombe, P.P., R.D. Mateja, K. Tachampa, Y. Ait Mou, G.P. Farman, and T.C. Irving. 2010. Myofilament length dependent activation. *J. Mol. Cell. Cardiol.* 48:851-858.

Dobesh, D.P., J.P. Konhilas, and P.P. De Tombe. 2002. Cooperative activation in cardiac muscle: imapct of sarcomere length. *Am J Physiol Heart Circ Physiol*. 282:1055-1062.

Dou, Y., P. Arlock, and A. Arner. 2007. Blebbistatin specifically inhibits actin-myosin interaction in mouse cardiac muscle. *Am J Physiol. Cell Physiol*. 293:C1148-1153.

Ebashi, S., F. Ebashi, and A. Kodama. 1967. Troponin as the Ca^{2+}-receptive protein in the contractile system. *J Biochem*. 62:137-138.

Ebashi, S., and M. Endo. 1968. Calcium ion and muscle contraction. *Prog. Biophys. Mol. Biol.* 18:123-183.

Ebashi, S., M. Endo, and I. Otsuki. 1969. Control of muscle contraction. *Q. Rev. Biophys.* 2:351-384.

Endo, M. 1972. Stretch-Induced Increase in Activation of Skinned Muscle Fibers by Calcium. *Nat-New Biol*. 237:211-&.

Fabiato, A. 1981. Myoplasmic free calcium concentration reached during the twitch of an intact isolated cardiac cell and during calcium-induced release of calcium from the sarcoplasmic reticulum of a skinned cardiac cell from the adult rat or rabbit ventricle. *J. Gen. Physiol.* 78:457-497.

Fabiato, A., and F. Fabiato. 1975. Dependence of the contractile activation of skinned cardiac cells on the sarcomere length. *Nature*. 256:54-56.

Fabiato, A., and F. Fabiato. 1978. Myofilament-Generated Tension Oscillations during Partial Calcium Activation and Activation Dependence of Sarcomere Length-Tension Relation of Skinned Cardiac Cells. *J. Gen. Physiol.* 72:667-699.

Farah, C.S., C.A. Miyamoto, C.H. Ramos, A.C. da Silva, R.B. Quaggio, K. Fujimori, L.B. Smillie, and F.C. Reinach. 1994. Structural and regulatory functions of the NH_2- and COOH-terminal regions of skeletal muscle troponin I. *J. Biol. Chem.* 269:5230-5240.

Farman, G.P., E.J. Allen, K.Q. Schoenfelt, P.H. Backx, and P.P. de Tombe. 2010. The Role of Thin Filament Cooperativity in Cardiac Length-Dependent Calcium Activation. *Biophys. J.* 99:2978-2986.

Farman, G.P., D. Gore, E. Allen, K. Schoenfelt, T.C. Irving, and P.P. de Tombe. 2011. Myosin head orientation: a structural determinant for the Frank-Starling relationship. *Am J Physiol-Heart C*. 300:H2155-H2160.

Farman, G.P., K. Tachampa, R. Mateja, O. Cazorla, A. Lacampagne, and P.P. de Tombe. 2008. Blebbistatin: use as inhibitor of muscle contraction. *Pflugers Arch.* 455:995-1005.

Farman, G.P., J.S. Walker, P.P. de Tombe, and T.C. Irving. 2006. Impact of osmotic compression on sarcomere structure and myofilament calcium sensitivity of isolated rat myocardium. *Am J Physiol-Heart C*. 291:H1847-H1855.

Ferguson, R.E., Y.B. Sun, P. Mercier, A.S. Brack, B.D. Sykes, J.E.T. Corrie, D.R. Trentham, and M. Irving. 2003. In Situ Orientations of Protein Domains:Troponin C in Skeletal Muscle Fibers. *Mol. Cell*:865-874.

Fitzsimons, D.P., and R.L. Moss. 1998. Strong binding of myosin modulates length-dependent Ca^{2+} activation of rat ventricular myocytes. *Circ. Res.* 83:602-607.

Flicker, P.F., G.N. Phillips, Jr., and C. Cohen. 1982. Troponin and its interactions with tropomyosin. An electron microscope study. *J. Mol. Biol.* 162:495-501.

Ford, L.E., K. Nakagawa, J. Desper, and C.Y. Seow. 1991. Effect of osmotic compression on the force-velocity properties of glycerinated rabbit skeletal muscle cells. *J. Gen. Physiol.* 97:73-88.

Frey, N., M. Luedde, and H.A. Katus. 2012. Mechanisms of disease: hypertrophic cardiomyopathy. *Nat Rev Cardiol*. 9:91-100.

Fuchs, F., and D.A. Martyn. 2005. Length-dependent Ca^{2+} activation in cardiac muscle: some remaining questions. *J Muscle Res Cell M*. 26:199-212.

Fuchs, F., and S.H. Smith. 2001. Calcium, cross-bridges, and the Frank-Starling relationship. *News Physiol Sci*. 16:5-10.

Fuchs, F., and Y.P. Wang. 1996. Sarcomere length versus interfilament spacing as determinants of cardiac myofilament Ca^{2+} sensitivity and Ca^{2+} binding. *J. Mol. Cell. Cardiol.* 28:1375-1383.

Fujii, T., A.H. Iwane, T. Yanagida, and K. Namba. 2010. Direct visualization of secondary structures of F-actin by electron cryomicroscopy. *Nature*. 467:724-728.

Fukuda, N., and H.L. Granzier. 2005. Titin/connectin-based modulation of the Frank-Starling mechanism of the heart. *J Muscle Res Cell M*. 26:319-323.

Fukuda, N., H. Kajiwara, S. Ishiwata, and S. Kurihara. 2000. Effects of MgADP on length dependence of tension generation in skinned rat cardiac muscle. *Circ. Res.* 86:E1-E6.

Fukuda, N., T. Terui, I. Ohtsuki, S. Ishiwata, and S. Kurihara. 2009. Titin and Troponin Central Players in the Frank-Starling Mechanism of the heart. *Current Cardiology Reviews*. 5:119-124.

Gasmi-Seabrook, G.M., J.W. Howarth, N. Finley, E. Abusamhadneh, V. Gaponenko, R.M. Brito, R.J. Solaro, and P.R. Rosevear. 1999. Solution structures of the C-terminal domain of cardiac troponin C free and bound to the N-terminal domain of cardiac troponin I. *Biochemistry (Mosc).* 38:8313-8322.

Geeves, M.A., and K.C. Holmes. 1999. Structural mechanism of muscle contraction. *Annu. Rev. Biochem.* 68:687-728.

Godt, R.E., and D.W. Maughan. 1981. Influence of osmotic compression on calcium activation and tension in skinned muscle fibers of the rabbit. *Pflugers Arch.* 391:334-337.

Goo, S., P. Joshi, G. Sands, D. Gerneke, A. Taberner, Q. Dollie, I. LeGrice, and D. Loiselle. 2009. Trabeculae carneae as models of the ventricular walls: implications for the delivery of oxygen. *J. Gen. Physiol.* 134:339-350.

Gordon, A.M., E. Homsher, and M. Regnier. 2000. Regulation of contraction in striated muscle. *Physiol. Rev.* 80:853-924.

Gordon, A.M., A.F. Huxley, and F.J. Julian. 1966. The variation in isometric tension with sarcomere length in vertebrate muscle fibres. *J Physiol*. 184:170-192.

Gordon, A.M., M. Regnier, and E. Homsher. 2001. Skeletal and cardiac muscle contractile activation: tropomyosin "rocks and rolls". *News Physiol Sci*. 16:49-55.

Gordon, A.M., and E.B. Ridgway. 1993. Cross-bridges affect both TnC structure and calcium affinity in muscle fibers. *Adv. Exp. Med. Biol.* 332:183-192; discussion 192-184.

Granzier, H.L., and T.C. Irving. 1995. Passive tension in cardiac muscle: contribution of collagen, titin, microtubules, and intermediate filaments. *Biophys. J.* 68:1027-1044.

Greaser, M.L., and J. Gergely. 1971. Reconstitution of troponin activity from three protein components. *J. Biol. Chem.* 246:4226-4233.

Hamdani, N., V. Kooij, S. van Dijk, D. Merkus, W.J. Paulus, C.D. Remedios, D.J. Duncker, G.J. Stienen, and J. van der Velden. 2008. Sarcomeric dysfunction in heart failure. *Cardiovasc. Res.* 77:649-658.

Hanft, L.M., F.S. Korte, and K.S. McDonald. 2008. Cardiac function and modulation of sarcomeric function by length. *Cardiovasc. Res.* 77:627-636.

Hanson, J., and H.E. Huxley. 1953. Structural basis of the cross-striations in muscle. *Nature*. 172:530-532.

Haselgrove, J.C., and H.E. Huxley. 1973. X-ray evidence for radial cross-bridge movement and for the sliding filament model in actively contracting skeletal muscle. *J. Mol. Biol.* 77:549-568.

Herzberg, O., and M.N. James. 1985. Structure of the calcium regulatory muscle protein troponin-C at 2.8 A resolution. *Nature*. 313:653-659.

Hibberd, M.G., and B.R. Jewell. 1982. Calcium- and length-dependent force production in rat ventricular muscle. *J Physiol*. 329:527-540.

Hofmann, P.A., and F. Fuchs. 1987a. Effect of Length and Cross-Bridge Attachment on Ca^{2+} Binding to Cardiac Troponin-C. *Am J of Physiol*. 253:C90-C96.

Hofmann, P.A., and F. Fuchs. 1987b. Evidence for a Force-Dependent Component of Calcium-Binding to Cardiac Troponin-C. *Am J of Physiol*. 253:C541-C546.

Hofmann, P.A., and F. Fuchs. 1988. Bound calcium and force development in skinned cardiac muscle bundles: effect of sarcomere length. *J. Mol. Cell. Cardiol.* 20:667-677.

Holmes, K.C., D. Popp, W. Gebhard, and W. Kabsch. 1990. Atomic model of the actin filament. *Nature*. 347:44-49.

Holroyde, M.J., S.P. Robertson, J.D. Johnson, R.J. Solaro, and J.D. Potter. 1980. The calcium and magnesium binding sites on cardiac troponin and their role in the regulation of myofibrillar adenosine triphosphatase. *J. Biol. Chem.* 255:11688-11693.

Hopkins, S.C., C. Sabido-David, J.E. Corrie, M. Irving, and Y.E. Goldman. 1998. Fluorescence polarization transients from rhodamine isomers on the myosin regulatory light chain in skeletal muscle fibers. *Biophys. J.* 74:3093-3110.

Hopkins, S.C., C. Sabido-David, U.A. van der Heide, R.E. Ferguson, B.D. Brandmeier, R.E. Dale, J. Kendrick-Jones, J.E. Corrie, D.R. Trentham, M. Irving, and Y.E. Goldman. 2002. Orientation changes of the myosin light chain domain during filament sliding in active and rigor muscle. *J. Mol. Biol.* 318:1275-1291.

Huxley, A.F., and R. Niedergerke. 1954. Structural changes in muscle during contraction; interference microscopy of living muscle fibres. *Nature*. 173:971-973.

Huxley, H., and J. Hanson. 1954. Changes in the Cross-Striations of Muscle during Contraction and Stretch and their Structural Interpretation. *Nature*. 173:973-976.

Huxley, H.E. 1953a. Electron microscope studies of the organisation of the filaments in striated muscle. *Biochim. Biophys. Acta*. 12:387-394.

Huxley, H.E. 1953b. X-ray analysis and the problem of muscle. *Proc. R. Soc. Lond. B. Biol. Sci.* 141:59-62.

Huxley, H.E. 1957. The double array of filaments in cross-striated muscle. *J Biophys Biochem Cytol*. 3:631-648.

Irving, M. 1996. Steady-state polarization from cylindrically symmetric fluorophores undergoing rapid restricted motion. *Biophys. J.* 70:1830-1835.

Irving, M., T. St Claire Allen, C. Sabido-David, J.S. Craik, B. Brandmeier, J. Kendrick-Jones, J.E. Corrie, D.R. Trentham, and Y.E. Goldman. 1995. Tilting of the light-chain region of myosin during step length changes and active force generation in skeletal muscle. *Nature*. 375:688-691.

Irving, T.C., J. Konhilas, D. Perry, R. Fischetti, and P.P. De Tombe. 2000. Myofilament lattice spacing as a function of sarcomere length in isolated rat myocardium. *Am J Physiol-Heart C*. 279:H2568-H2573.

Jewell, B.R. 1977. A reexamination of the influence of muscle length on myocardial performance. *Circ. Res.* 40:221-230.

Johnson, J.D., J.H. Collins, S.P. Robertson, and J.D. Potter. 1980. A fluorescent probe study of Ca^{2+} binding to the Ca^{2+}-specific sites of cardiac troponin and troponin C. *J. Biol. Chem.* 255:9635-9640.

Julien, O., Y.B. Sun, A.C. Knowles, B.D. Brandmeier, R.E. Dale, D.R. Trentham, J.E. Corrie, B.D. Sykes, and M. Irving. 2007. Toward protein structure in situ: comparison of two bifunctional rhodamine adducts of troponin C. *Biophys. J.* 93:1008-1020.

Kabsch, W., H.G. Mannherz, D. Suck, E.F. Pai, and K.C. Holmes. 1990. Atomic structure of the actin:DNase I complex. *Nature*. 347:37-44.

Kawai, M., J.S. Wray, and Y. Zhao. 1993. The effect of lattice spacing change on cross-bridge kinetics in chemically skinned rabbit psoas muscle fibers. I. Proportionality between the lattice spacing and the fiber width. *Biophys. J.* 64:187-196.

Kentish, J.C., H.E. ter Keurs, L. Ricciardi, J.J. Bucx, and M.I. Noble. 1986. Comparison between the sarcomere length-force relations of intact and skinned trabeculae from rat right ventricle. Influence of calcium concentrations on these relations. *Circ. Res.* 58:755-768.

Kirschenlohr, H.L., A.A. Grace, J.I. Vandenberg, J.C. Metcalfe, and G.A. Smith. 2000. Estimation of systolic and diastolic free intracellular Ca^{2+} by titration of Ca^{2+} buffering in the ferret heart. *Biochem. J.* 346 Pt 2:385-391.

Knowles, A.C., M. Irving, and Y.B. Sun. 2012. Conformation of the Troponin Core Complex in the Thin Filaments of Skeletal Muscle during Relaxation and Active Contraction. *J. Mol. Biol.* 421:125-137.

Kobayashi, T., L. Jin, and P.P. de Tombe. 2008. Cardiac thin filament regulation. *Pflugers Arch.* 457:37-46.

Kobayashi, T., and R.J. Solaro. 2005. Calcium, thin filaments, and the integrative biology of cardiac contractility. *Annu. Rev. Physiol.* 67:39-67.

Kobayashi, T., X. Zhao, R. Wade, and J.H. Collins. 1999. Ca^{2+}-dependent interaction of the inhibitory region of troponin I with acidic residues in the N-terminal domain of troponin C. *Biochim. Biophys. Acta*. 1430:214-221.

Kohler, J., Y. Chen, B. Brenner, A.M. Gordon, T. Kraft, D.A. Martyn, M. Regnier, A.J. Rivera, C.K. Wang, and P.B. Chase. 2003. Familial hypertrophic cardiomyopathy mutations in troponin I (K183D, G203S, K206Q) enhance filament sliding. *Physiol Genomics*. 14:117-128.

Konhilas, J.P., T.C. Irving, and P.P. de Tombe. 2002a. Frank-Starling law of the heart and the cellular mechanisms of length-dependent activation. *Pflug Arch Eur J Phy*. 445:305-310.

Konhilas, J.P., T.C. Irving, and P.P. de Tombe. 2002b. Myofilament calcium sensitivity in skinned rat cardiac trabeculae - Role of interfilament spacing. *Circ. Res.* 90:59-65.

Konhilas, J.P., T.C. Irving, S.H. Smith, and P.P. de Tombe. 2001. Length-dependent activation compared in three striated muscle types of the rat. *Biophys. J.* 80:258a-259a.

Konhilas, J.P., T.C. Irving, B.M. Wolska, E.E. Jweied, A.F. Martin, R.J. Solaro, and P.P. de Tombe. 2003. Troponin I in the murine myocardium: influence on length-dependent activation and interfilament spacing. *J Physiol-London*. 547:951-961.

Korte, F.S., E.R. Feest, M.V. Razumova, A.Y. Tu, and M. Regnier. 2012. Enhanced Ca^{2+} binding of cardiac troponin reduces sarcomere length dependence of contractile activation independently of strong crossbridges. *Am J Physiol Heart Circ Physiol*. 303:H863-870.

Kovacs, M., J. Toth, C. Hetenyi, A. Malnasi-Csizmadia, and J.R. Sellers. 2004. Mechanism of blebbistatin inhibition of myosin II. *J. Biol. Chem.* 279:35557-35563.

Labeit, S., and B. Kolmerer. 1995. Titins: giant proteins in charge of muscle ultrastructure and elasticity. *Science*. 270:293-296.

Lakatta, E.G., and B.R. Jewell. 1977. Length-dependent activation: its effect on the length-tension relation in cat ventricular muscle. *Circ. Res.* 40:251-257.

Lehman, W., R. Craig, and P. Vibert. 1994. Ca^{2+}-induced tropomyosin movement in Limulus thin filaments revealed by three-dimensional reconstruction. *Nature*. 368:65-67.

Lehman, W., P. Vibert, P. Uman, and R. Craig. 1995. Steric-blocking by tropomyosin visualized in relaxed vertebrate muscle thin filaments. *J. Mol. Biol.* 251:191-196.

Lehrer, S.S. 1994. The regulatory switch of the muscle thin filament: Ca^{2+} or myosin heads. *J. Muscle Res. Cell Motil.* 15:232-236.

Li, A.Y., C.M. Stevens, B. Liang, K. Rayani, S. Little, J. Davis, and G.F. Tibbits. 2013. Familial hypertrophic cardiomyopathy related cardiac troponin C L29Q mutation alters length-dependent activation and functional effects of phosphomimetic troponin I*. *PLoS One*. 8:e79363.

Li, M.X., L. Spyracopoulos, and B.D. Sykes. 1999. Binding of cardiac troponin-I147-163 induces a structural opening in human cardiac troponin-C. *Biochemistry (Mosc).* 38:8289-8298.

Li, X.E., L.S. Tobacman, J.Y. Mun, R. Craig, S. Fischer, and W. Lehman. 2011. Tropomyosin position on F-actin revealed by EM reconstruction and computational chemistry. *Biophys. J.* 100:1005-1013.

Linke, W.A., M. Ivemeyer, N. Olivieri, B. Kolmerer, J.C. Ruegg, and S. Labeit. 1996. Towards a molecular understanding of the elasticity of titin. *J. Mol. Biol.* 261:62-71.

Llinas, P., O. Pylypenko, T. Isabet, M. Mukherjea, H.L. Sweeney, and A.M. Houdusse. 2012. How myosin motors power cellular functions: an exciting journey from structure to function: based on a lecture delivered at the 34th FEBS Congress in Prague, Czech Republic, July 2009. *FEBS J*. 279:551-562.

Luther, P.K. 2009. The vertebrate muscle Z-disc: sarcomere anchor for structure and signalling. *J. Muscle Res. Cell Motil.* 30:171-185.

Luther, P.K., H. Winkler, K. Taylor, M.E. Zoghbi, R. Craig, R. Padron, J.M. Squire, and J. Liu. 2011. Direct visualization of myosin-binding protein C bridging myosin and actin filaments in intact muscle. *Proc. Natl. Acad. Sci. U. S. A.* 108:11423-11428.

Martyn, D.A., B.B. Adhikari, M. Regnier, J. Gu, S.G. Xu, and L.C. Yu. 2004. Response of equatorial X-ray reflections and stiffness to altered sarcomere length and myofilament lattice spacing in relaxed skinned cardiac muscle. *Biophys. J.* 86:1002-1011.

Martyn, D.A., and A.M. Gordon. 2001. Influence of length on force and activation-dependent changes in troponin C structure in skinned cardiac and fast skeletal muscle. *Biophys. J.* 80:2798-2808.

Martyn, D.A., M. Regnier, D. Xu, and A.M. Gordon. 2001. Ca^{2+} - and cross-bridge-dependent changes in N- and C-terminal structure of troponin C in rat cardiac muscle. *Biophys. J.* 80:360-370.

Mateja, R.D., and P.P. de Tombe. 2012. Myofilament length-dependent activation develops within 5 ms in guinea-pig myocardium. *Biophys. J.* 103:L13-15.

McDonald, K.S., L.J. Field, M.S. Parmacek, M. Soonpaa, J.M. Leiden, and R.L. Moss. 1995. Length dependence of Ca^{2+} sensitivity of tension in mouse cardiac myocytes expressing skeletal troponin C. *J Physiol*. 483 (Pt 1):131-139.

McDonald, K.S., and R.L. Moss. 1995. Osmotic compression of single cardiac myocytes eliminates the reduction in Ca^{2+} sensitivity of tension at short sarcomere length. *Circ. Res.* 77:199-205.

McKillop, D.F., and M.A. Geeves. 1993. Regulation of the interaction between actin and myosin subfragment 1: evidence for three states of the thin filament. *Biophys. J.* 65:693-701.

McLachlan, A.D., and M. Stewart. 1982. Periodic charge distribution in the intermediate filament proteins desmin and vimentin. *J. Mol. Biol.* 162:693-698.

Mercier, P., R.E. Ferguson, M. Irving, J.E. Corrie, D.R. Trentham, and B.D. Sykes. 2003. NMR structure of a bifunctional rhodamine labeled N-domain of troponin C complexed with the regulatory "switch" peptide from troponin I: implications for in situ fluorescence studies in muscle fibers. *Biochemistry (Mosc).* 42:4333-4348.

Milligan, R.A., and P.F. Flicker. 1987. Structural relationships of actin, myosin, and tropomyosin revealed by cryo-electron microscopy. *J. Cell Biol.* 105:29-39.

Millman, B.M. 1998. The filament lattice of striated muscle. *Physiol. Rev.* 78:359-391.

Moss, R.L., and D.P. Fitzsimons. 2002. Frank-Starling relationship: long on importance, short on mechanism. *Circ. Res.* 90:11-13.

Moss, R.L., L.O. Nwoye, and M.L. Greaser. 1991. Substitution of Cardiac Troponin C into Rabbit Muscle Does Not Alter the Length Dependence of Ca^{2+} Sensitivity of Tension. *J Physiol-London*. 440:273-289.

Moss, R.L., M. Razumova, and D.P. Fitzsimons. 2004. Myosin crossbridge activation of cardiac thin filaments: implications for myocardial function in health and disease. *Circ. Res.* 94:1290-1300.

Mueller, H., and S.V. Perry. 1962. The degradation of heavy meromyosin by trypsin. *Biochem. J.* 85:431-439.

Ohtsuki, I. 1979. Molecular arrangement of troponin-T in the thin filament. *J Biochem*. 86:491-497.

Ohtsuki, I., Y. Onoyama, and F. Shiraishi. 1988. Electron microscopic study of troponin. *J Biochem*. 103:913-919.

Pan, B.S., and R.J. Solaro. 1987. Calcium-binding properties of troponin C in detergent-skinned heart muscle fibers. *J. Biol. Chem.* 262:7839-7849.

Parry, D.A., and J.M. Squire. 1973. Structural role of tropomyosin in muscle regulation: analysis of the x-ray diffraction patterns from relaxed and contracting muscles. *J. Mol. Biol.* 75:33-55.

Pearlstone, J.R., and L.B. Smillie. 1983. Effects of troponin-I plus-C on the binding of troponin-T and its fragments to alpha-tropomyosin. Ca^{2+} sensitivity and cooperativity. *J. Biol. Chem.* 258:2534-2542.

Potter, J.D., and J. Gergely. 1975. The calcium and magnesium binding sites on troponin and their role in the regulation of myofibrillar adenosine triphosphatase. *J. Biol. Chem.* 250:4628-4633.

Previs, M.J., H. Yu, S.B. Previs, J. Gulick, J. Robbins, and D.M. Warshaw. 2013. Dephosphorylated Cardiac Myosin-Binding Protein C (cMyBP-C) Activates Native Cardiac Thin Filaments within the C-Zone of Native Cardiac Thick Filaments. *Biophys. J.* 104:186a.

Putkey, J.A., W. Liu, X. Lin, S. Ahmed, M. Zhang, J.D. Potter, and W.G. Kerrick. 1997. Fluorescent probes attached to Cys 35 or Cys 84 in cardiac troponin C are differentially sensitive to Ca^{2+}-dependent events in vitro and in situ. *Biochemistry (Mosc).* 36:970-978.

Rayment, I., H.M. Holden, M. Whittaker, C.B. Yohn, M. Lorenz, K.C. Holmes, and R.A. Milligan. 1993a. Structure of the actin-myosin complex and its implications for muscle contraction. *Science*. 261:58-65.

Rayment, I., W.R. Rypniewski, K. Schmidt-Base, R. Smith, D.R. Tomchick, M.M. Benning, D.A. Winkelmann, G. Wesenberg, and H.M. Holden. 1993b. Three-dimensional structure of myosin subfragment-1: a molecular motor. *Science*. 261:50-58.

Razumova, M.V., A.E. Bukatina, and K.B. Campbell. 2000. Different myofilament nearest-neighbor interactions have distinctive effects on contractile behavior. *Biophys. J.* 78:3120-3137.

Regnier, M., H. Martin, R.J. Barsotti, A.J. Rivera, D.A. Martyn, and E. Clemmens. 2004. Cross-bridge versus thin filament contributions to the level and rate of force development in cardiac muscle. *Biophys. J.* 87:1815-1824.

Regnier, M., A.J. Rivera, C.K. Wang, M.A. Bates, P.B. Chase, and A.M. Gordon. 2002. Thin filament near-neighbour regulatory unit interactions affect rabbit skeletal muscle steady-state force-Ca^{2+} relations. *J Physiol*. 540:485-497.

Rieck, D.C., K.L. Li, Y. Ouyang, R.J. Solaro, and W.J. Dong. 2013. Structural basis for the in situ Ca^{2+} sensitization of cardiac troponin C by positive feedback from force-generating myosin cross-bridges. *Arch. Biochem. Biophys.* 537:198-209.

Robinson, J.M., W.J. Dong, J. Xing, and H.C. Cheung. 2004. Switching of troponin I: Ca^{2+} and myosin-induced activation of heart muscle. *J. Mol. Biol.* 340:295-305.

Rome, E. 1972. Relaxation of glycerinated muscle: low-angle x-ray diffraction studies. *J. Mol. Biol.* 65:331-345.

Rosenfeld, S.S., and E.W. Taylor. 1985. Kinetic studies of calcium binding to regulatory complexes from skeletal muscle. *J. Biol. Chem.* 260:252-261.

Ruegg, C., C. Veigel, J.E. Molloy, S. Schmitz, J.C. Sparrow, and R.H. Fink. 2002. Molecular motors: force and movement generated by single myosin II molecules. *News Physiol Sci*. 17:213-218.

Ruegg, J.C. 1998. Cardiac contractility: how calcium activates the myofilaments. *Naturwissenschaften*. 85:575-582.

Sevrieva, I. 2014. Structural and functional effects of troponin C cardiomyopathy mutations studied by polarized fluorescence. *King's Thesis*.

Sevrieva, I., A.C. Knowles, T. Kampourakis, and Y.B. Sun. 2014. Regulatory domain of troponin moves dynamically during activation of cardiac muscle. *J. Mol. Cell. Cardiol.* 75:181-187.

She, M., D. Trimble, L.C. Yu, and J.M. Chalovich. 2000. Factors contributing to troponin exchange in myofibrils and in solution. *J. Muscle Res. Cell Motil.* 21:737-745.

Shiels, H.A., and E. White. 2008. The Frank-Starling mechanism in vertebrate cardiac myocytes. *J. Exp. Biol.* 211:2005-2013.

Shiner, J.S., and R.J. Solaro. 1984. The Hill coefficient for the Ca^{2+}-activation of striated muscle contraction. *Biophys. J.* 46:541-543.

Sia, S.K., M.X. Li, L. Spyracopoulos, S.M. Gagne, W. Liu, J.A. Putkey, and B.D. Sykes. 1997. Structure of cardiac muscle troponin C unexpectedly reveals a closed regulatory domain. *J. Biol. Chem.* 272:18216-18221.

Smith, S.H., A.F. Martin, R.J. Solaro, and P.P. de Tombe. 2003. Chimeric troponin I and the sarcomere length dependence of calcium sensitivity in skinned rat trabeculae. *Biophys. J.* 84:251a-251a.

Spudich, J.A. 2001. The myosin swinging cross-bridge model. *Nat Rev Mol Cell Biol*. 2:387-392.

Spudich, J.A., H.E. Huxley, and J.T. Finch. 1972. Regulation of skeletal muscle contraction. II. Structural studies of the interaction of the tropomyosin-troponin complex with actin. *J. Mol. Biol.* 72:619-632.

Spyracopoulos, L., M.X. Li, S.K. Sia, S.M. Gagne, M. Chandra, R.J. Solaro, and B.D. Sykes. 1997. Calcium-induced structural transition in the regulatory domain of human cardiac troponin C. *Biochemistry (Mosc).* 36:12138-12146.

Starling, E.H., and M.B. Visscher. 1927. The regulation of the energy output of the heart. *J Physiol*. 62:243-261.

Straight, A.F., A. Cheung, J. Limouze, I. Chen, N.J. Westwood, J.R. Sellers, and T.J. Mitchison. 2003. Dissecting temporal and spatial control of cytokinesis with a myosin II Inhibitor. *Science*. 299:1743-1747.

Strauss, J.D., C. Zeugner, J.E. Van Eyk, C. Bletz, M. Troschka, and J.C. Ruegg. 1992. Troponin replacement in permeabilized cardiac muscle. Reversible extraction of troponin I by incubation with vanadate. *FEBS Lett.* 310:229-234.

Sumandea, M.P., W.G. Pyle, T. Kobayashi, P.P. de Tombe, and R.J. Solaro. 2003. Identification of a functionally critical protein kinase C phosphorylation residue of cardiac troponin T. *J. Biol. Chem.* 278:35135-35144.

Sun, Y.B., B. Brandmeier, and M. Irving. 2006. Structural changes in troponin in response to Ca^{2+} and myosin binding to thin filaments during activation of skeletal muscle. *Proc. Natl. Acad. Sci. U. S. A.* 103:17771-17776.

Sun, Y.B., and M. Irving. 2010. The molecular basis of the steep force-calcium relation in heart muscle. *J. Mol. Cell. Cardiol.* 48:859-865.

Sun, Y.B., F. Lou, and M. Irving. 2009. Calcium- and myosin-dependent changes in troponin structure during activation of heart muscle. *J Physiol*. 587:155-163.

Syska, H., J.M. Wilkinson, R.J. Grand, and S.V. Perry. 1976. The relationship between biological activity and primary structure of troponin I from white skeletal muscle of the rabbit. *Biochem. J.* 153:375-387.

Szent-Gyorgyi, A.G. 1953. Meromyosins, the subunits of myosin. *Arch. Biochem. Biophys.* 42:305-320.

Tachampa, K., H. Wang, G.P. Farman, and P.P. de Tombe. 2007. Cardiac troponin I threonine 144: role in myofilament length dependent activation. *Circ. Res.* 101:1081-1083.

Takacs, B., N. Billington, M. Gyimesi, B. Kintses, A. Malnasi-Csizmadia, P.J. Knight, and M. Kovacs. 2010. Myosin complexed with ADP and blebbistatin reversibly adopts a conformation resembling the start point of the working stroke. *Proc. Natl. Acad. Sci. U. S. A.* 107:6799-6804.

Takeda, S., T. Kobayashi, H. Taniguchi, H. Hayashi, and Y. Maeda. 1997. Structural and functional domains of the troponin complex revealed by limited digestion. *Eur. J. Biochem.* 246:611-617.

Takeda, S., A. Yamashita, K. Maeda, and Y. Maeda. 2003. Structure of the core domain of human cardiac troponin in the Ca^{2+}-saturated form. *Nature*. 424:35-41.

Talbot, J.A., and R.S. Hodges. 1981. Synthetic studies on the inhibitory region of rabbit skeletal troponin I. Relationship of amino acid sequence to biological activity. *J. Biol. Chem.* 256:2798-2802.

Tanokura, M., Y. Tawada, A. Ono, and I. Ohtsuki. 1983. Chymotryptic subfragments of troponin T from rabbit skeletal muscle. Interaction with tropomyosin, troponin I and troponin C. *J Biochem*. 93:331-337.

ter Keurs, H.E., W.H. Rijnsburger, R. van Heuningen, and M.J. Nagelsmit. 1980. Tension development and sarcomere length in rat cardiac trabeculae. Evidence of length-dependent activation. *Circ. Res.* 46:703-714.

Tobacman, L.S. 1996. Thin filament-mediated regulation of cardiac contraction. *Annu. Rev. Physiol.* 58:447-481.

Tskhovrebova, L., and J. Trinick. 2003. Titin: properties and family relationships. *Nat Rev Mol Cell Biol*. 4:679-689.

Uyeda, T.Q., P.D. Abramson, and J.A. Spudich. 1996. The neck region of the myosin motor domain acts as a lever arm to generate movement. *Proc. Natl. Acad. Sci. U. S. A.* 93:4459-4464.

Uyeda, T.Q., and J.A. Spudich. 1993. A functional recombinant myosin II lacking a regulatory light chain-binding site. *Science*. 262:1867-1870.

van der Heide, U.A., S.C. Hopkins, and Y.E. Goldman. 2000. A maximum entropy analysis of protein orientations using fluorescence polarization data from multiple probes. *Biophys. J.* 78:2138-2150.

van Eerd, J.P., and K. Takahshi. 1976. Determination of the complete amino acid sequence of bovine cardiac troponin C. *Biochemistry (Mosc).* 15:1171-1180.

Vibert, P., R. Craig, and W. Lehman. 1997. Steric-model for activation of muscle thin filaments. *J. Mol. Biol.* 266:8-14.

Wang, Y.P., and F. Fuchs. 1994. Length, Force, and Ca^{2+}-Troponin-C Affinity in Cardiac and Slow Skeletal-Muscle. *Am J of Physiol*. 266:C1077-C1082.

Wang, Y.P., and F. Fuchs. 1995. Osmotic compression of skinned cardiac and skeletal muscle bundles: effects on force generation, Ca^{2+} sensitivity and Ca^{2+} binding. *J. Mol. Cell. Cardiol.* 27:1235-1244.

Wannenburg, T., G.H. Heijne, J.H. Geerdink, H.W. Van Den Dool, P.M. Janssen, and P.P. De Tombe. 2000. Cross-bridge kinetics in rat myocardium: effect of sarcomere length and calcium activation. *Am J Physiol Heart Circ Physiol*. 279:H779-790.

Wannenburg, T., P.M. Janssen, D. Fan, and P.P. de Tombe. 1997. The Frank-Starling mechanism is not mediated by changes in rate of cross-bridge detachment. *Am. J. Physiol.* 273:H2428-2435.

White, S.P., C. Cohen, and G.N. Phillips, Jr. 1987. Structure of co-crystals of tropomyosin and troponin. *Nature*. 325:826-828.

Wu, Y., O. Cazorla, D. Labeit, S. Labeit, and H. Granzier. 2000. Changes in titin and collagen underlie diastolic stiffness diversity of cardiac muscle. *J. Mol. Cell. Cardiol.*

32:2151-2162.

Xu, C., R. Craig, L. Tobacman, R. Horowitz, and W. Lehman. 1999. Tropomyosin positions in regulated thin filaments revealed by cryoelectron microscopy. *Biophys. J.* 77:985-992.

Zhao, Y., M. Kawai, and J. Wray. 1993. The effect of lattice spacing change on cross-bridge kinetics in rabbit psoas fibers. *Adv. Exp. Med. Biol.* 332:581-592.

Zhou, X., E.P. Morris, and S.S. Lehrer. 2000. Binding of troponin I and the troponin I-troponin C complex to actin-tropomyosin. Dissociation by myosin subfragment 1. *Biochemistry (Mosc).* 39:1128-1132.

Zhou, Z., K.L. Li, D. Rieck, Y. Ouyang, M. Chandra, and W.J. Dong. 2012. Structural dynamics of C-domain of cardiac troponin I protein in reconstituted thin filament. *J. Biol. Chem.* 287:7661-7674.

Zimmer, H.G. 2002. Who discovered the Frank-Starling mechanism? *News Physiol Sci*. 17:181-184.